

DIET-INDUCED DYSLIPIDEMIA DRIVES STORE-
OPERATED Ca^{2+} ENTRY, Ca^{2+} DYSREGULATION, NON-
ALCOHOLIC STEATOHEPATITIS, AND CORONARY
ATHEROGENESIS IN METABOLIC SYNDROME

Zachary Paul Neeb

Submitted to the faculty of the University Graduate School
in partial fulfillment of the requirements
for the degree
Doctor of Philosophy
in the Department of Cellular and Integrative Physiology,
Indiana University

February 2010

Accepted by the Faculty of Indiana University, in partial fulfillment of the requirements for the degree of Doctor of Philosophy.

Michael Sturek, PhD, Chair

Jeffrey A. Breall, PhD

Doctoral Committee

Robert V. Considine, PhD

December 16, 2009

Alexander Obukhov, MD

Johnathan D. Tune, PhD

Dedication

To the family that raised me, Mom, Dad, Mamaw, and Drew, to the family I married, Dave, Joyce, Grandma, Granny, and Lindsey, and to my family, Jessica and Paul, I loved you then, I love you now, and I will always love you. There are no words to describe my gratitude.

Acknowledgements

My advisor, Michael Sturek, PhD, for his wisdom, guidance, and support; my committee Johnathan D. Tune, PhD, Alexander Obukhov, PhD, Robert V. Considine, PhD, and Jeffrey A. Breall, MD, PhD, for greatly improving and influencing my thesis; Jason M. Edwards, MD, PhD, and Ian N. Bratz, PhD, for changing my outlook on life and contributing to the science; Mouhamad Alloosh, MD, James Wenzel, Reverend, James Byrd, and Xin Long, PhD, for their immense contributions; and the Cellular and Integrative Physiology Department, for providing an excellent environment and opportunity.

ABSTRACT

Zachary Paul Neeb

DIET-INDUCED DYSLIPIDEMIA DRIVES STORE-OPERATED Ca^{2+} ENTRY, Ca^{2+} DYSREGULATION, NON-ALCOHOLIC STEATOHEPATITIS, AND CORONARY ATHEROGENESIS IN METABOLIC SYNDROME

Risk of coronary artery disease (CAD), the leading cause of death, greatly increases in metabolic syndrome. Metabolic syndrome (MetS; obesity, insulin resistance, glucose intolerance, dyslipidemia, and hypertension) is increasing in prevalence with sedentary lifestyles and poor nutrition. Non-alcoholic steatohepatitis (NASH; i.e. MetS liver) is progressive and decreases life expectancy, with CAD as the leading cause of death. Pathogenic Ca^{2+} regulation transforms coronary artery smooth muscle from a healthy, quiescent state to a diseased, proliferative phenotype thus majorly contributing to the development of CAD. In particular, store-operated Ca^{2+} entry (SOCE) in vascular smooth muscle is associated with atherosclerosis. Genetic predisposition may render individuals more susceptible to Ca^{2+} dysregulation, CAD, NASH, and MetS. However, the metabolic and cellular mechanisms underlying these disease states are poorly understood. Accordingly, the goal of this dissertation was to investigate the role of dyslipidemia within MetS in the development of Ca^{2+} dysregulation, CAD, and NASH. The overarching hypothesis was that dyslipidemia within MetS would be necessary for induction of NASH and increased SOCE that would primarily mediate development of CAD. To test this hypothesis we utilized the Ossabaw miniature swine model of MetS. Swine were fed one of five diets for different lengths of time to induce varying severity of MetS. Lean swine were fed normal maintenance chow diet. F/MetS swine were fed high

Fructose (20% kcal) diet that induced normolipidemic MetS. TMetS were fed excess high Trans-fat/cholesterol atherogenic diet that induced mildly dyslipidemic MetS and CAD. XMetS were TMetS swine with eXercise. DMetS (TMetS + high fructose) were moderately dyslipidemic and developed MetS and extensive CAD. sDMetS (Short-term DMetS) developed MetS with mild dyslipidemia, but no CAD. MMetS (Mixed-source-fat/cholesterol/fructose) were severely dyslipidemic, exhibited NASH, and developed severe CAD. Dyslipidemia in MetS predicted NASH severity (all groups < DMetS << MMetS), CAD severity (i.e. Lean, F/MetS, sDMetS < XMetS < TMetS < DMetS < MMetS), and was necessary for STIM1/TRPC1-mediated SOCE, which preceded CAD. Exercise ameliorated SOCE and CAD compared to TMetS. In conclusion, dyslipidemia elicits TRPC1/STIM1 SOCE that mediates CAD, is necessary for and predictive of NASH and CAD, and whose affects are attenuated by exercise.

Michael Sturek, PhD, Chair

Table of Contents

List of Tables	xiii
List of Figures	xiv
List of Appendices	xvii
List of Abbreviations	xviii
Chapter 1 – Introduction	
Metabolic syndrome	1
Diabetes mellitus.....	1
Type 2 diabetes.....	2
Non-alcoholic steatohepatitis.....	3
Coronary artery disease	3
Coronary circulation	4
Treatment of coronary artery disease	5
Swine in cardiovascular research	6
Ossabaw model of metabolic syndrome and coronary artery disease	7
Ca ²⁺ regulation in coronary smooth muscle	8
Major hypotheses tested in this thesis.....	12
Introduction figure legends	13
Chapter 2 – Novel metabolic syndrome and coronary artery disease in Ossabaw compared to Yucatan swine	21
Title page	21

Abstract.....	22
Introduction	23
Materials and methods	26
Animal care and use.....	26
Body composition.....	26
Intravenous glucose tolerance test.....	27
Plasma lipid assays.....	27
Stent procedure.....	28
Coronary blood flow	28
Intracellular Ca ²⁺ measurements	29
Histology	29
Assessment of native atheroma	29
Statistical analysis.....	29
Results	30
Discussion.....	35
Acknowledgements	42
Grants	42
Figure legends	43

Chapter 3 – Dyslipidemia in metabolic syndrome is necessary to elicit severe

coronary artery disease and non-alcoholic steatohepatitis.....	58
Title page	58
Abstract.....	59
Introduction	60
Results	62
Lipids and integrated cardiovascular phenotype.....	62

Glucose intolerance.....	62
Insulin resistance	62
Serum fatty acid methyl esters and unbound free fatty acids.....	63
Atherosclerosis in Ossabaw swine	63
Fatty acid methyl esters and fatty acid metabolism in metabolic syndrome, coronary artery disease, and non-alcoholic steatohepatitis	64
Predictive dyslipidemia, non-alcoholic steatohepatitis, and coronary artery disease relationships.....	65
Discussion.....	66
Methods	72
Animal care and use.....	72
Intravenous glucose tolerance test.....	72
Insulin resistance	72
Plasma lipid assays.....	72
Assessment of coronary artery disease.....	73
Assessment of collagen content and non-alcoholic steatohepatitis.....	73
Assessment of insulin positive area.....	73
Fatty acid methyl esters	73
Statistical analysis.....	74
Acknowledgements	75
Figure legends	80

Chapter 4 – Exercise training decreases store-operated Ca²⁺ entry associated

with metabolic syndrome and coronary atherosclerosis.....	86
Title page	86
Abstract.....	87

Introduction	89
Methods	91
Animal care and use.....	91
Exercise training.....	91
Intravenous glucose tolerance test.....	92
Plasma lipid assays.....	92
Stent procedure.....	93
Intra-stent histology	94
Cell dispersion.....	94
Intracellular Ca ²⁺ measurements	94
Patch clamp electrophysiology	94
Reverse transcription polymerase chain reaction	95
Quantitative reverse transcription polymerase chain reaction	95
Immunoblots.....	95
Assessment of coronary artery disease.....	96
Results	97
Discussion.....	101
Funding	105
Acknowledgements	105
Figure legends	107

Chapter 5 – Store-operated Ca²⁺ influx predicts coronary artery disease and is

induced by dyslipidemia in metabolic syndrome and type 2 diabetes	114
Title page	114
Abstract.....	115
Condensed abstract	116

Introduction	117
Methods	119
Animal care and use.....	119
Intravenous glucose tolerance test.....	119
Plasma lipid assays.....	119
Assessment of insulin positive area.....	119
Assessment of coronary artery disease.....	120
Cell dispersion.....	120
Intracellular Ca ²⁺ measurements	120
Patch clamp electrophysiology	120
Statistical analysis	120
Results	122
Discussion.....	125
Acknowledgements	131
Figure legends	132
Chapter 6 – Conclusion	139
General overview	139
Porcine model of metabolic syndrome.....	140
Porcine model of type 2 diabetes	141
Fructose and dyslipidemia mediated non-alcoholic steatohepatitis.....	143
Dyslipidemia is necessary for coronary artery disease	145
Fatty acid methyl esters, not free fatty acids, predict coronary artery disease and non-alcoholic steatohepatitis	147
Stent-induced neointimal hyperplasia in metabolic syndrome.....	148

Short-term exercise training effects on metabolic syndrome and coronary artery disease	149
Ca ²⁺ signaling events in coronary smooth muscle cells	150
Effects of dyslipidemia in metabolic syndrome on transient receptor potential-mediated Ca ²⁺ influx	152
Revised model of coronary smooth muscle cell Ca ²⁺ regulation	156
Future directions	157
Figure Legends	160
Appendices	166
Appendix A	166
Appendix B	
Appendix C	
Appendix D	
Appendix E	
Appendix F	
Appendix G	
Appendix H	
Appendix I	
Appendix J	
References	212
Curriculum Vitae	

List of Tables

Table 2.1	Phenotypic characteristics of Yucatan and Ossabaw swine fed control chow or high fat/cholesterol atherogenic diet.....	47
Table 2.2	Brief review of Ossabaw and Yucatan metabolic disease and Ca^{2+} regulation.....	48
Table 3.1	Phenotypic characteristics of Ossabaw swine at the end of the study.....	76
Table 3.2	Fatty acid methyl esters predict coronary artery disease and non-alcoholic steatohepatitis in Ossabaw swine.....	77
Table 3.3	Fatty acid methyl esters groups predict coronary artery disease and non-alcoholic steatohepatitis in Ossabaw swine.....	78
Table 3.4	Liver enzyme function predicts non-alcoholic steatohepatitis in Ossabaw swine.....	79
Table 4.1	Phenotypic characteristics of Ossabaw miniature swine groups at end of study.....	106
Table 5.1	Metabolic syndrome characteristics of Ossabaw swine.....	134
Table 6.1	Summary of disease state affect on coronary smooth muscle Ca^{2+} regulation.....	162

List of Figures

Figure 1.1	Coronary artery (wall) anatomy.....	17
Figure 1.2	Progression to type 2 diabetes in humans.....	18
Figure 1.3	Stent revascularizes stenotic coronary artery in Ossabaw pig.....	19
Figure 1.4	Regulation of intracellular Ca ²⁺ in coronary smooth muscle.....	20
Figure 2.1	Body fat is greater and leptin increase is blunted in Ossabaw swine compared to Yucatan on calorie-matched diets.....	50
Figure 2.2	Ossabaw swine are glucose intolerant and insulin resistant compared to Yucatan.....	51
Figure 2.3	Ossabaw swine exhibit coronary microvascular dysfunction compared to Yucatan.....	52
Figure 2.4	Diffuse atherosclerosis is prominent in Ossabaw compared to Yucatan.....	53
Figure 2.5	In-stent stenosis is greater in Ossabaw compared to Yucatan.....	54
Figure 2.6	Peri-stent coronary artery disease is greater in Ossabaw compared to Yucatan and hyperlipidemia increases proximal non-stent and peri-stent coronary artery disease.....	55

Figure 2.7	Dysfunctional Ca ²⁺ efflux in Ossabaw vs. Yucatan coronary smooth muscle	56
Figure 2.8	Sarco/endoplasmic reticulum Ca ²⁺ ATPase Ca ²⁺ buffering function progresses from increased function to virtually complete dysfunction with severity of coronary artery disease	57
Figure 3.1	Insulin resistance and glucose intolerance	82
Figure 3.2	Elevated serum fatty acid methyl esters and free fatty acids in metabolic syndrome	83
Figure 3.3	Coronary artery disease is increased with severity of metabolic syndrome	84
Figure 3.4	Atheromous plaques contain less collagen with increased severity of metabolic syndrome	85
Figure 3.5	LDL gram-years predicts strongly correlated coronary artery disease and non-alcoholic steatohepatitis	86
Figure 4.1	Ossabaw swine fed excess atherogenic diet are glucose intolerant and insulin-resistant and exercise training improves physical work capacity....	109

Figure 4.2	Greater coronary atherosclerosis in metabolic syndrome swine versus Lean is attenuated by exercise training, but in-stent neointimal hyperplasia is not affected.....	110
Figure 4.3	Intra-stent histology.....	111
Figure 4.4	Store-operated Ca^{2+} entry is increased in MetS and attenuated by exercise.....	112
Figure 4.5	Increased canonical transient receptor potential 1 and stromal interaction molecule 1 in metabolic syndrome is abolished by exercise.....	113
Figure 5.1	Intravenous glucose tolerance test reveals glucose intolerance and insulin resistance in MetS and type 2 diabetes in DMetS.....	134
Figure 5.2	Coronary artery disease is increased in DMetS, but not MetS.....	136
Figure 5.3	Metabolic syndrome induces Ca^{2+} dysregulation in coronary smooth muscle.....	137
Figure 5.4	Dysfunctional mono- and di-valent cation conductances in DMetS compared to Lean.....	138
Figure 6.1	Type 2 diabetes and pre-diabetes in humans and Ossabaw swine.....	164
Figure 6.2	Proposed model of Ca^{2+} regulation.....	165

List of Appendices

Appendix A Angiography.....	166
Appendix B Intravascular ultrasound.....	176
Appendix C Stent procedure.....	183
Appendix D <i>In vivo</i> coronary blood flow measurements of anesthetized Ossabaw swine using percutaneous vascular access.....	188
Appendix E Sterile dissection of coronary artery from intact heart.....	193
Appendix F Fura-2 digital imaging methods.....	195
Appendix G Mechanical isolation of in-stent media from in-stent media.....	201
Appendix H Sterile organ culture.....	203
Appendix I Intracellular pipette solutions for recording of ionic currents (whole cell) ..	204
Appendix J Extracellular solutions.....	210

List of Abbreviations

APV	Average peak velocity
Ca ²⁺ _i	Intracellular Ca ²⁺
Ca ²⁺ _o	Extracellular Ca ²⁺
CAD	Coronary artery disease
Caff	Caffeine
CBF	Coronary blood flow
CFR	Coronary flow reserve
CFX	Left circumflex coronary artery
CPA	Cyclopiazonic acid
CSM	Coronary smooth muscle
DES	Drug-eluting stent
E _{Rev}	Reversal potential
ET-1	Endothelin-1
FDA	Food and Drug Administration
GES	Gene-eluting stent
HDL	High-density lipoprotein
HOMA	Homeostasis model assessment
IP ₃	Inositol trisphosphate
IPV	Instantaneous peak velocity
IVGTT	Intravenous glucose tolerance test
IVUS	Intravascular ultrasound
LAD	Left anterior descending coronary artery
LDL	Low density lipoprotein
L-type	High voltage-gated Ca ²⁺ channel
MetS	Metabolic syndrome (also group code)
MOC	Multiple-operated Ca ²⁺ channel
M _v	Membrane potential
NAFLD	Non-alcoholic fatty liver disease
NASH	Non-alcoholic steatohepatitis
NCX	Na ⁺ /Ca ²⁺ exchanger
PMCA	Plasmalemmal Ca ²⁺ ATPase
RC	Right coronary artery
ROC	Receptor-operated Ca ²⁺ channel
RyR	Ryanodine receptor
SERCA	Sarco/endoplasmic reticulum Ca ²⁺ ATPase
SOC	Store-operated current
SOCE	Store-operated Ca ²⁺ entry
SR	Sarcoplasmic reticulum
STOCs	Spontaneous transient outward current
TG	Thapsigargin
TRP	Transient receptor potential
TRPC1	TRP canonical 1
TRPM4	TRP melanostatin 4
T-type	Low-voltage gated Ca ²⁺ channel
VLDL	Very-low density lipoprotein

Chapter 1

Metabolic syndrome

Metabolic syndrome (MetS; “prediabetes”) afflicts up to 27% of the United States population while continuing to dramatically increase in prevalence (30). No precise definition of MetS has been universally accepted with three competing, although similar, criteria set forth first by the World Health Organization, followed by the Adult Treatment Panel III, then the International Diabetes Federation, and most recently through a joint scientific statement (with American Diabetes Association notably abstaining) (31-33). Although the clinical necessity of MetS classification has recently been questioned (34-37), MetS is generally diagnosed with the presence of three or more of the following conditions: obesity, insulin resistance, glucose intolerance, dyslipidemia (e.g. increased low density lipoprotein [LDL], decreased high density lipoprotein [HDL], increased LDL/HDL, and increased triglycerides), and hypertension.

MetS is strikingly prevalent (38) with the incidence of MetS continuing to rise with obesity and sedentary lifestyle (33). This is important as MetS is a strong predictor of several comorbidities including the incidence, severity, and interventional outcome in atherosclerosis (36;39;40), progression from non-alcoholic fatty liver disease (NAFLD) to non-alcoholic steatohepatitis (NASH; (41;42)), and progression from pre-diabetes to type 2 diabetes mellitus (43).

Diabetes mellitus

Diabetes mellitus is a condition most commonly defined simply by elevated fasting blood glucose (hyperglycemia; (44)). The fasting blood glucose threshold for diagnosis in humans is 126 mg/dL (45) and a vast majority of patients with diabetes are classified as either type 1 or type 2 diabetic. While the etiology of type 1 and type 2 diabetes was not determined until the 1970’s, it has been recognized for over a century

that fat (*gras*) and skinny (*maigre*) diabetes are diametrically opposed (reviewed in (46)). Whereas type 1 diabetes (insulin-dependent) is initiated by auto-immune response ablation of insulin-producing pancreatic β -cells, the progression towards type 2 diabetes (non insulin-dependent) is mediated by increased circulating insulin and the inability of various tissues/organs to appropriately respond to insulin (insulin resistance).

Type 2 diabetes

Type 2 diabetes is a progressive disease (reviewed elsewhere (44)) that is often preceded by years of mildly elevated blood glucose levels, hyperinsulinemia, and insulin resistance before the threshold of diagnosis is achieved (progression outlined in **Figure 1.2**; (47)). Elevated fasting and post-prandial blood glucose precede the diagnosis of type 2 diabetes. During this “prediabetes” stage, insulin resistance and elevated plasma insulin contribute to increased pancreatic β -cell work and decreasing function. Hyperinsulinemia drives progressively worse hepatic and peripheral insulin sensitivity, while continual stress and hyper-production of insulin lead to failed compensatory pancreas insulin production. Diagnosis of type 2 diabetes occurs when fasting blood glucose reaches the threshold of 126 mg/dL. In summary, the onset of type 2 diabetes is primarily mediated by three defects: increased hepatic glucose production, diminished insulin secretion, and insulin resistance (48).

Slow progression and often negligible symptoms of early stage type 2 diabetes lead to under-diagnosis of prediabetes (49). However, early diagnosis and treatment are vital for long-term outcomes and quality of life (50). Medical management of type 2 diabetes focuses primarily on limiting hyperglycemia, but reducing concomitant risk factors of MetS and CAD are also important (reviewed elsewhere (51)). Despite dietary, exercise, and medical intervention CAD is the leading cause of death in patients with

diabetes (52;53). Additionally, NAFLD is closely associated with incidence of type 2 diabetes mellitus (54).

Non-alcoholic steatohepatitis

NAFLD, considered the hepatic manifestation of MetS (55), is one of the most common chronic liver diseases present in about one third of the general population (41;56-58) and continues to increase in incidence (59;60). NAFLD is histologically characterized by microvesicular steatosis without additional signs of liver injury (8). NAFLD is benign when presented as simple steatosis, however NASH, a progressive form of NAFLD, can lead to advanced fibrosis, cirrhosis, and liver failure (41;56-58). NASH is histologically characterized by macrovesicular steatosis, inflammation, hepatocyte ballooning, and fibrosis (61). Up to 25% of patients with NAFLD typically progress to NASH (42;62). Importantly, patients with NASH have increased risk of death from cardiovascular disease (63), such that death from CAD exceeds even that of liver cirrhosis in NASH (64).

Coronary artery disease

Coronary artery disease (CAD) is the leading cause of heart disease and stroke. The risk for CAD increases 3- to 4-fold in the presence of MetS (65;66). Sedentary living, hypercaloric/lipidemic diet, diabetes, metabolic syndrome, non-alcoholic steatohepatitis, and gender are major risk factors for the progression of CAD (reviewed elsewhere (67)). There are several striking features of MetS CAD; in particular, pervasive, "diffuse CAD" is a hallmark of diabetic CAD (68-73;73-87). MetS also increases CAD: 1) plaque cellularity, 2) instability, 3) inflammation, and 4) calcification compared to non-diabetic patients (82).

Atherosclerosis (reviewed elsewhere (67;88)) is ubiquitous, often evident in early childhood of even healthy individuals (89), and progressive, advancing through eight stages characterized in detail by Stary (**Figure 1.1**; (90)). Monocytes infiltrate the vessel wall to scavenge fatty acids and cholesterol that have accumulated between endothelial cells and the internal elastic lamina. Lipid-laden monocytes transform to foam cells, contributing to the inflammatory response in the vessel wall leading to coronary smooth muscle (CSM) dedifferentiation, migration through the internal elastic lamina, proliferation, and secretion of connective collagen and elastin fibrils thus contributing to the building plaque (**Figure 1.1**).

Coronary circulation

Left and right coronary artery ostia (openings) originate from the left and right sinuses of Valsalva (bulges of the ascending aorta immediately distal to aortic valve; **Figure 1.1**). Coronary arteries are primarily apical, residing on top of the cardiac muscle, however Ossabaw swine, unlike canine, coronary artery branches dive into the cardiac muscle almost immediately after branching. The left coronary ostium connects with an almost undetectable left main artery, which bifurcates to form the left anterior descending (LAD) and circumflex (CFX) arteries. The LAD largely follows the cardiac septum all the way to the apex of the heart, while the CFX wraps around the base of the left ventricle just apical to the left atrium. The right coronary artery wraps around the base of the right ventricle, apical to the right atrium, until the septum where it abruptly turns towards the apex of the heart, providing blood flow to the posterior septal wall and thereby defining the pig as right dominant. This is one of the many striking similarities to the human coronary circulation.

The walls of coronary arteries are comprised of three major sections: adventitia, media, and intima (**Figure 1.1**). Two circumferential fibrous bands composed primarily of

elastin, the external and internal elastic laminae, form distinct borders between the three sections. Adventitia surrounds the exterior of the artery and is composed primarily of collagen fibrils and fibroblasts. The medial layer is bounded by the internal and external laminae and composed primarily of CSM. CSM cells in healthy arteries are quiescent, proliferating at very low levels, and contractile, mediating vessel tone. Intercellular connexins allow movement of small molecules and ions between neighboring CSM and endothelial cells. Endothelial cells form a thin monolayer on the luminal side of the internal elastic lamina in direct contact with blood flowing through the artery. The primary functions of endothelial cells are the production of vasoreactive compounds that influence the contractile state of the artery, formation of a tight barrier to allow proper blood flow and prevent interaction between blood and underlying CSM, and regulate growth and cytodifferentiation of CSM.

Treatment of CAD

The primary end-point for treatment of occlusive CAD is revascularization of the affected artery or arteries, thus relieving ischemia and preventing/minimizing tissue damage, necrosis, and reduced cardiac function. Coronary stenting is the primary surgical intervention for occlusive CAD (outlined in **Figure 1.3**; (68)).

Complications following revascularization include re-occlusion, thrombosis, myocardial infarction, and the need for repeat revascularization procedure (91-93). Despite similar completeness of revascularization compared to non-diabetics (68), complications are significantly greater in diabetics following revascularization (94). This is likely due to the diffuse nature of diabetic CAD and the effect of stent placement on “peri-stent” disease (95). The Food and Drug Administration (FDA) advises more studies are needed involving complex patients, including those with MetS and diabetes, receiving drug eluting stent (DES) treatment (96). However, no model of MetS and type

2 diabetes that naturally develops occlusive atherosclerosis has been available for clinical studies involving efficacy of revascularization attempts.

Due to lack of significant native atherosclerosis in an animal model, the current FDA protocol for the study of stent efficacy involves mechanical injury of the vascular wall by over-expansion of stents to induce neointimal hyperplasia in completely healthy swine juvenile with no CAD (reviewed elsewhere (97-100)). The current study design recommended by the FDA is in sharp contrast to clinical practice where vascular wall injury during stent placement is avoided to minimize endothelial damage, vascular inflammation, and surgical complications (i.e. coronary dissection). As a result of the inability to generate significant native CAD, no pre-clinical study has ever involved stent placement in an artery with severe native CAD. It is entirely possible that recent questions regarding the safety of drug-eluting stents (99;101) could have been avoided had a more appropriate model of CAD been available.

Swine in cardiovascular research

Swine (*sus scrofa*) are an excellent model for cardiovascular research for several major reasons: 1) coronary anatomy is strikingly similar to humans (102) 2) neointimal structure and thrombosis cascade mimic and humans (103), 3) omnivorous diet and lipid metabolism similar to humans, 4) docile and sedentary behavior, and 5) size. Miniature swine are sexually mature at approximately 3 months of age, corresponding to ~50 kg. This allows serial blood sampling and tissue biopsy without adverse reactions. Additionally, swine are large enough to perform interventional surgical procedures common to those used in humans with cardiovascular disease (i.e. percutaneous intervention, angiography, stent placement, and etc.).

The Yucatan is a lean swine breed widely used for many years in cardiovascular research. Atherogenic diet induces dyslipidemia but not insulin resistance and/or

glucose intolerance in Yucatan swine (3;4;7-10). Correspondingly, mild atherosclerotic lesions, primarily focused in the proximal portion of the coronary vasculature, develop in Yucatan swine fed atherogenic diet (3;4;4;6;8;11;12;17-24). Several studies have produced severe CAD in Yucatan swine, however this was not due to naturally developing MetS or diabetes, but through streptozotocin-induced pancreatic β -cell ablation (104-107). Demonstrating the clinical utility of swine, experiments in Yucatan swine involving angioplasty overexpansion-injury have elucidated important mechanisms of vascular disease (108).

Göttingen swine (Yucatan x Göttinger cross-breed) is used less commonly than the Yucatan, but has been shown to produce dyslipidemia and coronary disease when fed atherogenic diet (109). As in Yucatan swine, streptozotocin has been used to induce diabetes in Göttingen. However, Göttingen swine did not develop fasting hyperglycemia in the absence of chemically-induced pancreatic β -cell ablation, as evidenced in a ~2-year study of Göttingen swine fed atherogenic diet (110), thus indicating that Göttingen develop dyslipidemia, but do not progress to type 2 diabetes.

Several animal models recapitulate MetS (111-116); however, none are able to fully reproduce symptoms of MetS and CAD, except Ossabaw swine. A major outcome of this thesis work is demonstration of progression to type 2 diabetes in Ossabaw swine.

Ossabaw model of MetS and CAD

Our laboratory characterized the Ossabaw miniature swine model which faithfully replicates many of the human characteristics of MetS when fed excess calorie atherogenic diet (3;4;7;8;29), including hypertension, central obesity, insulin resistance, glucose intolerance, dyslipidemia (elevated LDL, LDL/HDL ratio, and total cholesterol), and hypertriglyceridemia. Trans-fatty acids and fructose have been shown to be important in the development of severe dyslipidemia, mild atherosclerosis, and MetS

(3;29), while a modified atherogenic diet supplemented with fructose, trans-fatty acids, and lard produced severe MetS with accompanying NASH (7), the first report of NASH in a large animal model of MetS induced by atherogenic diet. In addition to developing NASH, MetS, and (outlined in this report) type 2 diabetes, Ossabaw swine faithfully develop CAD that is strikingly similar to CAD in humans with regard to plaque morphology and cellular composition. As such, Ossabaw swine provide an ideal opportunity for the study of cellular mechanisms underlying progressive CAD in MetS (e.g. Ca^{2+} signaling in CSM).

Ca^{2+} regulation in CSM

Ca^{2+} regulation is vital to cellular health and function (reviewed elsewhere (117)). CSM actively regulate Ca^{2+} using an elaborate system of intracellular depots, pumps, and channels (outlined in **Figure 1.4**). CSM differentiation (118), proliferation (119), gene expression (120), and contraction (121) are tightly associated with its ability to effectively moderate free (ionized) intracellular concentrations of Ca^{2+} (Ca^{2+}_i). Ca^{2+}_i must come from one of two sources, entry across the plasma membrane, or release from intracellular Ca^{2+} stores.

While the nucleus (122), mitochondria (123), and intracellular Ca^{2+} binding proteins (124) may contribute to the regulation of Ca^{2+}_i , the primary intracellular Ca^{2+} store in CSM is the sarcoplasmic reticulum (SR). SR Ca^{2+} regulation is mediated by Ca^{2+} uptake and extrusion across the SR membrane. Sarco/endoplasmic Ca^{2+} adenosine triphosphatase (SERCA), a Ca^{2+} pump located in the SR membrane, is primarily responsible for Ca^{2+} sequestration into the SR (reviewed elsewhere (125)). SERCA is continually functioning to counteract passive leak of Ca^{2+} out of the SR and into the cytosol (reviewed elsewhere (126)), and SERCA molecular (127) and functional expression (125) have been shown to be regulated by Ca^{2+}_i . Once Ca^{2+} enters the SR, it

is immediately chelated by Ca^{2+} -binding proteins, greatly increasing the functional ability of the SR as an intracellular Ca^{2+} store (128). Active release of Ca^{2+} from the SR store is mediated by inositol 1,4,5 trisphosphate (IP₃)- or ryanodine-sensitive channels (RyR; reviewed in (129)). RyR in the SR, in close apposition to the plasma membrane, work to mediate Ca^{2+} -induced Ca^{2+} release (130-132). Thus, SR Ca^{2+} regulation does not act in isolation, but rather is tightly orchestrated with Ca^{2+} permeability of the plasma membrane.

Strong electromotive and diffusion forces exist for Ca^{2+} influx across the plasma membrane. The electromotive force is a consequence of the negative membrane potential of CSM (M_V ; ~ -60 mV) and is mediated by relative rates of charged particle transport across the plasma membrane. In CSM, K^+ conductance is the major determinant of M_V under normal resting conditions (reviewed elsewhere (133)); however, Na^+ , Ca^{2+} , and Cl^- conductance also contribute to M_V .

The diffusion force is due to the tight regulation of resting Ca^{2+}_i in the range of $\sim 10^{-7}$ M. This diffusion force is established by Ca^{2+} pumps (e.g. plasma membrane Ca^{2+} ATPase; PMCA) and antiporters (e.g. $\text{Na}^+/\text{Ca}^{2+}$ exchanger; NCX) in the plasma membrane regulating intracellular Ca^{2+} near 100 nM, while *in vivo* extracellular Ca^{2+} (outside Ca^{2+} ; Ca^{2+}_o) ranges from 1-2 mM, an incredible 20,000-fold gradient (yielding an equilibrium potential for Ca^{2+} (E_{Ca}) of $\sim +120$ mV). The PMCA and NCX each are responsible for approximately one third of the Ca^{2+} buffering in CSM, with SERCA accounting for the remainder (134). The strong diffusion force produced by the PMCA and NCX allows Ca^{2+} influx that is mediated by voltage gated, receptor-operated, and store-operated Ca^{2+} channels (reviewed elsewhere (117)). Ca^{2+} influx through ligand-gated channels may occur, but does not likely account for large Ca^{2+}_i increases in CSM (135), although Na^+ influx may contribute to depolarization and activation of voltage gated Ca^{2+} channels (reviewed elsewhere (129)).

Voltage gated Ca^{2+} channels are mediated by perhaps the most intuitive mechanism in that voltage sensors within the channel move when membrane voltage changes causing activation of the channel, much like a switch. Two main types of voltage gated Ca^{2+} channels exist in CSM, low-voltage-activated (T-type) and high-voltage-activated (L-type) (136-138). While relatively little is known about T-type channel activity in CSM (139), it is well established that Ca^{2+} influx through L-type Ca^{2+} channels leads to contraction (138;140) and contributes to hypertension (141;142).

Receptor-operated Ca^{2+} channels (ROC) are activated by intracellular 2nd messengers potentiated by agonist binding to a separate receptor entity (reviewed elsewhere (143)). Importantly, this definition of ROC is operationally based, and not dependent on a particular molecular identity. Well described pathways activating ROC include 2nd messengers inositol trisphosphate (144), cyclic GMP (145), and cyclic AMP (146). G-protein coupled receptors are common initiators of the 2nd messenger cascade in ROC (147).

The previous definition of ROC allows for inclusion of the putative store-operated Ca^{2+} channels (SOC). The precise definition of what constitutes a SOC has been the focus of several excellent reviews (117). Rigorously defined, SOC activation demands only depletion of SR Ca^{2+} store (148), but this store depletion may be achieved physiologically through second messenger, hormone, and ROC pathways. While activation via store-depletion is a prerequisite feature of any SOC, it has become increasingly evident that particular SOC may also be activated via ROC-like mechanisms (149). This has led to the term multiple-operated Ca^{2+} channel (MOC; (149;150)). Regardless of MOC or ROC classification, a recent consensus in the literature concerning the mechanism of SOC activation upon store depletion has been reached.

It has been generally accepted that SOC are activated by SR membrane protein stromal interaction molecule 1 (STIM1) upon SR Ca^{2+} store depletion (151). STIM1 has been demonstrated to sense ER/SR Ca^{2+} store depletion, form puncta in regions of the ER/SR in close apposition to the plasma membrane, form protein interactions with several SOC proteins, and be necessary for SOC activation (reviewed elsewhere (117)). Previous to this revelation, three major mechanisms linking SR store depletion and SOC activation in the plasma membrane: a diffusible second messenger signaling between the SR and plasma membrane, vesicle translocation containing SOC, and direct protein interaction between a sensor protein and SOC (e.g. STIM1) (reviewed elsewhere (152)).

At least two SOC have been identified to be activated by STIM1, Orai1 and transient receptor potential canonical 1 (TRPC1) (153). STIM1, TRPC1, and Orai1 have been shown, in an overexpression model, to form ternary complexes with the putative identity of Ca^{2+} influx channels (154). Additionally, TRPC1-mediated store operated Ca^{2+} entry (SOCE) has been shown to be dependent on Orai1 expression (155), and TRPC1 expression has been shown to augment Orai1-mediated SOCE (156). While STIM1 and Orai1 have been shown to be necessary components for SOCE (153;155;156), there is a clear involvement of TRPC1 in SOCE. TRPC1-mediated SOCE is strongly associated with smooth muscle proliferation, migration, and *in vitro* atherosclerosis (reviewed elsewhere (157)). As such, it is yet undetermined if SOCE and TRPC1, Orai1, and STIM1 play a pivotal role in the development of CAD, especially within the context of MetS and diabetes.

Major Hypotheses Tested in this Thesis

1. TRPC1-mediated store-operated Ca^{2+} entry in coronary smooth muscle is a major contributor to the development of native coronary artery disease and stent-induced stenosis in metabolic syndrome.
2. Exercise attenuates TRPC1 expression and function in metabolic syndrome, thereby protecting against development of CAD and stent-induced stenosis.
3. Dyslipidemia is a primary component of metabolic syndrome necessary for the development of coronary artery disease and non-alcoholic steatohepatitis and synergizes progression to type 2 diabetes.
4. Ossabaw swine have a genetic propensity towards obesity and metabolic syndrome related coronary disease and dysfunction compared to the lean Yucatan swine breed.

Figure Legends

Figure 1.1 Coronary artery (wall) anatomy. A Left and right coronary artery ostia (openings) originate from the left and right sinuses of Valsalva (bulges of the ascending aorta immediately distal to aortic valve). Coronary arteries are primarily apical, residing on top of the cardiac muscle, however Ossabaw swine, unlike canine, coronary artery branches dive into the cardiac muscle almost immediately after branching. The left coronary ostium bifurcates to form the left anterior descending (LAD) and circumflex (CFX) arteries. The LAD largely follows the cardiac septum all the way to the apex of the heart. Swine are left coronary dominant, meaning the heart apex statuary is the left coronary artery. The CFX wraps around the base of the left ventricle just apical to the left atrium, while the right coronary artery wraps around the base of the right ventricle, apical to the right atrium, until the septum where it abruptly turns towards the apex of the heart.

B Masson's trichrome, a standard histological preparation, of a sectioned RCA stains the adventitia (primarily collagen) blue and media (primarily smooth muscle) in red. This section of RCA is mildly atherosclerotic with a small fibro-fatty lesion (*).

C Surrounding the lumen of coronary arteries (**a**), the wall is comprised of three major sections: intima (**b**), media (**c**), and adventitia (**d**). Two circumferential fibrous bands composed primarily of elastin, the external and internal elastic laminae, form distinct borders between the three sections. **d** Adventitia surrounds the exterior of the artery and is composed primarily of collagen fibrils and fibroblasts. **c** The medial layer is bounded by the internal and external laminae and composed primarily of smooth muscle cells. Smooth muscle cells (SMC) in healthy arteries are quiescent, proliferating at very low levels, and contractile, mediating vessel tone. Intercellular connexins allow movement of small molecules and ions between SMC and neighboring endothelial cells (EC). **b** EC form a thin monolayer on the luminal side of the internal elastic lamina in direct contact with blood flowing through the artery. The primary functions of EC are the production of

vasoreactive compounds that influence the contractile state of the artery and formation of a tight barrier to allow proper blood flow and prevent interaction between blood and underlying CSM.

Atherosclerosis is a progressive disease advancing through several stages characterized in detail by Starry (illustrated in **D**, (89)). Monocytes infiltrate the vessel wall to scavenge fatty acids and cholesterol that have accumulated between ECs and the internal elastic lamina. Lipid-laden monocytes transform to foam cells, contributing to the inflammatory response in the vessel wall leading to SMC dedifferentiation, migration through the internal elastic lamina, proliferation, and secretion of connective collagen and fibrin thus contributing to the building plaque.

Figure 1.2 Progression to type 2 diabetes in humans. Elevated fasting and post-prandial blood glucose precede the diagnosis of type 2 diabetes. During this “prediabetes” stage, insulin resistance and elevated plasma insulin contribute to increased pancreatic β -cell work and decreasing function. Hyperinsulinemia drives progressively worse hepatic and peripheral insulin sensitivity, while continual stress and hyper-production of insulin lead to failed compensatory pancreas insulin production. Diagnosis of type 2 diabetes occurs years to decades following onset of prediabetes when fasting blood glucose reaches the threshold of 126 mg/dL. Unless dietary, exercise, and medical intervention are successful in reversing/minimizing peripheral insulin resistance and hyperglycemia, β -cell collapse will ensue resulting in significantly diminished insulin production. While insulin production decreases, insulin resistance remains elevated leading to worsening hyperglycemia.

Figure 1.3 Stent revascularizes stenotic coronary artery in Ossabaw pig. A Angiography revealed stenotic lesion in proximal left anterior descending coronary artery (arrow). **B** Intravascular ultrasound (IVUS) image of cross-sectional stenosis demonstrates method of IVUS image quantification. **C** Custom bare metal stent (8-mm length, 3-mm diameter) deployed on angioplasty balloon (20-mm length) inflated to nominal pressure. **D** IVUS confirmed stenotic lesion with original lumen diameter of ~3-mm. **E** IVUS following stent deployment confirmed revascularization of target lesion to optimal diameter. Yellow arrows denote stent struts.

Figure 1.4 Regulation of intracellular Ca^{2+} in coronary smooth muscle. A Ratiometric analysis of Ca^{2+} handling in coronary smooth muscle (CSM), loaded with Ca^{2+} -sensitive fluorescent dye fura-2, that were enzymatically isolated from healthy artery. **B** Basal Ca^{2+} regulation primarily mediated by Ca^{2+} pumps in the plasma membrane (PM) and sarcoplasmic reticulum (SR). Low-level Ca^{2+} leak from the SR is compensated by sarco/endoplasmic reticulum ATPase (Serca; SERCA). PM Ca^{2+} flux is primarily mediated by plasma membrane Ca^{2+} ATPase (P; PMCA) and forward mode $\text{Na}^+/\text{Ca}^{2+}$ exchanger (Ncx; NCX), as receptor-operated (R) and voltage-gated (L; L-type) Ca^{2+} channels are active at low levels. Membrane potential is dominated by K^+ channel activity (K^+ ; reversal potential = ~-90mV in physiological extracellular solution). **C** High extracellular K^+ shifts the K^+ reversal potential to less negative values, depolarizing the membrane potential and activating L-type channels leading to massive Ca^{2+} influx. NCX, PMCA, and SERCA activity increase, but are unable to compensate for L-type-mediated Ca^{2+} influx until high K^+ is removed. Upon removal of high K^+ , cells return to baseline. **D** Caffeine (Caff; 5 mM) and cyclopiazonic acid (CPA; 10^{-5} M) inhibit SERCA and activate ryanodine receptors (Ry) in the SR, leading to massive depletion of the SR Ca^{2+} store into the cell, thus raising intracellular Ca^{2+} . NCX and PMCA mediated Ca^{2+} efflux return

cell to normal intracellular Ca^{2+} as the SR Ca^{2+} store remains depleted. Stromal interaction molecule 1 (STIM1; S) proteins in the SR membrane sense depletion of the SR Ca^{2+} store and homomultimerize into distinct puncta in regions of the SR in close apposition to the PM. **E** In CSM from metabolic syndrome swine, **F** STIM1 activates store-operated Ca^{2+} entry leading to elevated Ca^{2+}_i .

Figure 1.1

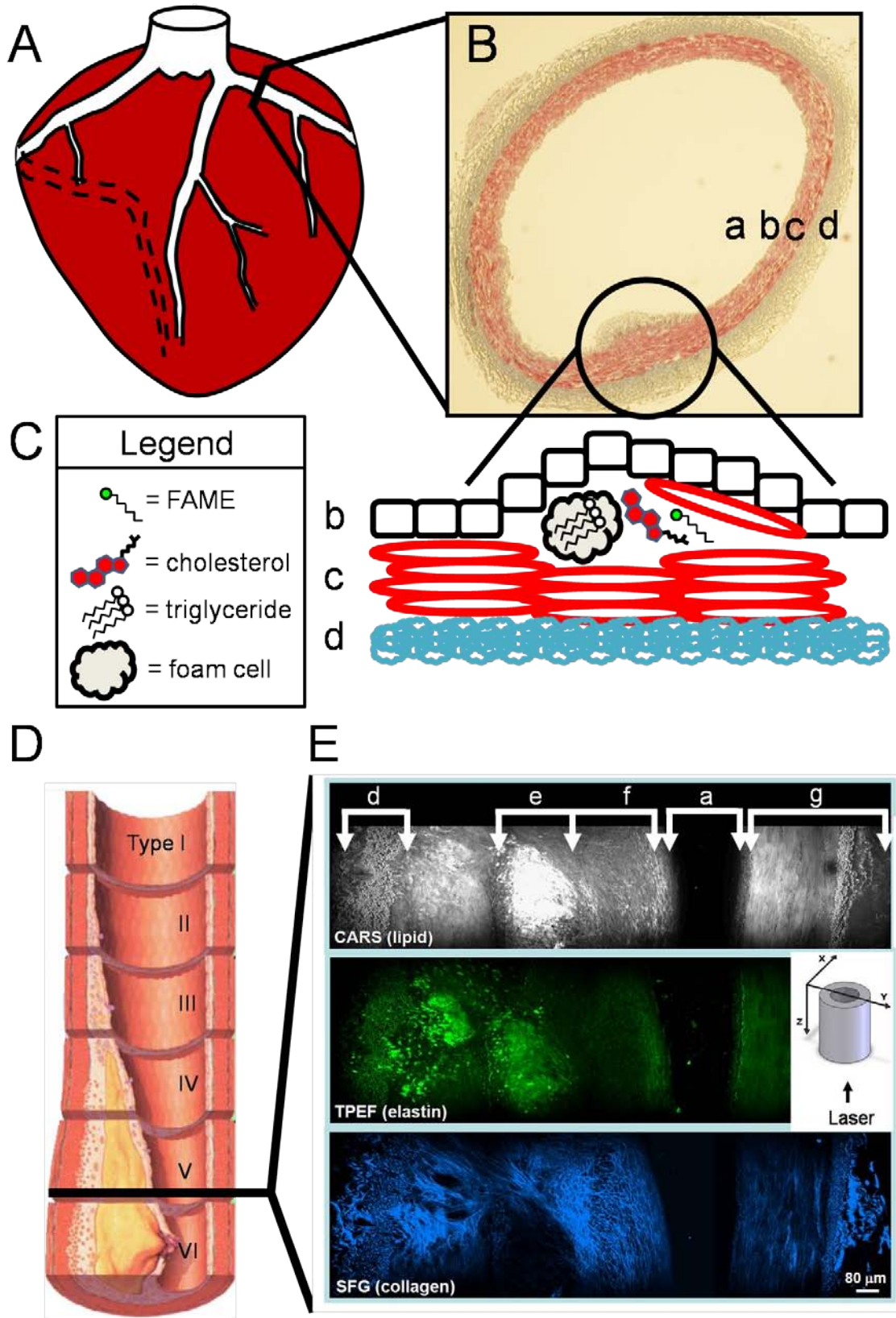


Figure 1.2

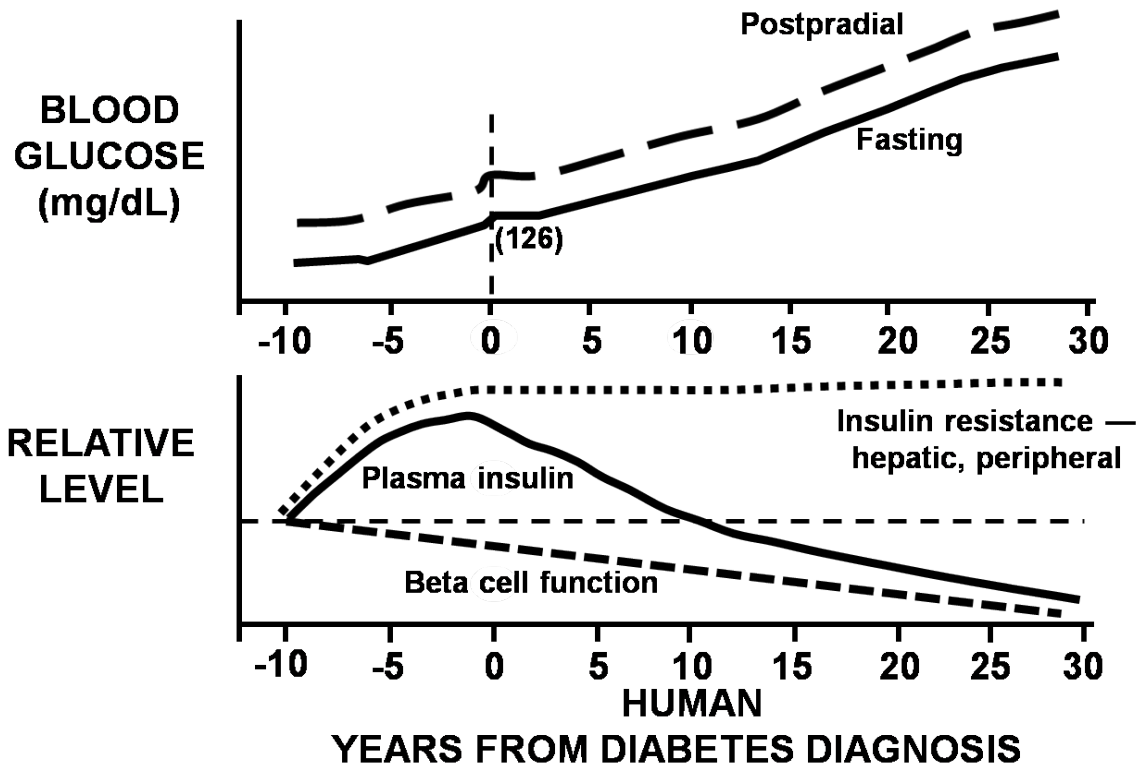


Figure 1.3

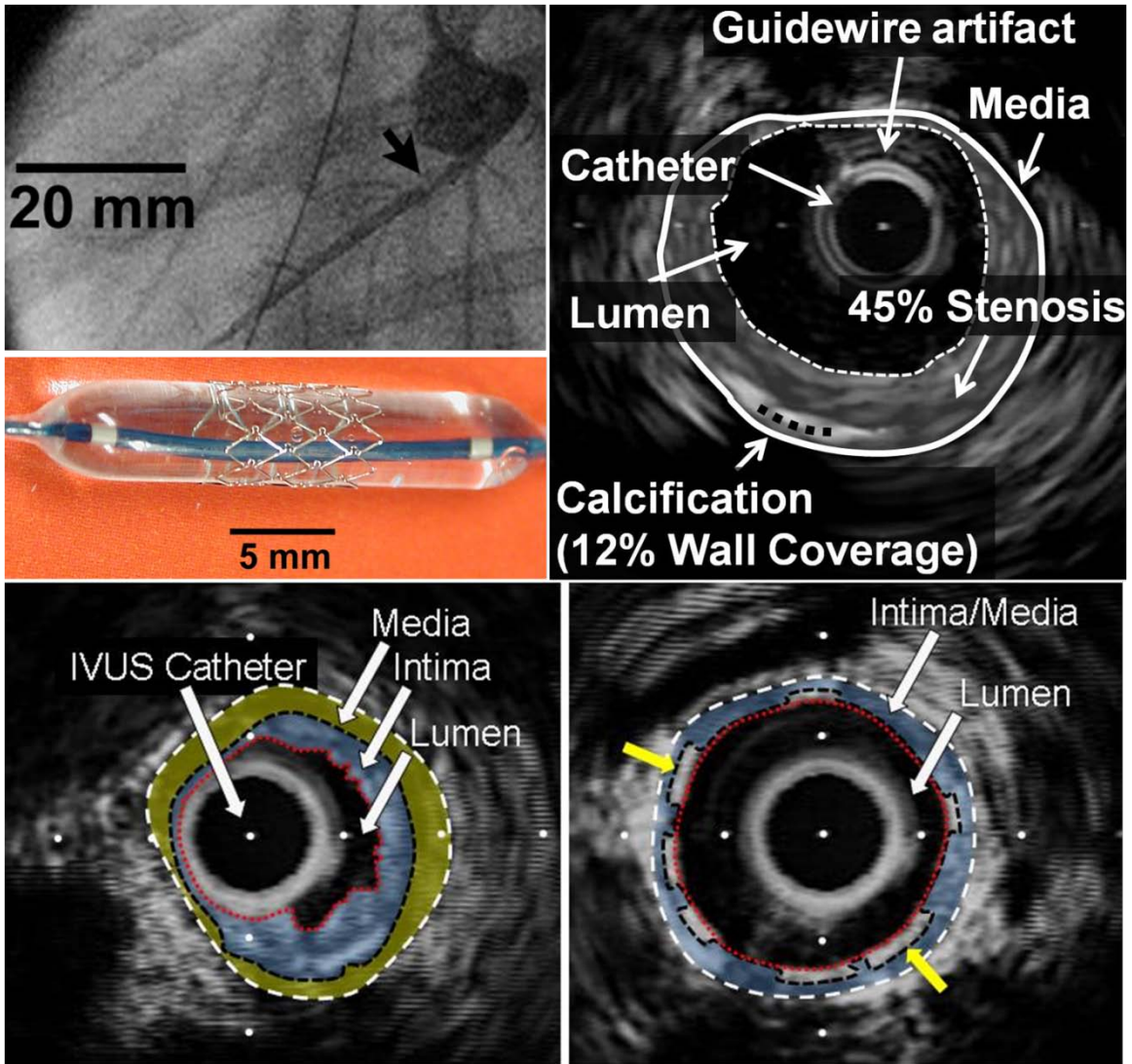
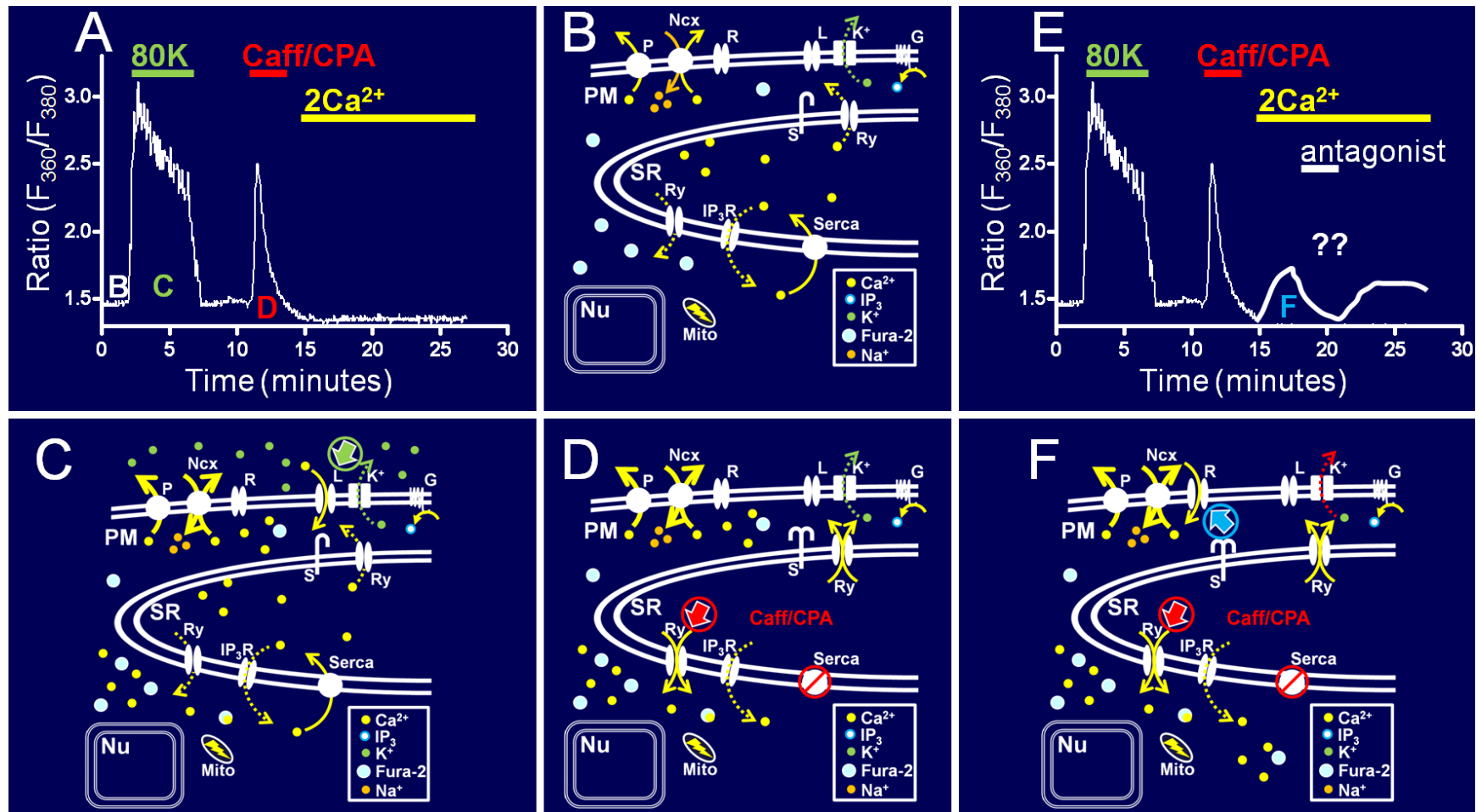


Figure 1.4



Chapter 2

Novel metabolic syndrome and coronary artery disease in Ossabaw compared to Yucatan swine

Zachary P. Neeb¹, Jason M. Edwards¹, Mouhamad Alloosh¹, Xin Long¹,
Eric A. Mokolke², and Michael Sturek¹

¹Department of Cellular and Integrative Physiology, Indiana University School of
Medicine

²Emerging Technology, Boston Scientific Corporation

Abstract

Metabolic syndrome (MetS), a compilation of associated risk factors, increases the risk of type 2 diabetes and coronary artery disease (CAD; atherosclerosis), which can progress to the point of occlusion. Stents are the primary interventional treatment for occlusive CAD and patients with MetS and hyperinsulinemia have increased restenosis. The Ossabaw pig is a model of MetS due to its thrifty genotype. We compared Ossabaw swine to the widely used Yucatan swine. Each breed was fed two separate diets which were calorie matched for normal growth maintenance of Yucatan and divided into two groups each for 40 weeks: control chow diet (C) and high fat/cholesterol atherogenic diet (H). A bare metal stent was deployed in the circumflex artery and pigs recovered 3 weeks. Characteristics of MetS, macrovascular and microvascular CAD, and in-stent stenosis and coronary smooth muscle Ca^{2+} signaling were evaluated. Ossabaw swine had greater characteristics of MetS, including obesity, glucose intolerance, hyperinsulinemia, and hypertension, compared to Yucatan. Ossabaw swine with MetS had more extensive and diffuse native CAD and in-stent stenosis and impaired coronary blood flow regulation compared to Yucatan. Atherosclerotic lesions in Ossabaw coronary arteries were less fibrous and more cellular. Coronary smooth muscle cells from Ossabaw had impaired Ca^{2+} efflux and intracellular sequestration vs. Yucatan cells. These comparative studies indicate that Ossabaw swine are a superior model of MetS, subsequent CAD, and cellular Ca^{2+} signaling defects, while Yucatan swine are leaner and relatively resistant to MetS and CAD.

Keywords: stent, coronary blood flow, calcium, SERCA, animal model

Introduction

Atherosclerotic coronary artery disease (CAD) is increased at least 2-fold in patients with metabolic syndrome (MetS) (39) and is accompanied by significant microvascular dysfunction that further impairs coronary blood flow (158). MetS is generally diagnosed by the presence of three or more of the following conditions: obesity, insulin resistance, glucose intolerance, dyslipidemia, and hypertension (159;160). Complications, including restenosis, thrombosis, and death (34;91;92;94) are significantly greater in diabetics following percutaneous coronary revascularization, e.g. stenting, (94). This is possibly due to the pervasive, “diffuse CAD” that is a hallmark of diabetic CAD and progression of vascular disease in regions adjacent to the stent, i.e. “peri-stent” disease (80;86;95). There is strong support for the role of the hyperinsulinemia component of MetS in increased restenosis after percutaneous coronary interventions (161-164). Further, our group has shown severe coronary microvascular dysfunction in MetS (8). Since MetS (“pre-diabetes”) afflicts up to 27% of the United States population, is drastically increasing in prevalence (30), and will progress to type 2 diabetes, there is an urgent need for basic research performed using animal models that accurately mimic MetS and the accompanying CAD. Clearly, there is need for study of MetS-induced CAD and in-stent stenosis and the underlying cellular and molecular mechanisms.

Several animal models recapitulate MetS (111-116); however, none are able to fully reproduce the combined symptoms of MetS and CAD. Further, transgenic mouse models are simply not adequate for coronary vascular interventions using stents identical to those used in humans (4;20;21;100;103;165-167), which is essential for translation to the clinic. Yucatan and domestic swine are commonly used large animal models for study of cardiovascular disease due to their ability to mimic neointimal formation and thrombosis observed in humans (103). For example, Gerrity et al. and

others produced severe CAD in swine, however this was not due to naturally developing MetS or diabetes, but through toxin-induced pancreatic β -cell ablation and atherogenic diet (2;9;12;14;17;18;104). Currently, there is a paucity of large animal models that reproduce MetS and CAD (115).

Research on the obesity-prone Ossabaw miniature swine (168) indicates clear MetS and cardiovascular disease when fed a high calorie atherogenic diet (3;4;6-8;22-24;29). Female Ossabaw swine on excess calorie atherogenic diet nearly doubled percent body fat in only 9 weeks, showed insulin resistance, impaired glucose tolerance, dyslipidemia (profound increase in LDL/HDL cholesterol, hypertriglyceridemia), hypertension, and early coronary atherosclerosis (3). These data are in contrast to male Yucatan miniature pigs, which did not develop MetS after 20 weeks on comparable excess calorie atherogenic diet (1;2;9). Yucatan swine do not develop MetS through diet manipulation, unlike Ossabaw swine, which consistently recapitulate all MetS characteristics. However, important differences in study design have not allowed direct comparison between Yucatan and Ossabaw swine.

It is clear that cytosolic Ca^{2+} signaling is involved in "phenotypic modulation" of coronary smooth muscle (CSM), characterized by proliferation and migration in several *in vitro* cell culture models (169-172) and *in vivo* rodent models of the peripheral circulation (e.g. (173)). In the Yucatan swine model of diabetic dyslipidemia there is altered Ca^{2+} extrusion (10), Ca^{2+} sequestration by the sarcoplasmic reticulum (13;16;174), and Ca^{2+} influx through voltage-gated Ca^{2+} channels (13). Currently, there are no direct comparisons of Ca^{2+} signaling in MetS Ossabaw compared to Yucatan swine.

Therefore, the purpose of this study was to compare male Ossabaw and Yucatan pigs on calorie matched standard chow and atherogenic diets (Yucatan maintenance diet, e.g. (1;2)). The goal was not to develop morbidly obese pigs, but to test the

hypothesis that Ossabaw swine have a greater propensity to MetS and CAD with impaired Ca^{2+} handling in CSM compared to Yucatan swine.

Materials and Methods

Animal care and use. All protocols involving animals were approved by an Institutional Animal Care and Use Committee and complied fully with recommendations outlined by the National Research Council and American Veterinary Medical Association (175;176). Eighteen male Ossabaw swine and 18 male Yucatan were assigned to one of four groups: Ossabaw control (Ossabaw C, N=9), Yucatan control (Yucatan C, N=9), Ossabaw high fat/cholesterol, atherogenic diet (Ossabaw H, N=9), and Yucatan H (Yucatan H, N=9). The control groups from both breeds were fed a calorie-matched diet for 43 weeks. The control diet contained 22% kcal from protein, 70% kcal from carbohydrates, and 8% kcal from fat. The pigs in the control groups ate 3200 kcal/day until sacrifice, which was a standard amount for maintaining lean, normal body growth in Yucatan swine (4). The H diet was composed of control chow supplemented with (percent by weight): cholesterol 2.0, coconut oil 17, corn oil 2.5, and sodium cholate 0.7. This mixture yielded a composition of 13% kcal from protein, 40% kcal from carbohydrates and 47% kcal from fat. The animals in the H groups ate 3200 kcal/day (calorie-matched the control diet) for 43 weeks until they were sacrificed. All animals were housed and fed in individual pens and provided a 12-hr light/12-hr dark cycle. Water was provided ad libitum.

Body composition. Backfat and carcass fat were measured as previously described (1;177). Body mass index (BMI) was determined, similar to that in humans (178), as body weight in kg divided by the square of the pig's length from the end of the snout to the base of the tail.

Intravenous glucose tolerance test. Swine were acclimatized to restraint in a specialized sling for 5-7 days before the IVGTT was conducted. Swine were then fasted overnight, and anesthetized with isoflurane (maintained at 2% by mask with supplemental O₂). The right jugular vein was catheterized percutaneously (3;4;179).

Following catheterization, swine were allowed to recover for 3 h. before the IVGTT to avoid any effect of isoflurane on insulin signaling (9). Conscious swine were restrained in the sling and baseline blood samples were obtained. Glucose (0.5 g/kg body weight; *i.v.*) was administered and timed blood samples were collected (9). Blood glucose was measured using YSI 2300 STAT Plus Glucose analyzer. Plasma insulin assays were performed by Linco Research Laboratories (St. Charles, MO).

Plasma lipid assays. Venous blood samples were obtained following overnight fasting and were analyzed for triglyceride and total cholesterol [fractionated into high density lipoprotein (HDL) and low density lipoprotein (LDL) components]. Cholesterol in lipoprotein fractions was determined after precipitation of HDL using minor modifications of standard methods (3;180). Specifically, apolipoprotein-B-containing lipoproteins were precipitated with heparin-MnCl₂ and the supernatant was assayed. LDL was calculated from the Friedewald equation: LDL = total cholesterol – HDL – (triglyceride ÷ 5).

Stent procedure. After 40 weeks on the diets a bare metal was deployed in the circumflex coronary artery of all pigs and then were euthanized after 3 weeks recovery, similar to previous reports (4;20;21;29). Swine received 325 mg aspirin as antiplatelet therapy starting the day prior to the stent procedure and continuing for the 3 weeks after stent deployment. Following an overnight fast, swine received (in mg/kg; IM) 0.05 atropine, 2.2 xylazine, and 5.5 telazol. Swine were intubated and anesthesia was maintained with isoflurane (2-4%, with supplemental O₂). The isoflurane level was adjusted to maintain anesthesia with stable hemodynamics. Heart rate, aortic blood pressure, respiratory rate, and electrocardiographic data were continuously monitored throughout the procedure. Under sterile conditions, a 7F vascular introducer sheath was inserted into the right femoral artery and heparin (200 U/kg) administered. A 7F guiding catheter (Amplatz L, sizes 0.75-2.0; Cordis) was advanced to engage the left main coronary ostium. A 3.2F, 30 MHz Intravascular Ultrasound (IVUS) catheter (Boston

Scientific) was advanced over a guide wire and positioned in the coronary artery. Automated IVUS pullbacks were performed at 0.5 mm/sec. Video images were analyzed off-line (Sonos Intravascular Imaging System; Hewlett Packard). The IVUS catheter was removed and a coronary stent (2.5-4.0 mm diameter by 8 mm length, Express2; Boston Scientific) catheter was deployed. Stents were chosen to match artery diameter at optimal inflation pressure. One stent was placed in the circumflex artery (CFX) at 1.0x lumen diameter. Angiography and IVUS were repeated to confirm proper stent deployment. The IVUS catheter, guide catheter, and introducer sheath were removed and the right femoral artery ligated. The incision was closed and the animal was allowed to recover. Cephalexin (1000 mg) was given twice a day for six days following the stent procedure.

Coronary blood flow. The ostium of the left main artery was engaged with the guiding catheter and a 0.014-inch diameter Doppler flow wire (JoMed Inc., Rancho Cordova, CA) was advanced down the circumflex artery (CFX) (17). After angiography-aided placement of the flow wire in a non-branching section of the CFX, flow velocity signals were allowed to stabilize for several minutes. The analog Doppler signals were continuously digitized both as instantaneous peak velocity (IPV) and averaged peak velocity (APV) values. Each APV value was calculated on-line as an average of instantaneous peak velocity over 2 consecutive cardiac cycles. All flow data were stored on videotape and personal computer for further off-line analysis. Data are shown as coronary flow reserve, which is the adenosine- or bradykinin-induced flow divided by baseline flow velocity.

Cell dispersion. The procedure for the isolation of the non-stented right coronary artery and the acute enzymatic dispersal of coronary smooth muscle cells has been previously described (10;13;16;26;169;174). Arteries were incubated in collagenase solution for 45 minutes to disperse endothelial cells, followed by a second period of 30

minutes for the smooth muscle cell fraction.

Intracellular Ca²⁺ measurements. Measurements of whole cell intracellular Ca²⁺ levels were obtained at room temperature (22–25°C) using the fluorescent Ca²⁺ indicator, fura-2, and the InCa++ Ca²⁺ Imaging System (Intracellular Imaging, Cincinnati, OH) as previously described by our laboratory (10;13;16;26;169;174).

Histology. Verhoeff-van Gieson and trichrome staining were performed on sections of stented arteries (20;29). Neointima formation was determined by obtaining area measurements bounded by the external elastic lamina and internal elastic lamina (tunica media) or internal elastic lamina and lumen (neointima) using commercially available software (ImagePro 3.0). The percent stenosis was calculated by dividing the area of the neointima by the area of the tunica media plus neointima and multiplying by 100. Collagen content in the sections of the stented arteries was determined by colorimetric analysis of trichrome histology. The adventitia, which is composed predominantly of collagen, was used as the reference color template against which the rest of the section was compared (11;29).

Assessment of native atheroma. IVUS pullbacks performed during the stenting procedure and before stent placement were used to assess native atheroma. Measurements were obtained every 2 mm through the length of the artery. Each cross-sectional IVUS image was divided into 16 equal segments. Percent wall coverage was calculated as (# segments containing atheroma ÷ 16) x 100 similar to previous reports (6;14;18;29).

Statistical analysis. Analyses were performed using commercially available software (Prism 4.0). One-way analysis of variance (ANOVA) or 2 x 2 ANOVA with student-Newman Keuls or Bonferroni *post hoc* tests, respectively, were used where appropriate. In all tests, $p < 0.05$ was the criterion for statistical significance.

Results

To test the hypothesis that Ossabaw swine were MetS-prone a metabolic profile was obtained for Ossabaw C and H and Yucatan C and H. Ossabaw C and H groups had a greater body weight and body mass index (BMI) than Yucatan C and H at sacrifice despite calorie matched diets in all groups throughout the study, (**Table 2.1**). Hyperlipidemic (H) diet increased total cholesterol, LDL, and HDL levels compared to control diet (C), although no increases in triglycerides were observed (**Table 2.1**). While systolic and diastolic blood pressure trended towards an increase in Ossabaw, mean arterial pressure (MAP) was significantly greater in Ossabaw compared to Yucatan swine.

To determine if increased adipose tissue was responsible for increased body weight and BMI observed in Ossabaw, back fat was measured by ultrasound. Backfat was increased in Ossabaw H compared to all groups while Ossabaw C was increased compared to Yucatan C and Yucatan H (**Figure 2.1A**). Ossabaw swine also demonstrated significantly greater whole carcass fat as a percent of body weight compared to Yucatan (**Figure 2.1B**), however they were not morbidly obese. Concurrently, plasma leptin levels were not increased in Ossabaw compared to Yucatan, while plasma leptin was increased in H diet compared to C diet (**Figure 2.1C**). In a subset of Ossabaw pigs fed a very high fat diet (VH) consisting of 75% total calories from fat, leptin levels were only 55% greater compared to Ossabaw C (**Figure 2.1D**). This increase is modest compared to Yucatan VH shown previously to have a 130% increase in plasma leptin over control Yucatan (1).

Hyperglycemia (glucose intolerance) defines diabetes, and is often preceded by primary insulin resistance in major target tissues, i.e. skeletal muscle and adipose. Both hyperglycemia and insulin resistance are major components of metabolic syndrome (MetS) and were assessed in this study using the intravenous glucose tolerance test.

After a 0.5 mg/kg bolus glucose injection Ossabaw H had significantly higher blood glucose concentrations at 5 and 10 minutes after bolus glucose injection compared to Yucatan C, Yucatan H, and Ossabaw C (**Figure 2.2A**). Further, peak plasma insulin was significantly elevated in Ossabaw C, Ossabaw H, and Yucatan H compared to Yucatan C. (**Figure 2.2C**). To evaluate the contribution of breed alone on blood glucose and plasma insulin during the IVGTT, we combined C and H groups in each pig breed. Ossabaw had significantly greater peak glucose at 5 and 10 minutes, and plasma insulin at 10 minutes after bolus glucose injection (**Figure 2.2 B&D**). Homeostasis model assessment (HOMA) is used to diagnose insulin resistance under fasting conditions (181). We measured insulin x glucose near the peak (10 minutes after bolus glucose injection) during the IVGTT resulting in a modified HOMA value (182). Modified HOMA values were significantly greater in both Ossabaw C and Ossabaw H compared to Yucatan C and Yucatan H (**Figure 2.2E**). When C and H diets are combined in each breed, we observed significantly greater modified HOMA values in Ossabaw over Yucatan (**Figure 2.2F**).

Microvascular dysfunction is a major characteristic of MetS (158). We assessed coronary microvascular function in Ossabaw and Yucatan swine by measuring blood flow velocity and calculating coronary flow reserve (CFR) in response to bradykinin and adenosine, two well characterized vasodilators of coronary vasculature (17). Placement of the flow wire in the circumflex artery is show in **Figure 2.3A**. CFR to adenosine was impaired in Ossabaw compared to Yucatan (**Figure 2.3B**). Additionally, endothelial cell dysfunction in response to bradykinin was apparent in Ossabaw compared to Yucatan (**Figure 2.3C**).

One hallmark of MetS CAD is diffuse atherosclerosis (95), which we assessed by measuring neointimal formation in proximal, intermediate, and distal segments of the left anterior descending (LAD) and circumflex (CFX) coronary arteries highlighted in a

coronary angiogram (**Figure 2.4A**) and schematic (**Figure 2.4B**) preceding stent placement. Atheroma was quantified by measuring the percent of the artery wall with neointimal formation demonstrated in **Figure 2.4C** in which a calcified lesion covers 15% of the cross-section of the coronary wall. Yucatan H had elevated atherosclerosis in the proximal segment, but was indistinguishable from Ossabaw and Yucatan C through the intermediate segment. Importantly, Ossabaw H remained elevated through all segments measured, demonstrating MetS Ossabaw swine develop diffuse CAD while Yucatan swine do not (**Figure 2.4D**).

Swine have been touted as the “ideal” model for studying stent efficacy (100;103;166;167), but recent clinical studies with complications not predicted in preclinical swine experiments suggest a better model is needed (183;184). Therefore, we tested the hypothesis that hyperinsulinemic Ossabaw swine have a propensity to increased in-stent CAD compared to Yucatan. **Figure 2.5A** is a coronary angiogram immediately before stent expansion. **Figure 2.5B** is a coronary angiogram during stent expansion with radio-opaque dye within the inflated balloon. Verhoeff’s elastin (**Figure 2.5 C&D**), hematoxylin and eosin (**Figure 2.5 E&F**), and trichrome collagen (**Figure 2.5 G&H**) stains were used to characterize in-stent CAD and stenosis in Ossabaw and Yucatan swine. All swine were allowed to recover three weeks following stent placement. In-stent neointimal hyperplasia was 2.5-fold greater in Ossabaw compared to Yucatan, regardless of diet (**Figure 2.5I**). Ossabaw also exhibited increased cells per mm² (**Figure 2.5J**) and decreased in-stent collagen content (**Figure 2.5K**) compared to Yucatan in-stent neointima. Thus, in-stent neointima of Ossabaw swine is more occlusive, less fibrous, and more cellular compared to Yucatan. Histological evaluation of the neointima of non-stent artery segments, revealed percent collagen was greater in Yucatan than in Ossabaw, with diet having no significant effect (**Figure 2.5L**), while cellularity was not changed (data not shown). CAD in non-stent segments proximal to

the stent and immediately adjacent to the stent, i.e. peri-stent, quantified with IVUS is shown in **Figure 2.6**. The most striking results were the ~5-fold greater peri-stent CAD in Ossabaw C compared to Yucatan C pigs and increases in peri-stent CAD after atherogenic diet.

We previously reported that intracellular Ca^{2+} signaling events are altered in coronary arteries with atherosclerotic lesions (6;10;13;16-18;174). High extracellular potassium (High K^+ , 80 mM) depolarizes the cell membrane activating voltage-gated Ca^{2+} channels in coronary smooth muscle (CSM) leading to Ca^{2+} influx and a rise in intracellular Ca^{2+} levels (**Figure 2.7A**). High K^+ application also maximally loads the sarcoplasmic reticulum (SR) Ca^{2+} store. The area under the curve of the High K^+ response was not different between Yucatan C and Ossabaw C (**Figure 2.7B**). Subsequent to SR Ca^{2+} release by caffeine, intracellular Ca^{2+} levels initially rise transiently, then fall over time due to Ca^{2+} extrusion (efflux) and sequestration mechanisms (**Figure 2.7A**). Baseline-subtracted peak Ca^{2+} response to caffeine was not different between Yucatan C and Ossabaw C (**Figure 2.7C**). Overall buffering of intracellular Ca^{2+} was measured as time from peak Ca^{2+} response to caffeine to $\frac{1}{2}$ the initial baseline. Ossabaw C CSM displayed increased time to $\frac{1}{2}$ minimum from peak Ca^{2+} response to caffeine compared to Yucatan C in Ca^{2+} -containing and Ca^{2+} -free solution (**Figure 2.7D**), thus providing evidence for decreased Ca^{2+} efflux in Ossabaw C compared to Yucatan C. CSM from peri-stent and non-stent artery segments of Yucatan C, Yucatan H, Ossabaw C, and Ossabaw H were assessed for sarcoplasmic reticulum (SR) / endoplasmic reticulum Ca^{2+} ATPase (SERCA) function. CSM were depolarized with High K^+ to load the SR (**Figure 2.8A**). SR Ca^{2+} release was elicited by application of endothelin-1 (ET-1, 30 nM), while thapsigargin (TG, 1 μ M) prevented Ca^{2+} uptake into the SR by blocking SERCA. SERCA buffering of Ca^{2+} was assessed by the effect of full SERCA inhibition by thapsigargin on the peak Ca^{2+} response to ET-1. SERCA buffering

of Ca^{2+} was not involved in Ca^{2+} response to ET-1 in Yucatan C in either peri- or non-stent CSM (**Figure 2.8 B&C**). SERCA significantly contributed to buffering ET-1 released Ca^{2+} in CSM from non-stent Yucatan H segments as evidenced by increased peak Ca^{2+} response to ET-1 with application of TG (**Figure 2.8D**). In other words, SERCA function was increased in native atherosclerotic arterial segments. Importantly, peri-stent CSM from Yucatan H have SERCA dysfunction, because the peak Ca^{2+} response to ET-1 is similar to non- and peri-stent with full inhibition of SERCA by TG. Ossabaw C CSM from non- and peri-stent segments have increased SERCA function evidenced by increased peak Ca^{2+} response to ET-1 in the presence of TG (**Figure 2.8E**). Incredibly, SERCA function is virtually non-existent in CSM from Ossabaw H non- and peri-stent as peak Ca^{2+} response to ET-1 is elevated in the absence of TG (**Figure 2.8F**). In summary, SERCA function in the buffering of peak Ca^{2+} response to ET-1 transitions of from increased SERCA function in mild CAD through dysfunction in more severe CAD.

Discussion

The major findings of this study are that Ossabaw swine compared to Yucatan have: 1) greater in 4 metabolic features of MetS, 2) coronary microvascular dysfunction in response to adenosine (primarily smooth muscle mediated) and bradykinin (endothelial mediated), 3) significantly greater native atheroma, diffuse atheroma, in-stent neointimal hyperplasia, and peri-stent atheroma, 4) less fibrous and more cellular atherosclerotic lesions within non-stented and stented segments of coronary artery, and 5) impaired coronary smooth muscle intracellular Ca^{2+} buffering and efflux following Ca^{2+} release from the sarcoplasmic reticulum. This is the first study to directly compare multiple symptoms of the MetS, CAD, and in-stent restenosis between Ossabaw swine and Yucatan fed calorie matched control chow and high fat/cholesterol atherogenic diet.

Phenomenal work has been done on transgenic and gene ablation (knockout) mouse models (e.g. (113)) and summarized recently from work of the Animal Models of Diabetic Complications Consortium (AMDCC) (116) to understand mechanisms of obesity and MetS. However, transgenic mouse models are simply not adequate for vascular interventions using stents identical to those used in humans (4;20;21;100;103;165-167), which is essential for translation to the clinic. Since the Ossabaw miniature swine model of MetS also develops mature, clinically significant atheroma (24), there is potential to improve vastly over all other stenting studies that employed injury of healthy arteries (100;103;166;167).

A primary advantage of Ossabaw miniature swine use in research is the predisposition to obesity and natural occurrence of MetS and progression to type 2 diabetes, which is unique for the Ossabaw. **Table 2.2** compares the major features of MetS (items 1-6) present (Yes) or not (No) in Yucatan vs. Ossabaw miniature swine and their utility as cardiovascular disease models and comparison of Ca^{2+} signaling (items 7-12). The Yucatan is our comparison because of our extensive, ~20 years of work with

this genetically leaner pig that is the predominantly used miniature swine for laboratory research. Relatively mild differences in metabolic parameters (e.g. body mass index, hyperglycemia, hyperinsulinemia, and hypercholesterolemia) were induced by atherogenic diet feeding compared to previous reports in Ossabaw and Yucatan swine (summary in **Table 2.2**). This was a direct result of our study's aim to sensitively measure breed differences by calorie matching C and H diets to that required for maintenance of normal body weight in adult Yucatan swine, rather than inducing maximal MetS by overfeeding the H groups. Rigorous comparison shows much greater propensity to obesity, i.e. "thriftiness" of Ossabaw compared to Yucatan. Increased back and carcass fat were noted in Ossabaw H vs. C, but no increase in Yucatan H vs. C (**Figure 2.1 A&B**).

In healthy humans, leptin limits the accumulation of ectopic fat accumulation, whereas in obese humans, leptin levels rise and the body develops leptin insensitivity. Leptin insensitivity leads to ectopic lipid accumulation, in turn contributing to insulin insensitivity (185). Although Ossabaw H have greater backfat and carcass fat compared to Yucatan H, plasma leptin was similarly and modestly elevated in Ossabaw H and Yucatan H above their respective control. Lending support to this idea are our previously published data, which revealed hypercaloric H fed Yucatan had an 84% increase in leptin above Yucatan H in this study ((1), **Figure 2.1C**). In contrast, hypercaloric H fed Ossabaw (VH) only displayed an 11% increase in plasma leptin above Ossabaw H (**Figure 2.1 C&D**), although VH were much more obese (data not shown). This suggests Ossabaw pigs may have a relatively deficient (blunted) leptin response to increased adipose, which may in part explain increased weight gain which contributes to metabolic syndrome, a situation strikingly similar to leptin deficiency, obesity, and MetS in humans (186). In summary, Ossabaws clearly show greater propensity to obesity than Yucatan

and direct measures show a greater accumulation of visceral fat on rigorously controlled experimental diets.

Despite intensive efforts to induce insulin resistance and glucose intolerance in Yucatan swine on high fat, high cholesterol, and high sucrose diets, we have found that currently available Yucatan pigs do not naturally develop obesity-associated insulin resistance ((9;111;187;188); **Table 2.2**, items 2, 3). In contrast, Ossabaw swine fed a high caloric diet display a natural pathogenesis of MetS with hyperinsulinemia and eventual progression to type 2 diabetes, as evidenced by significantly increased fasting blood glucose. Other miniature swine breeds currently available for laboratory animal medicine, i.e. Yucatan and Gottingen, do not progress to type 2 diabetes (e.g. (9;111;189)). Gottingen pigs (110;189-191), however, will develop mild MetS. Although outstanding work shows that a line of crossbred domestic pigs with familial hypercholesterolemia will develop MetS (115), use of the standard sized domestic swine is not practical because they weigh >250 kg and are 2 years of age before type 2 diabetes occurs. A 250 kg pig is not amenable to use of conventional angiography instrumentation needed for stent deployment compared to the convenient small stature of Ossabaw miniature swine (**Table 2.2**, item 8; see below). Dyslipidemia of Yucatan and Ossabaw was comparable in the present study (**Table 2.2**, items 4, 5), but other studies using hypercaloric diets showed robust increases LDL/HDL ratio and triglycerides in Ossabaws. Genetically leaner Yucatan pigs made mildly obese and hyperlipidemic by consumption of excess calorie atherogenic diet did not become hypertensive ((2;9;10), **Table 2.2**, item 6). In contrast, in all of our chronic studies of hypercaloric feeding Ossabaw swine hypertension was a clear finding, thus indicating MetS. Convincing evidence for “obesity hypertension” (192) is the robust, 5-fold increases in plasma renin and aldosterone in Ossabaw swine (193).

In the current study, we show mild MetS in Ossabaw swine increases CAD. Although Ossabaw H and Yucatan H have similar levels of CAD in proximal segments, Ossabaw H, the only group to exhibit elevated peak glucose in response to glucose tolerance test, have diffuse atherosclerosis, a hallmark of patients with diabetes ((80;86;95); **Table 2.2**, item 7). This difference in CAD between Yucatan and Ossabaw is especially striking considering the modest metabolic differences.

MetS patients have increased incidence of CAD (39), and those presenting with flow-limiting coronary occlusions are primarily treated by stent deployment. Drug eluting stents have significantly reduced restenosis rates; however, restenosis is still a major concern when treatment is complicated by diffuse and severe atheroma which progresses much more aggressively in regions adjacent to the stent (“peri-stent” CAD) (80;86;95). Ossabaw swine, which we show have 6 features of MetS (**Table 2.2**), have increased peri- and in-stent CAD (**Figures 2.5** and **2.6**) compared to Yucatan. Interestingly, pig breed, but not diet, is associated with increased in-stent stenosis. This differs from non-stent segments in that only the combination of the Ossabaw breed and high fat/cholesterol atherogenic diet elicited diffuse atherosclerosis. These findings suggest factors key to Ossabaw swine CAD drive the greater peri- and in-stent CAD compared to Yucatan swine, including possibilities such as: 1) other MetS milieu components not measured in our study, 2) other inflammatory mediators, or 3) other genetic components beyond the thrifty genotype, e.g. vascular wall differences, that render coronary arteries more sensitive to stenting. The most likely difference, however, is hyperinsulinemia, which was present in Ossabaw compared to Yucatan. Although some reports indicate no greater coronary restenosis in MetS compared to non-MetS patients (194), there is strong support for the role of the hyperinsulinemia component MetS in increased restenosis after percutaneous coronary interventions (161-164). Especially compelling support for the role of hyperinsulinemia is the study of Takagi et

al. (163) showing serial intravascular ultrasound measures of coronary restenosis in humans.

One possibility for underlying mechanisms of greater CAD and in-stent neointimal hyperplasia in MetS is the coronary smooth muscle cell (CSM), the predominant cell type in atherosclerotic tissue (195). Mechanisms underlying CAD and vascular response to injury are not completely understood, but we and others have reported altered CSM Ca^{2+} signaling is involved in diabetic CAD (10;13;14;16;18;29;174;196). Intracellular free Ca^{2+} concentration is determined by three major mechanisms: Ca^{2+} influx, Ca^{2+} extrusion, and intracellular Ca^{2+} sequestration by the sarcoplasmic reticulum (SR). Important observations in this study include no difference in Ca^{2+} influx in response to depolarizing extracellular solution (**Figure 2.7B**; quantifies mainly voltage-gated Ca^{2+} channel activity in plasma membrane (13;16)) or peak Ca^{2+} in response to caffeine treatment (**Figure 2.7C**; quantifies SR Ca^{2+} store (26;197;198)) between Ossabaw and Yucatan swine. In the presence and absence of extracellular Ca^{2+} , increased time to $\frac{1}{2}$ minimum in response to caffeine indicates decreased Ca^{2+} extrusion across the plasma membrane (Ca^{2+} efflux (13;26)) in Ossabaw CSM vs. Yucatan (**Figure 2.7D**). Importantly there was no difference in time to $\frac{1}{2}$ minimum despite the presence or absence of extracellular Ca^{2+} for either breed (**Figure 2.7D**), suggesting store-operated Ca^{2+} entry (SOCE) was not a major factor.

The lack of SOCE in Ossabaw CSM may appear to contradict recently published results from our laboratory (Edwards et al. (29)) implicating the SOCE channel transient receptor potential classical 1 (TRPC1) in MetS- and stent-induced CAD in Ossabaw swine (29). However, an important difference in Edwards et al. (hypercaloric atherogenic diet) is the induction of robust MetS and severe CAD compared to the relatively mild MetS and CAD induced in this study. The finding of this study that SOCE is not evident in Yucatan CSM confirms previous reports by our laboratory (e.g. (27;28)), although we

have observed robust SOCE in endothelial cells (199). Interestingly, sarcoplasmic reticulum/endoplasmic reticulum Ca^{2+} ATPase (SERCA) does not influence the peak response to endothelin-1 (ET-1) in CSM from Yucatan C non- and peri-stent (**Figure 2.8C**). The Ca^{2+} response is maintained at normal levels with increased SERCA function in both non- and peri-stent Ossabaw C CSM (**Figure 2.8E**), compared to Yucatan C. SERCA function increases in CSM from Yucatan H non-stent with maintained peak response compared to Yucatan C, but Yucatan H peri-stent CSM are unable to maintain peak response despite increased SERCA function (**Figure 2.8D**). Incredibly, SERCA is virtually non-functional in CSM from Ossabaw H non- and peri-stent (**Figure 2.8F**), as assessed by peak response to ET-1 with or without TG.

Complex and unstable plaque formation lead to increased risk of thrombosis (200), resulting in acute myocardial infarction. We have observed more than 500 Yucatan coronary arteries without documenting calcified coronary lesions, however Ossabaw coronary arteries contain calcified lesions as shown in **Figure 2.3C** (references in **Table 2.2**). Previously published data demonstrated collagen-rich atherosclerotic tissue in restenotic specimens was greater in humans with diabetes than in non-diabetic patients (201). In contrast, we show a 34-fold greater increase in percent collagen in stented segments in Yucatan compared to Ossabaw. One possible explanation is that the atherosclerotic tissue in the human study is more mature, whereas the atherosclerotic tissue in our study is in early stage of progression which is characterized by less stable plaque formation. The complex (highly cellular, calcified, and less fibrous) neointimal composition observed in stented segments of Ossabaw coronary artery suggests a complex, mature, proliferative, and/or lipid-laden composition; thus potentially more vulnerable plaque rupture.

Ossabaw swine were used as a laboratory animal model almost 40 years ago (168) and may be more relevant now than ever due to the increasing incidence of MetS

and type 2 diabetes in western society (30). Ossabaw swine remarkably mimic MetS and advanced CAD observed in humans and serve as an excellent large animal model for study metabolic abnormalities and coronary artery disease in the future.

Acknowledgements

We thank the many outstanding coworkers who contributed to this work, especially J. Bryd, J. Wenzel, R. Boullion, and Dr. C.A. Witczak. We thank J.M. Sturek for initial strategies for segmental analysis of intravascular ultrasound images to characterize diffuse coronary artery disease.

Grants

This work was supported by the National Institutes of Health grant numbers HL062552 and RR013223 and an Innovation Award from the American Diabetes Association to M.S. the Purdue-Indiana University Comparative Medicine Program, and the Fortune-Fry Ultrasound Research Fund of the Department of Cellular & Integrative Physiology at Indiana University School of Medicine. J.M.E. and Z.P.N. are the recipients of a Translational Research Fellowship from the Indiana University School of Medicine, Z.P.N. was the recipient of a Translational Fellowship from NIH UL1 RR025761, and X.L. was the recipient of a Predoctoral Fellowship from the American Heart Association.

Figure Legends

Figure 2.1 Body fat is greater in Ossabaw swine and leptin increase is blunted compared to Yucatan on calorie-matched diets. **A** Backfat measured by ultrasound at 5th rib. * $p < 0.05$ Ossabaw C vs. all other groups, ** $p < 0.05$ Ossabaw H vs. all other groups. **B** Percentage of carcass as fat measured by direct chemical analysis. * $p < 0.05$ Ossabaw H vs. all other groups. **C** Plasma leptin is increased similarly by H diet in both Ossabaw and Yucatan. * $p < 0.05$ H vs. C. **D** Plasma leptin is increased in a subset of Ossabaw fed a very high (VH) fat diet consisting of 75% of kcal from fat. * $p < 0.05$ Ossabaw C vs. VH.

Figure 2.2 Ossabaw swine are glucose-intolerant and insulin-resistant compared to Yucatan. Intravenous glucose tolerance test (IVGTT) in Yucatan and Ossabaw swine was initiated by infusion of 0.5 g glucose/kg body weight at time 0. **A** Time course of blood glucose responses in Yucatan C (filled circles), Yucatan H (open circles), Ossabaw C (filled triangles), and Ossabaw H (open triangles), * indicates Ossabaw H greater than all groups. **B** Combined C and H diets to compare glucose in breeds. **C** Simultaneous measurement of insulin responses during IVGTT, * indicates all groups greater than Yucatan C. **D** Combined C and H diets to compare insulin between breeds. **E** Ossabaw C and H have greater insulin x glucose at near peak (10 minutes) during IVGTT than Yucatan C and H. **F** Combined C and H diets to compare insulin x glucose at peak (10 minutes). A-D: * $p < 0.05$ by two-way repeated measures ANOVA with SNK *post-hoc* analysis. E-F: * $p < 0.05$ by 2x2 ANOVA.

Figure 2.3 Ossabaw swine exhibit coronary microvascular dysfunction compared to Yucatan. **A** Coronary schematic illustrates flow wire positioning in circumflex artery (from right anterior oblique view) and downstream microvasculature. **B** Ossabaw

coronary flow reserve is reduced in response to adenosine compared to Yucatan swine. **C** Ossabaw swine exhibit endothelial dysfunction compared to Yucatan swine in response to bradykinin. * $p < 0.05$ by two-way ANOVA with Bonferroni post-test.

Figure 2.4 Diffuse atherosclerosis is prominent in Ossabaw compared to Yucatan.

A Angiogram of left coronary arteries with circumflex (CFX) and left anterior descending (LAD) arteries labeled. **B** The most proximal segment (Proximal) is defined as 0 to 10 mm from the bifurcation of the LAD and CFX arteries. The middle segment (Intermediate) is defined as 20 to 30 mm from the bifurcation of the LAD and CFX. The most distal segment (Distal) is defined as (x-10 mm) to x mm where x is the most distal measurement of the intravascular ultrasound (IVUS) pullback. The right coronary (RC) artery shown here for completeness is not shown in the angiogram. IVUS recordings were acquired to assess native atheroma before stent placement as in Figure 6B. **C** IVUS image showing 15% wall coverage by calcified neointimal formation. Calcification is identified by signal dropout peripheral to the IVUS imaging transducer and is highlighted by dotted lines. **D** Native atheroma coverage of the artery wall as a percentage of the artery wall area (% wall coverage) is graphed along three segments of the CFX coronary artery. Each segment represents 10 mm of the CFX artery. Measurements of % wall coverage were taken every 2 mm. * $p < 0.05$ H vs. C; † $p < 0.05$ Ossabaw H vs. Yucatan H.

Figure 2.5 In-stent stenosis is greater in Ossabaw compared to Yucatan. A

Coronary angiogram in right anterior oblique 30° view prior to stent deployment and **B** during stent deployment. **C** Representative VVG stain of Yucatan C in-stent CAD. **D** Representative VVG stain of Ossabaw C in-stent CAD illustrating adventitia (A), neointima (Neo), media (M), lumen (L), pre-stent lumen border (dotted line), and post-

stent lumen border of neointimal hyperplasia (dashed line). **E** Image of hematoxylin and eosin stained cell nuclei in Yucatan and **F** Ossabaw neointima. **G&H** Histology using Masson's trichrome collagen staining (blue). Open spaces to the left and below NEO are from stent struts that were removed in sectioning. **I** Percent cross-sectional area stenosis calculated by histology is greater in Ossabaw C and H than Yucatan C and H, with no effect of atherogenic diet (H). **J** Ossabaw C and H have greater cell nuclei/unit area than Yucatan C and H. **K** Percent collagen in neointima area of in-stent and **L** non-stent artery segment. * $p < 0.05$ Ossabaw vs. Yucatan; † $p < 0.05$ C vs. H diet.

Figure 2.6 Peri-stent coronary artery disease is greater in Ossabaw compared to Yucatan and hyperlipidemia increases proximal non-stent and peri-stent coronary artery disease. **A&B** Representative IVUS images of Yucatan (**A**) and Ossabaw (**B**) peri-stent CAD. Solid and dotted lines show partial boundaries of lumen with neointima and neointima with echolucent media, respectively, used to calculate neointimal area and percent stenosis. White arrow in **B** illustrates IVUS guidewire artifact. **C** Hyperlipidemia increases both proximal non-stent and peri-stent CAD in Yucatan. **D** Peri-stent disease increased in Ossabaw H vs. C and vs. respective Yucatan C and H.. Group differences assessed by two-way ANOVA with Bonferroni post-test.

Figure 2.7 Dysfunctional Ca^{2+} efflux in Ossabaw vs. Yucatan coronary smooth muscle. **A** Duration of exposure to solutions is shown by horizontal lines. Representative Ca^{2+} tracing (fura-2 ratio) demonstrates Ca^{2+} influx response to 80 mM K^+ depolarizing solution (High K^+), peak Ca^{2+} response to caffeine (Caff, 5 mM), and time to half minimum from caffeine-induced Ca^{2+} peaks. **B** Integral of the intracellular Ca^{2+} response to depolarizing solution (High K^+ , 80 mM extracellular) is not different between Ossabaw control (C) and Yucatan C CSM. **C** Peak Ca^{2+} response to caffeine is not

different between Yucatan and Ossabaw CSM. **D** Time to $\frac{1}{2}$ minimum from peak is increased in Ossabaw C CSM compared to Yucatan C.

Figure 2.8 Sarco/endoplasmic reticulum Ca^{2+} ATPase Ca^{2+} buffering function progresses from increased function to virtually complete dysfunction with severity of CAD. **A** Duration of exposure to solutions is shown by horizontal lines. Representative Ca^{2+} tracing (fura-2 ratio) in Yucatan H demonstrates Ca^{2+} influx response to 80 mM K^+ depolarizing solution (High K^+) and peak Ca^{2+} response to endothelin-1 (ET-1, 30 nM) in coronary smooth muscle (CSM) cells in the presence (black tracing) or absence (gray tracing) of thapsigargin (TG, 1 μ M). **B** Coronary artery schematic illustrates non-stent and peri-stent segments from which CSM cells were dispersed. **C** SERCA function does not alter peak Ca^{2+} response to caffeine in CSM from lean, healthy Yucatan C. **D** TG inhibition of SERCA in Yucatan H CSM reveals increased role of SERCA in attenuating the ET-1 induced increase in intracellular Ca^{2+} in non- and peri-stent CSM. **E** SERCA attenuates peak Ca^{2+} response to ET 1 in Ossabaw C CSM. **F** SERCA function is inhibited in Ossabaw H CSM.

Table 2.1

	Yucatan C	Yucatan H	Ossabaw C	Ossabaw H	<i>p</i> < 0.05
Body weight (kg)	59 ± 2	58 ± 3	74 ± 2	76 ± 2	Y<O
Starting BMI (kg/m ²)	32 ± 1	34 ± 1	28 ± 1	28 ± 1	Y>O
End BMI (kg/m ²)	38 ± 1	38 ± 3	47 ± 6	45 ± 1	Y<O
Total cholesterol (mg/dL)	52 ± 4	420 ± 72	62 ± 3	338 ± 28	C<H
HDL (mg/dL)	30 ± 3	60 ± 10	34 ± 1	75 ± 9	C<H
LDL (mg/dL)	14 ± 3	351 ± 76	20 ± 4	255 ± 29	C<H
Triglycerides (mg/dL)	38 ± 6	41 ± 6	19 ± 3	41 ± 7	None
Systolic blood pressure (mm Hg)	77 ± 4	79 ± 9	88 ± 7	91 ± 3	None
Diastolic blood pressure (mm Hg)	48 ± 3	54 ± 1	59 ± 8	56 ± 3	None
Mean arterial pressure (mm Hg)	57 ± 4	62 ± 1	68 ± 7	67 ± 3	Y<O
Heart wt./ Body wt.	0.0039 ± .00012	0.00436 ± .00023	0.0031 ± .0001	0.003 ± .00006	Y>O
Coronary artery diameter (mm)	2.7 ± 0.1	2.5 ± 0.1	2.3 ± 0.3	2.3 ± 0.1	Y>O

Table 2.1. Phenotypic characteristics of Yucatan and Ossabaw swine fed control chow (C) or high fat/cholesterol (H) atherogenic diet. BMI = body mass index; wt. = weight; Y = Yucatan swine; O = Ossabaw swine.

Table 2.2

Characteristic	Yucatan	Ossabaw	References, Figures and Table 2.1
1. Obesity	No	Oss>Yuc	(1-8); Table 2.1, Figure 2.1
2. Insulin resistance	No	Yes	(3;4;7-10); Figure 2.2
3. Glucose intolerance (or impaired glucose tolerance, [IGT])	No	Yes	(1-4;4;6-13); Figure 2.2
4. Dyslipidemia (↑LDL/HDL or ↑LDL/TC)	Yes	Yes	(3;4;7;8;11;13-15); Table 2.1
5. Dyslipidemia (↑ triglycerides)	No	Yes	(1;3;4;7;8;10-12;15;16)
6. Hypertension	No	Yes	(3;4;9); Table 2.1
7. Cardiovascular disease, atherosclerosis	Yes	Yes	(3;4;4;6;8;11;12;17-24); Figures 2.3-2.6
8. Small stature	Yes	Yes	(1-4;25); Table 2.1
9. Other – vascular calcification, AMP kinase alleles	No	Yes	(23;24); Figure 2.3
10. CSM Ca²⁺ efflux dysfunction	Yes	Oss>Yuc	(13;26); Figure 2.7
11. CSM SERCA dysfunction	Yes	Oss>Yuc	(13;16); Figure 2.8
12.. CSM store-operated Ca²⁺ entry	No	Yes	(27-29); Figure 2.8

Table 2.2 Brief review of Ossabaw and Yucatan metabolic disease and Ca²⁺ regulation. Oss = Ossabaw swine; Yuc = Yucatan swine; AMP = '5adenosine monophosphate -activated protein; CSM = coronary smooth muscle; SERCA = sarco/endoplasmic reticulum ATPase; TC = total cholesterol; LDL = low density lipoprotein; HDL = high density lipoprotein.

Figure 2.1

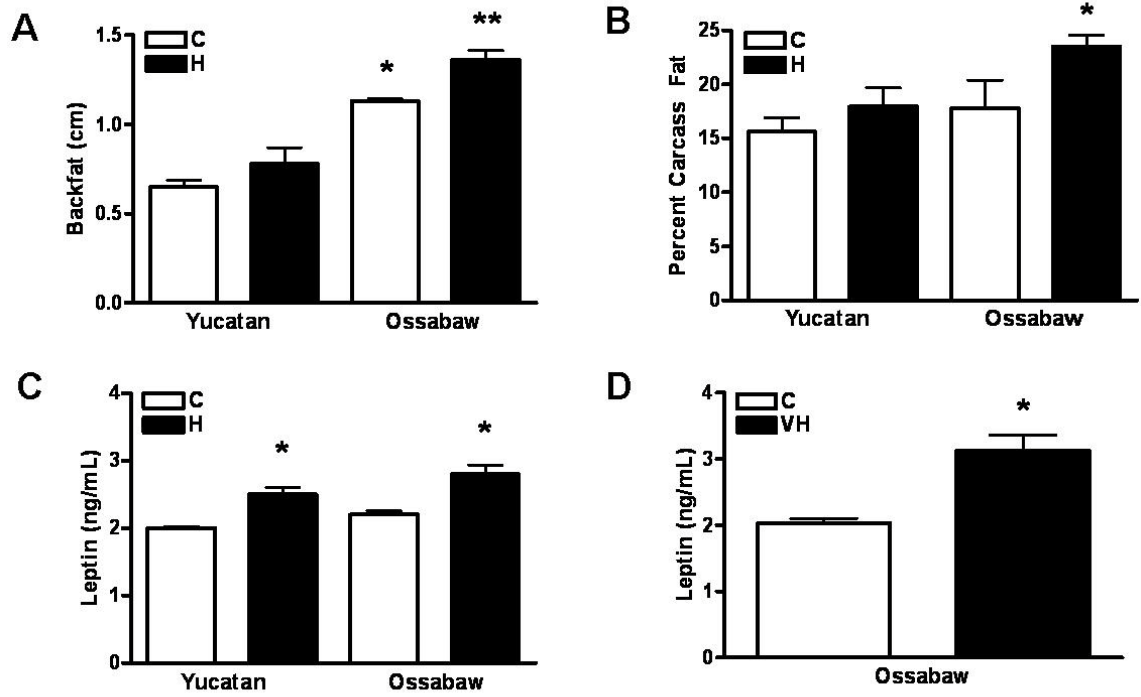


Figure 2.2

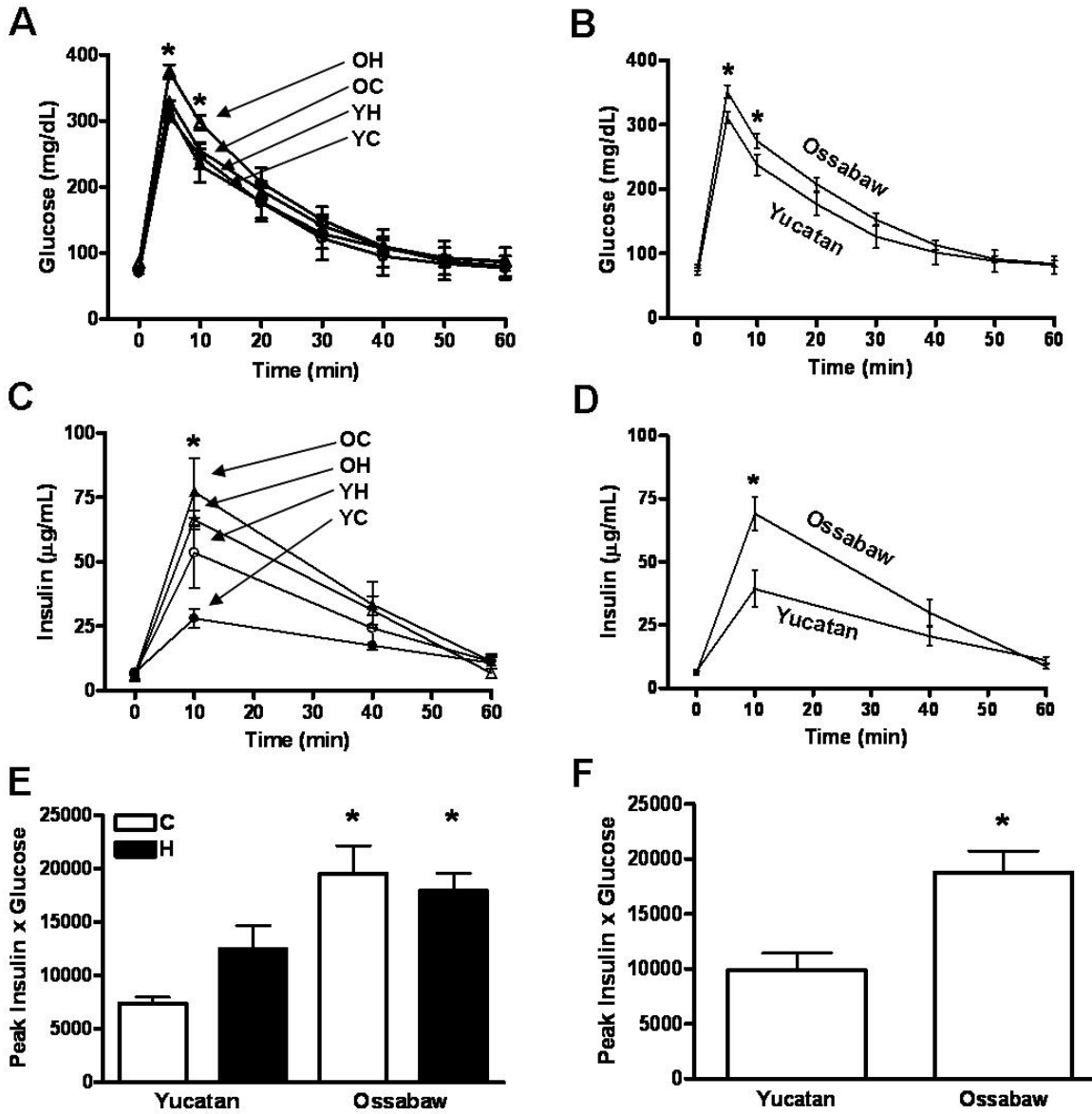


Figure 2.3

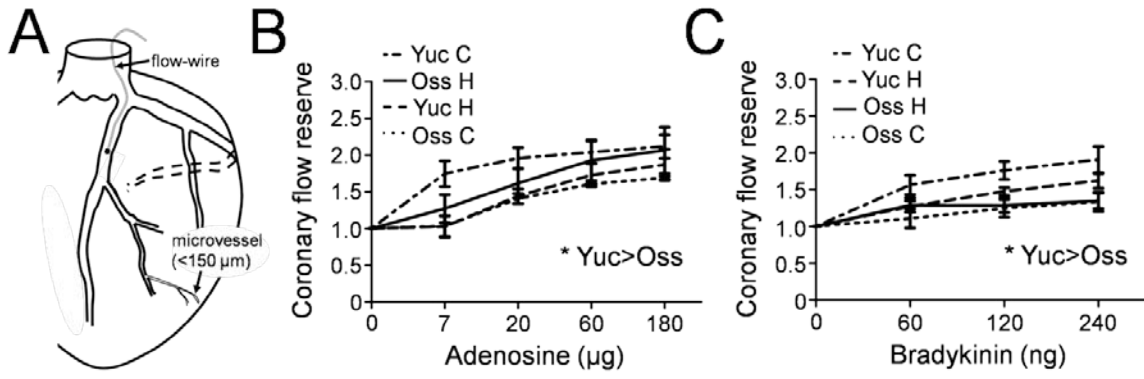


Figure 2.4

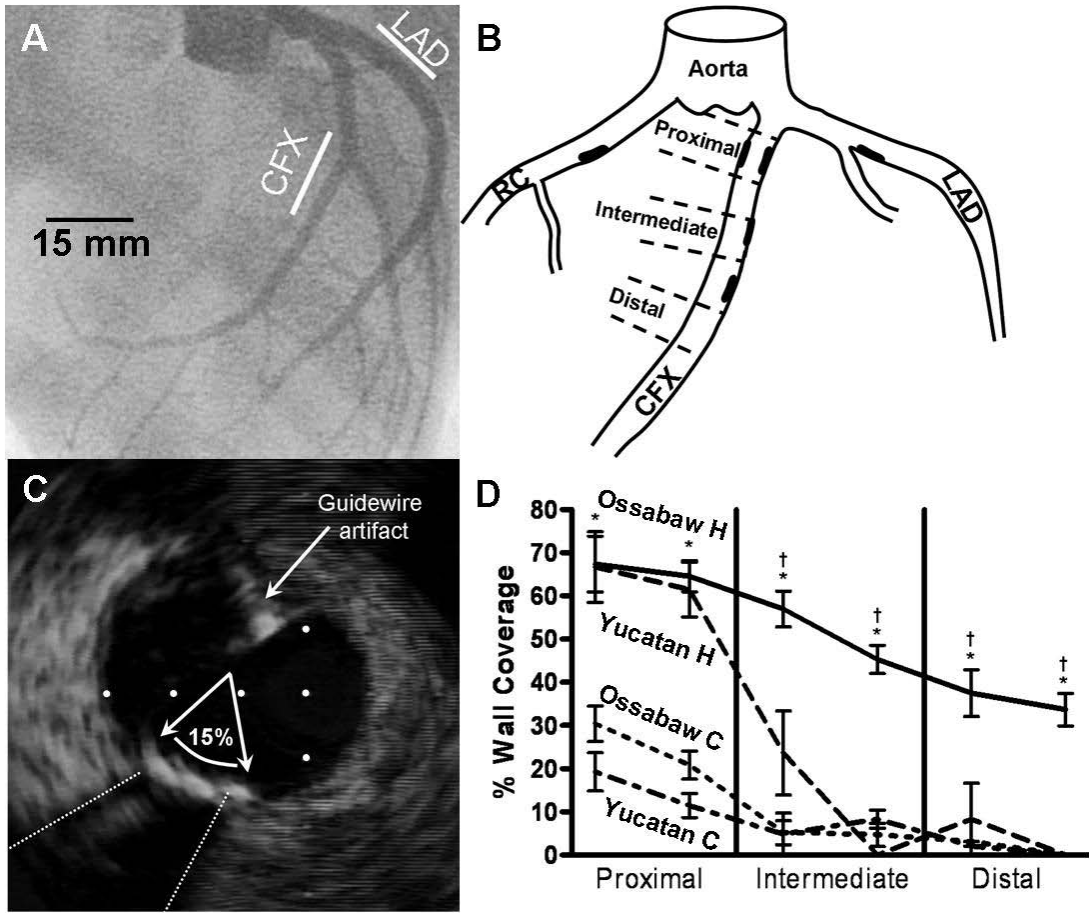


Figure 2.5

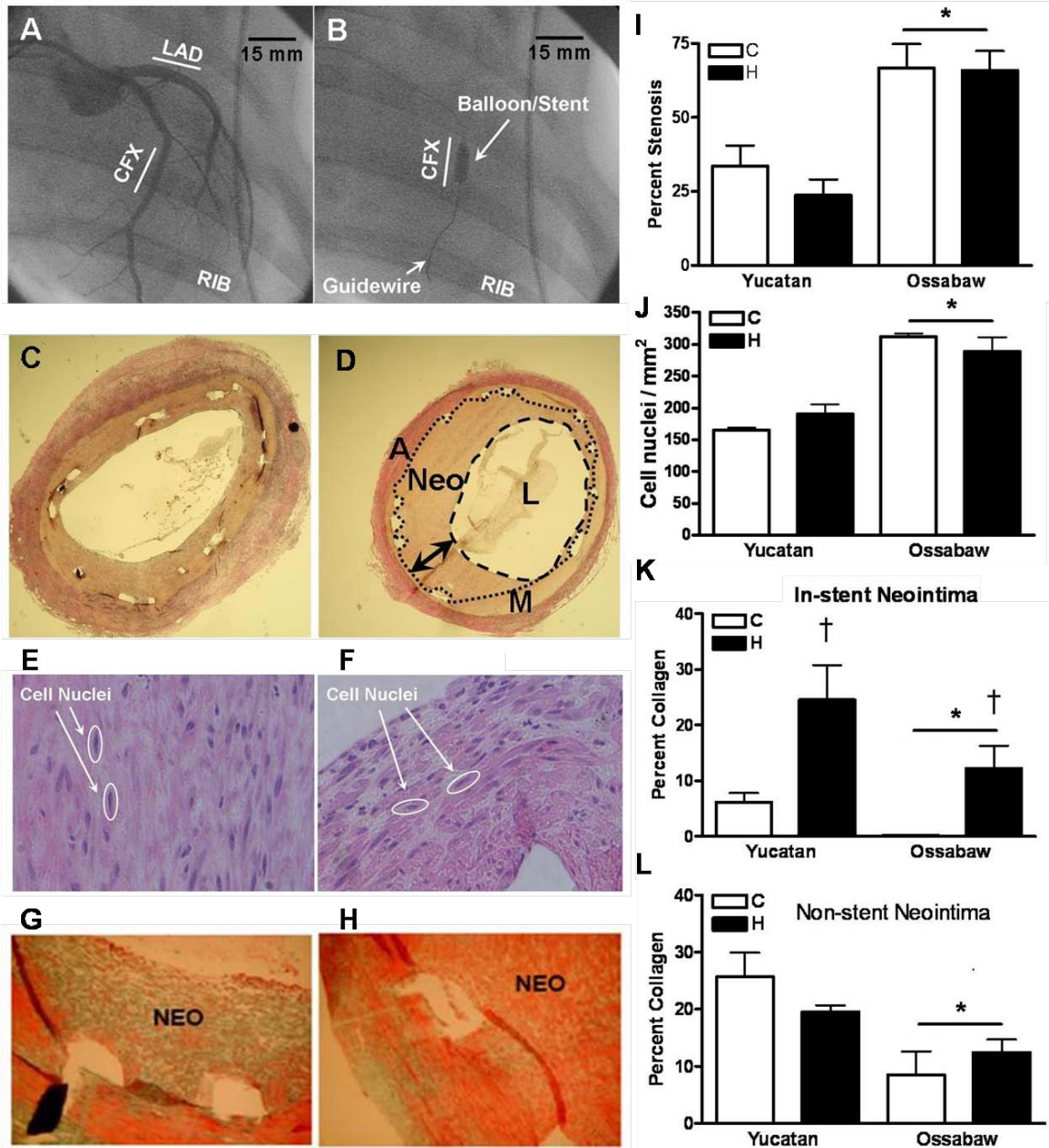


Figure 2.6

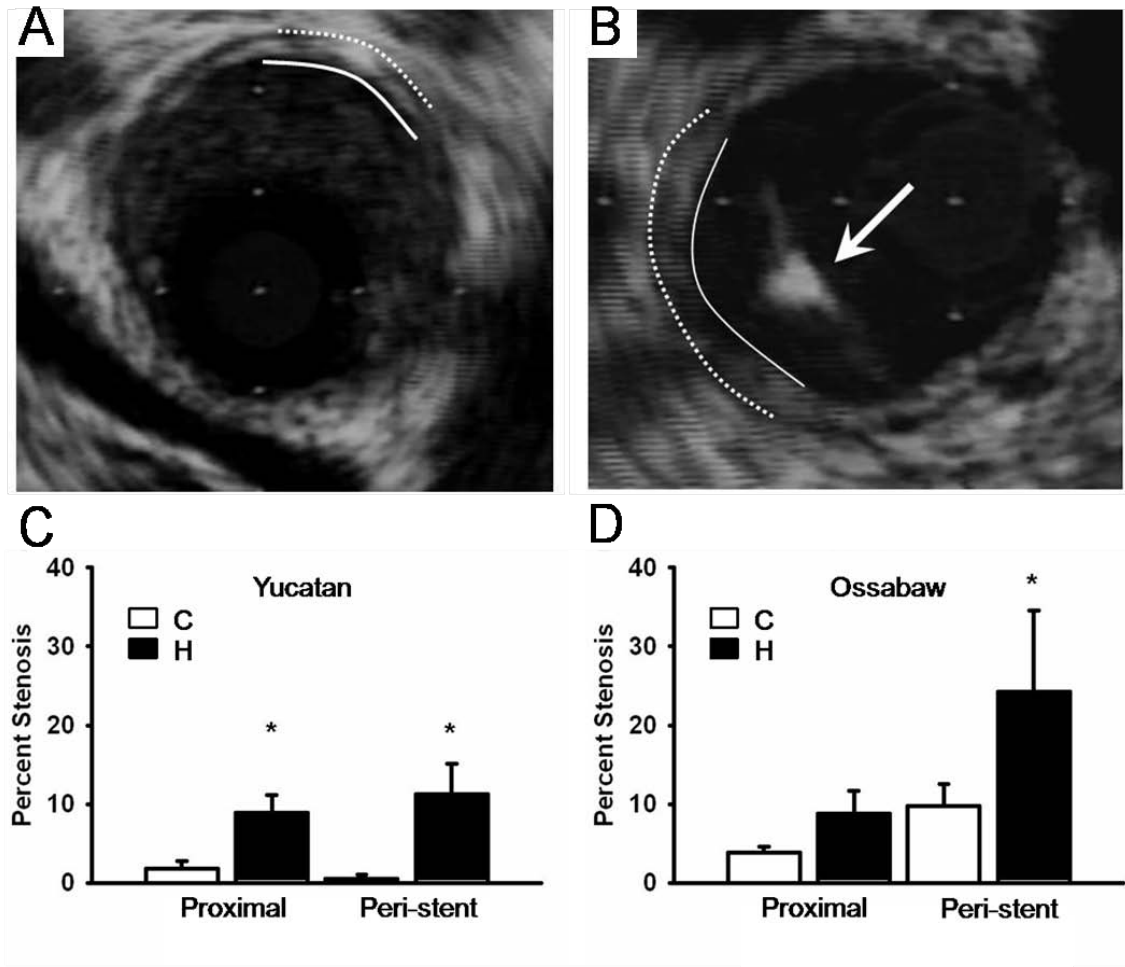


Figure 2.7

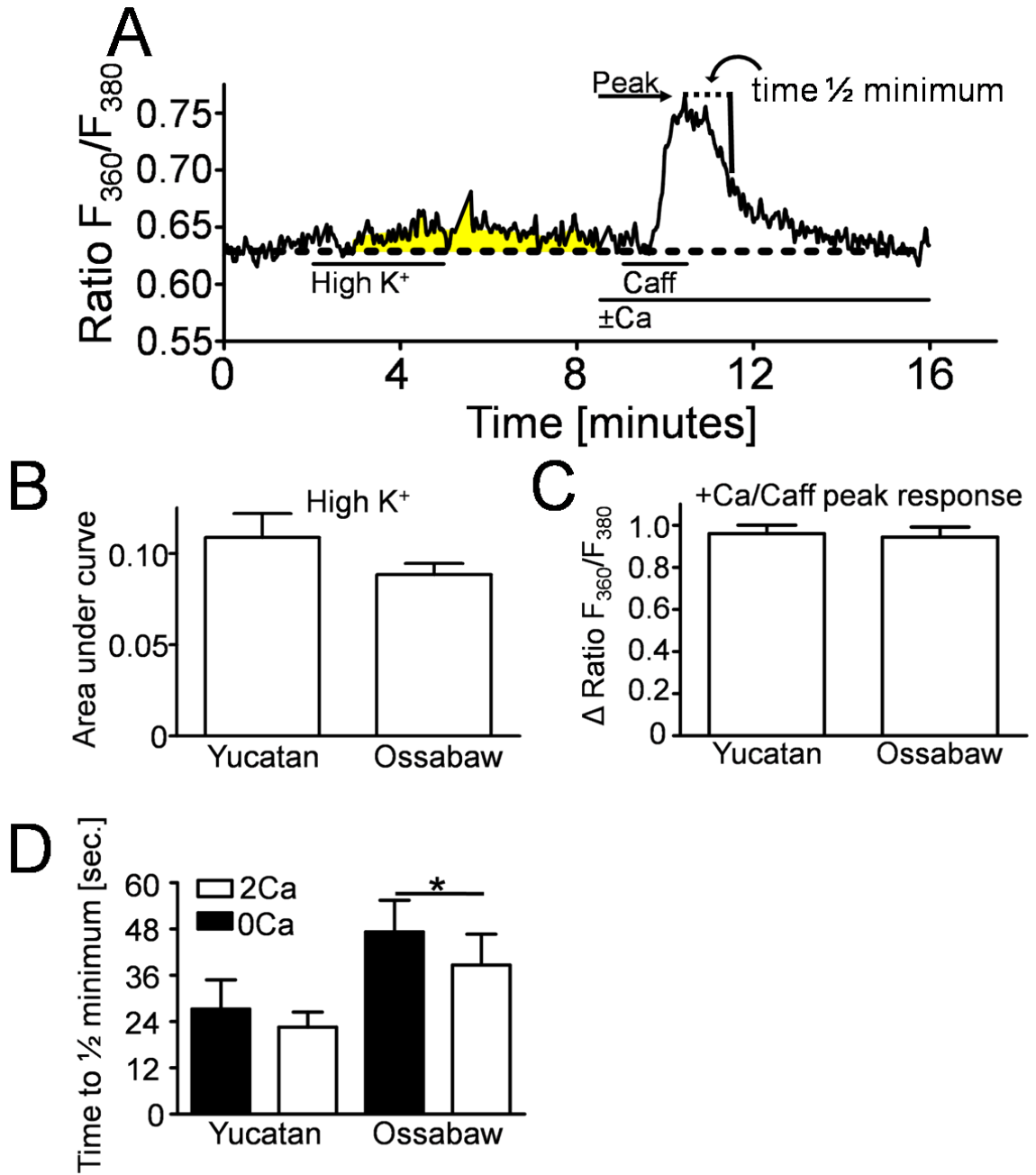
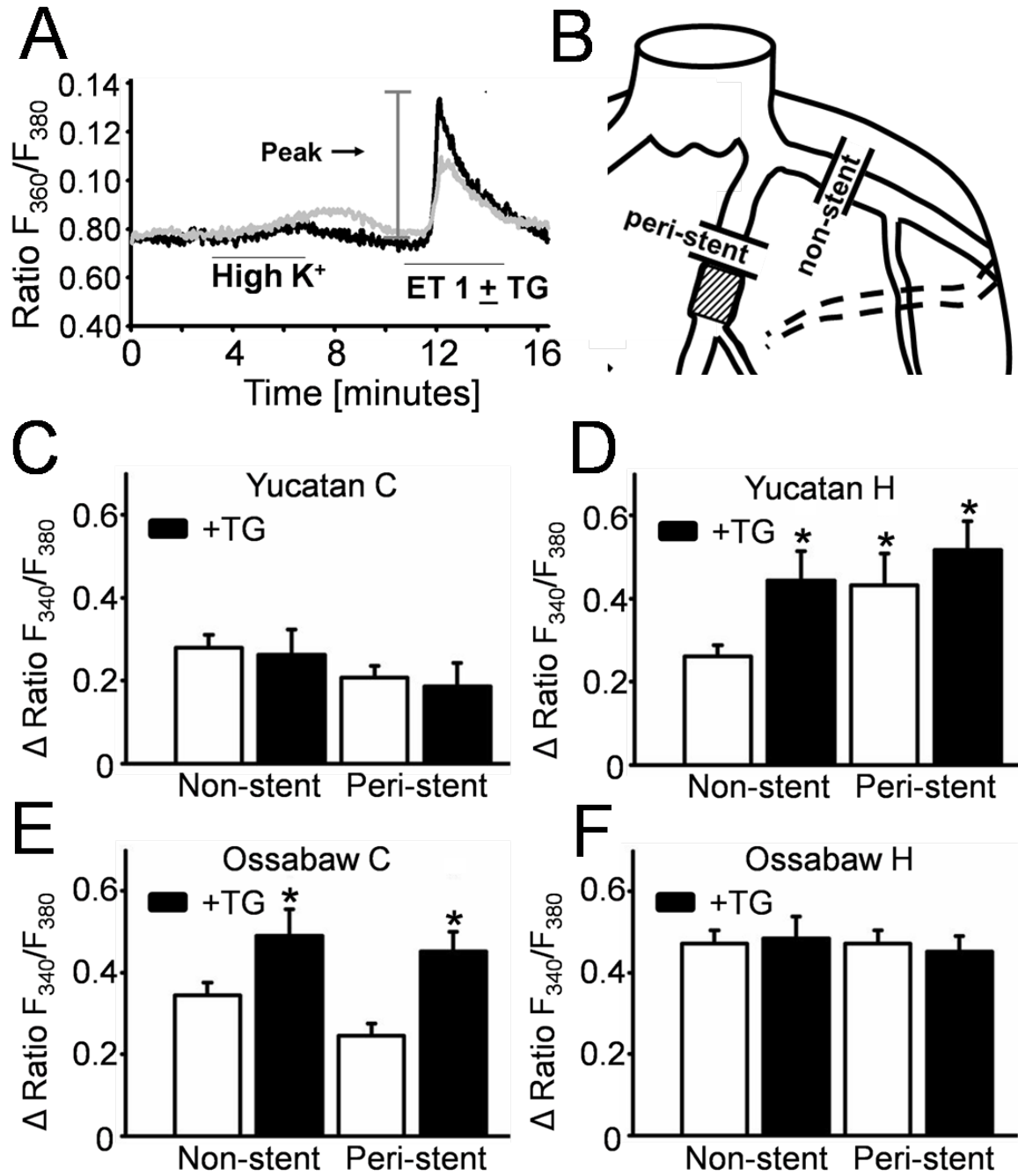


Figure 2.8



Chapter 3

Diet induced dyslipidemia in metabolic syndrome is necessary to elicit severe coronary artery disease and non-alcoholic steatohepatitis

Zachary P. Neeb¹, Mouhamad Alloosh¹, Ian N. Bratz⁴, Jason M. Edwards¹,
Ivan Mwesigwa¹, Lydia Lee², Romil Saxena³, Naga Chalasani², and Michael Sturek¹

Departments of ¹Cellular and Integrative Physiology, ²Medicine, and ³Pathology and Laboratory Medicine, Indiana University School of Medicine

²Department of Integrative Medical Sciences, Northeastern Ohio University College of Medicine

Abstract

Risk of coronary artery disease (CAD) is increased in patients with metabolic syndrome (MetS) and non-alcoholic steatohepatitis (NASH); however, the relative importance of each component of MetS (i.e. obesity, insulin resistance, glucose intolerance, dyslipidemia, hypertension) remains controversial. We hypothesized that occlusive and complex CAD and NASH are primarily driven by dyslipidemia within the MetS milieu and that all other components of MetS combined are not sufficient. Ossabaw swine were fed standard chow (Lean; N=16), chow with fructose (FMetS; N=9), trans-fat/cholesterol/fructose (TMetS; N=14), or mixed-source fat/cholesterol/fructose (MMetS; N=6) for 22-24 weeks. FMetS developed MetS without dyslipidemia. TMetS, and to a greater extent MMetS, developed MetS that included the dyslipidemia component. Lean demonstrated mild CAD and no NASH. Although FMetS developed MetS CAD and NASH were virtually non-existent. CAD and liver disease were directly related to dyslipidemia in MetS, with TMetS showing fatty/fibrous atheroma and MMetS progressing to stenotic, diffuse, and complex CAD and NASH. Total monounsaturated/polyunsaturated fatty acid ratio and fatty acid metabolism enzyme indices were associated with CAD and NASH, however LDL-gram years most reliably predicted CAD and NASH. Thus, dyslipidemia was a necessary component of MetS for eliciting severe CAD and NASH in swine that superbly mimic human pathologies.

Keywords: Ossabaw miniature swine, intravascular ultrasound, fatty acid methyl ester, coronary artery disease, non-alcoholic steatohepatitis

Introduction

Patients with metabolic syndrome (MetS; “pre-diabetes”) have a 3- to 4-fold increase in the risk of coronary artery disease (CAD) (39). There are several striking features of MetS CAD; in particular, pervasive, “diffuse CAD” is a hallmark of diabetic CAD (80;86;95). MetS also increases plaque cellularity, instability, inflammation, and calcification compared to non-diabetic patients (82;202). Generally, the presence of three or more of the following risk factors renders a diagnosis of MetS (159;160): obesity, insulin resistance, glucose intolerance, increased proportion of low-density lipoprotein (LDL) cholesterol, decreased high-density lipoprotein (HDL) cholesterol, increased LDL:HDL ratio, increased triglycerides, and hypertension (159;160). However, it is not clear whether any individual component, specifically dyslipidemia, provides the principal driving mechanism in developing CAD and associated diseases.

MetS and CAD are strongly associated with non-alcoholic fatty liver disease (NAFLD), one of the most common chronic liver diseases (41;56-58). NAFLD is benign when presented as simple steatosis, however non-alcoholic steatohepatitis (NASH), a progressive form of NAFLD, can lead to advanced fibrosis, cirrhosis, and liver failure (41;56-58). Approximately 30% of U.S. adults have NAFLD, while up to 25% of those patients have progressed to NASH (42;62). Importantly, patients with NASH have increased risk of death from cardiovascular disease (63), such that death from coronary disease exceeds even that of liver cirrhosis in NASH (64).

Despite the growing need for preclinical models of MetS and CAD, no animal model of MetS has ever demonstrated diffuse, stenotic, calcified, or complex coronary artery lesions. Gerrity et al. and others have demonstrated profound coronary atherosclerosis in streptozotocin-induced diabetic hyperlipidemic swine, but never without pancreatic β -cell ablation (104;106;203). Our laboratory has characterized the Ossabaw miniature swine model which faithfully replicates many of the human

characteristics of MetS when fed excess calorie atherogenic diet (3;4;6-8;29), including hypertension, obesity, insulin resistance, glucose intolerance, elevated LDL cholesterol and LDL:HDL ratio, and hypertriglyceridemia. Lee et al. utilized a modified atherogenic diet supplemented with fructose, trans-fatty acids, and lard in Ossabaw swine and observed severe MetS with accompanying NASH (7), the first report of NASH in a large animal model of MetS induced by atherogenic diet.

Utilizing the only model of MetS that develops severe NASH and CAD, we focused on and eliminated dyslipidemia, while retaining all other major components in the MetS milieu. This experimental design provided a unique opportunity to test the hypothesis that dyslipidemia is the primary component of the complex MetS milieu necessary for the induction of NASH and CAD.

Results

Lipids and integrated cardiovascular phenotype (Table 3.1). In Ossabaw swine, a hypercaloric chow diet supplemented with fructose produced MetS (FMetS). Additionally, supplementation with fat/fructose/cholesterol also produced MetS in TMetS and MMetS, while the source of fat (i.e. trans-fat versus trans- and saturated fat) dictated the severity of the phenotype. Body weight was significantly higher in FMetS, TMetS, and MMetS compared to Lean. FMetS, TMetS, and MMetS heart rates were increased over Lean, with MMetS being greater than FMetS and TMetS. Dyslipidemia was apparent in TMetS and MMetS as total cholesterol, HDL, LDL, LDL:HDL ratio, and triglycerides were all elevated compared to Lean and FMetS. FMetS were not dyslipidemic as defined by total cholesterol and LDL not being different from Lean, although LDL:HDL ratio was significantly increased, due to decreased HDL cholesterol compared to Lean. In addition, total cholesterol, LDL cholesterol, LDL:HDL ratio, and triglycerides were higher in MMetS compared to TMetS. FMetS, TMetS, and MMetS were hypertensive with elevated resting heart rate, systolic and diastolic blood pressure, and mean arterial pressure over Lean.

Glucose intolerance. After bolus intravenous glucose load, grouped MetS swine had significantly elevated peak blood glucose above Lean, demonstrating glucose intolerance (**Figure 3.1A**). FMetS, TMetS, and MMetS blood glucose area-under-the-curve (AUC) was significantly higher than Lean, with TMetS and MMetS elevated above FMetS (**Figure 3.1D**). Elevated fasting blood glucose clinically defines type 2 diabetes. Consistent with MetS and type 2 diabetes MMetS fasting glucose was elevated above Lean, while FMetS and TMetS strongly trended toward an increase (**Figure 3.1C**).

Insulin resistance. To assess insulin resistance, plasma insulin was measured after overnight fast and during the IVGTT. MetS exhibited significantly higher insulin at every measured time point of the IVGTT following glucose bolus compared to Lean (**Figure 3.1B**). Further indicating insulin resistance, FMetS, TMetS, and MMetS plasma

insulin levels were significantly higher compared to Lean as measured by the integral (**Figure 3.1E**). FMetS, TMetS, and MMetS demonstrated elevated homeostasis model assessment (HOMA) index compared to Lean (**Figure 3.1F**). In the early stages of type 2 diabetes, pancreatic β -cells increase insulin production as a compensatory mechanism for reduced insulin sensitivity of peripheral tissues. Importantly, FMetS, TMetS, and MMetS swine demonstrated increased percent insulin-positive area compared to Lean in histological analysis of pancreatic tissue (**Figure 3.1 G,H,I**), suggesting a compensatory pancreatic β -cell response due to peripheral insulin resistance. Adipose tissue insulin resistance (Adipo-IR), calculated by the product of fasting insulin resistance (pM) and free fatty acids (mM), was elevated in FMetS, TMetS, and MMetS compared to Lean (**Table 3.1**) and correlated to NASH scores ($r = 0.53$, $p < 0.05$), but not CAD ($r = 0.42$, NS).

Serum fatty acid methyl esters and unbound free fatty acids. Total serum monounsaturated fatty acids (TOTM), polyunsaturated fatty acids, and unbound free fatty acids were quantified. TOTM increased with severity of MetS (**Figure 3.2A**; i.e. Lean < FMetS < TMetS < MMetS), whereas PUFA decreased with severity of MetS (**Figure 3.2B**). As such, TOTM:PUFA ratio increased with severity of MetS (**Figure 3.2C**). FFA were elevated in FMetS and MMetS compared to Lean, but not TMetS due to variability (**Figure 3.2D**).

Atherosclerosis in Ossabaw swine. The severity of atherosclerosis in MMetS swine was grossly apparent in the coronary arteries by “pearly atherosclerotic lesions” visible on the exterior of the heart (**Figure 3.3A**), which was a novel and profound finding. CAD was quantitatively assessed in the coronary arteries *in vivo* using intravascular ultrasound (IVUS). Three segments (proximal, intermediate, and distal) of the left anterior descending artery (LAD) (**Figure 3.3B**) were analyzed for CAD burden. A representative IVUS image from within the circumflex artery (CFX) shows the arterial

lumen and the anatomy of a complex lesion (**Figure 3.3C**). IVUS was used to measure plaque coverage of the LAD wall, percent lumen stenosis in the CFX, and plaque composition (e.g. calcified lesions). Diffuse CAD, as measured by percent circumferential wall coverage (defined in **Figure 3.3C**), was observed in TMetS and, to a much greater extent, in MMetS compared to Lean (**Figure 3.3D**). Amazingly, FMetS CAD was similar to Lean, despite FMetS having all of the 6 components of MetS, except dyslipidemia. Significant stenosis (**Figure 3.3F**) and calcifications (**Figure 3.3E**) were only observed in MMetS swine, which are novel findings in a swine model of MetS.

In patients with MetS, coronary atherosclerosis has a propensity for diffuse distribution, calcifications (e.g. MMetS in **Figure 3.3**), increased vulnerability, and cellularity (202). The stability of an atherosclerotic plaque can be attributed to many factors, including the collagen content of the plaque. Diffuse MMetS plaques contained a substantial lipid core (**Figure 3.4C**) and significantly less collagen as a percent of total plaque area compared to TMetS (**Figure 3.4F**), while the collagen content of the arterial media in Lean, TMetS, and MMetS remained unchanged (**Figure 3.4F**). Cellularity of the atherosclerotic lesions was less in MMetS compared to TMetS (**Figure 3.4J**) and MMetS, potentially due to the greater lipid content in MMetS (**Figure 3.4K**).

Fatty acid methyl esters and fatty acid metabolism in metabolic syndrome, coronary artery disease, and non-alcoholic steatohepatitis. FMetS, TMetS, and MMetS developed insulin resistant MetS with FMetS normolipidemic, TMetS dyslipidemic, and MMetS severely dyslipidemic (**Table 3.1**; **Figure 3.1**). This provided a unique opportunity to determine the relative importance of dyslipidemia within the complex MetS milieu in the development of CAD and NASH. FAME were measured in serum and from liver biopsies. Each individually quantified FAME (**Table 3.2**) and groupings of FAME (**Table 3.3**) were correlated to CAD along the length of the artery and to NASH scores. Saturated FAME 14:0 directly correlated to CAD and NASH (**Table 3.2**). Individual

mono-unsaturated fatty acids tended to directly correlate with severity of CAD and NASH, while individual PUFA tended to negatively correlate to CAD and NASH (**Table 3.2**). TOTM and the ratio of TOTM to PUFA strongly and directly correlated with diffuse CAD and NASH (**Table 3.3**). PUFA, in particular n-6 PUFA (**Table 3.3**), demonstrated strong, inverse correlations with CAD and NASH (**Table 3.3**). FFA did not correlate to CAD or NASH (**Table 3.3**). Fatty acid $\Delta 5$, $\Delta 6$, and $\Delta 9$ convertase indices (20:4n-6/20:3n-6, 18:3n-6/18:2n-6, and 16:1n-7/16:0, respectively), elongase index (18:0/16:0), lipogenic index (16:0/18:2n-6), and microsomal stearyl-CoA desaturase1 (SCD1; 18:1/18:0) from both serum and liver tissue samples significantly correlated to NASH scores (**Table 3.4**).

Predictive dyslipidemia, non-alcoholic steatohepatitis, and coronary artery disease relationship. Histological liver NASH scores were elevated in TMetS compared to FMetS and Lean, while MMetS demonstrated strikingly severe NASH compared to all groups (**Figure 3.5A**, as previously reported (7)). The relationship of NASH with CAD was shown by the strong direct correlation (**Figure 3.5B**). LDL-gram years had phenomenal predictive ability as to the severity of CAD as well as NASH (**Figure 3.5 C&D**).

Discussion

The most significant and novel finding was that dyslipidemia is the major component of the complex MetS that elicits occlusive, complex, and calcified atherosclerotic lesions and NASH. In the rare, naturally occurring Ossabaw swine breed that is genetically predisposed to obesity, feeding hypercaloric diets high in mixed fatty acids or high in trans fatty acids (MMetS and TMetS, respectively), high cholesterol and fructose, we produced MetS characterized by obesity, increased total cholesterol, increased LDL, increased LDL:HDL ratio, increased triglycerides, glucose intolerance, insulin resistance, and hypertension. Importantly, high fructose diet was sufficient to induce MetS with all these features, except dyslipidemia (FMetS) and no CAD or NASH. Additional important findings in this study include the strong associations between specific FAME and groups of FAME with diffuse CAD and NASH and associations of fatty acid metabolism indices and Adipo-IR to NASH.

MMetS Ossabaw swine developed diffuse atherosclerosis (**Figure 3.3**), a hallmark of patients with diabetes (80;204;205), and significantly elevated fasting blood glucose (**Figure 3.1C**), which defines diabetes. Additionally, MMetS Ossabaw swine were severely insulin resistant and glucose intolerant. Insulin resistance was defined by 1) prolonged insulin and glucose response to intravenous glucose load (**Figure 3.1 D&E**) and 2) fasting HOMA values (**Figure 3.1F**). Importantly, HOMA values in all MetS swine were directly comparable to values seen in patients with type 2 diabetes (181;206-208). Percent insulin-positive area in the pancreas was increased in all MetS swine (**Figure 3.1I**), indicating β -cell hypertrophy, again consistent with the pathogenesis of type 2 diabetes in humans (reviewed elsewhere (209)). Thus, MMetS swine progress to overt type 2 diabetes induced by excess atherogenic diet, providing future opportunity for high-throughput studies of type 2 diabetes in a large animal model of MetS, NASH, and CAD.

There is significant evidence that patients with the constellation of risk factors that manifest MetS have a much higher incidence of CAD and NASH (39). It is difficult, by definition, to separate the individual influence of specific MetS risk components on CAD and NASH in patients with MetS. We used the only animal model of MetS, NASH, and CAD to focus on and eliminate dyslipidemia from the MetS milieu. We also point out that “dyslipidemia” is often defined as the combination of dyslipoproteinemia and hypertriglyceridemia (210). Hypercaloric, high fructose fed swine (FMetS) developed MetS defined by insulin resistance, glucose intolerance, hypertension, and obesity without dyslipidemia (measured as increased total cholesterol, LDL, and triglycerides; **Table 3.1, Figure 3.1**) and without increases in CAD or NASH compared to Lean (CAD, **Figure 3.2**; NASH, **Figure 3.5** and as previously reported (7)). Supplementation with partially hydrogenated soybean oil and cholesterol, in addition to fructose, (TMetS) led to MetS comparable to FMetS, while the TMetS had the additional factor of dyslipidemia (**Table 3.1, Figure 3.1**). Dyslipidemic TMetS developed diffuse CAD, no NASH, and only mildly fatty liver (CAD, **Figures 3** and **4**; NASH, **Figure 3.5** as previously reported (7)). Mixed source fat, cholesterol, and fructose fed MMetS developed overt type 2 diabetes, defined by elevated fasting blood glucose, and severe dyslipidemia (**Table 3.1, Figure 3.1** and **5**). MMetS had advanced stenotic CAD (**Figures 3** and **4**) and severe NASH (**Figure 3.5** and as previously published by Lee et al. (7)). It was not the intent of this study to isolate the effects of specific diet components on MetS, CAD, and NASH, but to maximize the MMetS phenotype and investigate potential phenotypic differences that may provide a physiological mechanism for MetS, CAD, and NASH. Thus, we cannot discount that minor changes in the protein source and nutrient content (increased casein and mildly reduced choline) may have influenced the results; however, the direct association of progressive dyslipidemia (i.e. Lean < FMetS < TMetS < MMetS) with CAD

and NASH severity provides compelling evidence for the significant contribution of dyslipidemia to the development of CAD and NASH in Ossabaw swine.

Total serum free fatty acids (FFA) did not correlate with the extent of CAD or NASH (**Table 3.3**). These results are consistent with a recent study that revealed strong associations of FFA with MetS in cross-sectional analysis, while no relationship was found in longitudinal analysis, thus supporting the overall conclusion that FFA are not causative in MetS or diabetes (211). Our powerful study design allowed clear dissection of potential FFA effects on CAD and NASH without the confounding effects of dyslipidemia (i.e. FMetS). Thus, this is the first report that increased FFA per se are not a primary factor eliciting CAD and NASH within the MetS milieu.

Total FFA did not sufficiently predict CAD or NASH, so individual (**Table 3.2**) and grouped fatty acid methyl esters (FAME; **Figure 3.2** and **Table 3.3**) were investigated. Individual monounsaturated fatty acids (MUFA) had the most predictive power with serum palmitoleic acid (16:1n7), heptadecaenoic acid (17:1n7), vaccinate acid (18:1n7), and oleic acid (18:1n9) all directly correlated to diffuse CAD and all four of these MUFA derived from liver tissue (liver) directly correlated to NASH (**Table 3.2**). It follows that total MUFA (TOTM) also directly correlated to the extent of diffuse CAD and severity of NASH (**Table 3.3**). Linoleic acid (18:2n-6), an essential polyunsaturated fatty acid (PUFA), negatively correlated to diffuse CAD and NASH (serum and liver derived; **Table 3.2**). Total PUFA also negatively correlated to CAD and NASH (**Table 3.3**). The powerful ability of individual and grouped FAME to predict the extent of CAD strongly resonates with the recent Atherosclerosis Risk in Communities (ARIC) study which found directionally identical associations of palmitoleic acid, oleic acid, TOTM, linoleic acid, and PUFA to incidence of heart failure in humans (212). The ARIC study, however, did not address heptadecaenoic and vaccinate acid associations with CAD or any FAME associations with NASH. Thus, this is the first report addressing the predictive power of

individual and grouped FAME, derived from both serum and liver tissue, to the degree of NASH.

Fatty acid synthase and *de novo* lipogenesis are central to fatty acid metabolism and substantially increased in patients with NAFLD (213;214). The progression of *de novo* lipogenesis is mediated by several enzymes including elongase that have a strong, inverse association with insulin resistance and obesity (215;216). Ratios of product and precursor FAME from liver and serum samples were used to estimate *de novo* lipogenesis (lipogenic index; 16:0/18:2n-6) and elongase activity (18:0/16:0). Liver sample lipogenic index directly correlated with NASH score, as previously reported in human NAFLD (217), but serum sample lipogenic index was inversely correlated with NASH score (**Table 3.4**), suggesting increased liver and decreased adipose lipogenesis. These findings are consistent with previous reports that high fructose diet shifts primary lipogenesis from adipose to liver (218), as well as reports that adipose and liver fatty acid synthase mRNA expression are almost reciprocal (219). Conversely, liver sample elongase activity inversely correlated with NASH, while serum elongase activity positively correlated with NASH (**Table 3.4**). Taken together, we speculate these findings support a primary role of fructose in NASH, whereby *de novo* lipogenesis is increased in the liver in effort to reduce hepatic damage from oxidized fatty acids, despite elevated dietary lipid intake. Additionally, the relatively weak predictive ability of Adipo-IR in the development of NASH and its absolute inability to predict CAD (**Table 3.1**), especially compared to strongly determinant LDL-gram years (**Figure 3.5 C&D**), suggest peripheral insulin resistance does not play a primary role in the progression of NASH and development of CAD in MetS.

International studies have clearly demonstrated that long-term elevations in LDL levels are associated with drastically increased coronary mortality rates (reviewed elsewhere (220)). However, reduced LDL levels through statin treatment over a period of

five years has resulted in relatively low reduction in incidence of cardiac death (221). It has been recently put forth that integrated measure of high LDL exposure may be more predictive than static measures (222), similar to the utility of pack-years in quantifying a patient's life-time exposure to cigarette smoke (223). Here we report a compelling, direct association between NASH and CAD severity (**Figure 3.5B**), corresponding to liver cirrhosis trials finding CAD as the leading cause of death in patients with NASH (64). As such, the immensely predictive power of LDL gram-years for the severity of CAD and NASH (**Figure 3.5 C&D**) are the first of such measurements in a large animal model of CAD and/or NASH, and may provide further insight into the primary driving mechanism of CAD and NASH.

Until now, no animal model of MetS and type 2 diabetes that naturally develops occlusive atherosclerosis and NASH has been available for clinical studies involving complete and complex metabolic disease. For example, as a result of the inability to generate significant native CAD, no pre-clinical study of stent efficacy has ever involved stent placement in an artery with severe native CAD. It is entirely possible that recent questions regarding the safety of drug-eluting stents (99;101) could have been avoided had a more appropriate model of CAD been available. Additionally, while extensive studies of NAFLD have been completed in rodents, there has been no opportunity to directly investigate NASH in any model, until the groundbreaking report by Lee et al. (7), let alone a large animal model allowing longitudinal studies with serial blood sampling and liver biopsies. Our unique and powerful study design allowed us to be the first to elucidate 1) the absolute requirement of dyslipidemia in the development of macrovascular CAD within MetS, 2) the most severe and advanced CAD in any current animal model of MetS and type 2 diabetes, 3) strong associations between individual and group FAME and CAD and NASH that concur with and expand upon important human clinical studies, 4) no independent association between total FFA to CAD and

NASH without the confounding influence of concomitant dyslipidemia, and 5) phenomenally predictive integrative LDL exposure (LDL gram-years) for CAD and NASH.

Methods

Animal care and use. All protocols involving animals were approved by an Institutional Animal Care and Use Committee and complied fully with standards (175;176). Forty-five mixed gender Ossabaw swine at the age of ten to fifteen months (adult) were assigned to four diet groups for 22-24 weeks. Lean control swine (Lean, N=10) were fed standard chow. In all MetS groups, high calorie (~2-fold increase above Lean) feeding was necessary to induce components of MetS. The fructose (FMetS; N=9) was fed a high fructose (20% kcal) diet (7). The trans fatty acid MetS (TMetS, N=9) group was fed a high fat/fructose/2% cholesterol (w/w) atherogenic diet (hydrogenated soybean oil; 56% trans fatty acid) (6;7;29). The mixed fat (MMetS, N=8) was fed a high fat/fructose/2% cholesterol (w/w) atherogenic diet (mixture of lard, hydrogenated soybean oil, and hydrogenated coconut oil) (7). Pigs in FMetS and MMetS groups were the same as those used by Lee et al. (7).

Intravenous glucose tolerance test. IVGTT was performed between weeks 22 and 24 of the study as previously described by our lab (3;4;9;29). Briefly, conscious swine acclimatized to low-stress restraint in a sling were fasted overnight and baseline blood samples were obtained. Glucose (1g/kg body weight; i.v.) was administered and timed blood samples were collected.

Plasma lipid assays. Venous blood samples were obtained following overnight fasting and analyzed for triglyceride and total cholesterol [fractionated into high density lipoprotein (HDL) and low density lipoprotein (LDL) components]. Apolipoprotein-B-containing lipoproteins were precipitated with heparin-MnCl₂ and the supernatant was assayed to determine cholesterol in lipoprotein fractions (3). LDL was calculated from the Friedewald equation: $LDL = \text{total cholesterol} - HDL - (\text{triglyceride} \div 5)$.

Assessment of coronary artery disease. IVUS pullbacks performed at the end of the study were used to assess native atheroma and percent circumferential wall

coverage was calculated similar to previous reports (3;6;20;29). Severity of native atheroma was also quantified as percent stenosis calculated as (plaque area ÷ total lumen area) x 100%. To assess diffuse atheroma, three segments were defined as proximal (0-10 mm from the LAD/LCX bifurcation), intermediate (20-30 mm from the LAD/LCX bifurcation), and distal (0-10 mm from the most distal part of the IVUS pullback towards the LAD/LCX bifurcation). Calcified lesions defined by signal dropout peripheral to the IVUS imaging transducer were assessed along the length of the entire artery.

Assessment of collagen content and non-alcoholic steatohepatitis. After fixation by immersion in formalin, tissues were routinely processed and paraffin embedded for standard histological analysis (11;29). NASH score was determined on liver samples and included macrovesicular steatosis, microvesicular steatosis, hepatocyte ballooning, Kupffer cell vacuoles, Kupffer cell fat, inflammation, and fibrosis characteristics assessed blindly by a histopathologist.

Assessment of insulin-positive area. Pancreas tissue was sectioned and imaged as outlined in above section. The 5- μ m pancreas sections were mounted on glass slides and assessed for insulin-positive area using mouse anti-insulin primary antibody (Sigma #I2018; a generous gift from Dr. Deborah Thurmond, Indiana University Purdue University Indianapolis) and mouse biotinylated secondary antibody (Vectastain Elite ABC Kit PK-6102). DAB (Sigma Fast D-4168) was used for visualization as previously described (9). Sections were counterstained with Mayer's hematoxylin.

Fatty acid methyl esters. The analysis of FAME in serum and live tissues was conducted by the gas liquid chromatography, as previously described (7). FAME were identified based on the retention time determined from authentic standards (Nu-Chek-Prep Inc., Elysian, MN), and results are presented as area percentages. FMetS and MMetS FAME values were a subset of data from Lee et al. (7) for which CAD data was obtained.

Statistical analysis. One-way or two-way analysis of variance with Student-Newman-Kuels or Bonferroni post-hoc analysis, as appropriate, were performed using commercially available software (Prism 4.0) when comparing multiple groups. Independent t-test was used for comparing just two groups. In all tests, $p < 0.05$ was the criterion for statistical significance. Unless otherwise noted, the following symbols were used: *, $p < 0.05$ compared to Lean; **, $p < 0.05$ compared to Lean and FMetS; ***, $p < 0.05$ compared to all other groups.

Acknowledgements

We thank Jim P. Byrd, Indiana University School of Medicine, for his expert histological imaging; Dr. Kara Standley, Indiana University Wells Center for Diabetes Research, for feedback on an early outline of the manuscript; and Dr. Johnathan D. Tune for insightful comments on the study design. We recognize the steadfast efforts of summer interns Ashley Burdex, Tamayi Bwititti, and David Whitney. This work was supported by the National Institutes of Health grants HL062552 and RR013223 and an Innovation Award from the American Diabetes Association to M.S., the Purdue-Indiana University Comparative Medicine Program, and the Fortune-Fry Ultrasound Research Fund of the Department of Cellular & Integrative Physiology at Indiana University School of Medicine. K.S was supported by postdoctoral training grant T32 HL079995 to Dr. Keith L. March. A.B. and T.B. were supported by short-term minority training grant T35 HL007802 to M.S. J.M.E. and Z.P.N. were the recipients of a Translational Research Fellowship from the Indiana University School of Medicine and Z.P.N. was the recipient of a Translational Fellowship from NIH UL1 RR025761.

Table 3.1

	Lean	FMetS	TMetS	MMetS	Significance
Body Weight (kg)	51 ± 3	94 ± 6	91 ± 6	87 ± 13	Lean < FMetS, TMetS, MMetS
Heart rate (beats/min)	65 ± 1	87 ± 4	94 ± 2	101 ± 3	Lean < FMetS, TMetS < MMetS
Total cholesterol (mg/dL)	80 ± 4	60 ± 4	373 ± 40	666 ± 80	Lean, FMetS < TMetS < MMetS
HDL (mg/dL)	40 ± 3	25 ± 5	85 ± 6	90 ± 9	FMetS < Lean < TMetS, MMetS
LDL (mg/dL)	35 ± 2	35 ± 3	281 ± 35	553 ± 73	Lean, FMetS < TMetS < MMetS
LDL:HDL	0.9 ± 0.1	2.5 ± 0.7	3.2 ± 0.2	6.1 ± 0.5	Lean < FMetS < TMetS < MMetS
Triglycerides (mg/dL)	22 ± 4	30 ± 2	37 ± 2	120 ± 24	Lean, FMetS < TMetS < MMetS
Mean arterial pressure (mmHg)	94 ± 1	110 ± 5	131 ± 3	140 ± 4	Lean < FMetS < TMetS, MMetS
Adipo-IR	40 ± 9	139 ± 28	142 ± 24	149 ± 30	Lean < FMetS, TMetS, MMetS

Table 3.1 Phenotypic characteristics of Lean, TMetS, and MMetS Ossabaw swine at the end of the study. Statistical differences between groups are indicated in the right column. Adipo-IR, adipose tissue insulin resistance.

Table 3.2

FAME	CAD (Percent wall coverage)						NASH			
	Proximal		Intermediate		Distal		Serum		Liver	
	r	p	r	p	r	p	r	p	r	p
14:0	0.65	*	0.81	*	0.64	*	0.56	*	0.72	*
16:1t	0.44	*	0.49	*	0.50	*	0.75	*	0.18	NS
16:1n7	0.79	*	0.86	*	0.81	*	-0.22	NS	0.81	*
17:1n7	0.64	*	0.68	*	0.51	*	0.32	NS	0.83	*
18:0	-0.53	*	-0.52	*	-0.50	*	-0.85	*	-0.90	*
18:1n9	0.65	*	0.59	*	0.53	*	0.48	*	0.85	*
18:1n7	0.68	*	0.64	*	0.63	*	0.80	*	0.85	*
18:2n-6	-0.69	*	-0.64	*	-0.50	*	-0.75	*	-0.89	*

Table 3.2 Fatty acid methyl esters (FAME) predict coronary artery disease (CAD) and non-alcoholic steatohepatitis (NASH) in Ossabaw swine. Serum FAME correlations to proximal, intermediate, and distal CAD and serum or liver tissue FAME correlations to modified NASH score are reported as indicated. Correlations statistically significant at $p < 0.05$ are indicated with asterisks; NS = non-significant. FAME showing no correlations to both CAD and NASH were 15:0, 16:0, 17:0, 18:1t, 18:1, 18:3n6, 18:3n3, 20:1n9, 20:2n6, 20:3n6, 20:4n6, 20:3n3, 20:5n3, 22:4n6, 22:5n3, and 22:6n3 and shown in Supplemental Table 3.1.

Table 3.3

FAME	CAD (Percent wall coverage)						NASH			
	Proximal		Intermediate		Distal		Serum		Liver	
	r	p	r	p	r	p	r	p	r	p
Total FFA	0.33	NS	NC		0.35	NS	0.20	NS	NC	
TOTM	0.66	*	0.62	*	0.58	*	0.78	*	0.86	*
PUFA	-0.73	*	-0.69	*	-0.60	*	-0.75	*	-0.88	*
n-6 PUFA	-0.74	*	-0.70	*	-0.61	*	-0.73	*	-0.88	*
TOTS/TOTM	-0.51	*	-0.46	*	-0.45	NS	-0.72	*	-0.82	*
TOTM/PUFA	0.79	*	0.76	*	0.66	*	0.85	*	0.88	*
TOTS/PUFA	0.65	*	0.63	*	0.36	NS	0.51	*	0.39	*

Table 3.3 Fatty acid methyl esters (FAME) groups predict coronary artery disease (CAD) and non-alcoholic steatohepatitis (NASH) in Ossabaw swine. Serum FAME group correlations to proximal, intermediate, and distal CAD and serum or liver tissue FAME group correlations to modified NASH score are reported as indicated. Correlations statistically significant at $p < 0.05$ are indicated with asterisks; NS = non-significant; NC = not completed. FAME groups showing no correlations to both CAD and NASH were 16:1t + 18:1t, TOTS, TOTM + PUFA, n-3 PUFA, n-6 LC, n-3 LC, TOTS/(TOTM + PUFA), n-6 LC/n-3 LC, and n-6/n-3 and shown in Supplemental Table 3.2. Abbreviations: FFA, free fatty acids (FA), TOTS, total saturated FA; TOTM, total monounsaturated FA; PUFA, total polyunsaturated FA; n-6, unsaturation at carbon 6; n-3, unsaturation at carbon 3; LC, long chain FA.

Table 3.4

Enzyme function index	Serum		Liver	
	r	p	r	p
$\Delta 5$ desaturase (20:4n-6/20:3n-6)	-0.49	*	-0.61	*
$\Delta 6$ desaturase (18:3n-6/18:2n-6)	0.44	*	0.47	*
$\Delta 9$ desaturase (16:1n-7/16:0)	0.71	*	0.85	*
Elongase (18:0/16:0)	0.74	*	-0.83	*
Lipogenic index (16:0/18:2n-6)	-0.75	*	0.62	*
stearoyl-CoA desaturase 1 (18:1/18:0)	0.75	*	0.74	*

Table 3.4 Liver enzyme function predicts non-alcoholic steatohepatitis (NASH) in Ossabaw swine. Liver enzyme function indices derived from serum or liver FAME are correlated to NASH score. Correlations statistically significant at $p < 0.05$ are indicated with asterisks.

Figure Legends

Figure 3.1 Insulin resistance and glucose intolerance. Combined MetS groups (solid) blood glucose (A) and insulin (B) remained elevated compared to Lean (dotted) for all time points during the IVGTT. C Fasting blood glucose concentrations were elevated in MMetS compared to Lean, while FMetS and TMetS were not significantly elevated. D Integral (area-under-curve) of plasma glucose concentrations during IVGTT were elevated in FMetS, TMetS, and MMetS compared to Lean, while TMetS and MMetS were also increased above FMetS. E Integral of plasma insulin concentrations during IVGTT were elevated in FMetS, TMetS, and MMetS compared to Lean. F HOMA index values were elevated in FMetS, TMetS, and MMetS compared to Lean. Representative pancreatic sections from Lean (G) and MetS (H) showing insulin staining (arrow). I Positive insulin staining area as a percent of total pancreas tissue area is increased in FMetS, TMetS, and MMetS compared to Lean.

Figure 3.2 Elevated serum fatty acid methyl esters and free fatty acids in metabolic syndrome. A Serum total mono-unsaturated FAME (TOTM) increased with severity of MetS. B Serum poly-unsaturated FAME (PUFA) decrease with severity of MetS. C The ratio between TOTM and PUFA (TOTM:PUFA) increased with severity of MetS. D Serum free fatty acids are increased in FMetS and MMetS compared to Lean, while TMetS was not different compared to Lean.

Figure 3.3 Coronary artery disease is increased with severity of metabolic syndrome. A Representative heart taken from a MMetS pig. Inset grossly demonstrates severity of coronary atheroma in arteries on left and right of the image. B Representative angiography image with labeled LAD and LCX arteries, and proximal, intermediate, and

distal segments. **C** Sample IVUS image demonstrating complex atheroma and method of quantifying % wall coverage (**D&F**). **D** Diffuse atheroma of the LAD is present in MMetS and in TMetS to a much lesser extent. **E** Calcification is quantified as the percent of artery segments with calcification present. **F** Percent stenosis of the LCX illustrates massive atheroma load in the MMetS.

Figure 3.4 Atheromous plaques contain less collagen with increased severity of metabolic syndrome. **A** Representative image of trichrome staining in Lean right coronary artery. **B&D** Representative images of trichrome staining in TMetS. **C&E** Representative images of trichrome staining in MMetS. **F** (Upper) Coronary media collagen, quantified as percent of total medial area, is not different between groups. (Lower) Percent neointima collagen is decreased in MMetS compared to TMetS. **G** Representative image of hematoxylin and eosin (H&E) staining in MMetS illustrating calcifications. **Inset** Magnification on calcified region of artery wall (**e**). **H** Representative image of H&E staining in TMetS. **I** Representative image of H&E staining in MMetS. **J** Plaque cellularity, quantified as cells per unit area, decreased in MMetS compared to TMetS. **K** Representative image of Oil Red O illustrates massive amount of lipid accumulation in MMetS plaque. *, $p < 0.05$ compared to TMetS. a, adventitia; b, media; c, intima; d, lumen; e, calcification.

Figure 3.5 LDL gram-years predicts strongly correlated coronary artery disease and non-alcoholic steatohepatitis. **A** TMeTS and MMetS NASH are increased compared to FMetS and Lean, with MMetS NASH greater than TMetS. **B** NASH directly correlates to diffuse coronary artery disease. **C** and **D** LDL gram-years is strongly predictive of CAD and NASH.

Figure 3.1

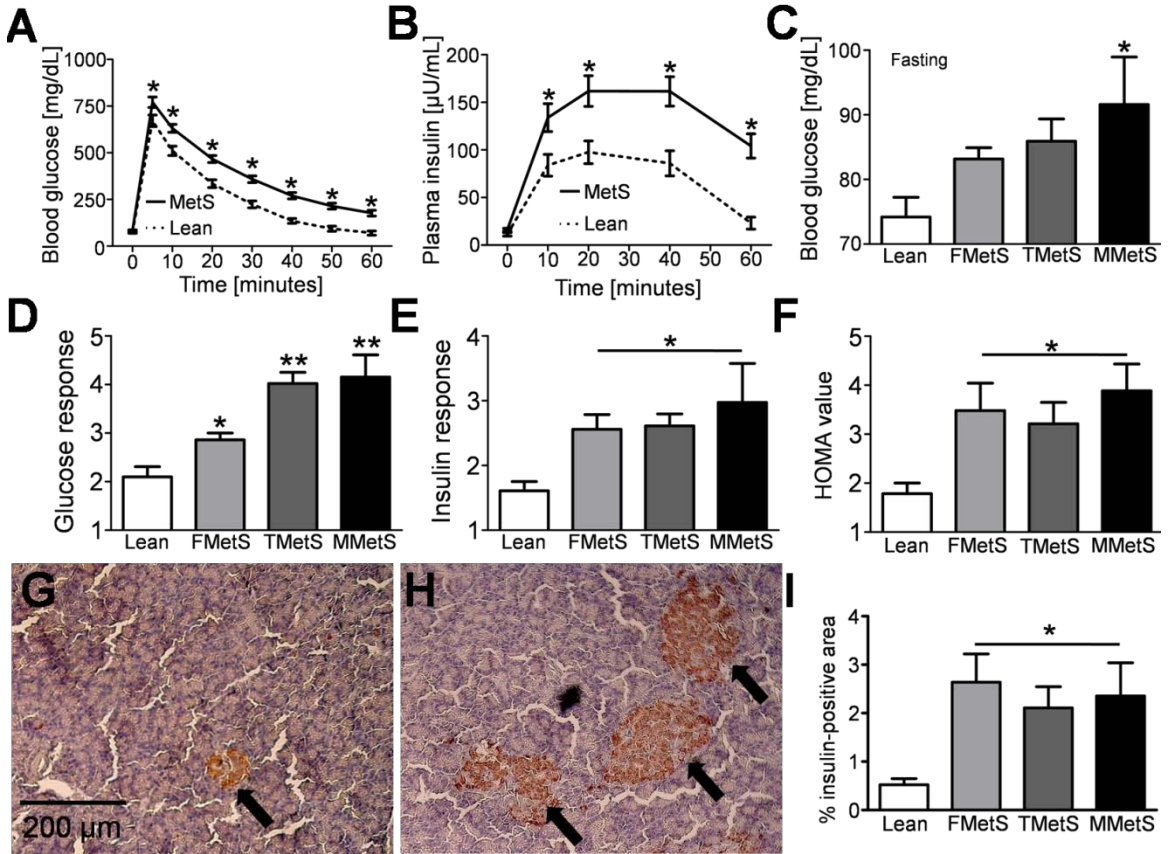


Figure 3.2

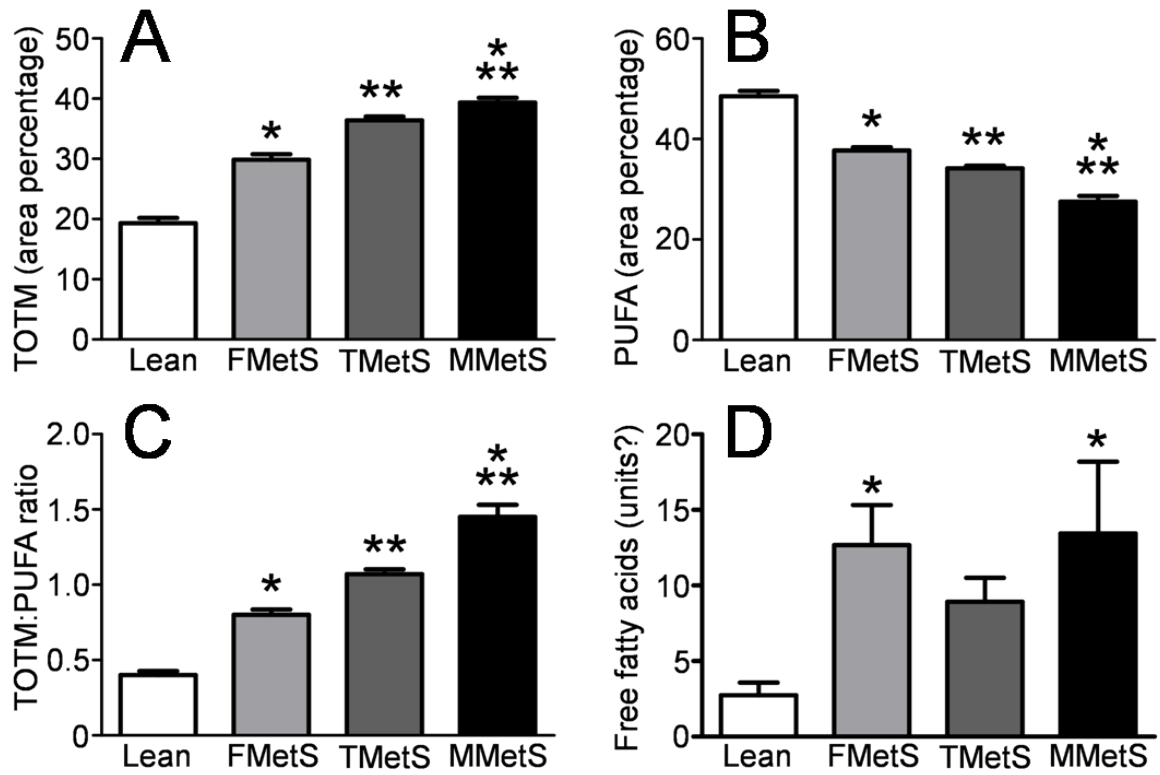


Figure 3.3

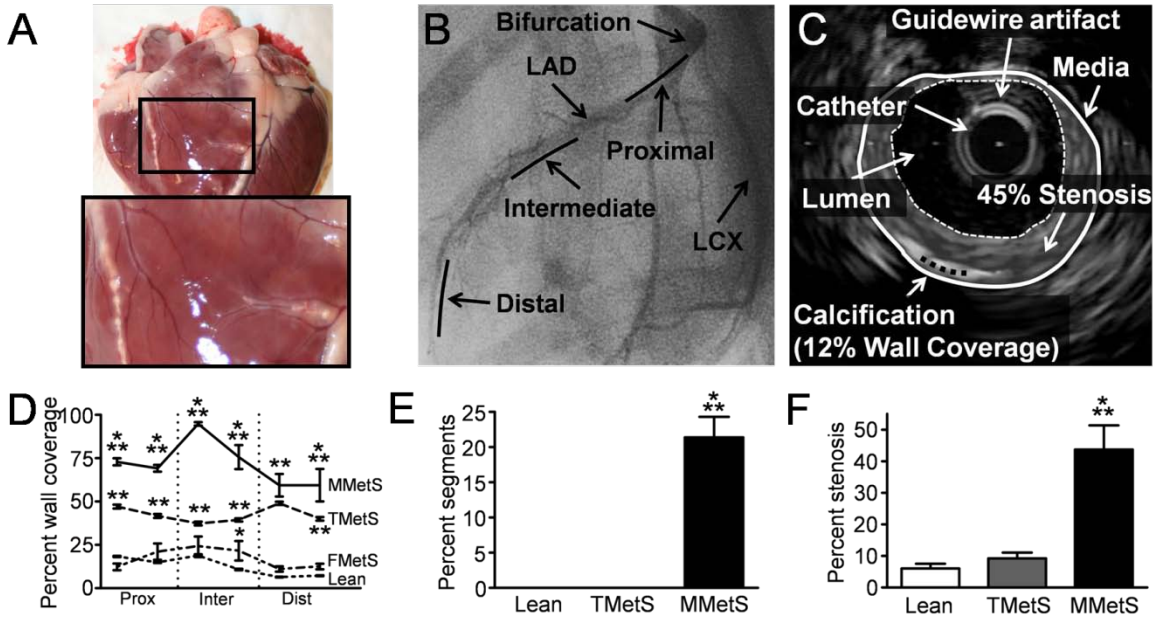


Figure 3.4

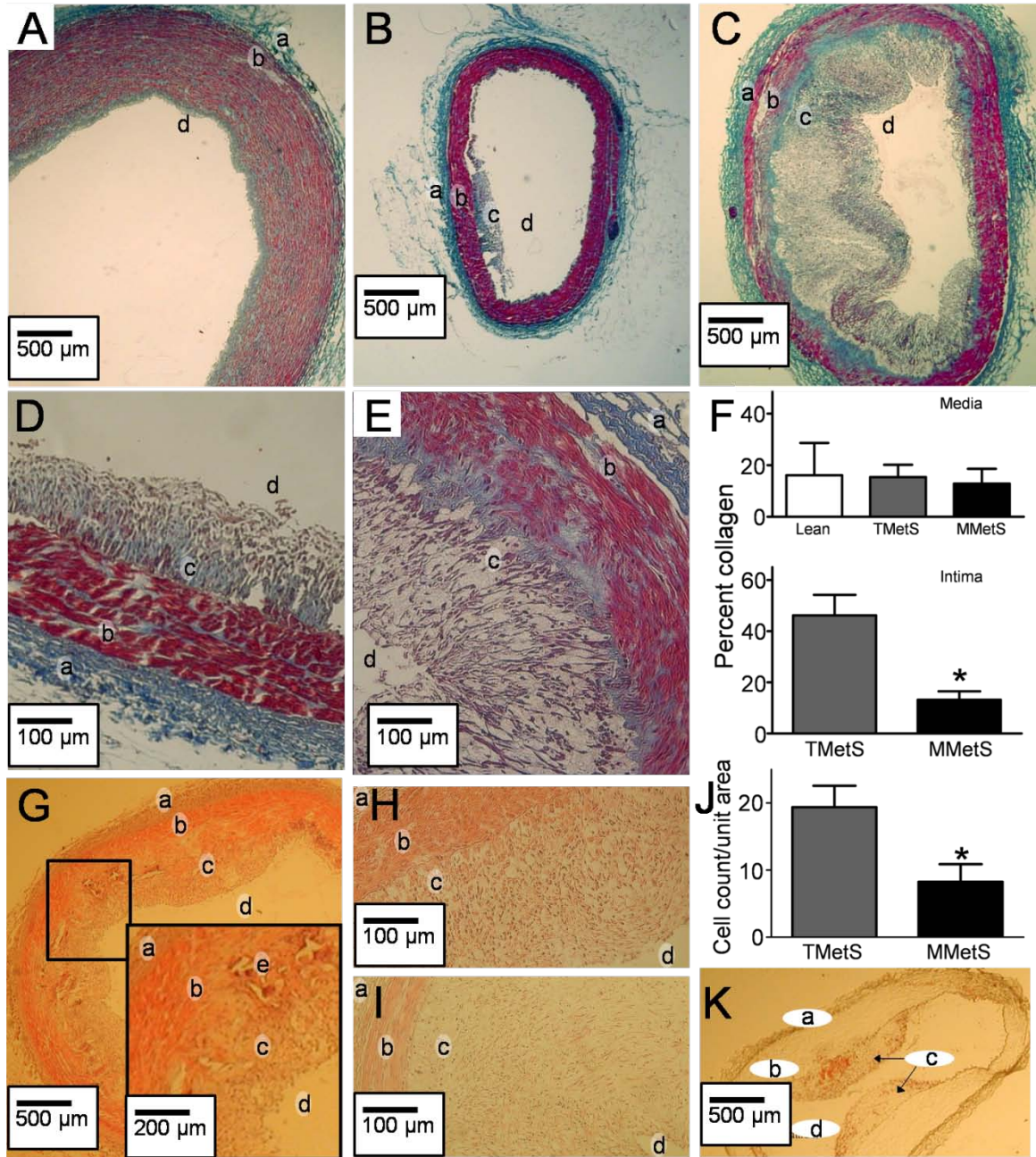
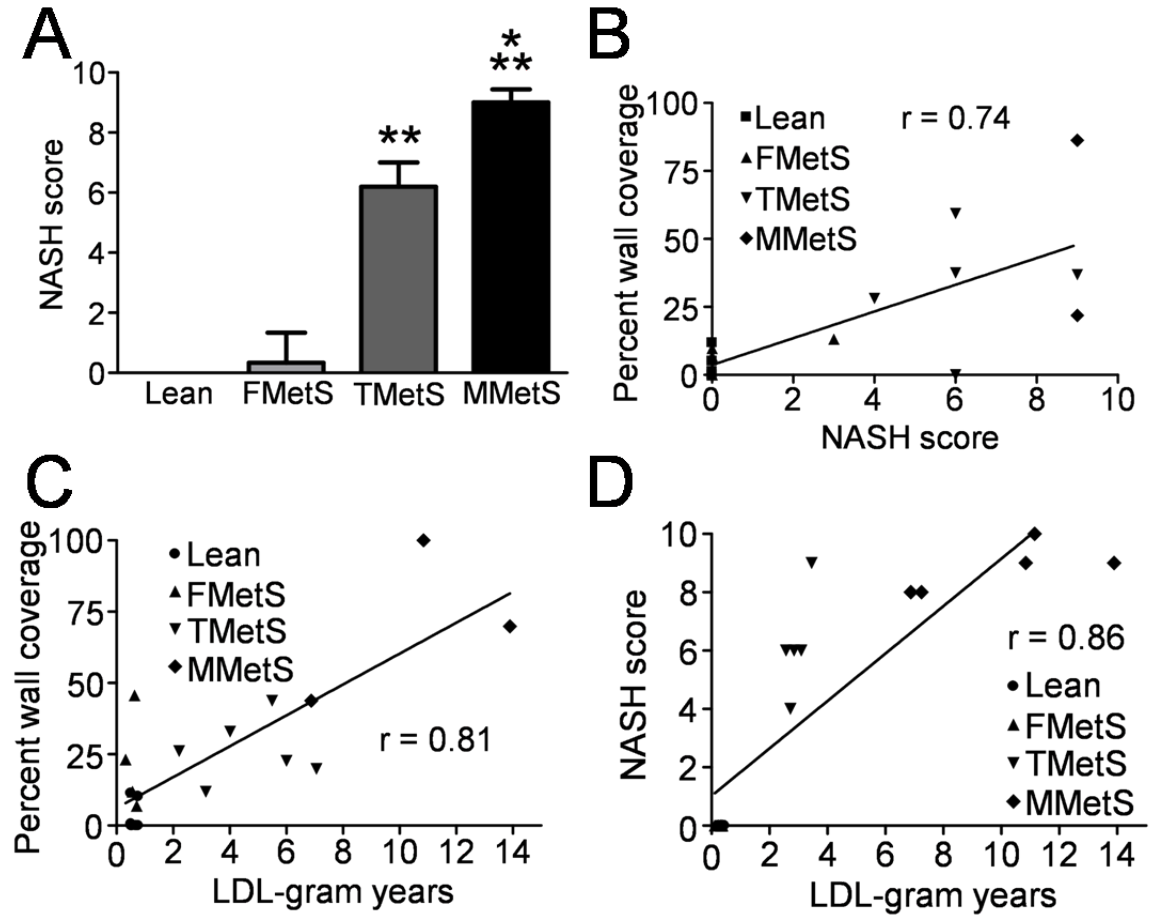


Figure 3.5



Chapter 4

Exercise training decreases store-operated Ca²⁺ entry associated with metabolic syndrome and coronary atherosclerosis

Jason M. Edwards*¹, Zachary P. Neeb*¹, Mouhamad A. Alloosh¹, Xin Long¹, Ian N. Bratz², Cassandra R. Peller¹, James P. Byrd¹, Sanjay Kumar¹, Alexander G. Obukhov¹,
Michael Sturek¹

¹Department of Cellular and Integrative Physiology, Indiana University School of Medicine

²Department of Integrative Medical Sciences, Northeastern Ohio Universities Colleges of Medicine

*Authors contributed equally to the manuscript.

Abstract

Aim. Stenting attenuates restenosis, but accelerated coronary artery disease (CAD) adjacent to the stent (peri-stent CAD) remains a concern in metabolic syndrome (MetS). Smooth muscle cell proliferation, a major mechanism of CAD, is mediated partly by myoplasmic Ca^{2+} dysregulation and store-operated Ca^{2+} entry (SOCE) via canonical transient receptor potential 1 (TRPC1) channels is proposed to play a key role. Exercise is known to prevent Ca^{2+} dysregulation in CAD. We tested the hypothesis that MetS increases SOCE and peri-stent CAD and exercise attenuates these events.

Methods. Groups (N=9 pigs each) were 1) healthy lean Ossabaw swine fed standard chow, 2) excess calorie atherogenic diet fed (MetS), and 3) aerobically exercise trained starting after 50 weeks of development of MetS (XMetS). Bare metal stents were placed after 54 weeks on diets and CAD and SOCE were assessed 4 weeks later. Coronary cells were dispersed proximal to the stent (peri-stent) and non-stented segments and fura-2 fluorescence assessed SOCE, which was verified by block by Ni^{2+} and insensitivity to nifedipine.

Results. XMetS pigs had increased physical work capacity and decreased LDL/HDL ($p < 0.05$), but no attenuation of robust insulin resistance, glucose intolerance, hypertriglyceridemia, or hypertension. CAD was greater in peri-stented vs. non-stented artery segments. MetS had the greatest CAD, SOCE, and TRPC1 and STIM1 mRNA and protein expression, which were all attenuated in XMetS.

Conclusion. This is the first report of the protective effect of exercise on native CAD, peri-stent CAD, SOCE, and molecular expression of TRPC1, STIM1, and Orai1 in MetS.

Keywords: transient receptor potential 1 (TRPC1) channel, STIM1, Orai1, store-operated calcium channel, intravascular ultrasound, coronary smooth muscle, Ossabaw miniature swine.

Introduction

Metabolic syndrome (MetS) is defined as the combination of several risk factors including: central obesity, dyslipidemia (increased LDL/HDL and triglycerides), hypertension, impaired glucose tolerance, and insulin resistance (160). Generally the presence of three of these characteristics renders a diagnosis of MetS (160). This combination of risk factors, also termed “pre-diabetes”, ultimately leads to type 2 diabetes and increased prevalence and severity of coronary artery disease (CAD) (224).

Untreated CAD will progress to the point where neointimal formation occludes coronary blood flow and impairs cardiac function. The primary interventional treatment for occlusive CAD is deployment of a coronary stent. Drug-eluting stents have substantially decreased such restenosis; however, artery segments adjacent to the stent's edge (peri-stent) are sites of significant stenosis (225). Accelerated peri-stent CAD progression increases the need for repeat stent procedures (68;225;226) and shows a greater prevalence in patients with diabetes (74). Since peri-stent CAD may be a milder representation of in-stent restenosis due to stent-induced injury, there is need for study of the cellular and molecular mechanisms underlying peri-stent CAD.

Clearly, coronary smooth muscle (CSM) proliferation is largely responsible for neointima formation after coronary stenting (227). Intracellular Ca^{2+} plays several roles in smooth muscle cells, such as regulation of contraction and gene expression (228), and altered intracellular Ca^{2+} signaling is associated with smooth muscle cell proliferation (169). The primary Ca^{2+} store within the CSM cell is the sarcoplasmic reticulum (SR). Depletion of the SR Ca^{2+} store leads to store-operated Ca^{2+} entry (SOCE) across the plasma membrane in smooth muscle (229). SOCE (or Ca^{2+} -release activated Ca^{2+} [CRAC] entry) historically has been described in purely electrophysiological terms, as the molecular entity was not known (as reviewed in (117;230)). In recent years, various candidates have been proposed to be involved in SOCE, including TRPC1, TRPC6,

STIM1, and Orai1 (as reviewed in (117;230)). Importantly, the transient receptor potential canonical 1 (TRPC1) channel that contributes to SOCE in smooth muscle is linked to hypertrophy and proliferation (196;228;229). Balloon injury-induced CSM cell proliferation in healthy juvenile swine is associated with upregulation of TRPC1 channels (196). In addition to pharmacological antagonism of aberrant Ca^{2+} signaling (18), we have shown that exercise therapy prevents CSM Ca^{2+} dysregulation in CAD (13;17). While TRPC1 channels are strongly associated with smooth muscle proliferation and have been implicated in CAD, no studies have examined changes in TRPC1 channels in native (non-stent) and peri-stent CAD in MetS or whether exercise training can attenuate these processes.

Our group has developed Ossabaw miniature swine as an excellent large animal model of MetS (3;4;7). We tested the hypothesis that MetS increases SOCE and CAD in non-stent and peri-stent segments of coronary artery and exercise attenuates these events. Our data provide the first cellular and molecular evidence that exercise protects against increases in SOCE, TRPC1, and STIM1 protein, and native and peri-stent CAD in MetS. These findings in the Ossabaw miniature swine model, which superbly mimics CAD in MetS, are critical links for translation to clinical medicine.

Methods

Animal care and use. The investigation conforms with the *Guide for the Care and Use of Laboratory Animals* published by the US National Institutes of Health (NIH Publication No. 85-23, revised 1996). All protocols involving animals were approved by an Institutional Animal Care and Use Committee and complied fully with recommendations in the *Guide for the Care and Use of Laboratory Animals* (176)¹ and the American Veterinary Medical Association Panel on Euthanasia²². Male Ossabaw swine at the age of seven months (sexually mature adult) were assigned to three diet groups for 55 weeks before stenting. Lean control swine (Lean, N=9) were fed lean chow containing 22% kcal from protein, 70% kcal from carbohydrates, and 8% kcal from fat. Pigs in the lean group ate 2500 kcal/day. Sedentary MetS (N=9) and exercise trained (XMetS, N=9) groups were fed a high fat/2% cholesterol atherogenic diet composed of lean chow supplemented with (percent by weight): cholesterol 2.0, hydrogenated soybean oil 16.7 (contains 56% trans fatty acids), corn oil 2.5, and sodium cholate 0.7. This mixture yielded a composition of 11% kcal from protein, 43% kcal from carbohydrates and 46% kcal from fat. Atherogenic diet groups ate 6000 kcal/day until sacrifice. All animals were housed in individual pens and provided a 12 hr light/12 hr dark cycle. Water was provided ad libitum.

Exercise Training. Pigs randomized to the exercise group began treadmill training 4 weeks prior to initial cardiac catheterization. To prevent any detrimental cardiac event in obese, MetS swine with CAD and after stenting, the endurance exercise training protocol was modified from our previous studies (e.g.¹⁵). This protocol complied fully with guidelines in the “*APS Resource Book for the Design of Animal Exercise Protocols*”²³. Briefly, exercise training consisted of treadmill running performed 4 days/week. During the first week of training, pigs were acclimated to the treadmill at 4 km/h (endurance) with 0% grade for 20-30 minutes and at 5.6 km/h for 15 minutes. After

acclimation the daily 45 minutes training bout consisted of four stages: 1) 5 minutes warm-up at 2.2 km/h, 2) 5 minutes at 6.1 km/h (~40-50% maximum heart rate), 3) 30 minutes at 7.7 km/h with a variable grade (~65-75% of maximum heart rate), and 4) 5 minutes cool down at 3.5 km/h. Heart rates were monitored continuously using an external monitor (T51H, Polar, Lake Success, NY). Throughout the total 7 week training period, training intensity was maintained in the desired heart rate range by altering the treadmill grade. Each pig resumed exercise training 48 hours following coronary stenting procedure and this regimen was maintained for 3 weeks following stenting before repeat cardiac catheterization and euthanasia.

Intravenous glucose tolerance test. Swine were acclimatized to low-stress restraint in a specialized sling for 5-7 days before the IVGTT was conducted¹⁷⁻¹⁹(3;4;9). Swine were then fasted overnight, and anesthetized with isoflurane (maintained at 4% by mask with supplemental O₂). The right jugular vein was catheterized percutaneously. Following catheterization, swine were allowed to recover for 3 h before the IVGTT to avoid any effect of isoflurane on insulin signaling¹⁹. For IVGTT, conscious swine were restrained by sling and baseline blood samples were obtained. Glucose (1g/kg body weight; *i.v.*) was administered and timed blood samples were collected¹⁹. Blood glucose was measured using YSI 2300 STAT Plus Glucose analyzer. Plasma insulin assays were performed by Linco Research Laboratories (St. Charles, MO).

Plasma lipid assays. Venous blood samples were obtained following overnight fasting. Fasting samples were analyzed for triglyceride and total cholesterol [fractionated into high density lipoprotein (HDL) and low density lipoprotein (LDL) components]¹⁷. Cholesterol in lipoprotein fractions was determined after precipitation of HDL using minor modifications of standard methods²⁴. Specifically, apolipoprotein-B-containing lipoproteins were precipitated with heparin-MnCl₂ and the supernatant was assayed.

LDL was calculated from the Friedewald equation: $LDL = \text{total cholesterol} - HDL - (\text{triglyceride} \div 5)$.

Stent procedure. Procedures were similar to previous reports^{18,25,26}. Swine received 325 mg aspirin and 25 mg Plavix (clopidogrel) daily as anti-platelet therapy which began one day prior to the stent procedure and continued for the duration of the study. Following an overnight fast, swine received (in mg/kg; *i.m.*) 0.05 atropine, 2.2 xylazine, and 5.5 telazol. Swine were intubated and anesthesia was maintained with isoflurane (2-4%, with supplemental O₂). The isoflurane level was adjusted to maintain anesthesia with stable hemodynamics. Heart rate, aortic blood pressure, respiratory rate, and electrocardiographic data were continuously monitored throughout the procedure. Under sterile conditions, a 7F vascular introducer sheath was inserted into the right femoral artery and heparin (200 U/kg) administered. A 7F guiding catheter (Amplatz L, sizes 0.75-2.0; Cordis) was advanced to engage the left main coronary ostium. A 3.2F, 30 MHz intravascular ultrasound (IVUS) catheter (Boston Scientific) was advanced over a guide wire and positioned in the coronary artery. Automated IVUS pullbacks were performed at 0.5 mm/sec. Video images were analyzed off-line (Sonos Intravascular Imaging System; Hewlett Packard). The IVUS catheter was removed and a coronary stent (2.5-4.0 mm diameter by 8 mm length, Express2; Boston Scientific) catheter was deployed. Stent diameter was chosen to match artery diameter using optimal balloon inflation pressure. Two stents were deployed in each animal. One stent was placed in the circumflex artery (CFX), while the second stent was placed in the left anterior descending artery (LAD). Angiography was performed to ensure proper longitudinal stent placement and IVUS was repeated to confirm deployment of the stent to the proper arterial lumen diameter (1.0x normal artery reference)^{18,25,26}. The IVUS catheter, guide catheter, and introducer sheath were removed and the right femoral

artery ligated. The incision was closed and the animal was allowed to recover. Cephalexin (1000 mg) was given twice a day for six days following the stent procedure.

Intra-stent histology. Stented coronary segments were placed in zinc-buffered formalin at sacrifice for histological analysis. Stent histology was performed by MicaGenix Corp. (Indianapolis, Indiana, USA, as we have described previously ²⁷. Images were captured with a Nikon CoolPix 990 (3.34 MegaPixel) digital camera. Measurements were made with Image Pro Plus v.4.1 software (Media Cybernetics, Silver Springs, Maryland, USA). Collagen content in the media and intima was determined as we previously described (11). Cell count was assessed using hematoxylin and eosin.

Cell dispersion. The procedure for the isolation of the right coronary artery and the enzymatic dispersal of porcine coronary smooth muscle cells has been previously described ^{9,15}. Briefly, arteries were freshly dissected and smooth muscle cells dispersed. Arteries were incubated in a physiological salt solution containing collagenase for 45 minutes to disperse endothelial cells, followed by a second period of 30 minutes to isolate the smooth muscle cell fraction.

Intracellular Ca²⁺ measurements. Whole cell intracellular Ca²⁺ levels were obtained at room temperature (22–23°C) using the fluorescent Ca²⁺ indicator, fura-2, and the InCa++ Ca²⁺ Imaging System (Intracellular Imaging, Cincinnati, OH) as previously described by our laboratory ^{9,14,15}.

Patch clamp electrophysiology. All electrophysiological experiments were performed using a Axopatch 200B integrating patch-clamp amplifier and a DigiData 1440A analog-digital converter and analyzed using Axon PCLAMP 10 software package. Cells were voltage-clamped at a holding potential of -60 mV and 300 ms voltage ramps from -100 to +100 mV were applied at 5 sec intervals similar to previous protocols (231). The pipette solution contained (mM): 135 CsMeSO₃, 10 CsCl, 2 MgCl₂, 10 EGTA, 20

HEPES (pH 7.2). Extracellular solutions contained (mM): 150 NaCl, 2 MgCl₂, 1.2 CaCl₂, 5.5 glucose, 10 HEPES (standard extracellular solution, pH 7.2) or divalent cation free solution having: 150 NaCl, 1 EGTA, 5.5 glucose, 10 HEPES (pH 7.2) and 5 mM caffeine added where indicated.

Reverse transcription-polymerase chain reaction. The total RNA from pig coronary arteries was isolated using TRIzol reagent (Invitrogen, Carlsbad, CA). The full-length transcripts of TRPC1 were amplified using the one-step SuperScript RT-PCR platinum Taq HiFi system (Invitrogen, Carlsbad, CA). Primers for PCR amplification of TRPC1 were designed for the Ossabaw TRPC1 sequence and were as follows: forward, ATGGCGGCCCTGTACCCGAG; reverse: CATAGCATATTTAGAAGTCCGAAAGCC. The transcripts were confirmed to be the pig TRPC1 by sequencing.

Quantitative reverse transcriptase polymerase chain reaction analysis. BioRad iScript cDNA Synthesis kit was used to reverse transcribe cDNA using total RNA isolated from coronary of 18 pigs (6 Lean, MetS, and XMetS) as templates. The Applied Biosystems 7500 Real Time PCR System was used and data were quantified using comparative Ct (ddCt) method. The endogenous control (18S rRNA) was amplified using TaqMan Universal PCR Master Mix (Applied Biosystems, Foster City, CA), whereas TRPC/Orai/Stim was amplified using SYBR Green Master mix (Applied Biosystems, Foster City, CA). The dissociation curves were run for all completed SYBR Green reactions to rule out non-specific amplifications and primer-dimers. The non-template control was performed as negative control.

Immunoblots. Protein extracts were subjected to 10.5% SDS-PAGE separating gel (4% stacking gel) and transferred to nitrocellulose membranes. The membrane (blocked with 5% casein) was incubated with the primary antibodies and then with an anti-rabbit or mouse HRP-conjugated antibody (Pierce, Rockford, IL, 1:20,000). Bound HRP-conjugates were detected using a SuperSignal West Femto Kit (Pierce), according

to the manufacturer's instructions. The monoclonal anti-TRPC1 antibody was a gift from Dr.Tsiokas (University of Oklahoma Health Sciences Center). STIM1 and ORAI1 antibodies were from Alomone labs (Rehovet, Israel).

Assessment of coronary artery disease. IVUS pullbacks performed during the stenting procedure and before stent placement were used to assess native atheroma^{16,26}. Measurements were obtained every 2 mm through the length of the artery. Each cross-sectional IVUS image was divided into 16 equal segments. Percent circumferential wall coverage was calculated as (# segments containing atheroma ÷ 16) x 100%, similar to previous reports^{17,26}.

Results

To determine if excess kcal atherogenic diet induces metabolic syndrome in Ossabaw swine, we evaluated the major parameters associated with MetS (**Table 4.1**). Several characteristics were elevated in MetS and XMetS above Lean, including bodyweight, LDL, systolic and diastolic blood pressure, and fasting blood glucose. LDL/HDL ratio was the only metabolic parameter attenuated by exercise training in XMetS vs. MetS. Efficacy of exercise training was evidenced as decreased resting heart rate, increased work load (treadmill grade) at a constant heart rate (65-75% maximum), and decreased heart rate at a constant work load during the treadmill stress test (**Figure 4.1A**).

Glucose intolerance and insulin resistance are major components of MetS and the development of type 2 diabetes. MetS had significantly greater blood glucose concentrations than Lean at 10, 20, 30, 40, and 50 minutes after bolus glucose injection (**Figure 4.1B**). In addition, XMetS had significantly elevated blood glucose above Lean at 10, 30, 40, and 50 minute time points (**Figure 4.1B**). MetS also elicited significant elevation in plasma insulin response above Lean at all times after glucose injection (**Figure 4.1C**). Likewise, XMetS plasma insulin was significantly elevated above Lean with the exception of the 60 minute time point (**Figure 4.1C**). Taken together, both glucose and insulin IVGTT results indicate glucose intolerance and primary insulin resistance in MetS and XMetS, with minimal effect of this short-term (7 weeks) exercise training program on these metabolic parameters.

To determine the effects of metabolic syndrome on CAD, atherosclerosis was imaged by IVUS and quantified as percent circumferential wall coverage. **Figure 4.2A** is a schematic of the coronary vasculature showing the location of peri-stent and non-stent segments studied. **Figure 4.2B** illustrates an *in vivo* coronary angiogram at right anterior

oblique 30 angle. Representative IVUS image from the CFX artery demonstrates atherosclerotic neointima formation (**Figure 4.2C**). IVUS images before (**Figure 4.2D**) and after stent (**Figure 4.2E**) deployment verified proper stent diameter. Representative longitudinal IVUS analysis of CFX before and 4 weeks after stent deployment illustrates relatively mild and diffuse atherosclerosis through the more distal regions of the artery (**Figure 4.2F**). Increased percent wall coverage was found in proximal and distal non-stented segments of coronary arteries in MetS compared to Lean, which was attenuated with exercise (XMetS) (**Figure 4.2 G&H**). Similar to non-stent segments, exercise (XMetS) completely prevented the increase in percent wall coverage observed in MetS compared to Lean in peri-stent segments of coronary artery (**Figure 4.2I**), but did not affect in-stent neointimal hyperplasia (**Figure 4.2J**).

Verhoff-Van Giessen (VVG), Masson's trichrome, and hematoxylin and eosin (H&E) stains were performed to assess in-stent plaque morphology. **Figure 4.3 A&B** show representative in-stent plaque from trichrom and H&E, respectively. Neointimal hyperplasia was not different across groups (**Figure 4.3C**). Exercise reduced the amount of collagen (**Figure 4.3D**), but there was no difference in cell density between groups in the in-stent regions (**Figure 4.3E**).

Since alterations in SOCE signaling mechanisms have been associated with atherosclerosis (196;228;229), we studied SOCE in smooth muscle cells freshly isolated from non-stent and peri-stent artery segments of Lean, MetS, and XMetS groups. To assess SOCE, we first employed a typical store-depletion protocol similar to that reviewed by Landsberg et al. (229). **Figure 4.4A** shows a representative record of intracellular Ca^{2+} changes in a peri-stent MetS CSM cell obtained during such an experiment. Baseline intracellular $[Ca^{2+}]$ was established from minutes 0-2 in physiological salt solution containing normal 2 mM Ca^{2+} . From minutes 3-7, the caffeine-sensitive SR Ca^{2+} stores were depleted in the presence of caffeine and the SERCA

inhibitor cyclopiazonic acid (CPA) in Ca^{2+} free solution. At minutes 17-22, Ca^{2+} was reintroduced and SOCE was quantified in non-stent and peri-stent cells. CSM SOCE was sensitive to the non-selective Ca^{2+} channel blocker Ni^{2+} , but insensitive to the L-type Ca^{2+} channel blocker nicardipine. Peak SOCE was not significantly different in the CSM cells from peri-stent segments of Lean and MetS in Ca^{2+} imaging experiments, but was markedly attenuated in XMetS (**Figure 4.4B**).

In a separate chronic study, SOCE was evaluated by Mn^{2+} quench in cells of non-stent and peri-stent segments. A Mn^{2+} -dependent decrease in the fluorescence intensity of fura-2 excited at 360 nm (the fura-2 Ca^{2+} -insensitive isosbestic point) is indicative of divalent cation influx. Caffeine and CPA were used to deplete intracellular Ca^{2+} stores in CSM cells. Mn^{2+} quench confirmed that store-depletion resulted in divalent cation influx sensitive to the non-selective Ca^{2+} channel blocker Ni^{2+} (**Figure 4.4C**). Mn^{2+} -influx was significantly greater in MetS compared to Lean in both non-stent and peri-stent cells (**Figure 4.4D**).

A less extreme Ca^{2+} store depletion protocol using caffeine alone in the absence of CPA demonstrated significant Mn^{2+} quench (**Figure 4.4E**), which was greater in MetS compared to the Lean group (**Figure 4.4F**). Mn^{2+} quench observed in **Figure 4.4 D&F** confirmed that store-depletion results in divalent cation influx in CSM cells without inhibition of SERCA. Whole cell patch clamp electrophysiology was performed using a similar protocol to **Figure 4.4E**. Caffeine-induced inward current was sustained for longer than 5 minutes (**Figure 4.4G**), indicating it was not due to transient Ca^{2+} -sensitive Cl^- channels activated by Ca^{2+} - release stimulated by caffeine. A current-voltage relationship plot of the sustained inward current was ohmic with a reversal potential of approximately 0 mV (**Figure 4.4H**).

While our patch clamp data suggested SOCE was due to TRPC1, we determined if changes in the molecular expression of TRPC1 or other SOCE related proteins (e.g.

STIM1 and Orai1) could account for the increased SOCE. In RT-PCR experiments the presence of TRPC1, STIM1, and Orai1 was shown in all groups (**Figure 4.5 A-D**). Group data demonstrated significantly greater TRPC1 mRNA expression in the MetS group compared to Lean, which was attenuated by exercise training (**Figure 4.5B**). STIM1 and Orai1 mRNA expression were also increased in the MetS group, but remained increased even with exercise (**Figure 4.5 C&D**). Immunoblots from coronary lysates showed TRPC1 protein in MetS was attenuated in XMetS and STIM1 protein in MetS was abolished in XMetS compared to Lean (**Figure 4.5 F&G**), while Orai1 protein expression shows no statistical difference between any group ($p=0.1$) (**Figure 4.5H**). Agarose gel images demonstrate the expression of only TRPC1 and TRPC6 gene in MetS coronary arteries (**Figure 4.5 I&J**). TRPC6 mRNA was increased in MetS compared to Lean (**Figure 4.5K**).

Discussion

The novel findings of this study are: 1) exercise decreases A) non-stent and peri-stent CAD, B) store-operated Ca^{2+} channel function and TRPC1/STIM1 molecular expression, and C) in-stent collagen content in MetS and 2) SOCE current-voltage relationship in coronary smooth muscle is ohmic and non-selective, which is consistent with TRPC1. Excess kcal atherogenic diet elicited robust MetS, which accompanied greater atherosclerosis in peri-stent segments of coronary arteries than in non-stented arteries. Functional store-depletion mediated Ca^{2+} influx and TRPC1/STIM1 molecular expression correlated with the extent of atherosclerosis amongst groups, while Orai1 protein expression did not change. The effect of exercise to attenuate progression of peri-stent CAD, but not in-stent stenosis, in Ossabaw miniature swine with MetS is consistent with the clinical study in humans by Belardinelli (226) and non-diabetic swine (232). Our Ca^{2+} signaling and molecular expression data provide evidence of cellular and molecular events underlying this vitally important clinical phenomenon and extend those findings (226;232) to MetS.

Patient complication following stent deployment is well documented (233) with diabetes increasing patient risk (234). Consistent with human data, MetS Ossabaw swine displayed increased atherosclerosis in non-stent artery segments compared to Lean. Peri-stent CAD has been observed by several groups and is more prevalent in patients with diabetes (74); which may be due to the overall greater diffuse CAD in MetS and diabetes (86). Despite this remarkable clinical observation, no studies have examined mechanisms which underlie peri-stent atherosclerosis in MetS. Similar to previous findings, peri-stent atherosclerosis, although augmented in all groups, mirrored non-stent atherosclerosis in that it was greater in MetS than Lean. Exercise has an independent role in primary prevention of CAD (235;236), reduction of coronary stenosis, and rates of hospital readmission after coronary angioplasty (226).

Nonetheless, mechanisms which underlie these changes are unclear. In the current study, seven weeks of exercise training attenuated the increased non-stent atherosclerosis and abolished increased peri-stent atherosclerosis observed in MetS. Although 20 weeks of exercise training of non-diabetic swine attenuated neointimal hyperplasia, i.e. progression to stenosis, after angioplasty balloon induced injury (232), in the present study MetS and the shorter training duration (7 weeks) are key differences that may have minimized the protective effects of exercise.

Our group captured feral swine from Ossabaw Island, GA, which naturally developed a thrifty genotype in response to the evolutionary selection pressure of seasonal shortages of food (4). When fed excess calorie atherogenic diet, Ossabaw swine develop MetS similar to humans (3;4;7). Also, MetS Ossabaw swine, like humans (but different from many other laboratory animal models), develop CAD. Consistent with these findings, male Ossabaw swine in this study show increased bodyweight, plasma LDL, LDL/HDL ratio, and triglyceride, systolic and diastolic pressure, and heart rate. A major extension of this work is our finding that short term exercise training reverses the elevated LDL/HDL ratio observed in MetS.

Obese, MetS Ossabaw swine showed classical cardiovascular adaptations to exercise training, including increased physical work capacity, resting bradycardia, and decreased heart rate response to a submaximal exercise stress test, indicating efficacy of the exercise program. The lack of exercise attenuation of other MetS characteristics is somewhat surprising, since exercise is a first line treatment for pre-diabetes / MetS (237). Factors may have mitigated the typical effects of exercise on MetS characteristics in Ossabaw swine. First, our study design was to maintain the atherogenic diet and obesity of the pigs, unlike the typical exercise training regimen and that in human clinical studies, in which diet improvements are also implemented (237). Second, Ossabaw miniature swine have a loss-of-function mutation in the AMP kinase gamma 3 subunit in

skeletal muscle, which is a pivotal enzyme in fatty acid oxidation and glucose uptake (238). Exercise is not as effective in activating AMP kinase in pigs having the mutation, thus the full benefit of exercise on skeletal muscle metabolism might not be seen in Ossabaw miniature swine (238).

Because of the widely reported occurrence of SOCE and distribution of TRPC channels in numerous cell types, including vascular cells (239), it might be considered dogma that SOCE and TRPC channels should be abundant in CSM and regulate Ca^{2+} signaling and contraction under normal conditions. We emphasize that we have never found activation of SOCE in Yucatan swine “healthy” CSM (13;240), despite robust SOCE in coronary endothelial cells (199). However, previous studies report increased expression of TRPC1 in diseased vascular smooth muscle cells (196;229). The results of our study are in agreement with the concept that TRPC1 channels are strongly associated with CAD, as shown by increased TRPC1 mRNA and protein expression, as well as the ohmic and non-selective current voltage relationship of SOCE in coronary smooth muscle consistent with current expected of TRPC1-channel (241). TRPC6 and Orai1, known SOCE mediators, expression is increased with MetS, however both TRPC6 (242) and Orai1 (243) have distinct and vastly different current-voltage relationships than that observed in this study. While STIM1 protein expression mirrors that of TRPC1, STIM1 operates as a sensor of the intracellular Ca^{2+} -store and not as a distinct functional ion channel (151). Additionally, TRPC1 protein is proportional to function, i.e. Ca^{2+} influx (**Figures 4, 5**). We can largely rule out other TRPC isoforms, because they are not expressed in coronary artery ((244), **Figure 4.5I**). The current study further extends our knowledge concerning the role of TRPC1 by the novel finding that metabolic syndrome increases SOCE and TRPC1 expression in conjunction with CAD, all of which are attenuated by exercise training.

Our findings indicate that TRPC1 is closely associated with neointimal hyperplasia, not only in non-stent, but also peri-stent segments of coronary artery. This is important because neointimal hyperplasia in non-stented segments is considered a natural progression of disease, whereas peri-stent atherosclerosis may be considered an arterial response to injury (245;246). Together these data suggest TRPC1 channels play a fundamental role promoting atherosclerosis in both non-stent and peri-stent segments of coronary artery. Thus, inhibition of TRPC1 channels may serve as a possible therapeutic target for the treatment of CAD. The concept of exercise and TRPC1 as potential therapeutic modes and targets is especially important because of the recent finding that treatment of conventional risk factors such as hyperglycemia had negligible effects on prevention of cardiovascular disease in type 2 diabetic humans and had detrimental side effects (247).

In conclusion, our data support the hypothesis that Ossabaw swine with robust MetS have increased SOCE and CAD in non-stent and peri-stent segments of coronary artery and exercise attenuates these events. Further, increased TRPC1/STIM1 protein expression was attenuated by exercise. The implications are that in human patients with metabolic syndrome who undergo coronary stenting and have attenuated peri-stent CAD with exercise training underlying cellular events may involve TRPC1 channels and STIM1. Future studies will focus on establishing a causative role of TRPC1 channels in the progression of CAD in *ex vivo* and *in vivo* models.

Funding

This work was supported by the National Institutes of Health grant numbers HL062552 and RR013223 to M.S, HL083381 to A.G.O., the Purdue-Indiana University Comparative Medicine Program, and the Fortune-Fry Ultrasound Research Fund of the Department of Cellular & Integrative Physiology at Indiana University School of Medicine. J.M.E. and Z.P.N. are the recipients of a Translational Research Fellowship from the Indiana University School of Medicine and Z.P.N. was the recipient of a Translational Fellowship from NIH UL1 RR025761

Acknowledgments

We thank Dr. Tsiokas, Ph.D. for his generous contribution of monoclonal TRPC1 antibody, Alice Nakatsuka and Gouqing Hu for RT-PCR analysis, and Keith L. March, M.D., Ph.D. for use of the Research Animal Angiography Laboratory of the Indiana Center for Vascular Biology and Medicine.

Table 4.1.

Parameter	Lean	MetS	XMetS	Significance
Weight (kg)	64 ± 3	111 ± 9	120 ± 5	XMetS, MetS > Lean
Total Cholesterol (mg/dL)	48 ± 2	215 ± 31	219 ± 6	XMetS, MetS > Lean
Low density lipoprotein (LDL, mg/dL)	26 ± 4	155 ± 4	136 ± 16	XMetS, MetS > Lean
High density lipoprotein (HDL, mg/dL)	18 ± 3	56 ± 10	83 ± 6	XMetS, MetS > Lean
LDL/HDL	1.8 ± 0.4	3.5 ± 0.7	1.7 ± 0.2	MetS > XMetS, Lean
Triglycerides (TG, mg/dL)	25 ± 3	39 ± 1	40 ± 2	XMetS, MetS > Lean
Systolic Blood Pressure (mm Hg)	116 ± 1	160 ± 1	146 ± 6	XMetS, MetS > Lean
Diastolic Blood Pressure (mm Hg)	77 ± 2	108 ± 5	94 ± 7	XMetS, MetS > Lean
Fasting Blood Glucose	67 ± 2	83 ± 2	82 ± 2	XMetS, MetS > Lean
Resting Heart Rate (bpm)	69 ± 3	93 ± 4	78 ± 1	MetS > XMetS > Lean
Resting heart rate start exercise training (bpm)	----	----	102 ± 1	End < Start training
Treadmill grade at 65-75% maximum heart rate				
Start exercise training	----	----	3%	----
End exercise training	----	----	8 ± 0.3 %	End > Start training
Submaximal stress test heart rate (bpm)				
Start exercise training	----	----	173 ± 2	----
End exercise training	----	----	150 ± 2	End < Start training

Table 4.1. Phenotypic characteristics of Ossabaw miniature swine groups at end of study. Lean control, MetS = metabolic syndrome, XMetS = exercise trained MetS.

Figure Legends

Figure 4.1 Ossabaw swine fed excess atherogenic diet are glucose intolerant and insulin-resistant and exercise training improves physical work capacity. A. Timeframe of study treatments and exercise stress test (See Methods). **B.** Time course of blood glucose responses during IVGTT. **C.** Time course of plasma insulin responses during IVGTT.

Figure 4.2 Greater coronary atherosclerosis in metabolic syndrome swine versus lean is attenuated by exercise training, but in-stent neointimal hyperplasia is not affected. A. Schematic of coronary vasculature. **B.** Coronary angiogram showing circumflex (CFX) and its large obtuse marginal branches and the left anterior descending (LAD) coronary arteries in right anterior oblique view. **C.** IVUS image. Dotted line indicates small section of internal elastic lamina and solid line indicates lumen boundary where showing 25% circumferential wall coverage of this cross-section of artery. Representative IVUS image of artery segment to receive stent immediately preceding stent placement in panel **D** and immediately following stent placement in panel **E** (arrows are stent struts). **F.** Representative percent wall coverage from IVUS data collected along the length of a stented artery both preceding stent placement (dotted) and after four weeks recovery post-stent (solid). **G.** Proximal non-stent percent wall coverage (N=9). ** $p < 0.05$ vs. Lean and XMetS, * $p < 0.05$ vs. Lean and MetS. **H.** Distal non-stent percent wall coverage (N=9). **I.** Percent wall coverage in peri-stent segments (N=9). **J.** In-stent percent wall coverage.

Figure 4.3 Intra-stent histology. A. Representative trichrome section. **B.** Representative H&E section. **C.** Intima / media cross-sectional area. **D.** Collagen in

XMetS as a percent of intra-stent media and intimal area. **E.** Cellularity (H&E section) in media and intima. a: adventitia; m: media; i: intima; l: lumen; s: stent; v: vasa vasorum.

Figure 4.4 Store-operated Ca^{2+} entry is increased in metabolic syndrome and attenuated by exercise. A&C. Representative data from standard protocols used to assess SOCE. Peak store depletion-mediated Ca^{2+} influx is assessed at minutes 17-20. **Duration of exposure to solutions is shown by horizontal lines;** caffeine (CAF, 5 mM); cyclopiazonic acid (CPA, 10 μM). **B.** Exercise attenuates peak SOCE compared to Lean and MetS in peri-stent sections of artery. **C.** Mn^{2+} as a Ca^{2+} surrogate quenches fura-2 fluorescence at the isosbestic (Ca^{2+} -insensitive) 360 nm wavelength verifying divalent cation influx. **D.** Increased SOCE in CSM from non-stent and peri-stent MetS coronary arteries compared to Lean. **E.** Only caffeine is used to deplete the Ca^{2+} store in this SOCE protocol. **F.** Increased SOCE in CSM from MetS swine. **G.** Whole-cell patch clamp data demonstrate sustained inward current by caffeine. **H.** Current-voltage relationship of leak subtracted control (blue) and SOCE (red).

Figure 4.5 Increased canonical transient receptor potential 1 and stromal interaction molecule 1 in metabolic syndrome is abolished by exercise. A. Representative agarose gel image quantifying TRPC1 using RT-PCR. **B.** TRPC1 mRNA normalized to β -actin. **C&D.** STIM1 (**Panel C**) and Orai1 (**Panel D**) mRNA using Q-RT-PCR normalized to β -actin. **E.** Immunoblot using anti- β -actin, STIM1, Orai1, and TRPC1 in Lean and MetS. **F-H.** TRPC1 (**F**), STIM1 (**G**), and Orai1 (**H**) protein expression using immunoblot analysis normalized to β -actin. **I.** Representative agarose gel image illustrating TRPC1 expression and no TRPC3, TRPC4, TRPC5, or TRPC7 expression. **J.** Agarose gel image illustrating TRPC6 expression in MetS coronary arteries. **K.** TRPC6 mRNA in MetS coronary arteries. **, $p < 0.5$ MetS compared to Lean and XMetS.

Figure 4.1

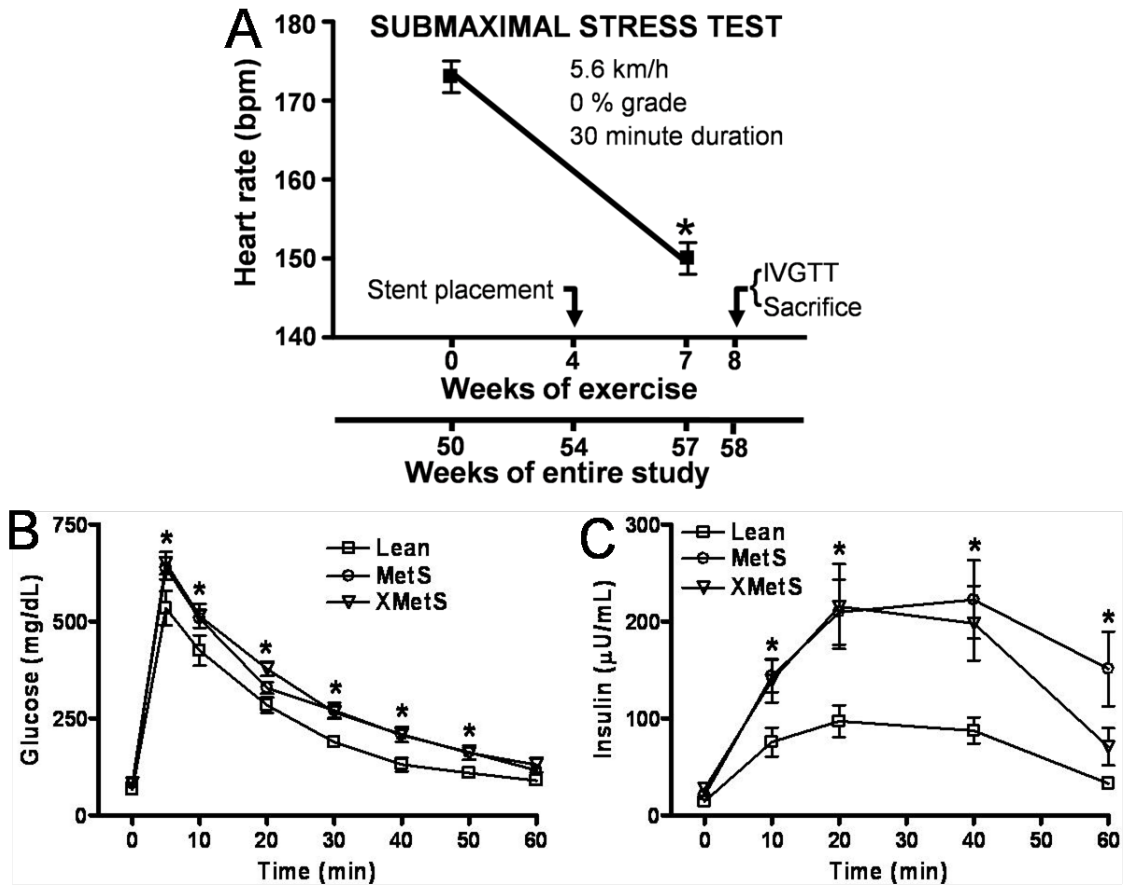


Figure 4.2

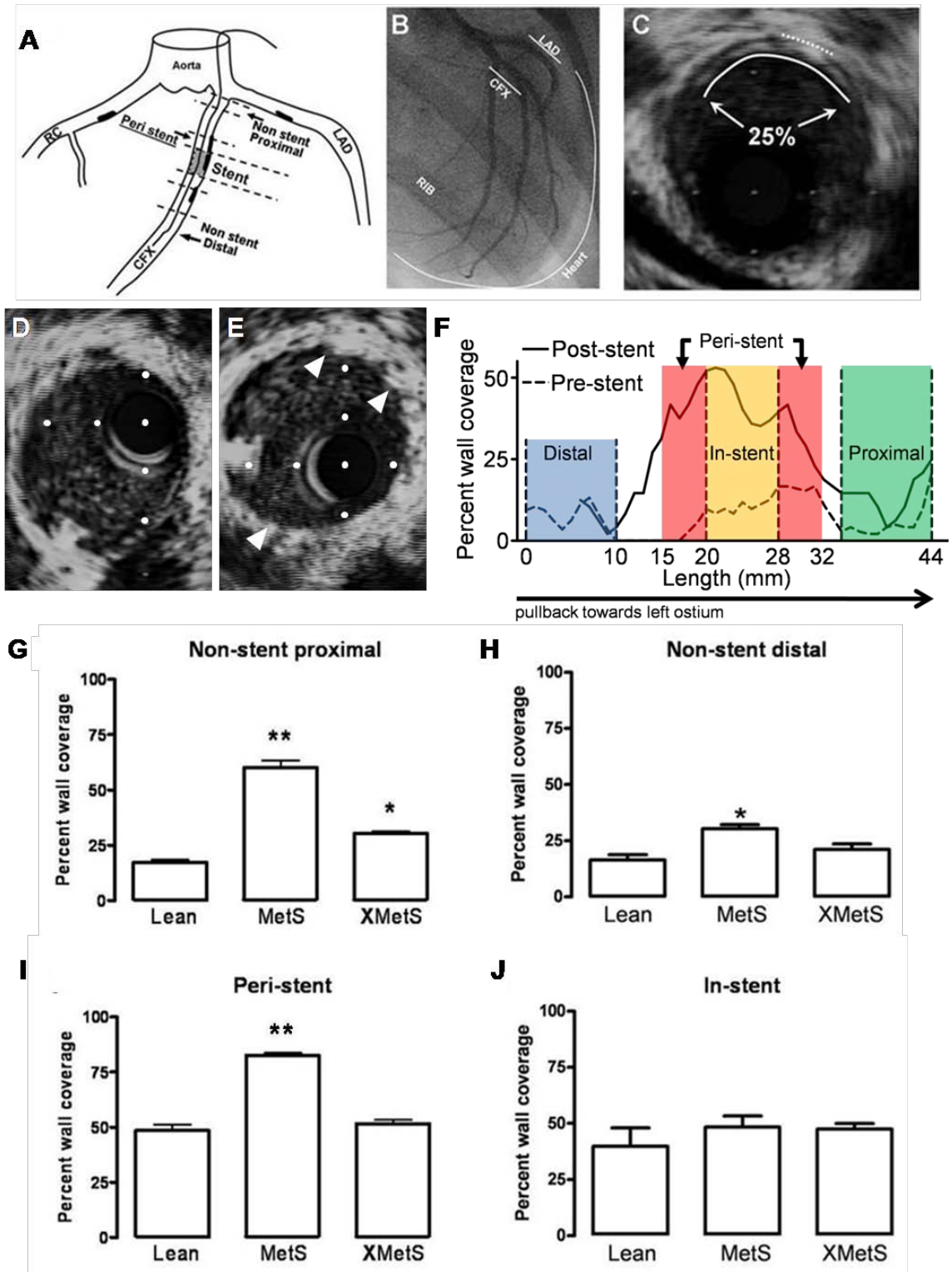


Figure 4.3

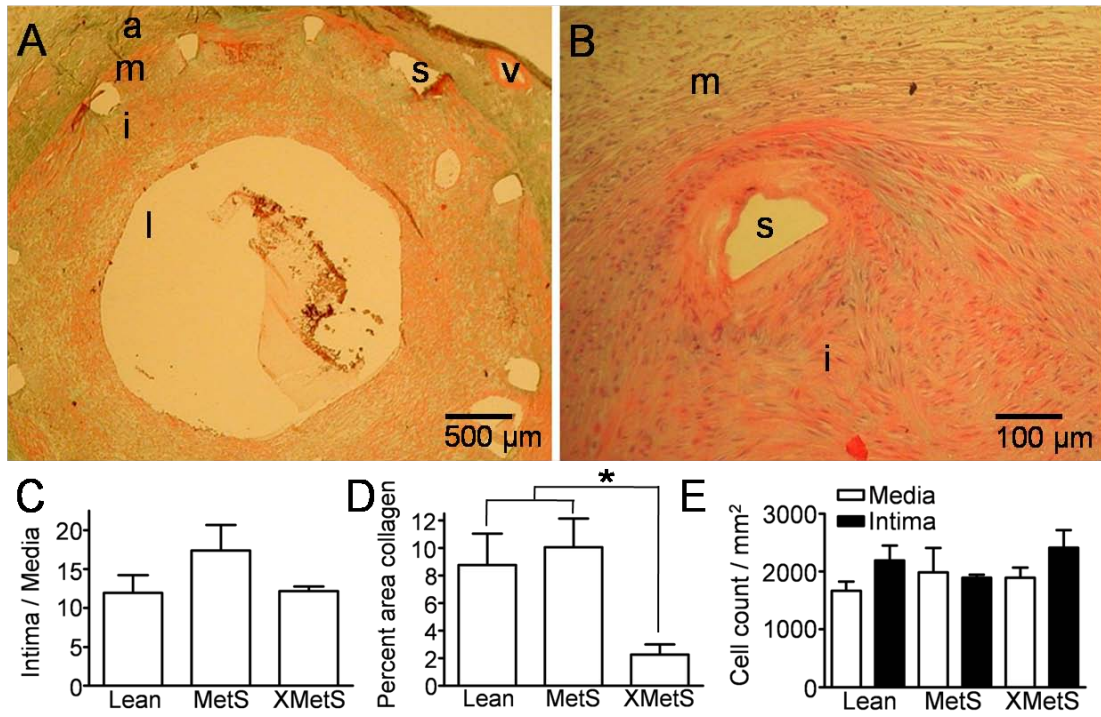


Figure 4.4

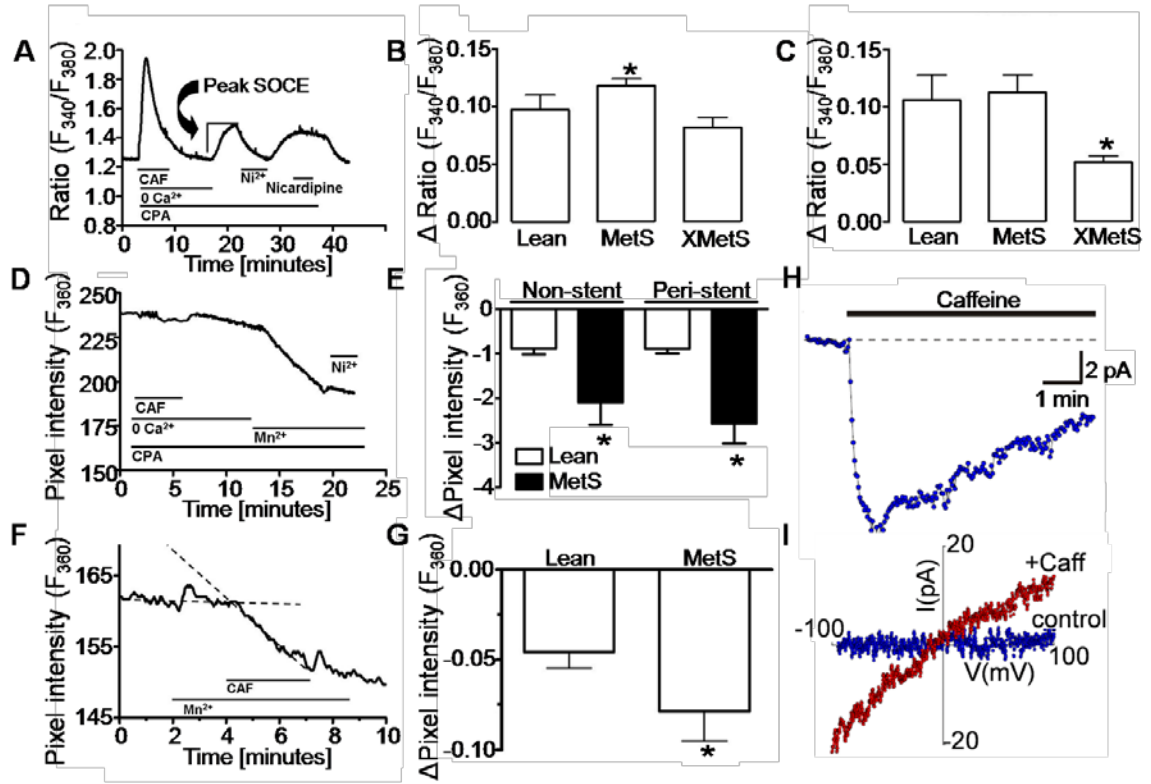
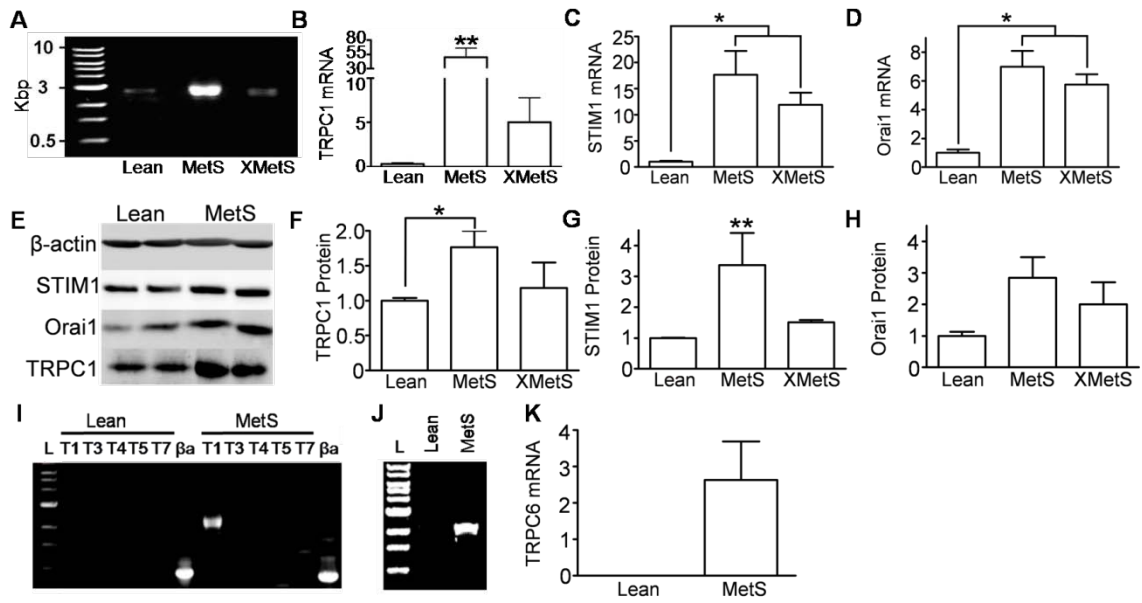


Figure 4.5



Chapter 5

Store-operated Ca²⁺ influx predicts coronary artery disease and is induced by dyslipidemia in metabolic syndrome and type 2 diabetes

Zachary P. Neeb¹, Mouhamad Alloosh¹, Jason M. Edwards¹, Ian N. Bratz²,
Michael Sturek¹.

¹Department of Cellular and Integrative Physiology, Indiana University School of Medicine

²Department of Integrative Medical Sciences, Northeastern Ohio University College of Medicine

Abstract

Objective. We tested the hypothesis that dyslipidemia was the principal component of metabolic syndrome (MetS; “prediabetes”) in the progression to type 2 diabetes and increased store-operated Ca^{2+} entry (SOCE) in coronary smooth muscle that contributes to coronary artery disease (CAD). Accordingly, we focused on and eliminated dyslipidemia from MetS allowing the contribution of dyslipidemia to be determined.

Methods and results. Ossabaw swine, an excellent humanoid model of MetS, were fed normal chow (Lean; N=9), high fructose diet that induced normolipidemic MetS (MetS; N=10), or high fructose/trans-fat/cholesterol diet that induced dyslipidemic MetS (DMetS; N=8) for 24 weeks before being assessed for MetS and CAD. MetS did not develop MetS, type 2 diabetes, increased SOCE, or CAD. DMetS developed MetS with type 2 diabetes, increased SOCE, and CAD. Swine fed the same atherogenic diet as DMetS, but short-term (sDMetS; N=?), developed dyslipidemic MetS with increased SOCE preceding CAD. Electrophysiology of coronary smooth muscle revealed absent Ca^{2+} -induced cation conductance and increased monovalent cation (Na^+) permeance via store-operated channels in DMetS compared to Lean.

Conclusions. Taken together, our results demonstrate dyslipidemia is the primary contributor to increased SOCE and the development of type 2 diabetes that precedes CAD in the metabolic syndrome.

Keywords: dyslipidemia, metabolic syndrome, coronary artery disease, type 2 diabetes, store-operated Ca^{2+} entry

Condensed abstract

We examined the hypothesis that dyslipidemia is the principal component of metabolic syndrome leading to type 2 diabetes, increased store-operated Ca^{2+} entry in coronary smooth muscle, and coronary artery disease. Our results confirm our hypothesis.

Introduction

Metabolic syndrome (MetS; “pre-diabetes”) is strongly associated with progression to type 2 diabetes (43), and both MetS and type 2 diabetes adversely increase incidence and severity of coronary artery disease (CAD) (39). CAD risk is elevated at least 3-fold in patients with diabetes, defined by elevated fasting blood glucose (39). Although some controversy exists over the precise definition of MetS, the presence of at least three metabolic risk factors (e.g. glucose intolerance, insulin resistance, increased triglycerides, increased LDL, decreased HDL, hypertension, and obesity) typically renders a diagnosis (159;160). By definition it is difficult to isolate individual MetS risk factor (e.g. dyslipidemia) contribution in the progression to type 2 diabetes and development of CAD in human clinical trials. Contributing to the opacity, there has been a paucity of suitable animal models of MetS that progress naturally to type 2 diabetes and develop substantial CAD (248).

Our group rescued the Ossabaw swine from their secluded island feast-and-famine environment and has since characterized the Ossabaw swine as the premier model for the study of MetS and CAD (3;4;6-8;29). A recent study by our group demonstrated that swine fed a diet high in fructose developed MetS without concomitant dyslipidemia or CAD, suggesting the necessity of dyslipidemia within the MetS for the development of CAD (249). However, when fed excess calorie atherogenic diet, Ossabaw swine recapitulate every aspect of MetS (including dyslipidemia), develop extensive CAD, and demonstrate dysfunctional Ca^{2+} regulation in coronary smooth muscle (CSM) (29).

While Ca^{2+} dysregulation is closely associated with CSM hyperplasia, a key contributor to the development of CAD (250), underlying mechanisms initiating CSM proliferation in MetS and type 2 diabetes remain unresolved. While our group was the first to show a strong association between increased CSM store-operated Ca^{2+} entry

(SOCE) and CAD in MetS (29), it has not been determined if SOCE is determinant or resultant in developing CAD. Additionally, while TRPC1 was implicated in contributing to increased SOCE, the molecular identity of the Ca^{2+} conducting pathway remains unclear.

Accordingly, this study was designed to test the hypothesis that dyslipidemia is the primary component of MetS for increased SOCE and the development of type 2 diabetes that subsequently contributes to the development of CAD in the MetS.

Methods

Animal care and use. All protocols involving animals were approved by an Institutional Animal Care and Use Committee and complied fully with standards (175;176). Forty-five mixed gender Ossabaw swine at the age of ten to fifteen months (adult) were assigned to four diet groups for 22-24 weeks. Lean control swine (Lean, N=10) were fed standard chow. The trans fatty acid MetS (TMetS, N=9) group was fed a high fat/fructose/2% cholesterol (w/w) atherogenic diet (hydrogenated soybean oil; 56% trans fatty acid) (6;7;29). The mixed fat (MMetS, N=8) was fed a high fat/fructose/2% cholesterol (w/w) atherogenic diet (mixture of lard, hydrogenated soybean oil, and hydrogenated coconut oil (7). See supplemental material for detailed methods.

Intravenous glucose tolerance test. IVGTT was performed as previously described by our lab (3;4;29). Briefly, conscious swine acclimatized to low-stress restraint in a sling were fasted overnight and baseline blood samples were obtained. Glucose (1g/kg body weight; i.v.) was administered and timed blood samples were collected.

Plasma lipid assays. Venous blood samples were obtained following overnight fasting and analyzed for triglyceride and total cholesterol as previously described by our laboratory (29). See supplement for detailed methods.

Assessment of insulin-positive area. Pancreas tissue was sectioned and imaged using standard histological technique (29). The 5- μ m pancreas sections were mounted on glass slides and assessed for insulin-positive area using mouse anti-insulin primary antibody (Sigma #I2018; a generous gift from Dr. Deborah Thurmond, Indiana University Purdue University Indianapolis) and mouse biotinylated secondary antibody (Vectastain Elite ABC Kit PK-6102). DAB (Sigma Fast D-4168) was used for visualization. Sections were counterstained with Mayer's hematoxylin.

Assessment of coronary artery disease. IVUS pullbacks performed at the end of the study were used to assess native atheroma (17;20;29). Percent circumferential wall coverage was calculated similar to previous reports (3;20;29). See supplemental material for detailed methods.

Cell dispersion. The procedure for the isolation of coronary arteries and the enzymatic dispersal of porcine coronary smooth muscle cells has been previously described (13;169). See supplement for detailed methods.

Intracellular Ca²⁺ measurements. Whole cell intracellular Ca²⁺ levels were obtained at room temperature (22–23°C) using the fluorescent Ca²⁺ indicator, fura-2, and the InCa++ Ca²⁺ Imaging System (Intracellular Imaging, Cincinnati, OH) as previously described by our laboratory (13;18;169). See supplement for detailed methods.

Patch clamp electrophysiology. Whole cell currents were measured at room temperature (22–23°C) using a standard whole cell voltage clamp technique as used routinely by our laboratory (29;138;182;251;252). Intracellular solution was (in mM) 120 CsCl, 10 NaCl, 1 MgCl₂, 20 HEPES, 5 Na₂ATP, 0.5 Tris GTP, with 7.2 pH. Currents were amplified with a List EPC-7 headstage filtered through an eight-pole low-pass filter with a cutoff frequency of 400 Hz. Capacity currents were filtered at low-pass cutoff frequency of 8.4 kHz. Normalization for membrane capacitance was not performed. Data acquisition and analyses were performed with a Labmaster analog-to-digital converter and AxoBASIC 1.0 data acquisition software (Axon Instruments, Sunnyvale, CA). Cells were constantly superfused at ~1–2 ml/min. See supplement for detailed methods.

Statistical analysis. One-way or two-way analysis of variance with Student-Newman-Kuels or Bonferroni post-hoc analysis, as appropriate, were performed using commercially available software (Prism 4.0) when comparing multiple groups. Independent t-test was used for comparing just two groups. In all tests, p <0.05 was the criterion for statistical significance. Unless otherwise noted; *, p <0.05 compared to

Lean; **, $p < 0.05$ compared to Lean and MetS; ***, $p < 0.05$ compared to all other groups.

Results

Three indicators of glucose intolerance were quantified from blood glucose measurements: 1) fasting glucose, 2) peak response to glucose, and 3) integral of glucose response curve. Peak response to glucose (**Figure 5.1A**) was elevated in MetS and DMetS compared to Lean. Fasting glucose was increased in DMetS ~33% above Lean and MetS (**Figure 5.1B**), providing strong evidence for type 2 diabetes in DMetS swine. Integral of the glucose response was elevated ~150% in DMetS compared to Lean and MetS, while MetS was elevated above Lean (**Figure 5.1C**). MetS insulin response was elevated above Lean and DMetS as evidenced by elevated peak (**Figure 5.1D**) and integral of the insulin response (**Figure 5.1F**). The homeostasis model assessment (HOMA) index is commonly used to diagnose insulin resistance clinically and MetS and DMetS HOMA index values were elevated ~200% above Lean (**Figure 5.1E**). Importantly, DMetS were unable to increase insulin secretion in response to the intravenous glucose load above Lean. The integral of the insulin response was also reflected in the relative pancreatic β -cell abundance, which was increased ~6-fold in MetS compared to Lean and DMetS (**Figure 5.1D**).

Angiography, used clinically to diagnose focal, stenotic atherosclerotic lesions, was performed on each pig and revealed no focal stenosis (**Figure 5.2A**) in any pig. Importantly, intravascular ultrasound (IVUS; **Figure 5.2B**) a more sensitive *in vivo* measure of CAD showed that DMetS developed extensive diffuse CAD compared to Lean and MetS (**Figure 5.2C**). Diffuse CAD was clearly evident by the ~2-fold greater arterial wall coverage with in proximal, intermediate, and distal coronary artery segments compared to MetS and Lean groups. MetS CAD was not significantly elevated compared to Lean.

. Analysis of coronary smooth muscle (CSM) Ca^{2+} regulation was conducted by fura-2 fluorescence imaging using a standard protocol (**Figure 5.3A**). Baseline

intracellular Ca^{2+} (Ca^{2+}_i) was elevated in DMetS CSM compared to Lean and MetS (**Figure 5.3B**). Caffeine and cyclopiazonic acid (Caff, 5 mM; CPA 10^{-5} M, respectively) treatment in the absence of extracellular Ca^{2+} (Ca^{2+}_o) rapidly release Ca^{2+} , resulting in a large amplitude Ca^{2+} and deplete the sarcoplasmic reticulum SR Ca^{2+} store (**Figure 5.3A**). MetS demonstrated increased Ca^{2+} efflux capacity compared to Lean and DMetS (**Figure 5.3C**), as assessed using time to $\frac{1}{2}$ minimum (time $\frac{1}{2}$ min.) recovery from Caff and CPA response in the absence of Ca^{2+}_o . In the absence of Ca^{2+}_o the peak Ca^{2+}_i response to Caff and CPA was elevated in DMetS compared to Lean and MetS, and MetS compared to Lean (**Figure 5.3D**), indicating increased SR Ca^{2+} -store. Store-operated Ca^{2+} entry (SOCE), was assessed by addition of extracellular Mn^{2+} (Mn^{2+}_o) following SR Ca^{2+} -store depletion. Mn^{2+}_o is permeant to Ca^{2+} conductance pathways, thus it served as a Ca^{2+}_o surrogate, quenching fura-2 (decreasing fluorescence) at its Ca^{2+} -insensitive isobestic excitation wavelength (F_{360}) and indicating inward divalent plasma membrane conductance (**Figure 5.3A**). SOCE was elevated ~2-fold in DMetS CSM compared to Lean and MetS, while MetS was not different than Lean (**Figure 5.3E**). Swine fed the same atherogenic diet as in DMetS for only 9 weeks (short-term DMetS; sDMetS) developed complete MetS (**Supplementary Table1**), but CAD (not shown), baseline CSM Ca^{2+}_i (**Figure 5.3F**) and peak CSM Ca^{2+} -response to Caff and CPA (**Figure 5.3G**) were not elevated above Lean cohorts. However, SOCE was elevated ~2-fold in sDMetS compared to Lean (**Figure 5.3H**). Thus, the development of CAD, increased CSM baseline Ca^{2+}_i , and increased SR Ca^{2+} -store were preceded by increased SOCE in CSM.

Whole-cell patch clamp experiments were conducted with Cs^+ -filled pipettes to block outward K^+ currents and optimize detection of inward cation currents. Rapid release of the SR Ca^{2+} store using Caff and CPA in the presence of 2 mM Ca^{2+} activated robust inward current at the peak of the Ca^{2+}_i transient (at ~90 s in **Figure 5.4A**) in Lean

CSM, which was completely abolished in DMetS (**Figure 5.4C**). The E_{Rev} of +34 mV indicates significant Na^+ and Ca^{2+} permeability. Following SR Ca^{2+} -store depletion, a store-operated cation conductance (SOCC) was not different in the presence or absence of 2 mM Ca^{2+}_o in Lean (**Figure 5.4D**), but was increased in DMetS CSM in 0 mM Ca^{2+}_o compared to 2mM Ca^{2+}_o (**Figure 5.4E**). Importantly, SOCC in the presence of 2 mM Ca^{2+}_o was mildly inward rectifying in Lean CSM, but ohmic in DMetS CSM (**Figure 5.4F,G**). The E_{rev} of +26 mV for SOCC indicates more Na^+ and Ca^{2+} permeability in CSM from Lean pigs, while the E_{rev} of 0 mV argues for non-selective SOCC in CSM from DMetS pigs. These patch clamp data suggest different proteins mediate SOCC between Lean and DMetS.

Discussion

The major novel findings of this study are that coronary smooth muscle (CSM) from Ossabaw swine with metabolic syndrome, coronary artery disease (CAD), and type 2 diabetes (DMetS) strikingly demonstrate a complete absence of Ca^{2+} -induced cation conductance (CICC), while profoundly increased store-operated cation conductance (SOCC) is completely non-selective. Importantly, increased SOCC precedes the development of CAD in short-term dyslipidemic MetS swine (sDMetS). Additional novel findings include greatly increased sarcoplasmic reticulum (SR) Ca^{2+} -store and basal intracellular Ca^{2+} (Ca^{2+}_i) in CSM from DMetS swine. CSM from Ossabaw swine that develop normolipidemic metabolic syndrome (MetS) demonstrate increased SR Ca^{2+} -store, but have increased Ca^{2+} efflux, no change in basal Ca^{2+}_i , no SOCC, and no CAD. Together, these results support a primary role of dyslipidemia in mediating increased SOCC, progression to type 2 diabetes, and development of CAD.

This is the first report of any swine model of MetS atherosclerosis progressing to type 2 diabetes mellitus characterized by ~30% increase in fasting blood glucose, elevated peak glucose and integral of glucose response without compensatory insulin response during intravenous glucose tolerance test (IVGTT), increased homeostasis model assessment (HOMA) index values, and the complete absence of pancreatic β -cell hypertrophy that typically compensates for decreased insulin sensitivity and glucose tolerance. MetS also develop glucose intolerance and insulin resistance, but are able to compensate through increased insulin output and pancreatic β -cell hypertrophy. The striking phenotypic contrast between normo- and dyslipidemic MetS swine, as well as the addition of sDMetS, provides absolutely unique experimental conditions to dissect the determinant mechanisms in the development of CAD.

Ossabaw swine have previously been characterized as possessing a uniquely thrifty phenotype (253), but suffered a nearly 30 year gap in the literature. Our group

responded to a timely appeal by Brisbin to save Ossabaw swine from eradication from their feast and famine ecology on Ossabaw Island, GA, USA (254). We removed Ossabaw swine from their coastal island to form the only large breeding and research herd of Ossabaw swine in the world. Our group has consistently reproduced the MetS phenotype in Ossabaw swine through selective breeding and feeding (3;29;182). However, this is the most convincing report that Ossabaw swine indeed develop overt type 2 diabetes, induced through the simple feeding of hypercaloric, atherogenic diet.

Diabetes mellitus is defined by an elevation in fasting blood glucose. While the threshold for diabetes is 126 mg/dL (7 mmol/L) in humans (45), it is expected that each species should have a different threshold as metabolism varies among species (255). Additionally, the mean fasting glucose for Lean in this study (74 mg/dL or 4.1 mmol/L; **Figure 5.1B**) is on the very low end of values observed in healthy humans (256). Thus, a lower threshold for diabetes should be considered in Ossabaw swine. MetS were clearly not diabetic with no elevation in fasting blood glucose (**Figure 5.1B**), however DMetS fasting blood glucose of 100 mg/dL (5.5 mmol/L; **Figure 5.1B**), representing an approximate 30% increase over Lean, should be considered significant evidence of type 2 diabetes. During the development of type 2 diabetes (see timeline in **Supplementary Figure 5.1**), hepatic and peripheral insulin resistance leads to a compensatory increase in insulin secretion by the pancreas thus instigating a further decreased insulin sensitivity. Increased insulin secretion leads to pancreatic β -cell hypertrophy and stress and eventually decreased β -cell function, resulting in deficient insulin response to glucose load. MetS and DMetS demonstrated clear insulin resistance, as homeostasis model assessment values were elevated compared to Lean (**Figure 5.1E**). However, DMetS were not able to compensate for insulin resistance by increasing insulin secretion during the IVGTT (**Figure 5.1 D&F**) and there was no β -cell hypertrophy in DMetS (**Figure 5.2D**). Directly juxtaposing was the compensatory increase in insulin secretion

and β -cell hypertrophy observed in MetS (**Figure 5.1 D&F and 2D**). Given the elevated fasting blood glucose and HOMA values, the lack of insulin response to glucose load suggests DMetS were progressing towards β -cell collapse and a total inability to produce insulin.

Pancreatic β -cell insulin signaling and hepatic and peripheral insulin sensitivity have been closely linked to dyslipidemia (257). Additionally, reducing circulating triglycerides and LDL cholesterol in patients with and without diabetes has been shown to lower the incidence of CAD (258). As such, the results of this study support a major contribution of dyslipidemia to the development of type 2 diabetes and, regardless of diabetic state, CAD. Specifically, MetS were normolipidemic and did not progress to type 2 diabetes or increased CAD, and DMetS were dyslipidemic and developed overt type 2 diabetes and CAD.

Consistent with a diabetic state, DMetS developed diffuse CAD (**Figure 5.3**). As CSM hyperplasia is a major contributor to advanced coronary atherosclerosis (227) and Ca^{2+} regulation is a key regulator of excitation-transcription coupling (120), we investigated Ca^{2+} regulation in CSM. CSM have three major mechanisms for regulating Ca^{2+}_i : Ca^{2+} entry across the plasma membrane, Ca^{2+} efflux across the plasma membrane, and Ca^{2+} buffering by intracellular Ca^{2+} stores (e.g. sarcoplasmic reticulum [SR]). Elevated baseline Ca^{2+}_i suggested severe Ca^{2+} dysregulation in DMetS CSM compared to Lean and MetS (**Figure 5.4B**). Elevated peak Ca^{2+}_i change in response to Caff and CPA demonstrated increased SR Ca^{2+} store (i.e. (26;197)) in MetS and DMetS CSM compared to Lean, with DMetS also elevated above MetS (**Figure 5.4D**). Importantly, SR Ca^{2+} store capacity is strongly determined by Ca^{2+}_i and Ca^{2+} influx (259;260).

No difference in time to $\frac{1}{2}$ minimum in response to Caff and CPA in the absence of extracellular Ca^{2+} (Ca^{2+}_o) suggests Ca^{2+} efflux across the PM was not different

(13;26;261) between Lean and DMetS, while Ca^{2+} efflux was elevated in MetS (**Figure 5.4C**). Decreased time to $\frac{1}{2}$ minimum in MetS may suggest a compensatory mechanism contributing to normal Ca^{2+} ; through increased Ca^{2+} efflux, despite significantly increased SR Ca^{2+} -store, consistent with previously reported up-regulation of Ca^{2+} sequestration by the SR in diabetic dyslipidemic Yucatan pigs (13;16;174). This would also suggest MMetS are not able to compensate a similar mechanism.

Complete SR Ca^{2+} -store depletion is accomplished in the presence of Caff and CPA, activating store-operated cation conductance (SOCC) pathways. SOCC has been strongly associated with CSM proliferation, migration, and CAD development, by our group and others (29;196). Indeed, CSM from DMetS exhibited a ~3-fold increase in SOCC compared to Lean and MetS (**Figure 5.4E**). Our group has previously shown that SOCC is mediated primarily through canonical transient receptor potential 1 (TRPC1), which is elevated in CSM from MetS swine (29). Importantly, this is the first report of increased SOCC in CSM preceding the development of CAD (i.e. sDMetS in **Figure 5.4H**) that, along with the absence of SOCC and CAD in MetS, provides compelling evidence for the necessity of 1) dyslipidemia in SOCC induction and 2) SOCC in CAD development in MetS swine.

Divalent cation influx, as measured by Mn^{2+} quench of fura-2 fluorescence, was significantly increased in DMetS compared to Lean and MetS when SR depletion was accomplished in Ca^{2+} -free media. Electrophysiological analysis of SOCC revealed monovalent SOCC was not changed in Lean CSM compared to divalent SOCC (**Figure 5D**), but non-selective monovalent SOCC was greatly increased in DMetS CSM (**Figure 5E**). Increased non-selective monovalent SOCC in DMetS is consistent with previous findings from our lab indicating TRPC1 mediates increased SOCC in CSM from MetS swine (29) and suggests an exciting mechanism involving the $\text{Na}^+/\text{Ca}^{2+}$ exchanger. Under normal circumstances NCX antiports three Na^+ ions into the cell and one Ca^{2+} ion

out of the cell, thus reducing Ca^{2+}_i . However increased intracellular Na^+ potentiates reverse mode NCX mediated Ca^{2+} influx (262). Additionally, decreased membrane polarity, reported in MetS Ossabaw CSM via decreased K^+ channel function (140), would be induced by Na^+ influx and further potentiate reverse mode NCX (262). Increased reverse mode NCX in regions of the plasma membrane closely associated with the SR membrane would lead to elevated SR Ca^{2+} -store (e.g. **Figure 5.4D**; (260;263)). SR Ca^{2+} depletion leads to conformational changes in stromal interaction molecule 1 (STIM1) in the SR membrane, in turn leading to direct physical interaction with and activation of TRPC1 in the plasma membrane (264). Thus, a close apposition of plasma membrane and SR membrane is essential for SOCC induction and provides an ideal opportunity for SOCC-induced reverse mode NCX. Other TRPC isoforms are known to directly induce reverse mode NCX through Na^+ influx involving receptor operated, but not store-operated, mechanisms of TRPC3/6 activation (265;266). Taken together, previous publications and the results of this study strongly suggest increased Na^+ influx conducted by TRPC1-mediated SOCC leads to reverse mode NCX and divalent cation influx in CSM from DMetS (outlined in **Supplementary Figure 5.2**).

Voltage-gated Ca^{2+} channels (VGCC) provide a significant Ca^{2+} conductance pathway in depolarized CSM, contributing to CSM contraction (267;268). Previous reports showed an ostensibly counter-intuitive decrease in voltage-gated Ca^{2+} conductance (VGCC) in CSM from hyperlipidemic and alloxan-induced diabetic Yucatan swine (13;267). However, strong evidence indicates that Ca^{2+} influx through VGCC preserves vascular smooth muscle contractile phenotype and genes, while down-regulation of VGCC induces de-differentiation associated with proliferation and migration (172). While this study cannot rule out VGCC contribution to Ca^{2+} -dysregulation in MetS CSM, decreased VGCC Ca^{2+} conductance would not increase Ca^{2+}_i . Also, it is evident

that VGCC do not significantly contribute to SOCC, as nifedipine does not inhibit SOCC (**Supplementary Figure 5.3**).

TRPM (melanostatin) 4 has been shown to directly inhibit SOCC in T lymphocytes (269). CSM from Lean demonstrated a cation conductance activated by increased Ca^{2+}_i . This Ca^{2+} -induced cation conductance (CICC) is strikingly similar to previous biophysical characterizations of TRPM4b (270) (**Figure 5C**). This provides the exciting possibility that, although Lean CSM express TRPC1 (29) and minimal SOCC (**Figure 5.4&5**; (29)), the co-expression of TRPM4 provides an inhibitory mechanism preventing increased SOCC that is not present in DMetS, thus resulting in potentiation of SOCC in DMetS CSM. This intriguing hypothesis, while not directly assessed in this study, should be considered in future studies investigating the involvement of TRPM4 in smooth muscle from diabetic coronary arteries demonstrating elevated SOCC.

This study provided compelling evidence of the first swine model of metabolic syndrome that progressed to type 2 diabetes mellitus and developed diffuse coronary artery. Extensive fura-2 based Ca^{2+} imaging studies clearly defined Ca^{2+} dysregulation in coronary smooth muscle from diabetic, dyslipidemic Ossabaw miniature swine characterized by 1) elevated baseline Ca^{2+}_i , 2) increased SR Ca^{2+} -store, 3) and increased SOCC. This is the first report of SOCC preceding the development of CAD, thus providing compelling evidence for a causative role. Patch clamp studies revealed robust TRPM4-like CICC in Lean CSM and no evidence of CICC and, correspondingly, increased non-selective SOCC in DMetS CSM. It is evident that dyslipidemia is a primary mediator of increased CSM SOCC, progression to diabetes, and diffuse CAD.

Acknowledgements

This work was supported by the National Institutes of Health grants HL062552 and RR013223 and an Innovation Award from the American Diabetes Association to M.S., the Purdue-Indiana University Comparative Medicine Program, and the Fortune-Fry Ultrasound Research Fund of the Department of Cellular & Integrative Physiology at Indiana University School of Medicine. J.M.E. and Z.P.N. were the recipients of a Translational Research Fellowship from the Indiana University School of Medicine, Z.P.N. was the recipient of a Translational Fellowship from NIH UL1 RR025761. The authors have no conflicts of interest to disclose.

Figure Legends

Figure 5.1 Intravenous glucose tolerance test reveals glucose intolerance and insulin resistance in MetS and type 2 diabetes in DMetS. A Peak glucose is elevated in MetS and DMetS compared to Lean. **B** Fasting glucose was elevated ~30% in DMetS compared to Lean and MetS. **C** Integral of the glucose response is elevated in DMetS compared to MetS and Lean, while MetS was elevated compared to Lean. **D** Peak insulin response is elevated in MetS compared to DMetS and Lean. **E** HOMA index values were increased in MetS and DMetS compared to Lean. **F** Integral of the insulin response is elevated in MetS compared to DMetS and Lean. Immunohistochemistry was performed on pancreas histological sections targeting insulin (**G,H**). **G** Arrows show insulin positive islets in Lean group. **H** Increased insulin positive area shows beta cell expansion and increased adipocyte area in MetS (*). **I** Pancreas percent insulin positive area was increased in MetS compared to DMetS.

Figure 5.2 Coronary artery disease is increased in DMetS, but not MetS. A Representative angiogram of left anterior descending (LAD) and circumflex (CFX) coronary arteries with schematic of proximal (Prox.), intermediate (Inter.), and distal segments. **B** Representative DMetS IVUS image with 63 percent wall coverage. **C** DMetS percent wall coverage is increased compared to Lean and MetS.

Figure 5.3 Metabolic syndrome induces Ca²⁺ dysregulation in coronary smooth muscle. A Baseline Ca²⁺ concentration, SR Ca²⁺ store (peak), Ca²⁺ efflux (time to ½ min.), and store-operated Ca²⁺ entry (SOCE; slope in Mn²⁺) were assessed in CSM. CSM were in physiological salt solution before switching the extracellular superfusate to 0 Ca²⁺ solution containing 5 mM caffeine (Caff) and 10⁻⁶ M cyclopiazonic acid (CPA) followed by addition of 2 mM Mn²⁺. Each solution was applied for the duration indicated

by the horizontal lines. **B** Baseline intracellular Ca^{2+} was elevated in DMetS CSM compared to MetS and Lean. **C** The time from peak Ca^{2+} response to caffeine to $\frac{1}{2}$ minimum was significantly reduced in MetS compared to Lean and DMetS. **D** Peak Ca^{2+} response to caffeine was increased in MetS compared to Lean, and DMetS compared to Lean and MetS. **E** The rate of Mn^{2+} influx is increased in DMetS compared to Lean and MetS. Short-term DMetS (sDMetS) have no change in baseline (**F**) or peak response to caffeine (**G**), while Mn^{2+} permeability (SOCE; **H**) is increased in sDMetS compared to Lean.

Figure 5.4 Dysfunctional mono- and di-valent cation conductances in DMetS compared to Lean. Whole cell current was recorded in freshly dispersed CSM at -80 mV holding potential at 2-5 s intervals for **A** Lean and **B** DMetS. 2000-ms ramp functions (-100 mV to +70 mV) were inserted at (**C**) peak Ca^{2+} -induced conductance or peak store-operated cation conductance (SOCC) in the (**D**) presence or (**E**) absence of 2 mM extracellular Ca^{2+} . **C-G** Representative leak-subtracted currents with mean and SEM values at -90, -60, -30, +30, and +60 mV. **C** Ca^{2+} -induced cation conductance is completely abolished in DMetS (Reversal potential, $E_{\text{Rev}} = 0$) compared to Lean ($E_{\text{Rev}} = 34$). **D** In the presence (\bullet , +Ca) or absence (\circ , -Ca) of 2 mM extracellular Ca^{2+} , SOCC is not different in Lean. **E** Non-selective, ohmic SOCC is increased in DMetS ($E_{\text{Rev}} = 0$) in the absence of extracellular Ca^{2+} , consistent with TRPC1-mediated SOCC. In the presence of 2mM extracellular Ca^{2+} , expanded scale demonstrates (**F**) inward rectifying, Ca^{2+} -selective current in Lean ($E_{\text{Rev}} = 26$), consistent with Orai1-mediated SOCC and (**G**) ohmic, non-selective current in DMetS ($E_{\text{Rev}} = 0$), consistent with TRPC1-mediated SOCC.

Table 5.1

	Lean	MetS	DMetS	p < 0.05
Start body weight (BW, kg)	41.5 ± 1.8	45.7 ± 2.7	48.0 ± 2.5	
End BW (kg)	59.0 ± 2.4	94.4 ± 6.4	78.7 ± 5.3	*, †
Girth (cm)	86.9 ± 2	117.5 ± 5	100.2 ± 3	*, †
Total cholesterol (mg/dl)	52.8 ± 3.5	59.9 ± 4.3	244.7 ± 11.9	**
LDL (mg/dl)	17.3 ± 1.7	35.2 ± 3.1	168.9 ± 9.6	**
HDL (mg/dl)	34.7 ± 2.8	24.5 ± 5.3	75.8 ± 8.3	**
LDL/HDL Ratio	0.5 ± 0.1	2.4 ± 2.0	2.4 ± 0.8	*
Triglycerides (mg/dl)	17.2 ± 2.6	30.1 ± 2.3	36.4 ± 9.8	*
Systolic blood pressure (mmHg)	123.9 ± 8.6	147.7 ± 6.6	139.6 ± 3.6	*
Diastolic blood pressure (mmHg)	80.3 ± 6.5	92.6 ± 4.3	85.5 ± 3.1	*
Mean arterial pressure	94.8 ± 7.1	110.3 ± 5.0	103.6 ± 3.1	**

Table 5.1 MetS characteristics of Ossabaw swine. Comparisons between groups were made by one-way analysis of variance (ANOVA) with Newman-Keuls *post-hoc* analysis.

Figure 5.1

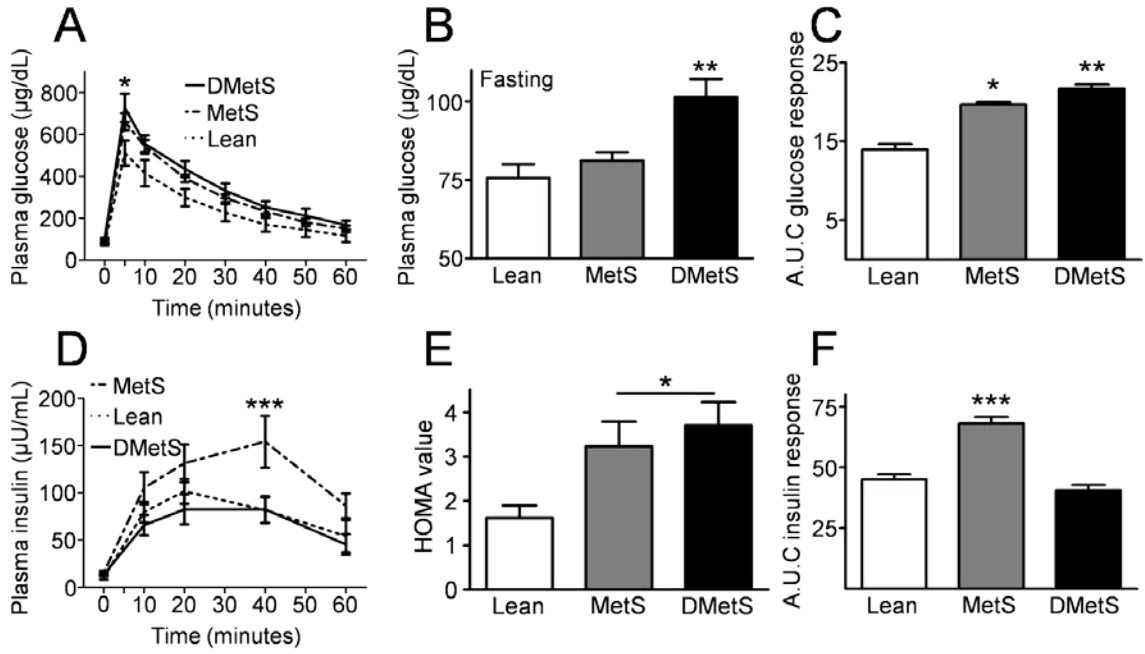


Figure 5.2

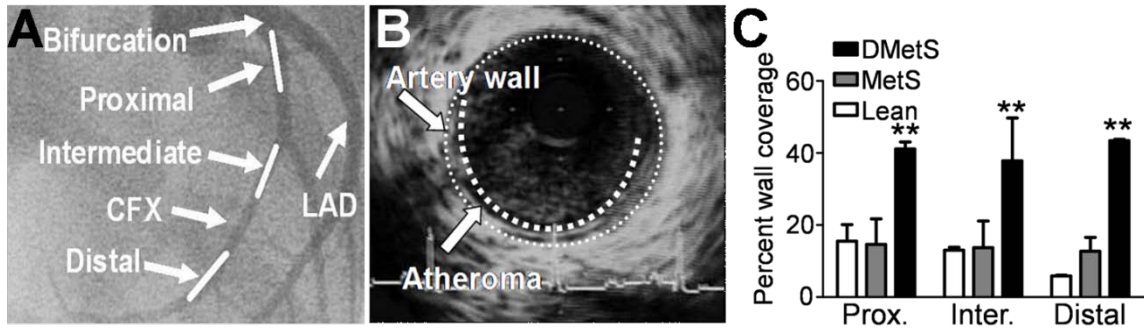


Figure 5.3

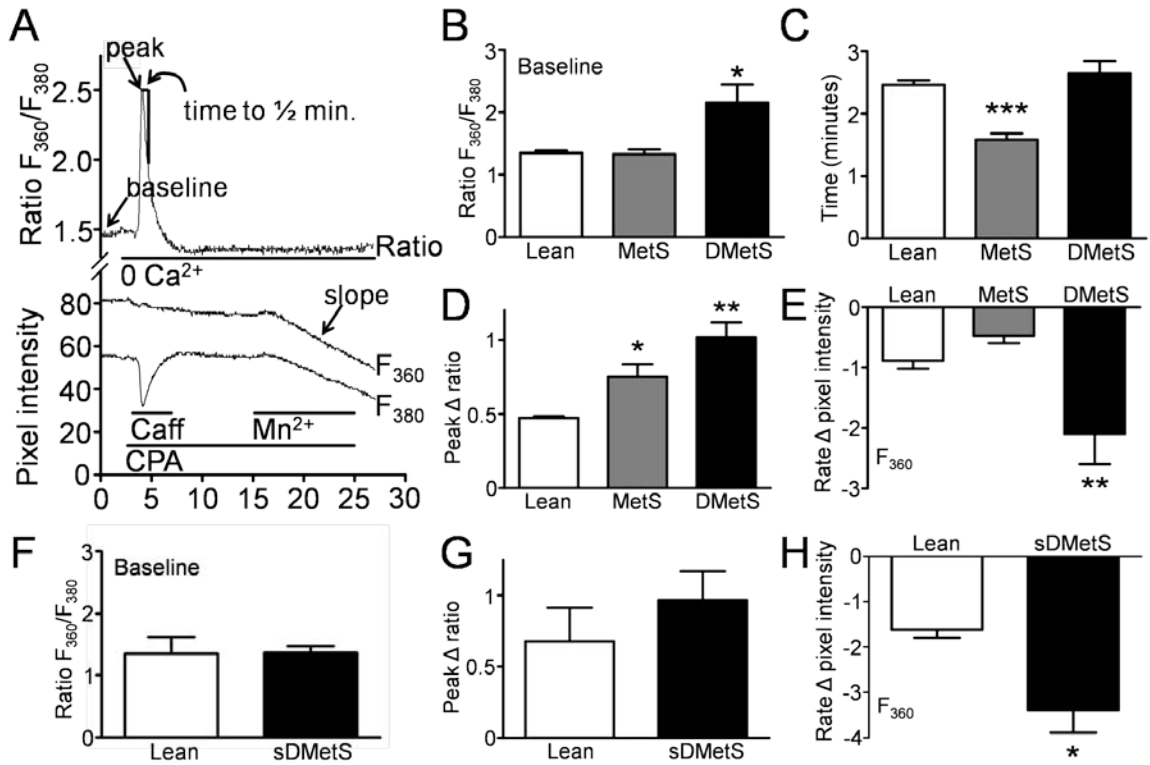
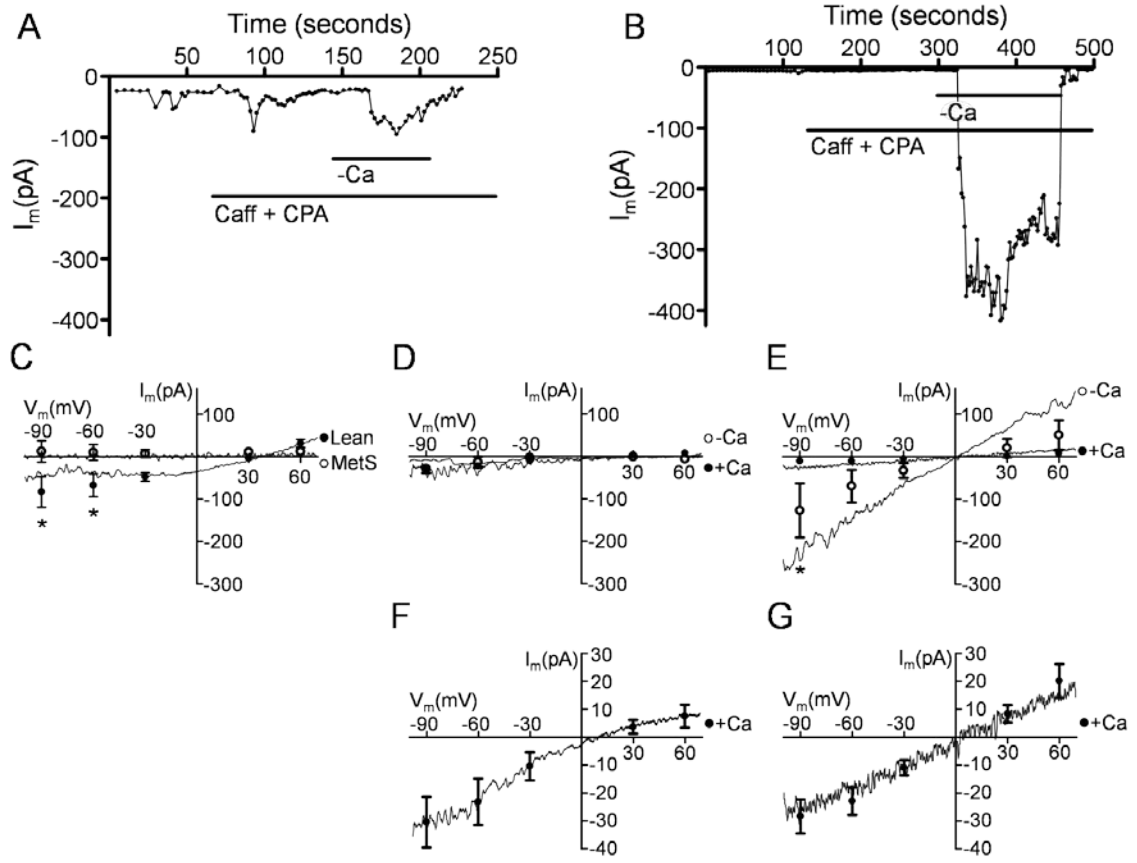


Figure 5.4



Chapter 6

General overview

The major hypotheses tested in this thesis were that 1) Ossabaw swine have a genetic predisposition for metabolic syndrome (MetS), type 2 diabetes, and coronary artery disease (CAD) compared to the lean Yucatan breed, 2) dyslipidemia is the primary component of MetS necessary for the development of non-alcoholic steatohepatitis, type 2 diabetes, and CAD, 3) MetS increases store-operated Ca^{2+} entry (SOCE) and CAD in non-stent and peri-stent segments of coronary artery and exercise attenuates these events, and 4) dyslipidemia is necessary for increased SOCE that significantly contributes to the development of CAD in MetS. Powerful study designs utilizing the only large animal model of MetS, type 2 diabetes, and CAD elucidated several novel findings with important implications for the fundamental treatment of human disease.

The major novel findings of this thesis were: 1) Ossabaw swine are predisposed to MetS, features of type 2 diabetes, and diffuse native and in-stent CAD compared to Yucatan swine. 2) Fructose is a necessary, but not sufficient, dietary component for induction of NASH. 3) The diet components of high fructose, mixed-source fat, and cholesterol uniquely synergize in the development of severe CAD. 4) Insulin resistance in MetS, while possibly permissive and synergistic, is not predictive of NASH or CAD. 5) Individual fatty acid methyl esters (FAME) heptadecaenoic and vaccinate acid (among others previously reported in CAD trials) are strongly associated with severity of CAD. 6) Several individual and group FAME are strongly associated with NASH. 7) Dyslipidemia, defined by dyslipoproteinemia and hypertriglyceridemia, is a necessary component of MetS for the development of NASH and CAD. 8) Elevated integral of LDL cholesterol (LDL gram-years) is strongly predictive of NASH and CAD in MetS. 9) SOCE is elevated in coronary smooth muscle (CSM) of atherosclerotic arteries, and this increased SOCE

precedes the development of CAD. 10) Ca^{2+} induced cation conductance in completely abolished in MetS. 11) Increased monovalent permeance through store-operated pathways in CSM is primarily mediated by dyslipidemia in MetS. 12) Biophysical properties of SOCE in CSM are consistent with TRPC1 as the molecular mediator of SOCE. 13) Exercise training decreases SOCE function and transient receptor potential canonical 1 (TRPC1) and stromal interaction molecule 1 (STIM1) in CSM from native CAD in MetS. 14) Exercise training attenuates native CAD in MetS.

Porcine model of metabolic syndrome

Swine are commonly used in the study of diabetes (12;142;271-273) and cardiovascular disease (4;110;165;274-276) because of their similarities to human lipid metabolism, insulin signaling, cardiovascular anatomy and function, size, activity level, and omnivorous diet (reviewed elsewhere (277)). Yucatan swine have been used extensively in cardiovascular research, although they develop sparse CAD in the absence of combined atherogenic diet and chemically-induced diabetes (reviewed elsewhere (115)). As such, Yucatan swine are a lean breed that never develop obesity, primary insulin resistance, glucose intolerance, elevated triglycerides, or hypertension when fed excess calorie atherogenic diet (reviewed elsewhere (278)). As demonstrated in this report and elsewhere, Ossabaw swine have been shown to be prone to obesity when compared to leaner breeds (**Chapter 2**, (3;168;253;279-281)) and develop all aspects of the MetS when fed excess calorie atherogenic diet (**Chapters 3, 4, and 5**, (3;4;6;29;282)). Additionally, Ossabaw swine demonstrated CAD mediated by excess atherogenic diet (3). Therefore, in **Chapter 2** we rigorously confirmed that Ossabaw swine have a propensity to obesity, MetS, cardiovascular dysfunction, native CAD, and in-stent stenosis compared to Yucatan swine when fed eucaloric diet (demonstrated to maintain healthy Yucatan body weight (4)) with either normal or high fat.

Similar to the Pima Indian population in the American southwest (283), Ossabaw swine developed a thrifty genotype through hundreds of years of natural selection in a harsh feast and famine ecology. While efficient storage of fat is beneficial when food supply is limited, when combined with long-term hypercaloric intake high in fat and carbohydrates (i.e. the modern diet) leads to obesity and propensity for type 2 diabetes (original thrifty genotype in modern times hypothesis outlined by Neel, J.V. in 1962 (284)). The strong evolutionary process of natural selection sets Ossabaw swine apart as a model of MetS compared to Göttingen minipigs that develop dyslipidemia, but not glucose intolerance or insulin resistance (110), Yucatan swine that develop high LDL cholesterol, but no other MetS component (1;2;9), and various Chinese minipigs that are relatively resistant to insulin resistance and glucose intolerance (142).

Chapter 4 and previous reports (3;4;20;21) induced MetS in Ossabaw swine using excess calorie atherogenic diet composed primarily of standard chow supplemented with partially hydrogenated soybean oil (high in trans-fat) and cholesterol. Excess high trans-fat/cholesterol induced complete MetS, including glucose and insulin resistance, mild atherosclerotic CAD, and no liver dysfunction or disease (7). Expanding on these studies, excess calorie high fructose alone was sufficient for the development of normolipidemic MetS, but was not sufficient for progression to type 2 diabetes, CAD, or NASH (**Chapter 3**). However, the addition of high fructose to excess calorie high fat (from varying source) and cholesterol diet enabled progression to type 2 diabetes and development of NASH and severe CAD (**Chapters 3 and 5**).

Porcine model of type 2 diabetes

Type 2 diabetes is clinically defined as fasting blood glucose above 126 mg/dL or 2-hour plasma glucose levels on oral glucose tolerance test above 200 mg/dL (reviewed elsewhere (256)). Although similar to humans, important differences in swine glucose

homeostasis should be taken into careful consideration when defining diabetes in swine (reviewed elsewhere (277)). Chief among these concerns are the lower fasting glucose levels (65-75 mg/dL swine (**Chapters 2-5**; (285), 74-106 human, reviewed elsewhere (256)) in healthy swine compared to humans. Also of importance, swine have relatively high glucose tolerance to oral glucose load and increased clearance following intravenous glucose load (**Chapters 2-5** (277)). Additionally, swine pancreatic β -cell:body mass ratio is twice that in humans, suggesting significant insulin secretory reserve in swine (286;287). Taken together, these observations suggest a lower threshold for the diagnosis of prediabetes and diabetes mellitus should be considered for swine.

Chapters 3 and 5 provide the most compelling evidence of progression to type 2 diabetes in the Ossabaw swine model of MetS. OssH (**Chapter 2**), F/MetS (**Chapters 3 and 5**), TMetS (**Chapter 4**), and XMetS (**Chapter 4**) swine groups in this report demonstrated fasting blood glucose levels between 75 and 90 mg/dL, consistent with a prediabetic state in swine, as outlined in **Figure 6.1**. Additionally, MMetS and DMetS fasting blood glucose were elevated above 90 mg/dL, the threshold for Ossabaw swine diabetes outlined in **Figure 6.1**. Additionally, histological analysis of pancreas insulin positive area was used to assess the relative density of pancreatic β -cells. MMetS demonstrated a significant increase in insulin positive pancreatic β -cell area compared to Lean, suggesting compensatory β -cell hypertrophy (**Figures 3.1 and 6.1**). DMetS fasting blood glucose were the highest of any group in this report, while insulin response during intravenous glucose tolerance test (IVGTT) and insulin positive pancreatic β -cell area was not different than their Lean cohorts (**Figure 5.2**). These results are suggestive of progression through pancreatic β -cell hypertrophy and into β -cell collapse, the late stages of type 2 diabetes (timeline outlined in **Figure 6.1**). It is possible that DMetS simply failed to compensate for peripheral insulin resistance by increasing insulin

secretion, however the underlying mechanism of such an event is uncertain. Importantly, 50-75% of patients with diabetes demonstrate significant fatty liver (63). Additionally, non-alcoholic fatty liver disease predicts the future diagnosis of type 2 diabetes (288).

Fructose and dyslipidemia mediate non-alcoholic steatohepatitis

NAFLD is generally considered the manifestation of MetS in the liver (289). As such, insulin resistance (peripheral and hepatic), dyslipidemia, and elevated triglycerides are defining characteristics of NAFLD (290). The progression of NAFLD to NASH is poorly understood (57), and diagnosis of NASH is relatively intensive, typically requiring histological analysis following liver biopsy (291). NASH is characterized by steatosis, inflammation, hepatocyte ballooning, and increased fibrosis (57). While NAFLD is fairly benign, NASH is associated with cirrhosis and reduced life expectancy (292) adding to the importance of early detection. Until the recent description of NASH in Ossabaw swine with MetS (7), there was absolutely no animal model of NASH available. As such, **Chapter 3** is the first report of NASH in a model of type 2 diabetes and MetS.

NASH was never observed in swine fed high fat/cholesterol atherogenic diet (**Chapters 2, 4, and 5**), even when the diet regimen lasted 2-3 times as long as the current studies (293), until the addition of high fructose (7). However, high fructose alone was not sufficient to induce NAFLD or NASH, although it was sufficient for induction of MetS (e.g. FMetS in **Chapter 3**). This suggests that fructose within an atherogenic diet is permissive for the development of NAFLD and NASH. The exact mechanism of this action is not known, however a volume of literature showing altered fatty acid metabolism with high fructose feeding may provide clues. High fructose feeding for only six days in human subjects was shown to stimulate *de novo* lipogenesis, elevate fasting triglycerides, blunt suppression of endogenous glucose production during hyperinsulinemic-euglycemic clamp, indicating hepatic insulin resistance, and impaired

suppression of non-esterified fatty acids, indicating adipose insulin resistance (294). Chronic high fructose feeding in rats inhibited *de novo* lipogenesis in adipose tissue, while hepatic lipogenesis was elevated under the same condition (218). Importantly, *de novo* lipogenesis was significantly elevated in patients with NAFLD and NASH (214). Taken together, these observations suggest high fructose intake leads to significantly elevated triglycerides, both circulating and hepatic, that is an essential step in the development of NAFLD and NASH (295).

We selectively eliminated dyslipidemia from the MetS milieu and tested the hypothesis that dyslipidemia, defined as the combination of dyslipoproteinemia and hypertriglyceridemia (210), is necessary for the development of NASH in the MetS (**Chapter 3**). Testing the role of dyslipidemia was important as many reports suggest that insulin resistance may be the primary mediator of NAFLD progression (reviewed elsewhere (296)). FMetS swine developed MetS without concomitant dyslipidemia, DMetS developed MetS with relatively mild dyslipidemia, and MMetS developed MetS with severe dyslipidemia and type 2 diabetes (**Figure 3.1** and **Table 3.1**). This powerful study design allowed dissection of the dyslipidemic contribution and clearly demonstrated the necessity of dyslipidemia in NASH within the MetS. The major findings that cumulative LDL cholesterol (LDL gram-years) powerfully predicted NASH severity ($r = 0.88$; **Figure 3.5**) and adipose insulin resistance weakly (**Chapter 3 discussion**) and fasting insulin levels and homeostasis model assessment HOMA values (data not shown) do not predict NASH, provide powerful evidence that dyslipidemia is the primary mediator of NASH in the MetS, while insulin resistance may play a facilitatory and synergistic role. While NASH increases the risk of liver-related mortality (e.g. cirrhosis and hepatocellular carcinoma), the leading cause of death in patients with NASH is in fact CAD (64).

Dyslipidemia is necessary for coronary artery disease

CAD and NASH are very tightly associated (**Figure 5.5** and (57;58)). Additionally, type 2 diabetes is a major contributor to the extent, severity, and complications associated with treatment of CAD (74;86;234), while MetS is associated with increased risk of CAD (224). As such, here we report the most severe CAD ever observed in any animal model of type 2 diabetes and MetS (**Figure 3.2**). CAD in Ossabaw swine fed atherogenic diet is diffuse (**Figures 2.4, 3.2, 4.2, and 5.2**).

Diffuse CAD is expected of CAD in diabetic humans (297), but this is a completely novel observation for any animal model of CAD. Interestingly, excess atherogenic diet, severe MetS, and overt type 2 diabetes are not prerequisite of diffuse CAD as observed in OssH (**Figure 2.4**). This leads to the speculation that diffuse CAD may be a preceding event to the onset of diabetes and that predilection to both disease states may in fact be driven by some primary defect, an interesting hypothesis which has not been tested either clinically or in any experimental model. Diffuse CAD is at highest risk of plaque rupture and thrombosis (reviewed elsewhere (298)) and drastically complicates treatment options of flow-limiting stenosis (76). Thus, Ossabaw swine may serve as an excellent model for studying thrombosis and plaque rupture, especially considering the total metabolic disease reliably demonstrated by Ossabaw swine with MetS.

While it is clear that MetS is predictive of CAD (224), the relative contribution of individual factors is, by definition, difficult to discern in the complicated metabolic disease. F/MetS, demonstrating MetS without dyslipidemia (**Chapters 3 and 5**), were used to test the hypothesis that dyslipidemia is necessary for the development of CAD within MetS. The striking and absolutely clear requirement of dyslipidemia was made evident as F/MetS did not develop CAD despite similar insulin resistance, glucose intolerance, obesity, and hypertension compared to DMetS, MetS with addition of

dyslipidemia, that developed extensive CAD (**Figures 3.2** and **5.2**). Additionally, LDL gram-years showed immense predictive power for CAD (**Figure 3.5**), while all markers of insulin resistance and glucose intolerance that were investigated did not predict CAD (**Chapter 3** and data not shown).

TMetS (hypercaloric high trans-fat/cholesterol) developed MetS and mild CAD similar to DMetS (hypercaloric high fructose/trans-fat/cholesterol), however DMetS was fed atherogenic diet only 24 weeks compared to the 54 weeks of TMetS (**Chapters 4** and **5 Methods**). Importantly, dyslipidemia was not different between TMetS and DMetS (**Tables 4.1** and **5.1**), suggesting that the addition of high fructose to atherogenic diet accelerates the progression of CAD in the MetS through a mechanism independent of increased dyslipidemia. These results are consistent with human clinical trials showing high fructose addition independently increases risk of CAD (reviewed elsewhere (299)). Accordingly, fructose should remain an important part of any atherogenic diet interested in maximizing CAD, as fructose represents an independent risk factor for CAD in MetS.

While elevated dietary fructose is important, it is clearly not the only component of atherogenic diets mediating CAD, as the source of dietary fats greatly determines the physiological effects (reviewed elsewhere (300)). For many years, atherogenic diets high in saturated and cis-fat and cholesterol were used to produce mild atherosclerosis in Yucatan swine (10-19;174;301-309). More recently, human studies have shown hydrogenated cooking oil high in trans-fat acids result in more extreme increases in total LDL and decreases in HDL (310), implying a more atherogenic profile. As such, high trans-fat/cholesterol atherogenic diet produced elevated CAD in female Ossabaw swine (3); recent studies from our laboratory have almost exclusively used atherogenic diets high in trans-fatty acids (**Chapters 2-5** and (4;6;20-22;29;311-314)). In collaboration with Purina TestDiets®, we formulated a unique atherogenic diet high in fructose/cholesterol/mixed-source fat (MMetS).

MMetS CAD was severe, with focal lesions in excess of 75% stenosis, and complex, with calcifications in 25% of the artery segments analyzed by IVUS (**Figure 3.2**). Histological analysis of MMetS CAD revealed advanced, complicated lesions ranging from fibro-fatty streaks to lipid-laden cores surrounded by fibrous caps (**Figure 3.3**). Compared to DMetS (high fructose/trans fat/cholesterol), MMetS intima contained less collagen and more cells/unit area, consistent with decreased plaque stability (**Figure 3.3**). Thus, **Chapter 3** outlined the most severe CAD phenotype ever reported in a model of MetS and type 2 diabetes.

Fatty acid methyl esters, not free fatty acids, predict coronary artery disease and non-alcoholic steatohepatitis

Free fatty acids (FFA) have been demonstrated to not be predictive of MetS or diabetes in longitudinal analysis, although cross-sectional analysis suggested FFA were highly associated with MetS and diabetes (211). Our results are in complete agreement, as total serum FFA did not correlate to either CAD or NASH (**Table 3.3**). Our study was powerfully designed to dissect any effect of FFA on CAD and NASH without the confounding effects of dyslipidemia already discussed (**Figure 3.5**). Accordingly, studies with concomitant dyslipidemia and elevated FFA should be interpreted with caution.

Total FFA did not correlate to CAD or NASH. However, the recent Atherosclerosis Risk in Communities (ARIC) study found powerful associations between individual and grouped fatty acid methyl esters (FAME) and incidence of heart failure (212). Our results agreed with associations between heart failure and palmitoleic acid, oleic acid, linoleic acid, total monounsaturated fatty acids (TOTM), and total polyunsaturated fatty acids (PUFA), as each shared directionally identical associations with development of CAD and severity of NASH in Ossabaw swine (**Table 3.2 and 3.3**). Heptadecanoic and vaccinate acid, monounsaturated fatty acids, were not assessed in

the ARIC trial, but also strongly and directly correlated with CAD and NASH (**Table 3.2**). Thus, monounsaturated fatty acids demonstrated the most reliable direct predictive power, while polyunsaturated acids inversely correlated with CAD and NASH. Given that some FAME were directly associated while others were inversely associated with CAD and NASH, it should be of no surprise that total FFA showed no significant association with either. Although some FAME correlations to heart disease (e.g. CAD) outlined in **Chapter 3** have been reported elsewhere, **Chapter 3** was the first report of heptadecanoic and vaccinate acid associations with CAD, nonetheless in an animal model of CAD in type 2 diabetes and MetS. Additionally, **Chapter 3** was the first report of any FAME associations with NASH.

Stent-induced neointimal hyperplasia in metabolic syndrome

Coronary stents are the most common form of treatment for flow-limiting stenoses (68). While the advent of drug-eluting stents has greatly diminished acute restenosis of the stented region, their use has led to increased risk of late stage thrombosis (315). Additionally, stenting is contraindicated in many cases involving complex lesions or coronary anatomy (e.g. diabetic shock; (76;77)). Recent questions regarding the necessity and safety of drug-eluting stents (99;101) may have been avoided had a suitable animal model of native stenosis in type 2 diabetes and MetS been available for preclinical trials. Stent efficacy preclinical trials have utilized over-inflation injury in lean swine breeds (e.g. Yucatan). As such, Yucatan response to vascular injury is fairly well characterized, providing an opportunity to test the hypothesis that Ossabaw swine exhibit increased stent-induced neointimal hyperplasia.

This hypothesis was tested by deploying a single stent at nominal diameter in the left circumflex coronary artery of Yucatan and Ossabaw swine fed either eucaloric chow or atherogenic diets (YucC, YucH and OssC, OssH, respectively). Ossabaw in-stent

neointimal hyperplasia after 4-weeks was increased compared to Yucatan, irrespective of diet (**Figure 2.6I**). Additionally, in-stent neointima was more cellular and contained more collagen, both suggesting increased CSM proliferation (**Figure 2.6J** and **K**). Accelerated neointimal hyperplasia induced by stent deployment is not limited to the in-stent region, as artery segments outside the edges of the stent (peri-stent) also experience accelerated neointimal hyperplasia (29). Additionally, peri-stent disease is elevated in patients with complicated metabolic disease (e.g. diabetes (74)). Peri-stent CAD was elevated with atherogenic diet (**Figure 2.5**). Although there was no significant difference between peri-stent neointima in Ossabaw compared to Yucatan, there was a very strong trend for increased Ossabaw peri-stent disease irrespective of diet (**Figure 2.5**). Accordingly, Ossabaw swine are a suitable model to test efficacy of treatment against stent-induced injury.

Short term exercise training effects on metabolic syndrome and coronary artery disease

Exercise is very efficacious in inducing regression of native CAD (235;236) and improves long-term outcomes following revascularization of coronary arteries (226). As such, MetS swine exposed to 3 weeks of exercise following induction of MetS and before stent placement, and 3 weeks of exercise following stent placement (XMetS; high trans-fat/cholesterol; see **Figure 4.1** for study timeline) demonstrated significantly regressed native CAD and peri-stent neointima (**Figure 4.2**). These results are remarkably consistent with human clinical trials (226). However, angioplasty-induced neointimal hyperplasia was not changed with exercise (**Figure 4.2**) as previously demonstrated in non-diabetic swine (232). Key differences in study design may account for this discrepancy. First, our study employed a much shorter exercise regimen (7 weeks compared to 20 weeks); second, our study deployed bare metal stents compared to simple balloon angioplasty (**Chapter 4** and (232)).

Considering exercise has shown efficacy in treating MetS and prediabetes (237), it was somewhat surprising that exercise in XMetS did not improve any MetS characteristics (e.g. hypertension). However, exercise is typically prescribed along with dietary changes (237). As such, continued excess calorie atherogenic diet in our study may have ameliorated any effect of exercise. Additionally, Ossabaw swine have a loss-of-function mutation in AMP kinase gamma 3 subunit. AMPK γ 3 is an important mediating enzyme of skeletal muscle fatty acid oxidation and glucose utilization (238). Swine with loss-of-function AMPK γ 3 mutation are less responsive to exercise, as measured by AMPK activation (238). Thus XMetS may not have received the full benefit of exercise.

Ca²⁺ signaling events in coronary smooth muscle cells

CSM are the predominant cell type in atherosclerotic lesions (316). Ca²⁺ regulation has been shown to be important in mediating CSM proliferation, migration, and extracellular matrix deposition (169-171;196;316;317) that are all pivotal events in the development of CAD (318-320). Extensive studies of Ca²⁺ regulation in CSM from multiple disease states were completed and are summarized in **Table 6.1**.

Intracellular Ca²⁺ buffering, mediated primarily by SERCA (outlined in **Figure 2.5**), decreases are associated with CSM proliferation in diabetes (321). Ossabaw swine have been shown to be predisposed to prediabetes and CAD (**Chapter 2** and **Figure 6.2**). Accordingly, SERCA function was decreased in CSM from Ossabaw swine compared to Yucatan (**Figure 2.8**). This was the only measurement of SERCA function in this thesis, as all other Ca²⁺ imaging experiments were primarily designed to measure Ca²⁺ flux across the plasma membrane. However, caffeine-sensitive SR Ca²⁺ store was quantified in Lean and MetS swine.

SR Ca^{2+} store is primarily mediated by SERCA, ryanodine receptor, and IP3 receptor and Ca^{2+}_i (outlined in **Chapter 1**). Ryanodine- and IP3-sensitive SR Ca^{2+} stores have been shown to decrease in proliferating vascular smooth muscle cells (322;323), however the cells used in both studies were cultured aortic smooth muscle. Ossabaw CSM SR Ca^{2+} store was not different than Yucatan (**Figure 2.7**) or in short-term MetS (sDMetS; **Figure 5.3**). However, CSM from MetS demonstrated increased SR Ca^{2+} store in the absence of CAD, while DMetS was greater than MetS (**Figure 5.3**). SR Ca^{2+} store was decreased in peri-stent CSM. The relative distribution of ryanodine and IP3 receptors is not clearly defined in smooth muscle compared to other cell types (324;325). However, there is some evidence that, rather than distinct SR Ca^{2+} pools accessible to only one receptor type, there is relative heterogeneity in ryanodine and IP3 receptor distribution within the SR membrane of vascular smooth muscle (326-328). The implications of this are vital for proper interpretation of the caffeine-sensitive SR Ca^{2+} store results. In this report, the assumption is made that ryanodine (caffeine sensitive) and IP3 (caffeine insensitive) receptors access the same SR Ca^{2+} store, as the literature suggests. As such, the changes in caffeine response represent changes in bulk SR Ca^{2+} store (i.e. peri-stent < Lean < MetS < DMetS). It is not clear from these results if changes in SR Ca^{2+} store are due to Ca^{2+} leak from the SR or SERCA function.

Ca^{2+} permeance across the plasma membrane is the primary determinant of Ca^{2+}_i . As outlined in **Chapter 1**, plasma membrane Ca^{2+} conductance is tightly regulated. Ca^{2+} efflux is primarily determined by NCX, PMCA, and SERCA via NCX (outlined in **Figure 2.5**) and is quantified by the time $\frac{1}{2}$ minimum in response to caffeine (13;26). CSM from type 1 diabetic/dyslipidemic Yucatan swine with mild atherosclerosis demonstrated decreased PMCA-mediated Ca^{2+} efflux (13;26). Accordingly, total Ca^{2+} efflux in CSM from MetS-prone Ossabaw was decreased compared to the lean Yucatan breed (**Figure 2.7**). It is not clear whether this decreased Ca^{2+} efflux is mediated by

PMCA, NCX, or SERCA via NCX. All other studies measuring Ca^{2+} efflux in this report were completed in the presence of cyclopiazonic acid (10^{-5} M, selective SERCA antagonist), thus Ca^{2+} efflux was not mediated by SERCA via NCX. NCX-mediated Ca^{2+} efflux has been shown to not change in diabetic, dyslipidemic swine CSM, and PMCA has been shown to either primarily mediate decreased Ca^{2+} efflux due to diabetic dyslipidemia (13). However, it should not be assumed that CSM from Ossabaw swine will behave in a similar fashion (i.e. differential Ca^{2+} efflux in CSM from Lean Ossabaw and Yucatan swine, **Figure 2.7**) and studies in this report did not dissect the relative contribution. As such, “ Ca^{2+} efflux” refers to PMCA/NCX-mediated Ca^{2+} efflux hereafter.

Ca^{2+} efflux was decreased in CSM from peri-stent artery, accelerated, stent-induced neointimal hyperplasia, compared to non-stented segments (**Figure 6.4**). Contrarily, Ca^{2+} efflux was not different in DMetS CSM compared to Lean (**Figure 5.3**), although DMetS developed extensive CAD. In the same study, CSM from MetS, normolipidemic MetS without CAD, demonstrated increased Ca^{2+} efflux. Summarily, Ca^{2+} efflux was increased (OssC) and decreased (MetS) in CSM from relatively healthy arteries, while Ca^{2+} efflux did not change (DMetS) or was increased (peri-stent) in CSM from disease arteries. Given the variability of Ca^{2+} efflux in differing degrees of CAD, it seems unlikely that Ca^{2+} efflux is causative in CSM proliferation and development of CAD. Changes in Ca^{2+} efflux may serve as a compensatory mechanism for primary defects in Ca^{2+} buffering or influx mechanisms (16).

A major contributor to CSM Ca^{2+} influx is the voltage-gated Ca^{2+} channels (VGCC, reviewed elsewhere (329)). While general dogma equates elevated Ca^{2+}_i with cell cycle progression and proliferation, Ca^{2+} influx through the VGCC has been shown to be largely beneficial, leading to contractile and quiescent phenotype in vascular smooth muscle (172;330). As such, VGCC have been shown to be down-regulated in disease states such as dyslipidemia and diabetes, an effect reversed by exercise (13).

Table 6.1 summarizes nicely the lack of information obtained in this report on differential regulation of VGCC in Ossabaw CSM. One complete set of experiments suggested no change in VGCC between Ossabaw and Yucatan CSM, however this result should be interpreted with caution, as SERCA activity was not inhibited during the protocol (**Chapter 2**). Ca^{2+} influx through VGCC has been shown to refill the SR Ca^{2+} store in CSM (330). As such, differences in baseline SR Ca^{2+} store could alter Ca^{2+} buffering by SERCA of VGCC-mediated Ca^{2+} influx differentially in the two cell types.

Effect of dyslipidemia in metabolic syndrome on canonical transient receptor potential 1-mediated Ca^{2+} influx

Store-operated Ca^{2+} entry (SOCE) function is strongly associated with CSM proliferation and progression of atherosclerosis (**Chapter 4 and 5**, (196;331)). SOCE has been associated with atherosclerosis in MetS (**Chapter 4 and 5**) and diabetes (332). Additionally, SOCE has been shown to regulate gene expression distinct from those regulated by VGCC Ca^{2+} influx (333), VGCC Ca^{2+} influx drives cell differentiation and quiescence (172;330). While SOCE is clearly important in regulating vascular smooth muscle transcription and cell cycle, the molecular identity has not been as forthcoming.

Multiple proteins have been identified as the pore-forming subunit of SOCE pathways, such that the molecular identity responsible for SOCE may be dependent on the vascular bed (334;335). TRPC1 and Orai1 have recently become the leading candidates for mediating most vascular smooth muscle SOCE (reviewed elsewhere (336)). While prominent reviews have dismissed TRPC1 involvement in SOCE (117), there is now considerable evidence supporting TRPC1-mediated SOCE in vascular smooth muscle (337;338). Likewise, Orai1 is now dogmatically considered the molecular identity of the historical Ca^{2+} release activated Ca^{2+} current (I_{CRAC} ; (339;340)). In some reports significant interaction between Orai1 and TRPC1 have been demonstrated, such

that I_{CRAC} , mediated by Orai1, is potentiated by TRPC1 expression (341) and TRPC1 mediated SOCE relies on Orai1 expression (241).

Our studies have consistently indicated an ~3-fold increase of SOCE in CSM from TMetS and DMetS compared to Lean (**Figures 4.4** and **5.3**). These are currently the only reports of elevated SOCE in smooth muscle (i.e. CSM) from MetS CAD. Additionally, we reported increased SOCE preceded development of increased Ca^{2+}_i in CSM and CAD in sDMetS, dyslipidemic MetS after 9 weeks on atherogenic diet (**Figure 5.3**). Correspondingly, SOCE preceding development of arteriosclerosis was shown in aortic smooth muscle from ApoE^{-/-} mice, although it is possible the SOCE measured in that study was mediated by receptor operated Ca^{2+} entry (317). MetS were critical in concluding that dyslipidemia is the principal MetS factor responsible for SOCE and CAD. MetS developed normolipidemic MetS without CAD (**Figure 5.2**) whose CSM did not develop increased SOCE (**Figure 5.3**). These results supported our hypothesis that dyslipidemia initiates increased CSM SOCE that primarily mediates the development of CAD in the MetS.

CSM from Lean demonstrated a cation conductance activated by increased Ca^{2+}_i . This Ca^{2+} -induced cation conductance (CICC) is strikingly similar to previous biophysical characterizations of TRPM4b (270) (**Figure 5.5**). TRPM (melanostatin) 4 has been shown to directly inhibit SOC in T lymphocytes (269). This provides the exciting possibility that, although Lean CSM express TRPC1 (29) and minimal SOC (**Figure 4&5**; (29)), the co-expression of TRPM4 provides an inhibitory mechanism preventing increased SOC that is not present in DMetS, thus resulting in potentiation of SOC in DMetS CSM. This intriguing hypothesis should be considered in future studies investigating the involvement of TRPM4 in smooth muscle from diabetic coronary arteries demonstrating elevated SOC.

Ossabaw CSM have decreased intracellular Ca^{2+} buffering (i.e. SERCA) and increased SOCE compared to Yucatan (outlined in **Table 6.1**). These results and a recent report demonstrating TRPC1 upregulation following SERCA gene silencing (342) may suggest that that TRPC1 is the molecular identity of SOCE in CSM from MetS swine. Accordingly, we found that TRPC1 protein was increased ratiometrically with SOCE function (~3-fold) in TMetS compared to Lean (**Figure 4.5**). Increased TRPC1 protein and SOCE function were attenuated/abolished with exercise (**Figures 4.4 and 4.5**). While Orai1 protein trended towards an increase in coronary arteries from TMetS, there was no statistical difference (**Figure 4.5**). Supporting the role of TRPC1 as the molecular identity of SOCE in CSM from TMetS, was the non-selective, ohmic I-V relationship of SOCE in a handful of CSM cells (**Figure 4.4**). TRPC1-mediated SOCE has been demonstrated to be exactly ohmic and non-selective in striking contrast to the extremely Ca^{2+} -selective and inward rectifying current of Orai1 (243;343;344).

Further electrophysiological characterization provides additional detail concerning the molecular identity of store-operated current (SOC) in CSM from Lean and DMetS swine. SOC in Lean CSM was consistent with Orai1, as SOC was not increased in the absence of Ca^{2+}_o and demonstrated significant Ca^{2+} selectivity ($E_{\text{Rev}} = 26$; **Figure 5.4**). However, in CSM from DMetS, there was a significant shift in the SOC properties that were suggestive of TRPC1-mediated current, as SOC was non-selective, cation permeable, increased in the absence of Ca^{2+}_o , and demonstrated no Ca^{2+} selectivity ($E_{\text{Rev}} = 0$; **Figure 5.4**). Importantly, there was no change in SOC amplitude between CSM from Lean and DMetS, while SOC in the absence of Ca^{2+}_o was elevated in CSM from DMetS (**Figure 5.4**). This suggests SOC in CSM from DMetS is less of a Ca^{2+} entry pathway, instead demonstrating increased monovalent cation permeability compared to Lean.

Irrespective of the pore-forming subunit identity, STIM1 has been clearly demonstrated to be necessary in activation of SOCE in vascular smooth muscle, and upregulated concordantly with increased SOCE (151;331;345;346). Accordingly, increased STIM1 protein in coronary arteries from TMetS was proportional to increased SOCE, and both were attenuated with exercise (**Figure 4.5**). From previous reports and our novel findings, this report concludes that STIM1 is involved in SOCE in CSM from MetS CAD.

Revised model of coronary smooth muscle cell Ca^{2+} regulation

Resting Ca^{2+}_i and SR Ca^{2+} store were increased in CSM from DMetS compared to Lean (**Figure 5.3**). These Ca^{2+} regulation changes were preceded by increased SOCE in CSM from sDMetS (**Figure 5.3**). SOC was primarily mediated by Na^+ permeance at physiological membrane potentials (**Figure 5.4**). Additionally, SOC has been demonstrated to mediate increases in Ca^{2+}_i through the involvement of NCX (347-349). Taken together, these findings support a model of SOCE whereby store-operated Na^+ influx potentiates reverse mode NCX-mediated Ca^{2+} influx (outlined in **Figure 6.5**; first proposed by Ashida and Blaustein (262)).

Significant Ca^{2+} influx through reverse mode NCX was first proposed by Ashida and Blaustein in 1987 (262). If we assume that SOCE in sDMetS is similar to DMetS, then increased Na^+ permeance through SOCE precedes other Ca^{2+} signaling dysfunction. This would shift $E_{\text{Na/Ca}}$ to more negative values leading to more positive $V_{\text{Na/Ca}}$, shown to potentiate reverse mode NCX (262). DMetS CSM have less negative M_V compared to Lean because of decreased large-conductance Ca^{2+} -activated K^+ channels (BK) as demonstrated by Borbouse et al. (8), and BK channel function has been shown to be inhibited by increased TRPC1-mediated SOCE (350). NCX is voltage dependent such that depolarization leads to propensity for reverse mode function (262). Increased

Ca²⁺ entry via reverse mode NCX and as well as TRPC1 increases Ca²⁺_i, further inhibiting BK function, and SR Ca²⁺ store (262). Additionally, NCX reverse mode, by definition, does facilitate Ca²⁺ efflux. In this model, increased SOCE and reverse mode NCX lead to BK channel inhibition, increased SR Ca²⁺ store, and decreased Ca²⁺ efflux. It should be noted that the description of “store-operated Ca²⁺ entry” is accurate concerning TRPC1-mediated reverse mode NCX Ca²⁺ entry. While we have not directly tested the involvement of NCX in CSM SOCE, the results of this study are entirely consistent with the model proposed by Ashida and Blaustein. Further, the complete abolition of TRPM4-like Ca²⁺ induced cation current in CSM from DMetS suggests that TRPM4 may act as an inhibitory factor of TRPC1-mediated SOCE. This report concludes that SOC is mediated primarily by Orai1 in CSM from Lean, while SOCE is mediated by TRPC1/reverse mode NCX in CSM from DMetS.

Future directions

While the NASH and CAD in **Chapter 3** and type 2 diabetes in **Chapter 5** are striking, there is great opacity concerning the systemic, cellular, and molecular mechanisms underlying the gross phenotypes. It may be tempting to investigate which dietary components relate the greatest contribution to the individual pathological states. Indeed this approach has significant basic research and clinical implications, namely providing the opportunity to further improve the model and providing insight into dietary modifications that may be beneficial to the general population. However, the goal was not to confirm extensive clinical dietary studies in a different species. The impetus was to design a humanoid animal model of MetS and type 2 diabetes that develops CAD. In pursuit of these goals, we serendipitously produced an animal model of NASH, thus providing additional metabolic relevance and producing an ideal framework to investigate the underlying mechanisms of CAD as observed in the general population.

Having achieved the goal of properly framing the incredibly complex metabolic disease state, future studies should focus on the systemic, cellular, and molecular mechanisms driving the pathologic endpoint of CAD.

Great effort has focused on the contribution of Ca^{2+} signaling in CSM to atherosclerotic and stent-induced atheroma. The major findings of this thesis suggest TRPC1-, STIM1-, and Orai1-mediated SOCE may play a pivotal role in the development of CAD in stent-induced injury and MetS CAD. Future studies should utilize specific inhibition of TRPC1 *in vitro* using organ culture experiments to determine its relative contribution to CSM proliferation, medial thickening, and collagen deposition. Dr. Leonidas Tsiokas, University of Oklahoma, has available an excellent and specific TRPC1 antibody that inhibits channel function and has, in the past, offered it for investigative use. Additional studies should utilize short interfering RNA techniques to knock-down expression of TRPC1, STIM1, and Orai1 individually or in conjunction in organ culture. This will allow elucidation of individual protein contribution to organ culture CAD. Expanding these findings to *in vivo* settings will require advanced techniques including stents designed to elute antagonizing agents (e.g. DES).

Custom-made DES allow relatively expensive or toxic compounds to be administered with local specificity and controlled release kinetics. Thus, costs and systemic effects are ameliorated while targeting drug treatment to the area of interest. Additionally, DES with highly specific and efficacious antagonist compounds essentially eliminate the contribution of their target within the treated area. Significant efforts to produce a TRPC1-targeted DES were unsuccessful in the tenure of this author. However, in collaboration with other key investigators, successful inhibition of adenosine A1 receptor using specific antagonist DES proved efficacious in preventing stent-induced injury below control stent. Thus, as more antagonists of TRPC1 and/or Orai1 become available, *in vivo* studies using DES should be considered.

Any future study investigation into the role of SOCE in CAD should include extensive patch clamp, Ca^{2+} imaging, and expression analyses. These intensive measures will allow confident interpretation and facilitate publication of experimental results. However, the relative contribution of particular Ca^{2+} signaling pathways to CSM proliferation, migration, and plasticity remains unresolved, particularly in MetS, type 2 diabetes, and progression to advanced CAD.

Figure Legends

Figure 6.1 Type 2 diabetes and pre-diabetes in humans and Ossabaw swine. A Fasting blood glucose levels are used to define healthy (75-106 mg/dL; green), prediabetes (100-126 mg/dL; yellow) and diabetes (>126 mg/dL; red) in humans. Given variation in glucose homeostasis compared to humans, Ossabaw swine generally demonstrate overall lower fasting blood glucose values across normoglycemia (65-75 mg/dL; Lean), prediabetes (76-90 mg/dL), and overt type 2 diabetes (>90 mg/dL). *, $p < 0.05$ compared to respective study controls. **B** Genetic predisposition to type 2 diabetes accelerates the effects of environmental factors. Thus, lean swine breeds (**a**) are resistant to progression to type 2 diabetes compared to the metabolic syndrome-prone Ossabaw (**b**). OssH, NMetS, TMetS, and XMetS (**c**) are insulin resistant and glucose intolerant, while pancreatic β -cell function was sufficient to partially compensate and maintain moderately elevated fasting blood glucose. MMetS+ (**d**) represent the threshold of type 2 diabetes with hyperglycemia, elevated insulin response to glucose load, and pancreatic β -cell hypertrophy. TMetS+ (**e**) were unable to compensate for glucose load by increasing insulin response, demonstrated more severe hyperglycemia and fasting insulin values, and pancreatic β -cell staining that was not different than their Lean cohorts.

Figure 6.2 Revised model of Ca^{2+} regulation. A Ratiometric analysis of Ca^{2+} handling in coronary smooth muscle (CSM) from healthy swine (Lean), loaded with Ca^{2+} -sensitive fluorescent dye fura-2, reveals virtually no store-operated cation entry. Fura-2 fluorescence at excitation wavelength F360 nm is Ca^{2+} insensitive, and global fura-2 fluorescence is quenched by Mn^{2+} . **B** Caffeine (Caff; 5 mM) and cyclopiazonic acid (CPA; 10^{-5} M) inhibit SERCA and activate ryanodine receptors (Ry) in the SR, leading to massive depletion of the SR Ca^{2+} store into the cell, thus raising intracellular Ca^{2+} . Ca^{2+} -

induced cation conductance, consistent with transient receptor potential melanostatin 4 (TRPM; M), rapidly activates and (de/in)activates parallel to SR release Ca^{2+} transient. NCX and PMCA mediated Ca^{2+} efflux return cell to normal intracellular Ca^{2+} as the SR Ca^{2+} store remains depleted. Stromal interaction molecule 1 (STIM1; S) proteins in the SR membrane sense depletion of the SR Ca^{2+} store and homomultimerize into distinct puncta in regions of the SR in close apposition to the PM. TRP canonical 1 (TRPC1; R) is inhibited by presence of TRPM4. **C** Ratiometric analysis of Ca^{2+} handling in CSM from metabolic syndrome swine reveals elevated store-operated divalent cation ($\text{Mn}^{2+}/\text{Ca}^{2+}$) entry compared to Lean. **D** CSM from MetS swine have elevated baseline Ca^{2+}_i . Decreased L-type Ca^{2+} entry, Ca^{2+} efflux mediated by NCX and PMCA, and SERCA contribute to Ca^{2+} regulation abnormalities. TRPC1 and STIM1 protein is upregulated ~3-fold compared to Lean. **E** Reduced L-type channel activity in CSM from MetS leads to reduced Ca^{2+} influx upon high K^+ depolarization compared to Lean. **F** SR Ca^{2+} store depletion does not activate any Ca^{2+} induced current, suggesting lack of TRPM4. STIM1 activates store-operated cation entry increasing Na^+ concentrations in the superficial buffer barrier. Elevated resting Ca^{2+}_i , decreased MV, and sudden rise in local Na^+ via TRPC1 activation all contribute to NCX reverse mode that moves Na^+ out of the cell and $\text{Ca}^{2+}/\text{Mn}^{2+}$ into the cell.

Table 6.1

Ca ²⁺ regulation		Disease state						
Mechanism	Putative mediator	Ossabaw (genetic)	F/MetS	MetS	XMetS	DMetS	MMetS	sDMetS+
Basal Ca ²⁺ _i	multiple	No Δ Not Shown	No Δ Chapter 5	??	??	↑ Chapter 5	--	No Δ Chapter 5
Voltage gated Ca ²⁺ influx	VGCC	NC ?? Chapter 2	--	--	--	--	??	--
Store-operated Ca ²⁺ influx	NCX via TRPC1	monoval./ Dv↑ (s) Chapter 5 (13;240)	DvNC (l) Chapter 5	DvNC (s) Dv↑ (s/l) Chapter 4	Dv↓ (s) Chapter 4	Dv↑ (l) Chapter 5	monoval.↑ (s) DvNC (s) Chapter 5	Dv↑ (l) Chapter 5
Ca ²⁺ -induced cation influx	TRPM4	--	--	--	--	--	↓ Chapter 5	--
Sarcoplasmic reticulum Ca ²⁺ store	RyR, IP3, and SERCA	No Δ Chapter 2	↑ Chapter 5	??	??	↑ Chapter 5	--	No Δ Chapter 5
Plasmalemmal Ca ²⁺ extrusion	NCX, PMCA, SERCA	↓ Chapter 2	↑ Chapter 5	??	??	No Δ Chapter 5	--	??

Table 6.1 Summary of disease state affect on coronary smooth muscle Ca²⁺ regulation. Changes for Lean Ossabaw (genetic) are relative to Lean Yucatan. Changes for all other disease states are relative to Lean Ossabaw (genetic). Abbreviations: VGCC, voltage gated Ca²⁺ channel; NCX, Na⁺/Ca²⁺ exchanger; TRPC1, transient receptor potential canonical 1; TRPM4, TRP melanostatin 4; RyR, ryanodine receptor; IP3, inositol trisphosphate; SERCA, sarco/endoplasmic reticulum Ca²⁺ ATPase; PMCA, plasma membrane Ca²⁺ ATPase; --, did not test; ↑, increased; ↓, decreased; Ca²⁺_i, intracellular Ca²⁺; ??, not clear; Dv, divalent; monoval., monovalent. Group codes: **F/MetS**, fructose/normolipidemic metabolic syndrome; **MetS**, high trans-fat/cholesterol atherogenic diet;

XMetS, exercised MetS; **DMetS**, MetS with addition of high fructose; **MMetS**, high mixed-source-fat/cholesterol/fructose atherogenic diet; **sDMetS**, short-term DMetS (9 week on diet).

Figure 6.1

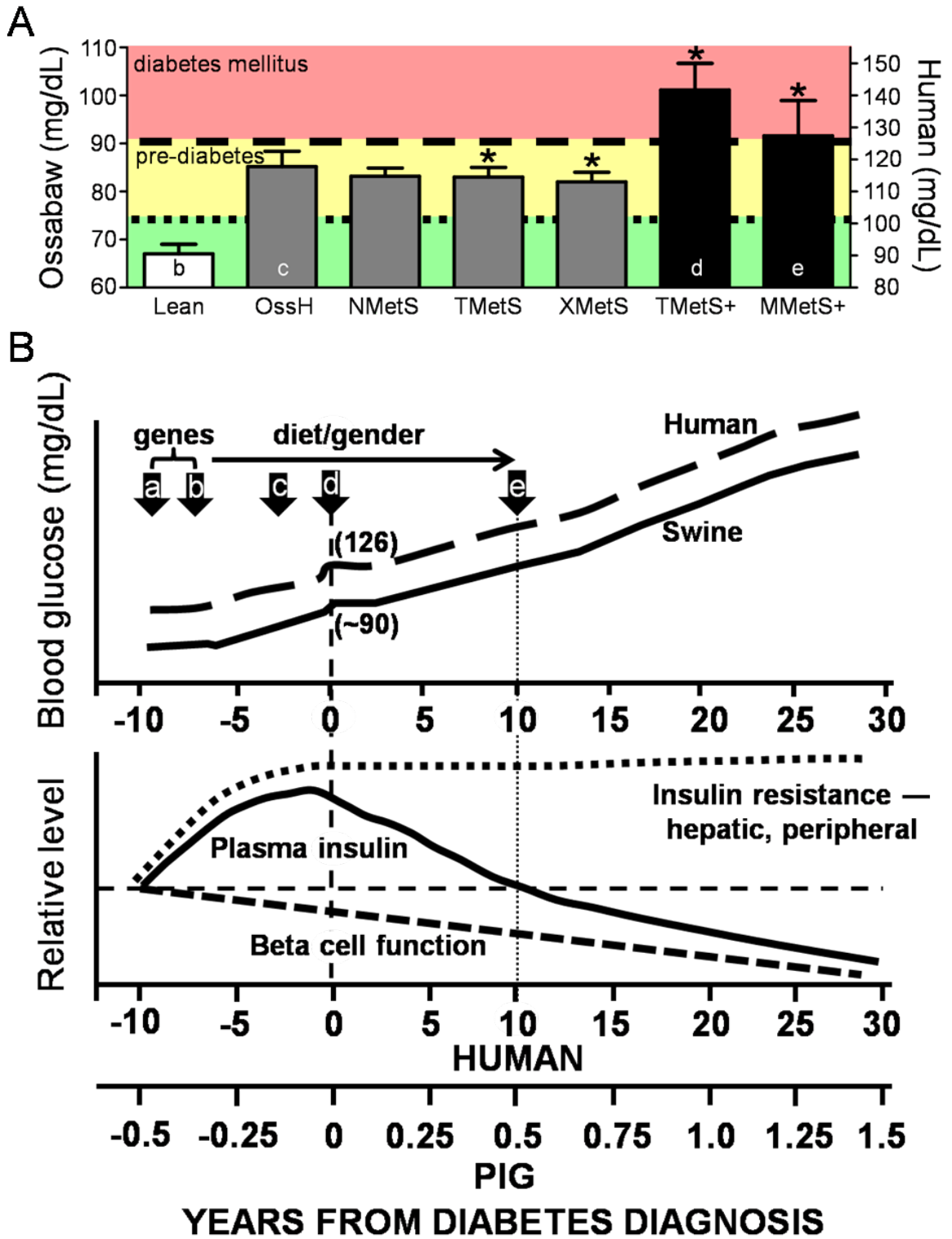
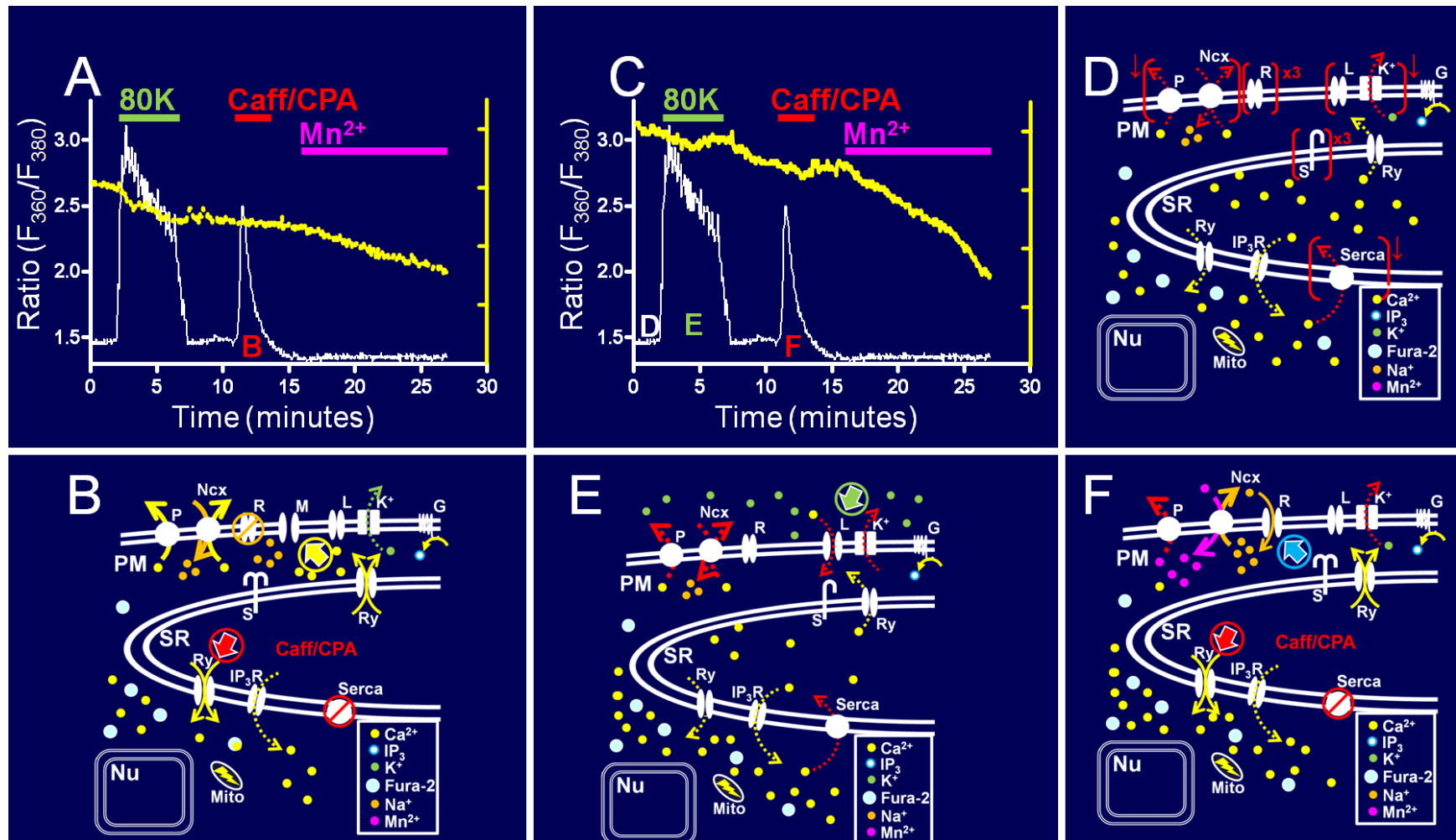


Figure 6.2



Appendices

Appendix A Angiography

See also reference 4 for figures and description of methods and references therein for more information.

1. All Radiation Safety protocols should be followed during all steps of procedure.
2. Sterile technique should be followed unless procedure is non-survival. During non-survival angiography, care should still be taken to perform tasks in sanitary fashion.

3. Anesthesia

Persons performing angiography procedure are all responsible for insuring a satisfactory plane of anesthesia is maintained during entire procedure. If isoflurane is used, check fill level on isoflurane dispenser. Generally 1.5-2% isoflurane and 2 L of O₂ is required for the health and sedation of intubated swine. Isoflurane should be adjusted based on blood pressure, heart rate, movement of pig, voluntary stomach contraction, or other visual cues during the procedure.

4. Secure pig to table.

Insure that swine is properly secured to table and table wheels are locked. This is essential for the safety of the pig and compliance with Institutional Animal Care and Use Committee protocol guidelines.

5. Intubation and respiration

Check proper intubation of pig. Chest should rise and fall with respirator without voluntary muscle contraction. Proper tidal volume is equal to 6-8 ml/kg body weight. Pressure should not exceed 20 atmospheres at any point during respiration and should fall to near zero on exhalation.

6. Insure angiography system is active and ready for use, but in a safe mode, such that no radiation is being emitted.
7. General cleanliness and organization
Work place should be clean, dry, and orderly. A proper angiography procedure minimizes fluid mess (e.g. blood or saline). This is especially important during sterile procedures, but should be a point of pride for any procedure.
8. Check that all necessary equipment for procedure is present and prepared for use. Steps 9-27.
9. Hang 1L saline bag, attach fluid line, and inflate to pressure (200-300 mm Hg).
10. Hang radio-opaque contrast, attach fluid line, and open vent on fluid line to prevent vacuum in contrast container.
11. Hang pressure transducer at same height as pig heart. Attach fluid line.
12. Connect pressure transducer to pressure transducer/ECG unit.
13. Attach three fluid lines, outflow line to three-way stopcock, and 12 mL NAMIC® Angiographic Control Syringes to NAMIC® Perceptor Manifold.
14. Open contrast to manifold/outflow and allow contrast to fill line. Close contrast at manifold. Insure no bubbles in line.
15. Open saline to manifold/outflow and allow saline to fill line. Open saline to syringe and fill syringe half way. Open saline to pressure transducer. Insure no bubbles in line or manifold.
16. Open pressure transducer to air and allow saline to fill line. Insure no bubbles. Close pressure transducer to air, keeping line open to saline at manifold. Close saline at manifold. Open outflow three-way stopcock to air. Pressure transducer should now be open to air. Zero pressure. Close pressure transducer at manifold.
 - a. Do not touch table, manifold, or tubing while zeroing pressure.
17. Attach extender to three-way stopcock away from manifold.

18. Attach NAMIC® Gateway™ Y-adapter to extender.
19. Attach guiding catheter to Y-adapter.
 - a. Typically a 7 French (F) 0.75 to 1.5 Amplatz left (AL) with side holes or hockey stick (HS) guiding catheter is used for cardiac procedures on the left main coronary artery. Side holes enable blood flow, which can minimize ischemia and arrhythmias when the coronary artery is selectively accessed by placement of the guiding catheter into the artery.
20. Open saline to guiding catheter, flushing any air out of three-way, tubing, Y-adapter, and guide catheter.
 - a. Be sure to flush deadspace in Y-adapter near hemostatic valve.
21. Open saline to syringe and fill, flushing any air out of manifold and into syringe.
 - a. If large amount of air is in syringe (>1 mL), take off syringe and empty of air, then attach to manifold and flush with saline again.
22. Surgical tub should be available with introducer, guide wire, PTCA wire, and torquer. Fill tub with sufficient saline to coat equipment. A small waste tub should be available on table. Several gauze pads and some paper towels should be readily available on table throughout procedure.
 - a. When not in use, wires should be coiled loosely (just enough to fit in surgical tub) with ends tucked into coil.
23. Percutaneous transluminal coronary angioplasty (PTCA) guidewire
 - a. Check quality of PTCA wire. PTCA wire (typically 0.04 inch diameter) should be without any bends, but may be slightly curved/bent at very tip (approximately 5-10° angle). Good care of PTCA wire is critical as it is very fragile and expensive.

- b. Insure there are no jagged edges or severe bends in the guide wire.
Guide wires are typically very durable and should be used for up to 30 cases. Tip should be curved back on itself and floppy.
- 24. Move table top back and forth until the center of movement is determined. Center table.
- 25. Adjust table to desired height. Generally, forearm of arm bent at elbow should be roughly parallel with table top.
- 26. If using C-arm system, position C-arm to the end of the table near pig's head.
 - a. Zero all axes of C-arm before moving.
 - b. Do not run over cords with wheels.
- 27. Don lead apron, thyroid protector, and glasses.
- 28. Wear radiation badges. Proper radiation procedures should be observed at all times.
- 29. If using C-arm, turn on key and set up C-arm. Move image transducer as close to pig as possible. Radiation exposure is reduced when the image transducer is close to the pig.
- 30. Run brief test image of pig.
 - a. Remove any metal or radio-opaque objects in field.
 - b. Never place any part of self in imaging zone while actively imaging.
 - c. All angiography should be kept to a minimum. Exposure is cumulative, so reducing a brief angiography from 3 to 2 seconds will reduce exposure by 30%.
- 31. Adjust angiography zoom to include as large field as possible without large air space on either side of pig. Proper zoom improves visualization and reduces radiation exposure.

32. Collimate to reduce visual field as much as possible. Advancement of guiding catheter/wire is easiest with large visual field, as a large distance is covered relatively quickly. Collimation reduces radiation exposure.
33. Move image intensifier close to legs.
34. Introduce 0.35 inch diameter guide wire into guiding catheter.
 - a. As the lead end of the guide wire is floppy, this is generally achieved by putting the stiff end of the guide wire into the tip of the guide catheter and pushing the wire through the catheter backwards.
 - b. When the back tip of the wire sticks out the Y-adapter hemostatic valve, pull the guide wire until the tip of the wire is just inside the tip of the guide catheter. It is important that the two tips be relatively close, as will be evident in steps below.
35. Insure all pre-heparin and pre-contrast blood samples have been collected.
36. Insure administration of heparin.
 - a. If heparin was not previously administered, wait 5-10 minutes after administration to allow proper circulation of heparin systemically.
37. Double check for air bubbles in tubing and manifold.
38. Flush guide catheter and hemostatic valve with saline.
39. Introduce guiding catheter into femoral sheath. Use care as the tip of guiding catheter is easily damaged. Advance just past side-holes on guiding catheter so that blood does not flood out of holes. Do not advance further.
40. Advance guide wire 2-3 cm out of tip of guiding catheter.
 - a. This will minimize any damage caused to vasculature by advancing guiding catheter and enables passage of the guiding catheter through the iliac bifurcation, past renal arteries, and over the aortic arch for placement near the tricuspid valve.

41. Keep Y-adapter hemostatic valve tightened throughout procedure to limit blood backflow.
42. Steadily advance guiding catheter about 10 cm. Stop advancing immediately if any resistance or tugging is felt.
43. Visualize guide wire/catheter with angiography.
44. Continue advancing guide wire/catheter to thoracic cavity visualizing each step of the way with angiography and using steady motions. Stop advancing immediately if any resistance or tugging is felt.
45. Rotate angiography image if needed to insure that cranial is up and caudal is down on the monitor.
46. Under angiography, advance guide wire/catheter until aortic arch is reached.
 - a. Twist guiding catheter clockwise slightly to pop catheter into arch and not advance up carotid artery.
 - b. Clockwise and counterclockwise refer to direction if pointing end of guiding catheter that attaches to Y-adapter at face.
 - c. After tip of guiding catheter is near tricuspid valve, then remove 0.35 inch diameter guidewire.
47. Rotate angiography unit to left anterior oblique 30° (LAO30) and center angiography image on heart.
48. Zoom, then collimate to improve view and reduce radiation exposure. The tip of the guiding catheter and the heart should be the only thing in the visual field.
49. Fill guiding catheter with contrast to visualize on angiography.
50. Advance guiding catheter into left coronary ostium, using bursts of contrast (approximately 5 mL) to determine position. Minimal contrast should always be used.

- a. Use a slight clockwise twist if necessary. (Accessing the right coronary ostium typically requires counterclockwise twists and is easier with a hockey stick guiding catheter.)
 - b. Do not advance the guiding catheter into the left ventricle. This can cause fibrillations.
 - c. Engage left main coronary artery, slowly rotating guiding catheter clockwise. Small bursts of contrast infusion will allow determination of catheter position.
51. Perform LAO30 cine.
- a. Person taking notes should record blood pressure and heart rate.
 - b. Announce cine.
 - c. Step on cine pedal immediately followed by bolus of 10 mL contrast. If pig is particularly sensitive to contrast, infusion should be 50% saline and 50% contrast.
 - d. Cine should last no longer than the time it takes for contrast to flush away.
52. Disengage guiding catheter from selective and deep access of left main coronary artery by slightly rotating counterclockwise.
- a. Do not disengage coronary ostium completely; instead, the tip of the guiding catheter should be close enough for quick angiograms, infusion of drugs, placement of PTCA guidewire, etc.
 - b. Remaining tightly engaged to left main coronary artery occludes blood flow and can lead to ischemia, fibrillation, and death.
 - c. If interrogation of the left anterior descending (LAD) is desirable at this point, go to step 63 for access methods.
53. Rotate angiography unit to right anterior oblique 30° (RAO30).

- a. Center heart in visual field by moving table.
 - b. The RAO30 view typically provides better views of the circumflex artery and branches
54. Engage left main coronary artery with guiding catheter as previously described.
- a. It is important to note that the electrocardiogram (ECG) provides the best evidence during angiography as to the health of the heart. Watch for any ECG abnormalities during all procedures, especially when occluding blood flow with the guiding catheter, wires, or balloons. Pull out if in doubt. An artery accessed once can be accessed again, but not on a dead pig.
55. Perform RAO30 cine as previously described for LAO30 cine.
56. Disengage guiding catheter from left main coronary artery as previously described in step 52.
57. Place floppy end of PTCA guide wire into PTCA introducer sheath and introducer into Y-adapter hemostatic valve.
- a. Do not allow PTCA wire to be exposed out the other end of the introducer.
58. Advance PTCA wire until the first demarcation on the wire reaches the Y-adapter.
59. Use angiography and advance the PTCA wire near the end of the guiding catheter, but still within the guiding catheter.
60. Engage left main coronary artery with guiding catheter as previously described.
61. Use angiography and advance PTCA wire into left main coronary artery. If engaged properly with guide catheter, PTCA wire will likely direct into either the left circumflex (CFX) or left anterior descending (LAD) coronary artery.
- a. Distinguishing both coronary arteries may be easier in LAO30.

62. If there is difficulty accessing the CFX, rotate the guiding catheter clockwise and advance down the left main to selectively access the CFX. Then, feed the PTCA wire into the artery and slowly retract the guiding catheter by pulling with a slight counterclockwise twist.
63. Accessing the LAD tends to be more difficult.
- a. Slightly bending the tip of the PTCA wire (described previously) before introduction and placement of torquer on PTCA wire may allow twisting the wire and allowing better access to select arteries.
 - b. Alternatively, selectively engaging the LAD with the guiding catheter is effective, but occludes flow to the LAD.
 - c. First move to LAO30 to provide the best possible distinction between LAD and CFX.
 - d. Advance guiding catheter down left main coronary artery into the CFX, this generally requires only slight advancement and no manipulation.
 - e. Then, while slowly retracting guiding catheter, provide very slight rotation in a clockwise direction.
 - f. Upon reaching the LAD/CFX bifurcation, the guiding catheter may “pop” into the LAD. It may also be a smooth transition made evident as the guiding catheter tip will twist in the direction of the screen and move upward and to the left of the screen.
 - g. As soon as the guiding catheter pops or slowly moves into place, cease movement of the guiding catheter. This is a precarious position and often the guiding catheter will pop completely out of the left main coronary artery because of the tension in the catheter.
 - h. Immediately advance the PTCA wire down the LAD and slowly twist the guiding catheter slightly counter-clockwise, thus relieving tension and

easing it into the left main coronary artery. If the guiding catheter pops out of place, it may bring the PTCA wire with it.

64. Complete intravascular ultrasound, stent placement, or flow measurements as required and described in other Appendices. To perform flow measurements, use a flow wire instead of a PTCA wire.

Appendix B Intravascular ultrasound (IVUS)

See also reference 4 for figures and description of methods and references therein for more information.

1. All Radiation Safety protocols should be followed during all steps of procedure.
2. Sterile technique should be followed unless procedure is non-survival. During non-survival angiography, care should still be taken to perform tasks in sanitary fashion.
3. Anesthesia
Persons performing angiography procedure are all responsible for insuring a satisfactory plane of anesthesia is maintained during entire procedure. If isoflurane is used, check fill level on isoflurane dispenser. Generally 1.5-2% isoflurane and 2 L of O₂ is required for the health and sedation of intubated swine. Isoflurane should be adjusted based on blood pressure, heart rate, movement of pig, voluntary stomach contraction, or other visual cues during the procedure.
4. Follow steps 1-27 under Appendix A Angiography to prepare angiography equipment for use.
5. Check that all additional equipment for IVUS procedure is present and prepared for use. Steps 6-26.
6. Turn on IVUS instrument (Hewlett Packard) and set up for recording.
 - a. Enter case information using rolling ball or arrows to move cursor and tab to change fields.
 - b. Include study, pig number, pig name, date, operators, and any other necessary identifying information.
7. Label VHS tape with case information and insert into IVUS machine.
 - a. Do not record over previous data on VHS tape.

8. Press Image to move from patient information to catheter selection screen.
9. Attach image transducer to pullback device.
 - a. During sterile procedure, image transducer and pullback device are to be kept at end of surgical table on top of sterile sheet and under sterile gown or Chucks pad with stationary arm of pullback device accessible.
10. Move image transducer/pullback 10 mm away from stationary arm of pullback device.
 - a. Rock image transducer/pullback tray away from front of pullback device to free from locking mechanism.
11. Attach extender tubing to IVUS catheter.
 - a. Attach three-way stopcock, 3 mL syringe, and 10 mL syringe to extender tubing.
12. Flush IVUS catheter with saline from 3 mL syringe. Insure no bubbles exist in the syringes, stopcock, extender or IVUS catheter.
 - a. IVUS catheter should be flushed with saline from only the 3 mL syringe to minimize pressure.
 - b. The 10 mL syringe should be used as saline reservoir to fill 3 mL syringe if needed.
13. Insert catheter into image transducer. Connection is unidirectional and catheter should click into place.
 - a. During sterile procedure IVUS catheter should not be beneath the cover of pullback device and image transducer should remain sterile.
14. Pull outer sheath of IVUS catheter away from image transducer just enough to connect it to stationary arm of pullback device.
15. Connect IVUS catheter to stationary arm of pullback device.

16. Rock image transducer/pullback tray all the way forward towards stationary arm of pullback device.
 - a. Keep IVUS catheter between image transducer and stationary arm straight and do not allow bending or crimping.
17. Press Image to move from catheter selection screen to imaging screen.
18. Select UltraCross 3.2F 30 MHz or 3F 40 MHz catheter as appropriate on IVUS machine.
19. Place imaging transducer (tip of IVUS catheter, yellow colored metal) in surgical tub of saline.
20. Flush IVUS catheter with saline.
21. Press (un)Freeze to start IVUS image collection. Image transducer will begin rotating.
22. Snap fingers near microphone and watch they audio voltmeter for reaction to insure audio is functioning properly and will record when appropriate.
23. Press image transducer to bottom of bowl. The bottom of bowl will appear as white arc on IVUS machine.
24. Position forceps over image transducer to visualize.
25. Calibrate gray scale of IVUS system.
 - a. Adjust brightness, contrast, and grayscale such that forceps are maximally bright.
 - b. Differences in plaque brightness between cases will convey actual morphological differences based on the maximum brightness (echogenicity) of metal forceps.
 - c. Record forceps calibration images on VHS tape.
26. Press Freeze to stop imaging collection.
27. IVUS machine is now ready to operate.

28. Follow steps 38-63 under Appendix A Angiography to access desired coronary artery with PTCA wire.
 - a. It is essential to record in the notes key landmarks of the angiogram, such as the most distinct branches, ribs, etc., for narrating the aspects of the IVUS images along a pullback through the artery. These precise notes will greatly assist everyone in analysis of the IVUS images.
29. Flush IVUS catheter with saline.
30. Insert stiff end of PTCA wire into lumen of IVUS catheter and feed out side-hole of IVUS catheter.
31. Operator number 2 (assistant to main operator) should secure end of PTCA wire already through IVUS catheter to table with fingers or thumb.
32. Operator number 1 should loosen Y-adapter hemostatic valve and advance IVUS catheter along PTCA wire without displacing PTCA wire from position in coronary artery. Holding the IVUS catheter only ~1 cm from the valve and advancing for the first ~10-15 cm is needed to protect the pliable section of the IVUS catheter where the imaging transducer is located. Beyond ~10-15 cm the IVUS catheter is stiffer and more durable.
33. Once the IVUS catheter is well advanced through Y-adapter (e.g. side-hole is through Y-adapter valve), operator number one should take control of both PTCA wire and IVUS catheter.
34. Advance IVUS catheter down PTCA wire until first white demarcation reaches valve, keeping PTCA wire stationary in coronary artery.
 - a. Because there often is slack in the PTCA guidewire, brief fluoroscopy should be done to make certain that the guidewire has not advanced further into the coronary artery, which could cause damage to the very small distal segments.

35. Continue advancing IVUS catheter using angiography to guide it to the end of the guiding catheter.
 - a. The IVUS catheter is radio-lucent, but a radio-opaque marker at the distal end allows visualization with angiography. Another radio-opaque marker is the imaging transducer (18-28 mm from the tip of the IVUS catheter).
36. Start IVUS imaging by pressing (un)Freeze.
37. Label IVUS image by pressing Text and using roller ball and keyboard. Once labeling is complete, press Text again.
38. Press record to start the VHS tape.
39. Advance IVUS catheter down PTCA wire into coronary artery such that image transducer is in desired position.
 - a. PTCA wire and IVUS catheter can be advanced together and/or separately at this point.
 - b. Do not allow IVUS catheter to come off end of PTCA wire as it may damage the artery and will lose ability to advance easily.
 - c. A very brief cine with or without contrast may be captured to document precisely the location of the IVUS imaging transducer.
40. Holding wires steady, operator 1 announces start of IVUS pullback (e.g. "IVUS pullback of X artery in 3, 2, 1, GO").
 - a. Operator 2 flips switch on pullback device to desired pullback speed, either 0.5 or 1.0 mm/sec (0.5 used almost exclusively).
 - b. Note taker or Operator 2 presses Pullback before IVUS pullback starts and then Start/Stop on "GO" to begin IVUS pullback on IVUS machine.
41. During IVUS pullback:
 - a. Operator 1 is responsible for maintaining steady wires.

- b. All operators are responsible for watching IVUS pullback and commenting on artery morphology and IVUS features along length of pullback and watching ECG for abnormalities.
 - c. The ribs are labeled in the notes as #1 in the most cranial position to #x (typically 3 or 4) in the most caudal position to be used as landmarks for narrating the position of the imaging transducer during the pullback.
 - d. A very brief cine without contrast may be captured to document precisely the location of the IVUS imaging transducer relative to ribs, locations of arterial branches, etc.
42. Once image transducer is in guiding catheter, IVUS pullback is stopped simultaneously on pullback device and IVUS machine (press Start/Stop again) and lengths are recorded on pullback device and IVUS machine.
43. IVUS of another artery can be performed by repeating steps 34-41.
- a. The IVUS catheter must first be pulled back into the guiding catheter proximal to the Amplatz or hockey stick bend.
 - b. The PTCA guidewire is pulled back within the tip of the guiding catheter and the artery of interest accessed as described in step 27 and Appendix A Angiography.
 - c. This is a challenging method for accessing an artery because the PTCA guidewire is not as easily maneuvered while the IVUS catheter is in place, so it may require complete removal of the IVUS catheter and reintroduction after the PTCA guidewire is in place in the artery.
44. Remove IVUS catheter by pulling back over the PTCA wire and advance image transducer/pullback device back towards stationary arm of pullback device.
- a. Do not bend or crimp IVUS catheter between image transducer and stationary arm.

- b. Upon completion of angiography/IVUS/stent/flow procedures, special care must be taken to preserve IVUS catheter.
- 1) Flush blood out of IVUS catheter with saline.
 - 2) Flush saline out with water.
 - 3) Flush water out with air.
 - 4) Hang IVUS catheter in gentle coil or in safe place in laboratory with the imaging transducer end down to enable any water residue to leak out and assist in drying.
45. Leave PTCA wire in artery if stent is to be placed. Otherwise, PTCA wire may be removed from artery when all procedures are complete.

Appendix C Stent procedure

1. All Radiation Safety protocols should be followed during all steps of procedure.
2. Sterile technique should be followed unless procedure is non-survival. During non-survival angiography, care should still be taken to perform tasks in sanitary fashion.
3. Anesthesia
Persons performing angiography procedure are all responsible for insuring a satisfactory plane of anesthesia is maintained during entire procedure. If isoflurane is used, check fill level on isoflurane dispenser. Generally 1.5-2% isoflurane and 2 L of O₂ is required for the health and sedation of intubated swine. Isoflurane should be adjusted based on blood pressure, heart rate, movement of pig, voluntary stomach contraction, or other visual cues during the procedure.
4. Follow steps 1-27 under Appendix A Angiography to prepare angiography equipment for use.
5. Follow steps 1-26 under Appendix B Intravascular ultrasound to prepare IVUS equipment for use.
6. Check that all additional equipment for stent procedure is present. Complete stent kit and necessary accessories include:
 - a. Pressure device (indeflator)
 - b. Extender tubes
 - c. Three-way stopcock
 - d. Percutaneous angioplasty balloon
 - e. Wire clip
 - f. Blunt needle
 - g. Syringes (2)

- h. Stents with varying diameter.
7. Follow steps 28-64 under Appendix A Angiography to access desired coronary artery with PTCA wire.
8. Follow steps 27-43 under Appendix B Intravascular ultrasound to collect IVUS data of desired coronary artery.
 - a. **Note carefully the diameter of the artery at distinct landmarks** that help determine where the stent(s) will be deployed, so that the stent will be deployed to the exact diameter.
9. Using IVUS and angiography, determine site to be stented.
10. Obtain lumen diameter for mildly diseased artery or reference lumen diameter for stenotic lesion and calculate stent deployment diameter.
11. Choose angioplasty balloon that will inflate to desired diameter.
12. Prepare angioplasty balloon for inflation.
 - a. Attach three-way stopcock to pressure device (indeflator).
 - b. Connect three-way stopcock to balloon catheter using extender tubing.
 - c. Fill 10 mL syringe with 5 mL saline and attach to three-way stopcock.
 - d. Open syringe to balloon catheter and put negative pressure on syringe.
This will cause balloon catheter to fill with saline without inflating balloon.
Syringe may be pulled to 10 mL mark and suddenly released. This technique may be helpful in removing bubbles from balloon catheter. Use a hemostat to tap any visible bubbles out of the line while negative pressure is applied with syringe.
 - e. Close balloon catheter from three-way stopcock.
 - f. Remove syringe from three-way stopcock.
 - g. Fill indeflator with saline.

- h. Rotate handle in clockwise motion to remove air from indeflator and tubing to three-way stopcock.
 - i. Open indeflator to balloon catheter.
 - j. Attach blunt needle to syringe filled with saline.
 - k. Insert blunt needle into lumen on end of balloon catheter nearest balloon.
 - l. Fill dead-space with saline.
 - m. Balloon catheter is now prepared for inflation.
13. If using custom-made Burpee stents (most typical), perform test inflation of angioplasty balloon to pressure necessary for inflation diameter. Deflate balloon.
- a. The deflated balloon will have folds in it that will help the stent grip onto balloon and not become dislodged when advancing through hemostatic valve, guiding catheter, and into artery.
14. Choose stent size within 10% of the desired diameter.
- a. Stents can be deployed to 90-110% of nominal diameter if necessary, because the stent surface area relative to the artery surface area will be similarly close.
 - b. A 3.0 mm diameter stent is the size used for >90% of the stents placed in Ossabaw pigs.
 - c. A stent length of 8 mm has been used exclusively in Ossabaws because it enables placement between arterial branches (i.e. branches are not “jailed”) and provides opportunity for easy placement of 2 stents per artery.
15. Place stent on balloon and center between two radio-opaque markers.
16. Gently crimp stent on balloon with fingers using great care to not damage stent architecture.

17. Insert the stiff, firm end of the PTCA guidewire into lumen of the balloon catheter and feed the guidewire out through a side hole.
18. Insert balloon/stent into guiding catheter through Y-adapter using the same technique as required for the IVUS catheter in Appendix B Intravascular ultrasound steps 30-33, except that the hemostatic valve is opened wider and saline from the pressurized bag is flowed through the valve to permit easier introduction and verification that the stent was introduced successfully.
19. Use angiography to guide balloon/stent over PTCA wire to desired region of artery.
 - a. Balloon is bounded by two radio-opaque markers.
 - b. PTCA wire and balloon catheter can be advanced together and/or separately at this point. Do not allow balloon catheter to come off end of PTCA wire as it may damage the artery and will lose ability to advance easily.
 - c. A very brief cine with or without contrast may be captured to document precisely the location of the stent in the artery.
20. Holding wires steady, operator 1 announces start of stent deployment (e.g. "Stent deployment in 3, 2, 1, GO").
 - a. Operator 2 quickly inflates the balloon to desired diameter adjusting pressure in the balloon by twisting the inflater handle.
 - b. Note taker or Operator 2 is responsible for watching the clock.
21. Balloon inflation should persist for 30 seconds.
 - a. During stent deployment, operator 1 is responsible for maintaining steady wires and watching the ECG.

- b. Operator 2 is responsible for maintaining constant desired pressure in the balloon, making adjustments as needed.
 - c. Note taker is responsible for keeping track of time and counting down last 10 seconds (e.g. 10, 9, 8, 7, 6, 5, 4, 3, 2, 1, DEFLATE).
 - d. Upon DEFLATE, Operator 2 presses the pressure release button on the side of the pressure device and deflating the balloon by pulling back on the handle sharply.
22. Remove balloon catheter by pulling back gently over the PTCA wire, which should be done with fluoroscopy to make certain the balloon moves successfully without snagging the stent.
23. Perform angiography (cine) with contrast infusion to visualize any damage, over-inflation of the stent, etc.
- a. Angiography should be performed in either LAO30 (Appendix A Angiography steps 57-52) or RAO30 (Appendix A Angiography steps 53-56) to obtain best resolution of stented artery.
24. Perform IVUS to insure proper deployment diameter, etc. following Appendix B Intravascular ultrasound steps 28-44.
25. Leave PTCA guidewire in artery if a second stent is to be placed. Otherwise, PTCA guidewire may be removed from artery when all procedures are complete. Typically, however, the PTCA guidewire retracts into the guiding catheter when the balloon is completely removed from the catheter.

Appendix D *In vivo* coronary blood flow measurements in anesthetized Ossabaw swine using percutaneous vascular access

1. All Radiation Safety protocols should be followed during all steps of procedure.
2. Sterile technique should be followed unless procedure is non-survival. During non-survival angiography, care should still be taken to perform tasks in sanitary fashion.
3. Anesthesia
Persons performing angiography procedure are all responsible for insuring a satisfactory plane of anesthesia is maintained during entire procedure. If isoflurane is used, check fill level on isoflurane dispenser. Generally 1.5-2% isoflurane and 2 L of O₂ is required for the health and sedation of intubated swine. Isoflurane should be adjusted based on blood pressure, heart rate, movement of pig, voluntary stomach contraction, or other visual cues during the procedure.
4. Follow steps 1-28 under Appendix A Angiography to prepare angiography equipment for use.
5. Follow steps 1-26 under Appendix B Intravascular ultrasound to prepare IVUS equipment for use.
6. Prepare flow equipment for use.
 - a. Connect flow transducer to flow machine.
 - b. Connect flow wire to flow transducer.
 - c. After starting ComboMap **flow machine**, flow and pressure wire must be zeroed while still in plastic sheath.
 - d. Connect flow machine to pressure transducer/ECG unit.
7. Follow steps 28-67 under Appendix A Angiography to access desired coronary artery with flow wire.

- a. Flow wire is very similar to PTCA wire. However, flow wire is very fragile and if bent or crimped will not work. Also, flow wires are very expensive relative to PTCA guide wire.
 - b. Before advancing flow wire out of guide catheter, line up very tip of flow wire with end of guide catheter and normalize proximal pressure reading for flow wire to pressure reading from aortic pressure transducer.
8. Position flow wire in proximal/intermediate section of target artery.
- a. Avoid branch points or acute bends in the artery trajectory.
 - b. Desirable position is achieved when consistent/low noise flow envelopes are strong enough to obtain reasonable flow velocity measurements.
9. Obtain first baseline flow measurements.
- a. This will allow reference point for normal flow preceding introduction of IVUS catheter and/or pharmacological agents.
 - b. Adenosine dose-response may be obtained now (outlined in [steps 15-17](#)).
10. Follow [steps 27-43](#) under Appendix **B** Intravascular ultrasound to collect IVUS data from desired coronary artery, if conduit artery diameter is needed.
- a. Use flow wire instead of PTCA guidewire to guide IVUS catheter into desired coronary artery.
11. To use IVUS catheter for steady-state infusion of drugs into the artery via the IVUS lumen, advance IVUS wire to very tip of flow wire and then retract flow wire to remove from IVUS catheter lumen.
- a. Do not allow IVUS catheter to slip out of target artery, as it cannot be guided back into artery without re-introducing flow wire into lumen of IVUS catheter.
 - b. IVUS catheter should not be advance, but may be retracted, while IVUS catheter is free from flow wire. This will prevent damage to target artery.

- c. Flow wire is now free to advance or retract as needed.
12. Reposition flow wire into optimal position for flow recording.
13. Retract IVUS catheter such that distal marker is proximal to the tip of the flow wire, but not less than ~10 mm distal to the coronary ostium within target artery.
 - a. This will insure minimal interaction of IVUS catheter with flow measurements.
 - b. This will also insure any solution infused into IVUS catheter will reach target artery with desired concentration.
14. Obtain second baseline flow measurements.
 - a. These measurements compared to first baseline measurements will reflect either 1) change in flow wire position or 2) affect of IVUS catheter on target artery flow.
15. All bolus injections through guiding catheter should equal ~3-fold of dead-space of guiding catheter (typically 3 mL dead space and 10 mL saline bolus).
 - a. Bolus through guiding catheter is achieved using three-way stop cock attached between manifold and guiding catheter.
 - b. Boluses should be through guiding catheter selectively accessing target coronary artery. If completely selective access of target artery cannot be achieved, selective access to left main coronary artery may suffice.
16. Bolus saline and measure any change in flow.
 - a. Strong flow artifact will be present as long as bolus is sustained. It should immediately stop when bolus stops.
 - b. If contrast solution is present in guiding catheter, variable flow response should be observed following initial flow artifact.
 - c. Pure saline does not typically elicit sustained flow response past initial flow artifact (17).

- d. Repeat 3-4 times for first bolus following angiography with contrast to properly flush contrast out of catheter.
 - e. Contrast will generally elicit strong vasodilatory response.
 - f. If saline elicits sustained flow response (elevated flow ~20-30 seconds following bolus), any following boluses should be normalized to saline response.
17. Adenosine dose-response should be obtained using bolus injections.
- a. Load guiding catheter with 3 mL of solution with desired adenosine concentration.
 - b. Make certain that selective access of the target artery with guiding catheter is maintained.
 - c. Obtain baseline average peak velocity (APV).
 - d. Bolus 10 mL of saline in less than 1 second, flushing adenosine into target artery.
 - e. Wait 5-10 seconds for flush artifact to subside.
 - f. Record flow measurements and obtain APV of maximal adenosine response in the following 45 seconds.
 - g. Repeat with each desired adenosine dose.
18. Begin continuous infusion of pharmacological agent through lumen of IVUS catheter, if desired. Continuous infusion should be maintained at constant rate, typically 1-2 mL/min.
- a. IVUS catheter dead-space is approximately 1 mL, so first mL of infusion can be fast.
 - b. If more than one continuous infusion in series are desired, IVUS catheter should be saline flushed into target artery with at least 3 mL saline immediately following previous drug infusion and with sufficient time

between serial infusions to allow previous drug to wash out or become inactive.

19. Time to efficacy will be drug-dependent, but may occur in as little as 5 minutes.
 - a. Be sure to record any changes in baseline flow to continuous infusion.
 - b. After drug is fully efficacious, compare flow to baseline flow.
 - c. Make certain that position of flow wire, etc. have remained constant during the continuous infusion.
20. Bolus dose responses can be obtained during continuous drug infusion. Be sure to include continuously infusing drug in bolus solution at desired concentration to prevent wash-out during bolus.
21. Reactive hyperemia data can be obtained using existing setup.
 - a. Following IVUS catheter detachment from flow wire, introduce angioplasty balloon catheter of appropriate diameter over flow wire.
 - b. Advance balloon catheter into coronary artery, but do not advance past flow wire. Insure IVUS catheter is not placed within balloon markers.
 - c. Deploy balloon while balloon catheter is still attached to flow wire. Flow measurements will decrease with increasing balloon inflation.
 - d. Inflate balloon rapidly to completely occlude flow measurements. Balloon should remain inflated for 15-45 seconds.
 - e. Deflate balloon and record flow measurements. Increased blood flow following occlusion is reactive hyperemia.

Appendix E Sterile dissection of coronary artery from intact heart

Procedures are adapted from "CORSMC1_METv2.doc", which was updated 6/25/08 by M. Sturek. Each step should be completed with sterile technique and in a sterile laminar flow hood whenever possible. All instruments, containers, dissecting dish, gloves, etc. should be sterile. Solutions should be sterile filtered with 0.2 µm filter.

"Sterilization" of tissue is facilitated by serial dilution technique noted below.

1. Rough / gross dissection of coronary arteries from heart ensues immediately after heart is obtained within 60 seconds following removal of heart from chest cavity.
 - a. Rinse coronary artery area on heart with cold, sterile 2CaNa + 2% PS.
 - b. Scissors are run from within 5 mm of coronary ostium into cardiac tissue on either side of each artery. Artery is cut away from heart with some cardiac tissue still attached. The aim of this step is expediency to place in sterile buffer solution.
 - c. Rinse dissected arteries again thoroughly with ~20-50 mL of 2CaNa + 2% PS.
2. Quickly plunge arteries into 500 mL ice-cold 2CaNa + 2% PS. Container should be kept on ice through entire dissection procedure.
3. Immediately take arteries to dissecting microscope in cell culture hood for further dissection.
4. Clean artery of excess adventitia, cardiac tissue, and adipose that may be attached to artery following rough / gross dissection in the cell culture hood in 100 x 20 mm culture dish in ~30 ml Low Ca. Treat artery gently (do not stretch excessively, if possible).
5. Any coronary artery that needs to be isolated/frozen for later molecular analysis should be attended to first.

6. At this point, the artery can be stored in the refrigerator in storage media for 2-5 days, if necessary.

Appendix F Fura-2 digital imaging methods

Michael Sturek, Ph.D.

Revised by Jason M. Edwards 4-14-06

Further revision by Zachary P. Neeb 12-30-09

PRELIMINARY NOTES

1. This text is for the "Rig 5" Intracellular Calcium Imaging experiments using multiple cells.
2. These procedures are mainly the "hows" of doing microfluorometry experiments with some of the "whys"
3. Check with Jason or Dr. Sturek if this text is unclear. Please make suggestions for improvement. A team effort will make these instructions better and the resulting uniform data collection procedures will make our data more reliable, etc.
4. Note the accompanying "BRIEF CHECKLIST" of procedures.

BEFORE STARTING EXPERIMENTS

1. Turn off all equipment: the computer, monitor, and the shutter on top of the lamp.
2. Turn on xenon lamp power supply (Blue box, power switch is in the back). You will hear the lamp switch on and the fan in the power supply will start.
3. **VERY IMPORTANT: MAKE SURE COMPUTERS IN THE ROOM ARE OFF BEFORE IGNITING XENON LAMP!**
The arc lamp igniter elicits 15,000 - 20,000 volt pulses to ignite the xenon lamp, thus damage to integrated circuits is possible. (To convince yourself, have a radio playing in the room as you ignite the lamp and listen to the static interference.)
 - a. The stability of the lamps is best if allowed to warm up for $\approx > 10$ -15 min. You should begin to put get your cells ready immediately, it will take at least 10 minutes by the time you start the experiment.
4. **Turn on Shutter**
5. During the 10-15 period of xenon lamp warm-up:
6. Turn on computer and monitor.
7. Prepare superfusion chamber.
(An illustration of the superfusion chamber can be found in Thayer, Sturek, and Miller. Measurement of neuronal Ca^{2+} transients using simultaneous microfluorimetry and electrophysiology. *Pflugers Arch.* 412:216-223, 1988.)
 - A) Apply vaseline to bottom side of chamber around the opening of the chamber with cotton swab, being careful not to slop vaseline on inside of chamber where cells are placed or in the inflow chamber.
 - B) Place coverslip on bottom using small forceps.
 - C) Place metal retaining ring on the four threaded screws and place one nut loosely on one of the screws to hold the coverslip loosely in place.
 - D) Verify that the coverslip is centered over the opening of the chamber and the retaining ring uniformly contacts the coverslip around the entire perimeter of the coverslip. This prevents leakage of solutions from the chamber. If small movements of the coverslip are needed for centering, care must be taken to avoid getting vaseline inside the chamber where the cells will be placed.
 - E) Place the remaining 3 nuts on the screws and tighten firmly with fingers.
 - F) Place 1-2 ml of solution (e.g. 2CaNa) in the superfusion chamber. This allows a quick check for leaks in the superfusion chamber/coverslip junction.
 - G) The objective on the scope is a 20x objective, make sure it is locked in place. This is a dry objective so **do not** place oil or water on it. Clean objective with lens paper.
8. Place superfusion chamber on microscope.

Metal ring should face down toward objective and the glass outflow tubing toward the back of the microscope.

9. Attach vacuum tubing to the glass outflow tubing on superfusion chamber. **Be careful not to break the glass tube.** If you do break a glass capillary tube, there are some spares either on the rig 5 table or on the lab bench behind you.

If the outflow tubing breaks, remove the superfusion chamber and replace the outflow tubing.

Always use a double trap in line with suction. Empty first trap after each use. It may be appropriate to partially fill the second trap with an absorbent material to prevent condensation in vacuum line.

10. Prepare solutions and cell superfusion reservoirs (syringes).

A) The superfusion syringe system must be checked for proper flow rate of \approx 1-2 ml/min, which is \approx > 1-2 drops/s.

1) Plunging of the 60 ml syringes, unclogging the needles with blasts of air, etc. may be needed to insure proper flow. Plunging may shread part of the black rubber on the plunger into the syringe. A better method may be to apply negative gauge pressure with a 20 ml syringe to the common outflow (with a needle).

2) Needles are 20 gauges, are cut with wire cutters, bent, and filed as needed to create a smoother edge.

B) Add desired solutions to the syringes and run solution through to be certain that each solution is in the tubing leading from the syringe to the valve. Solutions are collected in beaker marked "waste". Often it is necessary to tape the polyethylene (PE) tubing to the waste beaker to avoid slipping of the PE tubing out of the waste beaker and leakage of solutions on the bench, etc.

C) In the 7-syringe systems any chemicals that have rapid and/or irreversible actions should be placed in syringes 5, 6, or 7. The reason is that if some chemical is left in the dead space in tubing from the valve for syringes 1-4, a partial Ca_i response may be elicited in the cell.

D) Chemicals that notoriously stick to tubing (ie: Thapsigargin) , syringes, etc. should have a designated syringe and that syringe should not be used for any other chemical. For example, ionomycin is very stable and may stick to syringes. **Label the syringes** with appropriate numbers. Additional precaution should include rinsing syringes and tubing with ethanol following each use.

E) Always have list indicating contents of each syringe taped near the superfusion chamber for clarity. Confusion about what solution is in what syringe should be avoided during the experiment.

F) The superfusion flow is turned off by positioning the arrow between numbers on the valve control. Note that in the 4 and 7 syringe systems (Anspec, blue valve) the arrow on the control (handle) is very small and opposite of the direction of the handle. The 8 syringe Valco system is clearly marked.

1. Place superfusion system on left of the RIG.

2. Attach PE tubing from superfusion syringe system to superfusion inflow tubing (metal tube on right of chamber).

3. Turn on vacuum pump in room 366. Suction of the solution from the superfusion chamber should occur quickly and be evident from the brief slurping noise as the solution is aspirated from the superfusion chamber. The rate of flow should not be measured by the frequency of aspiration.

4. Verify solution flow characteristics of the superfusion system on the microscope stage.

This is **VERY IMPORTANT** because: a) it will insure rapid and complete exchange of solutions bathing the cell or tissue and, b) **AVOIDANCE OF FLOODING THE MICROSCOPE.**

- G) Turn on flow for physiological salt solution (PSS or 2CaNa) by turning handle on syringe system to appropriate syringe. The fluid level in the superfusion chamber should start rising and/or the slurping sound will start again.
- H) The fluid level should be ideally 1-2 mm for single cells and flow rate of \approx 1-2 ml/min. The higher the fluid level the greater the volume of solution in the superfusion chamber. Thus, even if the flow rate is very high it will require longer to exchange solutions if the superfusion chamber volume is greater.
- I) Fluid level may be changed by adjusting the outflow tubing (glass tubing), usually by turning the opening from side to side.
- J) Sometimes it is necessary to place wet the nylon mesh in front of the outflow tubing.
- K) Place a folded Kimwipe™ under inflow tubing and against the outside of the superfusion chamber (on top of microscope stage). This will serve the purpose of alerting the operator of any leak between inflow tubing and superfusion chamber. Also, if leak is slow, one Kimwipe™ will function as a sufficient wick for several hours of experiments. When performing patch clamp experiments, be sure wet Kimwipe™ does not touch any metal objects or it may introduce noise.

CONDUCTING EXPERIMENTS

1. Turn off PSS (2CaNa) and remove some solution from superfusion chamber by gentling swabbing with Kimwipe.
2. Add 1-3 drops of cell suspension (5-30uL) to the superfusion chamber on the coverslip directly at the objective aperture.
Do not add too much cell suspension because it might fill the superfusion chamber perhaps enough to cause the vacuum system to aspirate a large fraction of the solution (taking the cells, also). If you have few cells obtain the drop from the bottom of the conical centrifuge tube and take extra care to place the drop directly over the objective aperture.
3. Allow the cells to settle onto coverslips for 1 to 3 minutes depending on concentration of the cells, the longer you wait, the more cells will stick to the coverslip.
4. Observe cell through the binocular eyepieces.
 - a. Turn off room lights.
 - c. Turn on the arc lamp on the right. Excitation light will be transmitted to the microscope and the fura-2 loaded cells can thereby be visualized.
 - d. Focus on cells.
 - 1) The top slider rod should be pushed to the right of the binoculars to see the cells.
 - 2) Usually only fine adjustment of the focus is needed.
 - 3) If it is difficult to find cells the most common problems are too few cells or the cells are grossly out of the focal plane.
 - e. Adjust binocular eyepiece distance as needed to accommodate your eye spacing.
5. Start superfusion of PSS (2CaNa).
 - a. View through binocular eyepieces. The top slider is pushed to the right.
 - b. When superfusion is started some cells may be swept away (easily noted if looking in the binocular eyepieces). This is normal and usually an ample number of cells adhere to the coverslip. If cells are not adhering try changing

- the coverslip. It seems that after long usage of the same coverslip the adhesion properties decrease.
- c. Monitor closely the superfusion characteristics.
The nylon mesh sometimes becomes dried out during the several minutes required for the cells to adhere to the coverslip. Sometimes it is necessary to apply solution to the nylon mesh with a dispo pipette, change the vacuum line, etc. as described above.
 - d. Definitely start superfusion before searching for cells because it is very frustrating to select a cell, start an experiment, then have the cell swept away when the superfusion is started.
6. Search for a cell or cells.
- a. Vascular smooth muscle cells having a "glowing" appearance in brightfield view (through the bionocular eyepieces), thick looking, and elongated are usually reactive to vasoconstrictors. Refer to the book chapters for photomicrographs of smooth muscle and endothelial cells. These morphological criteria are not absolute. Some dispersions may yield many cells with this appearance, but the cells may be functionally unreactive. To our knowledge no laboratory can explain this.
 - b. Freshly dispersed endothelial cells typically clump together like a cluster of grapes and are spherical. A single cell at the edge of a clump or several cells in a clump may be studied.
 - c. After finding a good group of cells you may want to look for an even better group of cells.
 - 1) Search at right angles to cell because it is easier then to return to that same cell should you not find a better cell. Movement around the field is possible with X and Y stage movement controls located on lower right, toward back of microscope. The search area will be limited by objective hitting retaining ring of superfusion chamber.
 - 2) Make sure the cell is located near the middle 1/2 (x-y direction) of the superfusion chamber because the exchange of solutions is not complete in the peripheral 1/4 of the chamber. A cell located near the opening of the inflow chamber is ideal.
 - d. Place the cell near the cross hairs in the center of the field. For each Rig there is a unique location near the crosshairs that provides a view of the cell in the center of the video monitor. Also, the crosshair area is that which is excited by the arc lamp.
 - e. Check fluorescence of cells by blocking transillumination (with small piece of cardboard placed on phase condenser or by turning off the light) and observing visually. If no fluorescence signal or signal is weak then check several points along the excitation and emission path:
 - 1) Arc lamp shutter is open.
 - 2) If blue/violet light is not visible coming through the objective, push "local" on the filter controller then press 2 or 3. 2 and 3 are the 340 and 380 filters respectively, while 1 blocks the laser.
 - 3) Make sure Objective aperture is opened fully.
Your eyes are quite sensitive and usually if you see only faint fluorescence you will have to take extra care to measure the fluorescence with the optical processor. If the cells are too faintly fluorescent it may be necessary to load with dye again or obtain a different fraction of cells.
 - f. Record notes on cells if the morphology is unusual, etc.
7. Observe cell in video monitor.
- 1) Pull slider under the binoculars of the microscope over (to the left). Then open the program "Inca" and click **Experiment** on the top, then **New Experiment**.

- 2) Click **Video Preview** and fluorescent light will illuminate the cells. If this does not occur, adjust the power of the lamp by turning the black wheel on the front of the lamp clockwise. You may also need to reset the timer on the lamp by pushing the black button on the front of the lamp.
 - 3) Click **Check Brightness** and the screen will turn green and red. Adjust the stretch at the bottom of the screen until no red is present on the image.
8. Exposure time
- 1) Increase the exposure time as an alternative to increasing intensity of the lamp(which is done by turning the black wheel on the front of the laser). As you increase exposure time, you decrease the rate at which you collect images. The exposure times should be a 2:1 ratio with 340:380 respectively. Click **Ok**.
 - 2) Record background.
 - 1) Click **Record New Background**. Move the slide under the binoculars to the right and click **Accept new background**. Move slide back to the left.
 - 2) If background fluorescence is too high (>20% for single cells) try to reduce the background further by several methods.
 - a) Decrease transillumination light intensity. Light may be turned off, but this is rarely necessary.
 - b) Last resort - Close black curtains.
 - 3) Move cell back in measurement aperture.
9. Make "areas of interest" (AOI).
- 1) Click **Find cells and set Threshold**. Click **Freehand**. Then move mouse to cell perimeter and click the left mouse once and circle the cell once, then click the mouse again to complete the circumference. Repeat until all the desired cell are circled. Circle and note a background area.
 - 2) Adjust the threshold, Begin at **10** click **measure**. Look for the largest difference in the background (dark) circle compared to the cell intensity (bright). Readjust the number to higher or lower than 10 to obtain optimal conditions. Click **OK**.
10. Click **Select File Name**. Make a file name for the upcoming experiment.

Start experiment.

Press "**Start Experiment**"

11. TAKE MANY NOTES ON EXPERIMENTS BECAUSE:
- a. Precise observation of subtle, but consistent, changes in cells, etc. may lead to new avenues of experimentation.
 - b. "Audit" of research programs by NIH. Documentation of effort and results is essential to justify funding of grants and to resolve any issues regarding validity of our findings.
12. Other precautions during experiments:
- a. **VERY IMPORTANT: Check the superfusion chamber for leaks periodically throughout the experiment.** Usually a leak is noticed first as a fluid front between the superfusion chamber and the plastic ring on which it sits on the microscope stage. If a leak is remedied at this time there is little harm done. Putting a drop of solution purposely on the plastic ring before placing the superfusion chamber on the microscope will illustrate this. Be especially aware of leaks when using saponin, Triton X-100, or >70% ethanol because these agents dissolve the vaseline. If a leak goes unnoticed the solution may flow down onto the objective and into the body of the microscope. **Servicing the microscope requires IMMEDIATE ATTENTION** and involves disassembly of

the microscope. It is a major operation, but better than servicing the microscope after the solutions have dried in the joints of the microscope and the parts are immobilized. **If you ever suspect a leak please ask for help!!**

- b. Wipe solution spills from air suspension tables and microscopes immediately.
 - c. Check the fluid trap on right of the Rig cage.
If the trap is getting full empty it, otherwise the solution will be aspirated into the vacuum pump and ruin the pump.
13. Rinse chamber thoroughly between experiments on cells. Distilled water sprayed into the superfusion chamber with a wash bottle equipped with flexible tubing is ideal. Wiping of the chamber is also needed, because some cells are strongly adherent.
 14. Remember...cell heterogeneity -- not all cells will respond to all agents.

SHUTTING DOWN RIG AND CLEANING

1. **Very Important:** Turn off the filter wheel controller first, then the computer, then the Arc Lamp last.
2. Clean superfusion chamber.
 - a. Remove the chamber from the microscope.
 - b. Wash the chamber well with water. Then remove suction tube.
 - c. Remove coverslip and wipe vaseline from superfusion chamber.
 - d. Place nuts in jar.
 - e. Place coverslip in "SHARPS" trash (small box in each Rig).
3. Turn off other equipment in whatever order is convenient.
4. Flush distilled water through superfusion system.
5. Double check that all shutters are closed and turn off power strip for arc lamp fan.

Appendix G Mechanical isolation of in-stent neointima from in-stent media

First conduct all steps in **Appendix E Sterile dissection of coronary artery from intact heart.**

1. Separate stent from rest of artery by cutting as close to the stent edges as possible without crimping stent.
2. Under magnification, all adventitia and adipose should be carefully removed. Do not perforate artery wall. Do not crimp or otherwise disturb the artery wall. Healthy looking artery equals healthy cells and clean mechanical isolation.
3. The stent struts should be apparent through the wall of the artery. Pick a stent window longitudinally at the middle of the stent. Using very sharp, fine dissecting scissors, cut through the adventitia outside the stent window. The cut should be cross-sectional and only through the adventitia.
 - a. When cutting through adventitia, do not push the scissors into the stent. Sufficiently sharp scissors should cut without a lot of downward pressure.
 - b. Alternatively to scissors, a scalpel can be used to cut through the adventitia.
4. In the section of cut adventitia, poke one scissor through the media and neointima. If the adventitia was cut through and the scissor is sharp, it should poke through without crimping the stent.
5. Cut the media and neointima within the stent window in a cross-sectional direction.
6. Place sturdy, yet sharp scissors into the cut made. Use small cuts with the tips of the scissors to cut through the stent and tissue in a cross-sectional manner.
 - a. Large cuts result in crimping.

- b. The tissue may require a bit more up and down cutting. Cut through the tissue so that the scissors stop on the stent strut without cutting through. A sharp cutting motion should be used to cut through the stent to prevent twisting the stent struts or crimping the stent.
 - c. Rotate the stent with each cut, placing the scissors in optimal cutting position to minimize crimping pressure.
 - d. A clean cut will result in a cross-sectioned stent with no crimping.
- 7. One half of the stent may be used for molecular studies and should be immediately taken care of. Place the other half of the stent in ice-cold 2CaNa if there is a prolonged delay.
- 8. Cut one wall of the stent-half longitudinally. Crimping will not be an issue.
- 9. Pull the stent open using tweezers exposing the luminal side.
 - a. This causes tension in the neointima aiding mechanical isolation.
- 10. Firmly grab the thickest section of neointima near the cross-sectional cut with sharp tweezers. Optimally, grab the neointima near the corner of the cross-sectional and longitudinal cuts.
 - a. When grabbing the neointima with tweezers, one point of the tweezers should be between the stent and neointima and one point should be on the luminal side of the neointima.
- 11. Using sturdy tweezers or even clamps, grab a stent strut nearest the other tweezers.
- 12. Gently pull/peel the neointima up and away from the stent struts. It should come off in one intact sheet. The stent should remain apposed to the media.
- 13. Pull the stent away from the media. It should easily come away in one piece.

Appendix H Sterile organ culture

1. Complete **Appendix E Sterile dissection of coronary artery from intact heart**.
Cleanly dissect any adventitia and adipose because they will detract from quality of cell isolation later. Adipose cells lyse during organ culture, may secrete indeterminate adipokines, and consume media nutrients.
2. Cut artery segment into smaller segments of ~equal length.
3. Fill each well of 6-well culture dish with sterile phosphate buffered saline.
4. Transfer each artery segment separately into the top left well.
5. Allow to sit for several seconds before transferring to top middle well. Each segment should be moved separately and with as little solution from the previous well transferred as possible.
6. Continue to transfer artery segments in a clock-wise manner through each well.
7. Serial “sterilization” is achieved after each artery segment has been moved in sequence through each well of the plate.
8. Set up 6-well culture dish with 5 mL of sterile RPMI solution with 1% penicillin/streptomycin in each well.
9. Transfer one “sterilized” artery segment to each well.
10. Appropriate labeling is essential. Cover of 6-well dish should be marked with pig number, start date of organ culture, and any treatments unique to each well.
11. Culture dish should be transferred to 37°C incubator with 4.6% CO₂.
12. Depending on desired time of organ culture, media should be changed every 2-3 days using sterile technique.
 - a. Color of the media should be noted, as amber yellow indicates acidity and darker purple indicates alkalinity. Acidity is much more common and would indicate high cellular metabolism and need for nutrients, thus more frequent changing of media.

Appendix I Intracellular pipette solutions for recording of ionic currents (whole cell)

Adapted from hardcopy "SOLUT1.MET, 121787; Michael Sturek, PhD.

Always check notes and specific instructions below table.

1. Cs⁺ pipette, highly buffered Ca²⁺ (10 mM EGTA)

Cs10EGTA			
Components	Conc. (mM)	100 mL total	Notes
Cs ⁺ (CsCl)	100 +24 <u>+13</u> 137 Total	10 mL of 1 M pH'ed (~40 µL)	– from CsOH add to STOCK – from CsOH after add ATP system & GTP
MgCl ₂	1	1 mL of 0.1 M	
HEPES	10	1 mL of 1.0 M	
EGTA	10	380.4 mg	
pH	7.3 w/CsOH		
			Components above here → STOCK solution
MgATP	3.6	19.1 mg / 10 mL	Components below here add to STOCK (10 or 20 mL aliquots)
Tris ₂ CP	14	63.5 mg / 10 mL	
CPK	50 U/mL	4.0 mg / 10 mL	Lot# 96F-9555; optional
TrisGTP	1	6.4 mg / 10 mL	
Other?			enzymes, cofactors, etc.
GMPP(NH)P	60 µM	0.32 mg / 10 mL	Optional

Instructions:

- i. Dispense 10 mL of STOCK into small beaker with stirring bar. Add ATP and Tris₂CP → pH <6. Add >40 µL of dilute (1 CsOH stock:3 ddH₂O) CsOH → pH 7.3.
- ii. Add CPK (avoids possible adverse pH effect; optional) filtered with Millex-GS 0.22 µm filter.
- iii. Add 0.5 mL to micro centrifuge tubes and place at -80°C.
- iv. Store in plastic bottles in order to avoid leeching of Ca²⁺ from the container.
- v. Suck STOCK solution into electrode, then backfill with ATP system solution.

2. Cs⁺ pipette, slightly buffered Ca²⁺ (0.1 mM EGTA)

Cs0.1EGTA			
Components	Conc. (mM)	100 mL total	Notes
Cs ⁺ (CsCl)	120 +11 <u>+8</u> 140 Total	12 mL of 1 M pH'ed (~40 µL)	- from CsOH add to STOCK - from CsOH after add ATP system & GTP
MgCl ₂	1	1 mL of 0.1 M	
HEPES	10	1 mL of 1.0 M	
CsEGTA	0.1	1 mL of 10 mM	
pH	7.3 w/CsOH		
			Components above here → STOCK solution
MgATP	3.6	19.1 mg / 10 mL	Components below here add to STOCK (10 or 20 mL aliquots)
Tris ₂ CP	14	63.5 mg / 10 mL	
			; optional
TrisGTP	1	6.4 mg / 10 mL	
Other?			enzymes, cofactors, etc.
GMPP(NH)P	60 µM	0.32 mg / 10 mL	optional

Instructions:

1. Dispense 10 mL of STOCK into small beaker with stirring bar. Add ATP and Tris₂CP → pH <6. Add >40 µL of dilute (1 CsOH stock:3 ddH₂O) CsOH → pH 7.3.
2. Add CPK (avoids possible adverse pH effect) filtered with Millex-GS 0.22 µm filter.
3. Add 0.5 mL to micro centrifuge tubes and place at -80°C.
4. Store in plastic bottles in order to avoid leeching of Ca²⁺ from the container.
5. Suck STOCK solution into electrode, then backfill with ATP system solution.

3. Cs⁺ pipette, Fura-2 K5, slightly buffered Ca²⁺ (0.1 mM EGTA)

CsFura-20.1EGTA			
Components	Conc. (mM)	100 mL total	Notes
Cs ⁺ (CsCl)	120 +11 +8 140 Total	12 mL of 1M pH'ed (~40µL)	- from CsOH add to STOCK - from CsOH after add ATP system & GTP
MgCl ₂	1	1 mL of 0.1M	
HEPES	10	1 mL of 1.0M	
CsEGTA	0.1	1 mL of 10mM	
pH	7.3 w/CsOH		Components above here → STOCK solution
MgATP	3.6	19.1 mg / 10 mL	Components below here add to STOCK (10 or 20 mL aliquots)
Tris ₂ CP	14	63.5 mg / 10 mL	
CPK	50 U/mL	4.0 mg / 10 mL	Lot# 96F-9555
TrisGTP	1	6.4 mg / 10 mL	
Fura-2	100µM	0.1 mg / 1.0 mL	Only 1 mL; Fura-2 K5
Other?			enzymes, cofactors, etc.
GMPP(NH)P	60µM	0.32 mg / 10 mL	optional

Instructions:

1. Dispense 10 mL of STOCK into small beaker with stirring bar. Add ATP and Tris₂CP → pH <6. Add >40 µL of dilute (1 CsOH stock:3 ddH₂O) CsOH → pH 7.3.
2. Add CPK (avoids possible adverse pH effect) filtered with Millex-GS 0.22 µm filter.
3. Add 0.5 mL to micro centrifuge tubes and place at -80°C.
4. Store in plastic bottles in order to avoid leeching of Ca²⁺ from the container.
5. Suck STOCK solution into electrode, then backfill with ATP System solution.

4. K⁺ pipette, highly buffered Ca²⁺ (10 mM EGTA).

K ⁺ , 10 EGTA			
Components	Conc. (mM)	100 mL total	Notes
K ⁺ (KCl)	100 +29 +9 140 Total	10 mL of 1M pH'ed (~70µL)	- from KOH add to STOCK - from KOH after add ATP system & GTP
TEACl	10	10 mL of 1.0M	
MgCl ₂	1	1 mL of 0.1M	
HEPES	10	1 mL of 1.0M	
KEGTA	10	380.4 mg	
pH	7.3 w/KOH		Components above here → STOCK solution
MgATP	3.6	19.1 mg / 10 mL	Components below here add to STOCK (10 or 20 mL aliquots)
Tris ₂ CP	14	63.5 mg / 10 mL	
CPK	50 U/mL	4.0 mg / 10 mL	Lot# 96F-9555
TrisGTP	1	6.4 mg / 10 mL	
Other?			enzymes, cofactors, etc.
GMPP(NH)P	60µM	0.32 mg / 10 mL	optional

Instructions:

1. Dispense 10 mL of STOCK into small beaker with stirring bar. Add ATP and Tris₂CP → pH <6. Add >70 µL of 1M KOH → pH 7.3.
2. Add CPK (avoids possible adverse pH effect) filtered with Millex-GS 0.22 µm filter.
3. Add 0.5 mL to micro centrifuge tubes and place at -80°C.
4. Store in plastic bottles in order to avoid leeching of Ca²⁺ from the container.
5. Suck STOCK solution into electrode, then backfill with ATP System solution.

5. K⁺ pipette, slightly buffered Ca²⁺ (0.1 mM EGTA).

K ⁺ , 0.1 EGTA			
Components	Conc. (mM)	100 mL total	Notes
K ⁺ (KCl)	130 +5 <u>+9</u> 144 Total	13 mL of 1M pH'ed (~70µL)	- from KOH add to STOCK - from KOH after add ATP system & GTP
MgCl ₂	1	1 mL of 0.1M	
HEPES	10	1 mL of 1.0M	
KEGTA	0.1	1 mL of 10 mM	
pH	7.3 w/KOH		Components above here → STOCK solution
MgATP	3.6	19.1 mg / 10 mL	Components below here add to STOCK (10 or 20 mL aliquots)
Tris ₂ CP	14	63.5 mg / 10 mL	
CPK	50 U/mL	4.0 mg / 10 mL	Lot# 96F-9555
TrisGTP	1	6.4 mg / 10 mL	
Other?			enzymes, cofactors, etc.
GMPP(NH)P	60µM	0.32 mg / 10 mL	optional

Instructions:

1. Dispense 10 mL of STOCK into small beaker with stirring bar. Add ATP and Tris₂CP → pH <6. Add >70 µL of 1M KOH → pH 7.3.
2. Add CPK (avoids possible adverse pH effect) filtered with Millex-GS 0.22 µm filter.
3. Add 0.5 mL to micro centrifuge tubes and place at -80°C.
4. Store in plastic bottles in order to avoid leeching of Ca²⁺ from the container.
5. Suck STOCK solution into electrode, then backfill with ATP System solution.

6. K⁺ pipette, Fura-2 K5, slightly buffered Ca²⁺ (0.1 mM EGTA).

K ⁺ , Fura-2 K5, 0.1 EGTA			
Components	Conc. (mM)	100 mL total	Notes
K ⁺ (KCl)	130 +5 <u>+9</u> 144 Total	13 mL of 1M pH'ed (~70µL)	– from KOH add to STOCK – from KOH after add ATP system & GTP
MgCl ₂	1	1 mL of 0.1M	
HEPES	10	1 mL of 1.0M	
KEGTA	0.1	1 mL of 10mM	
pH	7.3 w/KOH		Components above here → STOCK solution
MgATP	3.6	19.1 mg / 10 mL	Components below here add to STOCK (10 or 20 mL aliquots)
Tris ₂ CP	14	63.5 mg / 10 mL	
CPK	50 U/mL	4.0 mg / 10 mL	Lot# 96F-9555
TrisGTP	1	6.4 mg / 10 mL	
Fura-2	100µM	0.1 mg / 1.0 mL	Only 1 mL; Fura-2 K5
Other?			enzymes, cofactors, etc.
GMPP(NH)P	60µM	0.32 mg / 10 mL	optional

Instructions:

1. Dispense 10 mL of STOCK into small beaker with stirring bar. Add ATP and Tris₂CP → pH <6. Add >70 µL 1M KOH → pH 7.3.
2. Add CPK (avoids possible adverse pH effect) filtered with Millex-GS 0.22 µm filter.
3. Add 0.5 mL to micro centrifuge tubes and place at -80°C.
4. Store in plastic bottles in order to avoid leeching of Ca²⁺ from the container.
5. Suck STOCK solution into electrode, then backfill with ATP System solution.

Appendix J Extracellular solutions

Adapted from hardcopy "SOLUT1.MET, 121787; Michael Sturek, PhD.

Always check notes and specific instructions below table.

1. 2CaNa or 2BaNa

2BaNa or 2CaNa				
Components	Conc. (mM)	4000 mL total	3000 mL total	11.5 L total
BaCl ₂ or CaCl ₂	2 2	80 mL of 0.1 M	60 mL of 0.1 M	230 mL of 0.1 M
NaCl	138	552 mL of 1.0M	414 mL of 1.0M	92.74 g
MgCl ₂	1	40 mL of 0.1M	30 mL of 0.1M	115 mL of 0.1M
KCl	5	200 mL of 0.1M	150 mL of 0.1M	57.5 mL of 1.0M
HEPES	10	40 mL of 1.0M	30 mL of 1.0M	115 mL of 1.0M
Glucose (D-glucose)	10	7.2 g	5.4 g	20.7 g
pH	7.4 w/NaOH	15-17 mL of 1.0M	10-12 mL of 1.0M	48-50 mL of 1.0M
Total Na ⁺	142			

2. 0.5Ca²⁺

Low Ca				
Components	Conc. (mM)	1000 mL total	500 mL total	Notes
CaCl ₂	0.5	5.0 mL of 0.1 M	2.5 mL of 0.1 M	
NaCl	140	140 mL of 1.0 M	70 mL of 1.0 M	
MgCl ₂	1	10 mL of 0.1 M	5 mL of 0.1 M	
KCl	5	50 mL of 0.1 M	40 mL of 0.1 M	
HEPES	10	10 mL of 1.0 M	5 mL of 1.0 M	
Glucose (D-glucose)	10	1.8 g	0.9 g	
pH	7.4 (w/NaOH)	3-5 mL of 1.0 M	2-3 mL of 1.0 M	
BSA	1.5%	15 g	7.5 g	

3. 0Ca

0CaNa				
Components	Conc. (mM)	1000 mL total	500 mL total	Notes
CaCl ₂	--	--	--	
NaCl	140	140 mL of 1.0 M	70 mL of 1.0M	
MgCl ₂	1	10 mL of 0.1M	5 mL of 0.1M	
KCl	5	50 mL of 0.1M	40 mL of 0.1M	
HEPES	10	10 mL of 1.0M	5 mL of 1.0M	
Glucose (D-glucose)	10	1.8 g	0.9 g	
EGTA	10 ⁻² (10 ⁻⁵ M)	3.8 mg	1.9 mg	
pH	7.4 (w/NaOH)	3-5 mL of 1.0M	2-3 mL of 1.0M	

References

1. Witczak,C.A., Mokolke,E.A., Boullion,R.D., Wenzel,J., Keisler,D.H., and Sturek,M. 2005. Noninvasive measures of body fat percentage in male Yucatan swine. *Comp. Med.* **55**:445-451.
2. Boullion,R.D., Mokolke,E.A., Wamhoff,B.R., Otis,C.R., Wenzel,J., Dixon,J.L., and Sturek,M. 2003. Porcine model of diabetic dyslipidemia: Insulin and feed algorithms for mimicking diabetes in humans. *Comp. Med.* **53**:42-52.
3. Dyson,M., Alloosh,M., Vuchetich,J.P., Mokolke,E.A., and Sturek,M. 2006. Components of metabolic syndrome and coronary artery disease in female Ossabaw swine fed excess atherogenic diet. *Comp. Med.* **56**:35-45.
4. Sturek,M., Alloosh,M., Wenzel,J., Byrd,J.P., Edwards,J.M., Lloyd,P.G., Tune,J.D., March,K.L., Miller,M.A., Mokolke,E.A. et al 2007. Ossabaw Island miniature swine: cardiometabolic syndrome assessment. In *Swine in the Laboratory: Surgery, Anesthesia, Imaging, and Experimental Techniques*. M.M.Swindle, editor. CRC Press. Boca Raton. 397-402.
5. Flum,D.R., Devlin,A., Wright,A.S., Figueredo,E., Alyea,E., Hanley,P.W., Lucas,M.K., and Cummings,D.E. 2007. Development of a porcine Roux-en-Y gastric bypass survival model for the study of post-surgical physiology. *Obesity Surgery* **17**:1332-1339.
6. Bender,S.B., Tune,J.D., Borbouse,L., Long,X., Sturek,M., and Laughlin,M.H. 2009. Altered mechanism of adenosine-induced coronary arteriolar dilation in early-stage metabolic syndrome. *Experimental Biology and Medicine* **234**:683-692.
7. Lee,L., Alloosh,M., Saxena,R., Van Alstine,W., Watkins,B.A., Klaunig,J.E., Sturek,M., and Chalasani,N. 2009. Nutritional model of steatohepatitis and metabolic syndrome in the Ossabaw miniature swine. *Hepatology* **50**:56-67.
8. Borbouse,L., Dick,G.M., Asano,S., Bender,S.B., Dincer,U.D., Payne,G.A., Neeb,Z.P., Bratz,I.N., Sturek,M., and Tune,J.D. 2009. Impaired function of coronary BK_{Ca} channels in metabolic syndrome. *Am. J. Physiol. Heart Circ. Physiol.* **(In press)**.
9. Otis,C.R., Wamhoff,B.R., and Sturek,M. 2003. Hyperglycemia-induced insulin resistance in diabetic dyslipidemic Yucatan swine. *Comp. Med.* **53**:53-64.
10. Witczak,C.A., and Sturek,M. 2004. Exercise prevents diabetes-induced impairment in superficial buffer barrier in porcine coronary smooth muscle. *J. Appl. Physiol.* **96**:1069-1079.
11. Dixon,J.L., Shen,S., Vuchetich,J.P., Wysocka,E., Sun,G., and Sturek,M. 2002. Increased atherosclerosis in diabetic dyslipidemic swine: protection by atorvastatin involves decreased VLDL triglycerides but minimal effects on the lipoprotein profile. *J. Lipid Res.* **43**:1618-1629.

12. Mokolke,E.A., Hu,Q., Song,M., Toro,L., Reddy,H.K., and Sturek,M. 2003. Altered functional coupling of coronary K⁺ channels in diabetic dyslipidemic pigs is prevented by exercise. *J. Appl. Physiol.* **95**:1179-1193.
13. Witczak,C.A., Wamhoff,B.R., and Sturek,M. 2006. Exercise training prevents Ca²⁺ dysregulation in coronary smooth muscle from diabetic dyslipidemic Yucatan swine. *J. Appl. Physiol.* **101**:752-762.
14. Lee,D.L., Wamhoff,B.R., Katwa,L.C., Reddy,H.K., Voelker,D.J., Dixon,J.L., and Sturek,M. 2003. Increased endothelin-induced Ca²⁺ signaling, tyrosine phosphorylation, and coronary artery disease in diabetic dyslipidemic swine are prevented by atorvastatin. *J. Pharmacol. Exp. Ther.* **306**:132-140.
15. Rector,R.S., Thomas,T.R., Liu,Y., Henderson,K.K., Holiman,D.A., Sun,G.Y., and Sturek,M. 2003. Effect of exercise on postprandial lipemia following a higher calorie meal in Yucatan miniature swine. *Metabolism* **53**:1021-1026.
16. Hill,B.J.F., Price,E.M., Dixon,J.L., and Sturek,M. 2003. Increased calcium buffering in coronary smooth muscle cells from diabetic dyslipidemic pigs. *Atherosclerosis* **167**:15-23.
17. Mokolke,E.A., Dietz,N.J., Eckman,D.M., Nelson,M.T., and Sturek,M. 2005. Diabetic dyslipidemia and exercise affect coronary tone and differential regulation of conduit and microvessel K⁺ current. *Am. J. Physiol. Heart Circ. Physiol.* **288**:H1233-H1241.
18. Wamhoff,B.R., Dixon,J.L., and Sturek,M. 2002. Atorvastatin treatment prevents alterations in coronary smooth muscle nuclear Ca²⁺ signaling associated with diabetic dyslipidemia. *J. Vasc. Res.* **39**:208-220.
19. Turk,J.R., Carroll,J.A., Laughlin,M.H., Thomas,T.R., Casati,J., Bowles,D.K., and Sturek,M. 2003. C-reactive protein correlates with macrophage accumulation in coronary arteries of hypercholesterolemic pigs. *J. Appl. Physiol.* **95**:1301-1304.
20. Lloyd,P.G., Sheehy,A.F., Edwards,J.M., Mokolke,E.A., and Sturek,M. 2008. Leukemia inhibitory factor is upregulated in coronary arteries of Ossabaw miniature swine after stent placement. *Cor. Art. Dis.* **19**:217-226.
21. Edwards,J.M., Alloosh,M., Long,X., Dick,G.M., Lloyd,P.G., Mokolke,E.A., and Sturek,M. 2008. Adenosine A₁ receptors in neointimal hyperplasia and in-stent stenosis in Ossabaw miniature swine. *Cor. Art. Dis.* **19**:27-31.
22. Le,T., Langohr,I.M., Locker,M.J., Sturek,M., and Cheng,J.-X. 2007. Label-free molecular imaging of atherosclerotic lesions using multimodal nonlinear optical microscopy. *J. Biomed. Opt.* **12**:054007.
23. Langohr,I.M., HogenEsch,H., Stevenson,G.W., and Sturek,M. 2008. Vascular-associated lymphoid tissue in swine (*sus scrofa*). *Comp. Med.* **58**:168-173.

24. Wang,H.-W., Langohr,I.M., Sturek,M., and Cheng,J.-X. 2009. Imaging and quantitative analysis of atherosclerotic lesions by CARS-based multimodal nonlinear optical microscopy. *Arterioscler. Thromb. Vasc. Biol.* **29**:1342-1348.
25. Bratz,I.N., Dick,G.M., Tune,J.D., Edwards,J.M., Neeb,Z.P., Dincer,U.D., and Sturek,M. 2008. Impaired capsaicin-induced relaxation of coronary arteries in a porcine model of the metabolic syndrome. *Am. J. Physiol. : Heart Circ. Physiol.* **294**:H2489-H2496.
26. Witczak,C.A., and Sturek,M. 2005. Training-induced sarcoplasmic reticulum Ca^{2+} unloading occurs without Ca^{2+} influx. *Med. Sci. Sports Exerc.* **37**:1119-1125.
27. Dick,G.M., and Sturek,M. 1996. Effects of a physiological insulin concentration on the endothelin-sensitive Ca^{2+} store in porcine coronary artery smooth muscle. *Diabetes* **45**:876-880.
28. Heaps,C.L., Sturek,M., Price,E.M., Laughlin,M.H., and Parker,J.L. 2001. Sarcoplasmic reticulum Ca^{2+} -ATPase uptake is impaired in coronary smooth muscle distal to chronic occlusion. *Am. J. Physiol. : Heart Circ. Physiol.* **281**:H223-H231.
29. Edwards,J.M., Neeb,Z.P., Alloosh,M.A., Long,X., Bratz,I.N., Peller,C.R., Byrd,J.P., Kumar,S., Obukhov,A.G., and Sturek,M. 2009. Exercise training decreases store-operated Ca^{2+} entry associated with metabolic syndrome and coronary atherosclerosis. *Cardiovasc. Res.* doi: **10.1093/cvr/cvp308**.
30. Wilson,P.W., D'Agostino,R.B., Parise,H., Sullivan,L., and Meigs,J.B. 2005. Metabolic syndrome as a precursor of cardiovascular disease and type 2 diabetes mellitus. *Circulation* **112**:3066-3072.
31. Alberti,K.G., and Zimmet,P.Z. 1998. Definition, diagnosis and classification of diabetes mellitus and its complications. Part 1: diagnosis and classification of diabetes mellitus provisional report of a WHO consultation. *Diabet. Med.* **15**:539-553.
32. 2001. Executive Summary of The Third Report of The National Cholesterol Education Program (NCEP) Expert Panel on Detection, Evaluation, And Treatment of High Blood Cholesterol In Adults (Adult Treatment Panel III). *JAMA* **285**:2486-2497.
33. Alberti,K.G., Eckel,R.H., Grundy,S.M., Zimmet,P.Z., Cleeman,J.I., Donato,K.A., Fruchart,J.C., James,W.P., Loria,C.M., and Smith,S.C., Jr. 2009. Harmonizing the metabolic syndrome: a joint interim statement of the International Diabetes Federation Task Force on Epidemiology and Prevention; National Heart, Lung, and Blood Institute; American Heart Association; World Heart Federation; International Atherosclerosis Society; and international association for the Study of Obesity. *Circulation* **120**:1640-1645.

34. Kahn,R., Buse,J., Ferrannini,E., and Stern,M. 2005. The metabolic syndrome: time for a critical appraisal. Joint statement from the American Diabetes Association and the European Association for the Study of Diabetes. *Diabetologia* **48**:1684-1699.
35. Stern,M.P., Williams,K., Gonzalez-Villalpando,C., Hunt,K.J., and Haffner,S.M. 2004. Does the metabolic syndrome improve identification of individuals at risk of type 2 diabetes and/or cardiovascular disease? *Diabetes Care* **27**:2676-2681.
36. Kip,K.E., Marroquin,O.C., Kelley,D.E., Johnson,B.D., Kelsey,S.F., Shaw,L.J., Rogers,W.J., and Reis,S.E. 2004. Clinical Importance of Obesity Versus the Metabolic Syndrome in Cardiovascular Risk in Women: A Report From the Women's Ischemia Syndrome Evaluation (WISE) Study. *Circulation* **109**:706-713.
37. Reaven,G.M. 2006. The metabolic syndrome: is this diagnosis necessary? *Am. J. Clin. Nutr.* **83**:1237-1247.
38. Ford,E.S., Giles,W.H., and Mokdad,A.H. 2004. Increasing prevalence of the metabolic syndrome among U.S. adults. *Diabetes Care* **27**:2444-2449.
39. Grundy,S.M. 2007. Metabolic Syndrome: A Multiplex Cardiovascular Risk Factor. *Journal of Clinical Endocrinology Metabolism* **92**:399-404.
40. Girman,C.J., Rhodes,T., Mercuri,M., Pyorala,K., Kjekshus,J., Pedersen,T.R., Beere,P.A., Gotto,A.M., and Clearfield,M. 2004. The metabolic syndrome and risk of major coronary events in the Scandinavian Simvastatin Survival Study (4S) and the Air Force/Texas Coronary Atherosclerosis Prevention Study (AFCAPS/TexCAPS). *Am. J. Cardiol.* **93**:136-141.
41. Angulo,P. 2005. Nonalcoholic fatty liver disease. *Rev. Gastroenterol. Mex.* **70 Suppl 3**:52-56.
42. Farrell,G.C. 2009. The liver and the waistline: Fifty years of growth. *J. Gastroenterol. Hepatol.* **24 Suppl 3**:S105-S118.
43. Stern,M.P. 1995. Diabetes and cardiovascular disease. The "common soil" hypothesis. *Diabetes* **44**:369-374.
44. Lin,Y., and Sun,Z. 2009. Current Views on Type II Diabetes. *J. Endocrinol.*
45. American Diabetes Association 2008. Diagnosis and Classification of Diabetes Mellitus. *Diabetes Care* **31**:S55-S60.
46. Gale,E.A.M. 2001. The discovery of type 1 diabetes. *Diabetes* **50**:217-226.
47. Ramlo-Halsted,B.A., and Edelman,S.V. 1999. The natural history of type 2 diabetes. Implications for clinical practice. *Primary Care* **26**:771-789.
48. DeFronzo,R.A., Bonadonna,R.C., and Ferrannini,E. 1992. Pathogenesis of NIDDM. A balanced overview. *Diabetes Care* **15**:318-368.

49. Harris,M.I. 1993. Undiagnosed NIDDM: clinical and public health issues. *Diabetes Care* **16**:642-652.
50. Colagiuri,S., Cull,C.A., and Holman,R.R. 2002. Are lower fasting plasma glucose levels at diagnosis of type 2 diabetes associated with improved outcomes?: U.K. prospective diabetes study 61. *Diabetes Care* **25**:1410-1417.
51. Nathan,D.M., Buse,J.B., Davidson,M.B., Ferrannini,E., Holman,R.R., Sherwin,R., and Zinman,B. 2009. Medical management of hyperglycemia in type 2 diabetes: a consensus algorithm for the initiation and adjustment of therapy: a consensus statement of the American Diabetes Association and the European Association for the Study of Diabetes. *Diabetes Care* **32**:193-203.
52. Moss,S.E., Klein,R., and Klein,B.E. 1991. Cause-specific mortality in a population-based study of diabetes. *Am. J. Public Health* **81**:1158-1162.
53. Fox,C.S., Coady,S., Sorlie,P.D., Levy,D., Meigs,J.B., D'Agostino,R.B., Sr., Wilson,P.W., and Savage,P.J. 2004. Trends in cardiovascular complications of diabetes. *JAMA* **292**:2495-2499.
54. Prashanth,M., Ganesh,H.K., Vima,M.V., John,M., Bandgar,T., Joshi,S.R., Shah,S.R., Rathi,P.M., Joshi,A.S., Thakkar,H. et al 2009. Prevalence of nonalcoholic fatty liver disease in patients with type 2 diabetes mellitus. *J. Assoc. Physicians India* **57**:205-210.
55. Khashab,M.A., Liangpunsakul,S., and Chalasani,N. 2008. Nonalcoholic fatty liver disease as a component of the metabolic syndrome. *Curr. Gastroenterol. Rep.* **10**:73-80.
56. Clark,J.M., Brancati,F.L., and Diehl,A.M. 2003. The prevalence and etiology of elevated aminotransferase levels in the United States. *Am. J. Gastroenterol.* **98**:960-967.
57. Vuppalanchi,R., and Chalasani,N. 2009. Nonalcoholic fatty liver disease and nonalcoholic steatohepatitis: Selected practical issues in their evaluation and management. *Hepatology* **49**:306-317.
58. Torres,D.M., and Harrison,S.A. 2008. Diagnosis and therapy of nonalcoholic steatohepatitis. *Gastroenterology* **134**:1682-1698.
59. Fraser,A., Longnecker,M.P., and Lawlor,D.A. 2007. Prevalence of elevated alanine aminotransferase among US adolescents and associated factors: NHANES 1999-2004. *Gastroenterology* **133**:1814-1820.
60. Charlton,M. 2004. Nonalcoholic fatty liver disease: a review of current understanding and future impact. *Clin. Gastroenterol. Hepatol.* **2**:1048-1058.
61. Chalasani,N., Wilson,L., Kleiner,D.E., Cummings,O.W., Brunt,E.M., and Unalp,A. 2008. Relationship of steatosis grade and zonal location to histological features of steatohepatitis in adult patients with non-alcoholic fatty liver disease. *J. Hepatol.* **48**:829-834.

62. Browning, J.D., Szczepaniak, L.S., Dobbins, R., Nuremberg, P., Horton, J.D., Cohen, J.C., Grundy, S.M., and Hobbs, H.H. 2004. Prevalence of hepatic steatosis in an urban population in the United States: impact of ethnicity. *Hepatology* **40**:1387-1395.
63. Targher, G., Bertolini, L., Poli, F., Rodella, S., Scala, L., Tessari, R., Zenari, L., and Falezza, G. 2005. Nonalcoholic fatty liver disease and risk of future cardiovascular events among type 2 diabetic patients. *Diabetes* **54**:3541-3546.
64. Rafiq, N., Bai, C., Fang, Y., Srishord, M., McCullough, A., Gramlich, T., and Younossi, Z.M. 2009. Long-term follow-up of patients with nonalcoholic fatty liver. *Clin. Gastroenterol. Hepatol.* **7**:234-238.
65. Lakka, H.M., Laaksonen, D.E., Lakka, T.A., Niskanen, L.K., Kumpusalo, E., Tuomilehto, J., and Salonen, J.T. 2002. The metabolic syndrome and total and cardiovascular disease mortality in middle-aged men. *JAMA* **288**:2709-2716.
26. Isomaa, B., Almgren, P., Tuomi, T., Forsen, B., Lahti, K., Nissen, M., Taskinen, M.R., and Groop, L. 2001. Cardiovascular morbidity and mortality associated with the metabolic syndrome. *Diabetes Care* **24**:683-689.
67. Lusis, A.J. 2000. Atherosclerosis. *Nature* **407**:233-241.
68. Sturek, M., and Reddy, H.K. 2002. Editorial: New tools for prevention of restenosis could decrease the 'oculostentor' reflex. *Cardiovasc. Res.* **53**:292-293.
69. Alderman, E.L., Kip, K.E., Whitlow, P.L., Bashore, T., Fortin, D., Bourassa, M.G., Lesperance, J., Schwartz, L., and Stadius, M. 2004. Native coronary disease progression exceeds failed revascularization as cause of angina after five years in the bypass angioplasty revascularization investigation (BARI). *J. Am. Coll. Cardiol.* **44**:766-774.
70. Moses, J.W., Leon, M.B., Popma, J.J., Fitzgerald, P.J., Holmes, D.R., O'Shaughnessy, C., Caputo, R.P., Kereiakes, D.J., Williams, D.O., Teirstein, P.S. et al 2003. Sirolimus-Eluting Stents versus Standard Stents in Patients with Stenosis in a Native Coronary Artery. *N Engl J Med* **349**:1315-1323.
71. Mehran, R., Dangas, G.D., Kobayashi, Y., Lansky, A.J., Mintz, G.S., Aymong, E.D., Fahy, M., Moses, J.W., Stone, G.W., and Leon, M.B. 2004. Short- and long-term results after multivessel stenting in diabetic patients. *J. Am. Coll. Cardiol.* **43**:1348-1354.
72. Kornowski, R., Mintz, G.S., Kent, K.M., Pichard, A.D., Satler, L.F., Bucher, T.A., Hong, M.K., Popma, J.J., and Leon, M.B. 1997. Increased restenosis in diabetes mellitus after coronary interventions is due to exaggerated intimal hyperplasia. A serial intravascular ultrasound study. *Circulation* **95**:1366-1369.
73. Gilutz, H., Russo, R.J., Tsameret, I., Fitzgerald, P.J., and Yock, P.G. 2000. Comparison of coronary stent expansion by intravascular ultrasonic imaging in younger versus older patients with diabetes mellitus. *Am. J. Cardiol.* **85**:559-562.

74. Finn,A.V., Palacios,I.F., Kastrati,A., and Gold,H.K. 2005. Drug-eluting stents for diabetes mellitus: A rush to judgment? *J. Am. Coll. Cardiol.* **45**:479-483.
75. Kuntz,R.E. 1999. Importance of considering atherosclerosis progression when choosing a coronary revascularization strategy. *Circulation* **99**:847-851.
76. Loutfi,M., Mulvihill,N.T., Boccalatte,M., Farah,B., Fajadet,J., and Marco,J. 2003. Impact of restenosis and disease progression on clinical outcome after multivessel stenting in diabetic patients. *Catheterization and Cardiovascular Interventions* **58**:451-454.
77. Singh,M., Gersh,B.J., McClelland,R.L., Ho,K.K.L., Willerson,J.T., Penny,W.F., and Holmes,D.R., Jr. 2004. Clinical and Angiographic Predictors of Restenosis After Percutaneous Coronary Intervention: Insights From the Prevention of Restenosis With Tranilast and Its Outcomes (PRESTO) Trial. *Circulation* **109**:2727-2731.
78. Yoon,S.C., Laskey,W.K., Assadourian,A., Kelly,D., Gellman,J., Herzog,W., and Stafford,J.L. 2002. Assessment of contemporary stent deployment using intravascular ultrasound. *Cath. Cardiovasc. Intervent.* **57**:150-154.
79. Kip,K.E., Faxon,D.P., Detre,K.M., Yeh,W.L., Kelsey,S.F., and Currier,J.W. 1996. Coronary angioplasty in diabetic patients - The National Heart, Lung, and Blood Institute percutaneous transluminal coronary angioplasty registry. *Circulation* **94**:1818-1825.
80. Natali,A., Vichi,S., Landi,P., Severi,S., L'Abbate,A., and Ferrannini,E. 2000. Coronary atherosclerosis in Type II diabetes: angiographic findings and clinical outcome. *Diabetologia* **43**:632-641.
81. Haffner,S.M., Lehto,S., Rönnemaa,T., Pyörälä,K., and Laakso,M. 1998. Mortality from coronary heart disease in subjects with type 2 diabetes and in nondiabetic subjects with and without prior myocardial infarction. *N. Engl. J. Med.* **339**:229-234.
82. Burke,A.P., Kolodgie,F.D., Zieske,A., Fowler,D.R., Weber,D.K., Varghese,P.J., Farb,A., and Virmani,R. 2004. Morphologic Findings of Coronary Atherosclerotic Plaques in Diabetics: A Postmortem Study. *Arterioscler. Thromb. Vasc. Biol.* **24**:1266-1271.
83. Schofer,J., Schlüter,M., Rau,T., Hammer,F., Haag,N., and Mathey,D.G. 2000. Influence of treatment modality on angiographic outcome after coronary stenting in diabetic patients: A controlled study. *J. Am. Coll. Cardiol.* **35**:1554-1559.
84. Ortolani,P., Ardissino,D., Cavallini,C., Bramucci,E., Indolfi,C., Aquilina,M., and Marzocchi,A. 2005. Effect of Sirolimus-Eluting Stent in Diabetic Patients With Small Coronary Arteries (A SES-SMART Substudy). *The American Journal of Cardiology* **96**:1393-1398.

85. Rosano,G.M.C., Vitale,C., and Fragasso,G. 2006. Metabolic Therapy for Patients with Diabetes Mellitus and Coronary Artery Disease. *The American Journal of Cardiology* **98**:14-18.
86. Morgan,K.P., Kapur,A., and Beatt,K.J. 2004. Anatomy of coronary disease in diabetic patients: an explanation for poorer outcomes after percutaneous coronary intervention and potential target for intervention. *Heart* **90**:732-738.
87. Grané, r,M., nne,M., Kahri,J., Nieminen,M.S., and Taskinen,M.R. 2007. Insulin resistance as predictor of the angiographic severity and extent of coronary artery disease. *Annals of Medicine* **39**:137-144.
88. Ross,R. 1993. The pathogenesis of atherosclerosis: a perspective for the 1990s. *Nature* **362**:801-809.
89. Stary,H.C. 1989. Evolution and progression of atherosclerotic lesions in coronary arteries of children and young adults. *Arteriosclerosis* **9 Suppl.**:I19-I32.
90. Stary,H.C. 1994. Changes in components and structure of atherosclerotic lesions developing from childhood to middle age in coronary arteries. *Basic Res. Cardiol.* **89 Suppl 1**:17-32.
91. Stone,G.W., Ellis,S.G., Colombo,A., Dawkins,K.D., Grube,E., Cutlip,D.E., Friedman,M., Baim,D.S., and Koglin,J. 2007. Offsetting impact of thrombosis and restenosis on the occurrence of death and myocardial infarction after paclitaxel-eluting and bare metal stent implantation. *Circulation* **115**:2842-2847.
92. Pfisterer,M., Brunner-La Rocca,H.P., Buser,P.T., Rickenbacher,P., Hunziker,P., Mueller,C., Jeger,R., Bader,F., Osswald,S., and Kaiser,C. 2006. Late Clinical Events After Clopidogrel Discontinuation May Limit the Benefit of Drug-Eluting Stents: An Observational Study of Drug-Eluting Versus Bare-Metal Stents. *J. Am. Coll. Cardiol.* **48**:2584-2591.
93. Aoki,J., Ong,A., Arampatzis,C.A., Vijaykumar,M., Granillo,G.A., Disco,C.M.C., and Serruys,P. 2004. Comparison of three-year outcomes after coronary stenting versus coronary artery bypass grafting in patients with multivessel coronary disease, including involvement of the left anterior descending coronary artery proximally. *The American Journal of Cardiology* **94**:627-631 (Abstr.)
94. Abizaid,A., Kornowski,R., Mintz,G.S., Hong,M.K., Abizaid,A.S., Mehran,R., Pichard,A.D., Kent,K.M., Satler,L.F., Wu,H.S. et al 1998. The influence of diabetes mellitus on acute and late clinical outcomes following coronary stent implantation. *J. Am. Coll. Cardiol.* **32**:584-589.
95. Nicholls,S.J., Tuzcu,E.M., Kalidindi,S., Wolski,K., Moon,K.W., Sipahi,I., Schoenhagen,P., and Nissen,S.E. 2008. Effect of Diabetes on Progression of Coronary Atherosclerosis and Arterial Remodeling: A Pooled Analysis of 5 Intravascular Ultrasound Trials. *J. Am. Coll. Cardiol.* **52**:255-262.

96. Isermann,B., Vinnikov,I.A., Madhusudhan,T., Herzog,S., Kashif,M., Blautzik,J., Corat,M.A.F., Zeier,M., Blessing,E., Oh,J. et al 2007. Activated protein C protects against diabetic nephropathy by inhibiting endothelial and podocyte apoptosis. *Nat Med* **13**:1349-1358.
97. Granada,J.F., Kaluza,G.L., Wilensky,R.L., Biedermann,B.C., Schwartz,R.S., and Falk,E. 2009. Porcine models of coronary atherosclerosis and vulnerable plaque for imaging and interventional research. *EuroIntervention* **5**:140-148.
98. Finn,A.V., Nakazawa,G., Joner,M., Kolodgie,F.D., Mont,E.K., Gold,H.K., and Virmani,R. 2007. Vascular Responses to Drug Eluting Stents: Importance of Delayed Healing. *Arterioscler. Thromb. Vasc. Biol.* **27**:1500-1510.
99. Nakazawa,G., Finn,A.V., Ladich,E., Ribichini,F., Coleman,L., Kolodgie,F.D., and Virmani,R. 2008. Drug-eluting stent safety: findings from preclinical studies. *Expert Review of Cardiovascular Therapy* **6**:1379-1391.
100. Schwartz,R.S., and Edelman,E.R. 2002. Drug-eluting stents in preclinical studies. Recommended evaluation from a consensus group. *Circulation* **106**:1867-1873.
101. Holmes Jr,D.R., Kereiakes,D.J., Laskey,W.K., Colombo,A., Ellis,S.G., Henry,T.D., Popma,J.J., Serruys,P.W.J.C., Kimura,T., Williams,D.O. et al 2007. Thrombosis and Drug-Eluting Stents: An Objective Appraisal. *J. Am. Coll. Cardiol.* **50**:109-118.
102. Crick,S.J., Sheppard,M.N., Ho,S.Y., Gebstein,L., and Anderson,R.H. 1998. Anatomy of the pig heart: comparisons with normal human cardiac structure. *J. Anat.* **193 (Pt 1)**:105-119.
103. Touchard,A.G., and Schwartz,R.S. 2006. Preclinical restenosis models: challenges and successes. *Toxicol. Pathol.* **34**:11-18.
104. Gerrity,R.G., Natarajan,R., Nadler,J.L., and Kimsey,T. 2001. Diabetes-induced accelerated atherosclerosis in swine. *Diabetes* **50**:1654-1665.
105. Artinger,S., Deiner,C., Loddenkemper,C., Schwimmbeck,P.L., Schultheiss,H.P., and Pels,K. 2009. Complex porcine model of atherosclerosis: induction of early coronary lesions after long-term hyperlipidemia without sustained hyperglycemia. *Can. J. Cardiol.* **25**:e109-e114.
106. Chatzizisis,Y.S., Jonas,M., Coskun,A.U., Beigel,R., Stone,B.V., Maynard,C., Gerrity,R.G., Daley,W., Rogers,C., Edelman,E.R. et al 2008. Prediction of the Localization of High-Risk Coronary Atherosclerotic Plaques on the Basis of Low Endothelial Shear Stress: An Intravascular Ultrasound and Histopathology Natural History Study. *Circulation* **117**:993-1002.
107. Mohler,E.R., III, Sarov-Blat,L., Shi,Y., Hamamdzcic,D., Zalewski,A., MacPhee,C., Llano,R., Pelchovitz,D., Mainigi,S.K., Osman,H. et al 2008. Site-Specific Atherogenic Gene Expression Correlates With Subsequent Variable Lesion Development in Coronary and Peripheral Vasculature. *Arterioscler. Thromb. Vasc. Biol.* **28**:850-855.

108. Tharp,D.L., Wamhoff,B.R., Wulff,H., Raman,G., Cheong,A., and Bowles,D.K. 2008. Local Delivery of the KCa3.1 Blocker, TRAM-34, Prevents Acute Angioplasty-Induced Coronary Smooth Muscle Phenotypic Modulation and Limits Stenosis. *Arterioscler. Thromb. Vasc. Biol.* **28**:1084-1089.
109. Hansen,A., Hehrlein,C., Hardt,S., Bekeredjian,R., Brachmann,J., Kubler,W., Bode,C., and Kuecherer,H.F. 2001. Is the "candy-wrapper" effect of (32)P radioactive beta-emitting stents due to remodeling or neointimal hyperplasia? Insights from intravascular ultrasound. *Catheter. Cardiovasc. Interv.* **54**:41-48.
110. Larsen,M.O., Juhl,C.B., Porksen,N., Gotfredsen,C.F., Carr,R.D., Ribel,U., Wilken,M., and Rolin,B. 2005. Beta-cell function and islet morphology in normal, obese, and obese beta-cell mass-reduced Gottingen minipigs. *Am J Physiol Endocrinol Metab* **288**:E412-E421.
111. Phillips,R.W., Panepinto,L.M., Spangler,R., and Westmoreland,N. 1982. Yucatan miniature swine as a model for the study of human diabetes-mellitus. *Diabetes* **31**:30-36.
112. Christoffersen,B.O., Grand,N., Golozoubova,V., Svendsen,O., and Raun,K. 2007. Gender-associated Differences in Metabolic Syndrome-related Parameters in Gottingen Minipigs. *Comp. Med.* **57**:493-504.
113. Masuzaki,H., Paterson,J., Shinyama,H., Morton,N.M., Mullins,J.J., Seckl,J.R., and Flier,J.S. 2001. A transgenic model of visceral obesity and the metabolic syndrome. *Science* **294**:2166-2170.
114. Peterson,R.G. 2001. The Zucker diabetic fatty (ZDF) rat. In *Animal Models of Diabetes: A Primer*. A.A.F.Sima, and Shafir,E., editors. Harwood Academic Publishers. Amsterdam. 109-128.
115. Bellinger,D.A., Merricks,E.P., and Nichols,T.C. 2006. Swine models of type 2 diabetes mellitus: insulin resistance, glucose tolerance, and cardiovascular complications. *ILAR J.* **47**:243-258.
116. Hsueh,W., Abel,E.D., Breslow,J.L., Maeda,N., Davis,R.C., Fisher,E.A., Dansky,H., McClain,D.A., McIndoe,R., Wassef,M.K. et al 2007. Recipes for Creating Animal Models of Diabetic Cardiovascular Disease. *Circ. Res.* **100**:1415-1427.
117. Clapham,D.E. 2007. Calcium signaling. *Cell* **131**:1047-1058.
118. Owens,G.K., Kumar,M.S., and Wamhoff,B.R. 2004. Molecular regulation of vascular smooth muscle cell differentiation in development and disease. *Physiol. Rev.* **84**:767-801.
119. House,S.J., Potier,M., Bisailon,J., Singer,H.A., and Trebak,M. 2008. The non-excitable smooth muscle: calcium signaling and phenotypic switching during vascular disease. *Pflugers Arch.* **456**:769-785.

120. Wamhoff,B.R., Bowles,D.K., and Owens,G.K. 2006. Excitation-Transcription Coupling in Arterial Smooth Muscle. *Circ. Res.* **98**:868-878.
121. Kim,H.R., Appel,S., Vetterkind,S., Gangopadhyay,S.S., and Morgan,K.G. 2008. Smooth muscle signalling pathways in health and disease. *J. Cell Mol. Med.* **12**:2165-2180.
122. Haller,H., Lindschau,C., Quass,P., Distler,A., and Luft,F.C. 1994. Nuclear calcium signaling is initiated by cytosolic calcium surges in vascular smooth muscle cells. *Kidney International* **46**:1653-1662.
123. Babcock,D.F., Herrington,J., Goodwin,P.C., Park,Y.B., and Hille,B. 1997. Mitochondrial participation in the intracellular Ca²⁺ network. *J. Cell Biol.* **136**:833-844.
124. Cheung,W.Y. 1980. Calmodulin plays a pivotal role in cellular regulation. *Science* **207**:19-27.
125. O'Donnel,M.E., and Owen,N.E. 1994. Regulation of ion pumps and carriers in vascular smooth muscle. *Physiol. Rev.* **74**:683-721.
126. Rasmussen,H., and Barrett,P.Q. 1984. Calcium messenger system: an integrated view. *Physiol. Rev.* **64**:938-984.
127. Wu,K.-D. 2000. Regulation of SERCA Ca²⁺ pump expression by cytoplasmic [Ca²⁺] in vascular smooth muscle cells. *Am. J. Physiol.* **280**:C843-C851.
128. Milner,R.E., Baksh,S., Shemanko,C., Carpenter,M.R., Smillie,L., Vance,J.E., Opas,M., and Michalak,M. 1991. Calreticulin, and not calsequestrin, is the major calcium binding protein of smooth muscle sarcoplasmic reticulum and liver endoplasmic reticulum. *J. Biol. Chem.* **266**:7155-7165.
129. Somlyo,A.P., and Somlyo,A.V. 1994. Signal transduction and regulation in smooth muscle. *Nature* **372**:231-236.
130. Endo,M. 1977. Calcium release from the sarcoplasmic reticulum. *Physiol. Rev.* **57**:71-108.
131. Lynn,S., and Gillespie,J.I. 1995. Basic properties of a novel ryanodine-sensitive, caffeine- insensitive calcium-induced calcium release mechanism in permeabilised human vascular smooth muscle cells. *FEBS Lett.* **367**:23-27.
132. Morel,J.L., Macrez-Leprêtre,N., and Mironneau,J. 1996. Angiotensin II-activated Ca²⁺ entry-induced release of Ca²⁺ from intracellular stores in rat portal vein myocytes. *Br. J. Pharmacol.* **118**:73-78.
133. Nelson,M.T., and Quayle,J.M. 1995. Physiological roles and properties of potassium channels in arterial smooth muscle. *Am. J. Physiol. Cell Physiol.* **268**:C799-C822.

134. Szewczyk,M.M., Davis,K.A., Samson,S.E., Simpson,F., Rangachari,P.K., and Grover,A.K. 2007. Ca²⁺-pumps and Na²⁺-Ca²⁺-exchangers in coronary artery endothelium versus smooth muscle. *J. Cell Mol. Med.* **11**:129-138.
135. Baek,E., Yoo,H., Park,S., Kim,H., Kim,S., Earm,Y., and Kim,S. 2008. Luminal ATP-induced contraction of rabbit pulmonary arteries and role of purinoceptors in the regulation of pulmonary arterial pressure. *Pflugers Archiv European Journal of Physiology* **457**:281-291.
136. Ganitkevich,V.Y., and Isenberg,G. 1990. Contribution of two types of calcium channels to membrane conductance of single myocytes from guinea-pig coronary artery. *J. Physiol. (Lond.)* **426**:19-42.
137. Hermsmeyer,K., Sturek,M., Marvin,W., Mason,R., and Puga,A. 1989. Vascular muscle calcium channel modulation in hypertension. *J. Cardiovasc. Pharmacol.* **14 Suppl. 6**:S45-S48.
138. Sturek,M., and Hermsmeyer,K. 1986. Calcium and sodium channels in spontaneously contracting vascular muscle cells. *Science* **233**:475-478.
139. Cribbs,L.L. 2001. Vascular smooth muscle calcium channels - Could "T" be a target? *Circ. Res.* **89**:560-562.
140. Borbouse,L., Dick,G.M., Asano,S., Bender,S.B., Dincer,U.D., Payne,G.A., Neeb,Z.P., Bratz,I.N., Sturek,M., and Tune,J.D. 2009. Impaired Function of Coronary BKCa Channels in Metabolic Syndrome. *Am. J. Physiol Heart Circ. Physiol.*
141. Moosmang,S., Haider,N., Bruderl,B., Welling,A., and Hofmann,F. 2006. Antihypertensive effects of the putative T-type calcium channel antagonist mibefradil are mediated by the L-type calcium channel Cav1.2. *Circ. Res.* **98**:105-110.
142. Moosmang,S., Schulla,V., Welling,A., Feil,R., Feil,S., Wegener,J.W., Hofmann,F., and Klugbauer,N. 2003. Dominant role of smooth muscle L-type calcium channel Cav1.2 for blood pressure regulation. *EMBO J.* **22**:6027-6034.
143. Barritt,G.J. 1999. Receptor-activated Ca²⁺ inflow in animal cells: a variety of pathways tailored to meet different intracellular Ca²⁺ signalling requirements. *Biochemical Journal* **337**:153-169.
144. Restrepo,D., Teeter,J.H., and Schild,D. 1996. Second messenger signaling in olfactory transduction. *J. Neurobiol.* **30**:37-48.
145. Finn,J.T., Grunwald,M.E., and Yau,K.W. 1996. Cyclic nucleotide-gated ion channels: An extended family with diverse functions. *Annu. Rev. Physiol.* **58**:395-426.
146. Lenz,T., and Kleineke,J.W. 1997. Hormone-induced rise in cytosolic Ca²⁺ in axolotl hepatocytes: properties of the Ca²⁺ influx channel. *Am. J. Physiol* **273**:C1526-C1532.

147. Guibert,C., Ducret,T., and Savineau,J.P. 2008. Voltage-independent calcium influx in smooth muscle. *Prog. Biophys. Mol. Biol.* **98**:10-23.
148. Lewis,R.S. 1999. Store-operated calcium channels. *Adv. Second Messenger Phosphoprotein Res.* **33**:279-307.
149. Saleh,S.N., Albert,A.P., Peppiatt,C.M., and Large,W.A. 2006. Angiotensin II activates two cation conductances with distinct TRPC1 and TRPC6 channel properties in rabbit mesenteric artery myocytes. *J. Physiol. (Lond.)* **577**:479-495.
150. Albert,A.P., Pucovsky,V., Prestwich,S.A., and Large,W.A. 2006. TRPC3 properties of a native constitutively active Ca²⁺-permeable cation channel in rabbit ear artery myocytes. *J. Physiol* **571**:361-369.
151. Mercer,J.C., Dehaven,W.I., Smyth,J.T., Wedel,B., Boyles,R.R., Bird,G.S., and Putney,J.W., Jr. 2006. Large store-operated calcium selective currents due to co-expression of Orai1 or Orai2 with the intracellular calcium sensor, Stim1. *J. Biol. Chem.* **281**:24979-24990.
152. Clapham,D.E. 2003. TRP channels as cellular sensors. *Nature* **426**:517-524.
153. Salido,G.M., Sage,S.O., and Rosado,J.A. 2009. Biochemical and functional properties of the store-operated Ca²⁺ channels. *Cell Signal.* **21**:457-461.
154. Cheng,K.T., Liu,X., Ong,H.L., and Ambudkar,I.S. 2008. Functional Requirement for Orai1 in Store-operated TRPC1-STIM1 Channels. *Journal of Biological Chemistry* **283**:12935-12940.
155. Alicia,S., Angelica,Z., Carlos,S., Alfonso,S., and Vaca,L. 2008. STIM1 converts TRPC1 from a receptor-operated to a store-operated channel: moving TRPC1 in and out of lipid rafts. *Cell Calcium* **44**:479-491.
156. Liao,Y., Erxleben,C., Yildirim,E., Abramowitz,J., Armstrong,D.L., and Birnbaumer,L. 2007. Orai proteins interact with TRPC channels and confer responsiveness to store depletion. *Proc. Natl. Acad. Sci. U. S. A* **104**:4682-4687.
157. Beech,D.J. 2005. TRPC1: store-operated channel and more. *Pflugers Arch.* **451**:53-60.
158. Camici,P.G., and Crea,F. 2007. Coronary Microvascular Dysfunction. *N Engl J Med* **356**:830-840.
159. Grundy,S.M., Brewer,H.B., Cleeman,J.I., Smith,S.C., Jr., and Lenfant,C. 2004. Definition of the metabolic syndrome. *Circulation* **109**:433-438.
160. Eckel,R.H., Kahn,R., Robertson,R.M., and Rizza,R.A. 2006. Preventing cardiovascular disease and diabetes: a call to action from the American Diabetes Association and the American Heart Association. *Circulation* **113**:2943-2946.

161. Tommasino,A., Burzotta,F., Trani,C., Giammarinaro,M., and Schiavoni,G. 2008. Impact of Metabolic Syndrome on Angiographic and Clinical Outcome After Stenting. *The American Journal of Cardiology* **101**:1679.
162. Pons,D., Monraats,P.S., Zwinderman,A.H., de Maat,M.P.M., Doevendans,P.A.F.M., de Winter,R.J., Tio,R.A., Waltenberger,J., and Jukema,J.W. 2009. Metabolic background determines the importance of NOS3 polymorphisms in restenosis after percutaneous coronary intervention: A study in patients with and without the metabolic syndrome. *Disease Markers* **26**:75-83.
163. Takagi,T., Yoshida,K., Akasaka,T., Kaji,S., Kawamoto,T., Honda,Y., Yamamuro,A., Hozumi,T., and Morioka,S. 2000. Hyperinsulinemia during oral glucose tolerance test is associated with increased neointimal tissue proliferation after coronary stent implantation in nondiabetic patients: A serial intravascular ultrasound study. *J. Am. Coll. Cardiol.* **36**:731-738.
164. Piatti,P., Di Mario,C., Monti,L.D., Fragasso,G., Sgura,F., Caumo,A., Setola,E., Lucotti,P., Galluccio,E., Ronchi,C. et al 2003. Association of Insulin Resistance, Hyperleptinemia, and Impaired Nitric Oxide Release With In-Stent Restenosis in Patients Undergoing Coronary Stenting. *Circulation* **108**:2074-2081.
165. Gal,D., and Isner,J.M. 1992. Atherosclerotic Yucatan microswine as a model for novel cardiovascular interventions and imaging. In *Swine as Models in Biomedical Research*. M.M.Swindle, Moody,D.C., and Phillips,L.D., editors. Iowa State University Press. Ames. 118-140.
166. Johnson,G.J., Griggs,T.R., and Badimon,L. 1999. The utility of animal models in the preclinical study of interventions to prevent human coronary artery restenosis: Analysis and recommendations. *Thromb. Haemost.* **81**:835-843.
167. Lowe,H.C., Schwartz,R.S., Mac Neill,B.D., Jang,I.K., Hayase,M., Rogers,C., and Oesterle,S.N. 2003. The porcine coronary model of in-stent restenosis: current status in the era of drug-eluting stents. *Catheterization and Cardiovascular Interventions* **60**:515-523.
168. Martin,R.J., Gobble,J.L., Hartsock,T.H., Graves,H.B., and Ziegler,J.H. 1973. Characterization of an obese syndrome in the pig. *Proc. Soc. Exp. Biol. Med.* **143**:198-203.
169. Hill,B.J.F., Katwa,L.C., Wamhoff,B.R., and Sturek,M. 2000. Enhanced endothelin_A receptor-mediated calcium mobilization and contraction in organ cultured porcine coronary arteries. *J. Pharmacol. Exp. Ther.* **295**:484-491.
170. Hill,B.J.F., Wamhoff,B.R., and Sturek,M. 2001. Functional nucleotide receptor expression and sarcoplasmic reticulum morphology in dedifferentiated porcine coronary smooth muscle cells. *J. Vasc. Res.* **38**:432-443.
171. Wamhoff,B.R., Bowles,D.K., Dietz,N.J., Hu,Q., and Sturek,M. 2002. Exercise training attenuates coronary smooth muscle phenotypic modulation and nuclear Ca²⁺ signaling. *Am. J. Physiol. Heart Circ. Physiol.* **283**:H2397-H2410.

172. Wamhoff,B.R., Bowles,D.K., McDonald,O.G., Sinha,S., Somlyo,A.P., and Owens,G.K. 2004. L-type voltage-gated Ca²⁺ channels modulate expression of smooth muscle differentiation marker genes via a Rho kinase/myocardin/SRF-dependent mechanism. *Circ. Res.* **95**:406-414.
173. Levy,J., Gavin,J.R., and Sowers,J.R. 1994. Diabetes mellitus: A disease of abnormal cellular calcium metabolism? *Am. J. Med.* **96**:260-273.
174. Hill,B.J.F., Dixon,J.L., and Sturek,M. 2001. Effect of atorvastatin on intracellular calcium uptake in coronary smooth muscle cells from diabetic pigs fed an atherogenic diet. *Atherosclerosis* **159**:117-124.
175. Beaver,B.V., Reed,W., Leary,S., McKiernan,B., Bain,F., Schultz,R., Bennett,B.T., Pascoe,P., Shull,E., Cork,L.C. et al 2001. 2000 Report of the AVMA panel on euthanasia. *JAMA* **218**:669-696.
176. National Research Council 1996. *Guide for the care and use of laboratory animals*. National Academy Press. Washington, D.C.
177. Graier,W.F., Paltauf-Doburzynska,B.J.F., Hill,E., Fleischhacker,E., Hoebel,B.G., Kostner,G.M., and Sturek,M. 1998. Submaximal stimulation of porcine endothelial cells causes focal Ca²⁺ elevation beneath the cell membrane. *J. Physiol. (Lond.)* **506**:109-125.
178. Greif,M., Becker,A., von Ziegler,F., Lebherz,C., Lehrke,M., Broedl,U.C., Tittus,J., Parhofer,K., Becker,C., Reiser,M. et al 2009. Pericardial Adipose Tissue Determined by Dual Source CT Is a Risk Factor for Coronary Atherosclerosis. *Arterioscler. Thromb. Vasc. Biol.* **29**:781-786.
179. Carroll,J.A., Daniel,J.A., Keisler,D.H., and Matteri,R.L. 1999. Non-surgical catheterization of jugular vein in young pigs. *Lab Animal* **33**:129-133.
180. Warnick,G., Benderson,J., and Albers,J.J. 1982. Dextran sulfate-Mg²⁺ precipitation procedure for quantitation of HDL cholesterol. *Clin. Chem.* **28**:1379-1388.
181. Wallace,T.M., Levy,J.C., and Matthews,D.R. 2004. Use and abuse of HOMA modeling. *Diabetes Care* **27**:1487-1495.
182. Mattern,H.M., Lloyd,P.G., Sturek,M., and Hardin,C.D. 2007. Gender and genetic differences in bladder smooth muscle PPAR mRNA in a porcine model of the metabolic syndrome. *Mol. Cell. Biochem.* **302**:43-49.
183. Sipido,K.R., Tedgui,A., Kristensen,S.D., Pasterkamp,G., Schunkert,H., Wehling,M., Steg,P.G., Eisert,W., Rademakers,F., Casadei,B. et al 2009. Identifying needs and opportunities for advancing translational research in cardiovascular disease. *Cardiov. Res.* **83**:425-435.

184. Young,J.J., Phillips,H.R., Marso,S.P., Granada,J.F., McPherson,J.A., Waksman,R., Steinhubl,S.R., Schwartz,R.S., and Stone,G.W. 2008. Vulnerable plaque intervention: State of the art. *Catheterization and Cardiovascular Interventions* **71**:367-374.
185. Lovejoy,J.C., Windhauser,M.M., Rood,J.C., and de la Bretonne,J.A. 1998. Effect of a controlled high-fat versus low-fat diet on insulin sensitivity and leptin levels in African-American and Caucasian women. *Metabolism* **47**:1520-1524.
186. Friedman,J.M. 2002. The function of leptin in nutrition, weight, and physiology. *Nutr. Rev.* **60**:S1-S14.
187. Panepinto,L.M., Phillips,R.W., Westmoreland,N.W., and Cleek,J.L. 1982. Influence of genetics and diet on the development of diabetes in Yucatan miniature swine. *J. Nutr.* **112**:2307-2313.
188. Phillips,R.W., Westmoreland,N., Panepinto,L., and Case,G.L. 1982. Dietary effects on metabolism of Yucatan miniature swine selected for low and high glucose utilization. *J. Nutr.* **112**:104-111.
189. Larsen,M.O., Rolin,B., Raun,K., Bjerre Knudsen,L., Gotfredsen,C.F., and Bock,T. 2007. Evaluation of beta-cell mass and function in the Gottingen minipig. *Diabetes, Obesity and Metabolism* **9, Suppl. 2**:170-179.
190. Larsen,M.O., Rolin,B., Sturis,J., Wilken,M., Carr,R.D., Porksen,N., and Gotfredsen,C.F. 2006. Measurements of insulin responses as predictive markers of pancreatic beta-cell mass in normal and beta-cell-reduced lean and obese Gottingen minipigs *in vivo*. *Am J Physiol Endocrinol Metab* **290**:E670-E677.
191. Larsen,M.O., Rolin,B., Wilken,M., Carr,R.D., and Svendsen,O. 2002. High-fat high-energy feeding impairs fasting glucose and increases fasting insulin levels in the Gottingen minipig: results from a pilot study. *Ann N Y Acad Sci.* **967**:414-423.
192. Hall,J.E. 2003. The kidney, hypertension, and obesity. *Hypertension* **41**:625-633.
193. Alloosh,M., Pratt,J.H., Sturek,M., and Basile,D.P. 2008. Elevated renin and enhanced adrenal steroidogenesis in the Ossabaw miniature swine model of the metabolic syndrome (abstract). *FASEB J.* **22**:736.7.
194. Rana,J.S., Monraats,P.S., Zwinderman,A.H., de Maat,M.P.M., Kastelein,J.J.P., Doevendans,P.A.F., de Winter,R.J., Tio,R.A., Frants,R.R., van der Laarse,A. et al 2005. Metabolic Syndrome and Risk of Restenosis in Patients Undergoing Percutaneous Coronary Intervention. *Diabetes Care* **28**:873-877.
195. Massoud,T.F., Vinters,V.H., Chao,K.H., Vinuela,F., and Jahan,R. 2000. Histopathologic characteristics of a chronic arteriovenous malformation in a swine model: preliminary study. *AJNR. Am. J. Neuroradiol.* **21**:1268-1276.

196. Kumar,B., Dreja,K., Shah,S.S., Cheong,A., Xu,S.Z., Sukumar,P., Naylor,J., Forte,A., Cipollaro,M., McHugh,D. et al 2006. Upregulated TRPC1 channel in vascular injury *in vivo* and its role in human neointimal hyperplasia. *Circ. Res.* **98**:557-563.
197. Stehno-Bittel,L., Laughlin,M.H., and Sturek,M. 1990. Exercise training alters Ca release from coronary smooth muscle sarcoplasmic reticulum. *Am. J. Physiol. Heart Circ. Physiol.* **259**:H643-H647.
198. Stehno-Bittel,L., Laughlin,M.H., and Sturek,M. 1991. Exercise training depletes sarcoplasmic reticulum calcium in coronary smooth muscle. *J. Appl. Physiol.* **71**:1764-1773.
199. Graier,W.F., Simecek,S., and Sturek,M. 1995. Cytochrome P450 mono-oxygenase-regulated signalling of Ca²⁺ entry in human and bovine endothelial cells. *J. Physiol. (Lond.)* **482**:259-274.
200. Daemen,J., Wenaweser,P., Tsuchida,K., Abrecht,L., Vaina,S., Morger,C., Kukreja,N., Juni,P., Sianos,G., Hellige,G. et al 2007. Early and late coronary stent thrombosis of sirolimus-eluting and paclitaxel-eluting stents in routine clinical practice: data from a large two-institutional cohort study. *Lancet* **369**:667-678.
201. Moreno,P.R., Fallon,J.T., Murcia,A.M., Leon,M.N., Simosa,H., Fuster,V., and Palacios,I.F. 1999. Tissue characteristics of restenosis after percutaneous transluminal coronary angioplasty in diabetic patients. *J. Am. Coll. Cardiol.* **34**:1045-1049.
202. Kimura,B.J., Bhargava,V., and DeMaria,A.N. 1995. Value and limitations of intravascular ultrasound imaging in characterizing coronary atherosclerotic plaque. *Am. Heart J.* **130**:386-396.
203. McDonald,T.O., Gerrity,R.G., Jen,C., Chen,H.J., Wark,K., Wight,T.N., Chait,A., and O'Brien,K.D. 2007. Diabetes and Arterial Extracellular Matrix Changes in a Porcine Model of Atherosclerosis. *J. Histochem. Cytochem.* **55**:1149-1157.
204. Granger,C.B., Califf,R.M., Young,S., Candela,R., Samaha,J., Worley,S., Kereiakes,D.J., and Topol,E.J. 1993. Outcome of patients with diabetes mellitus and acute myocardial infarction treated with thrombolytic agents. The Thrombolysis and Angioplasty in Myocardial Infarction (TAMI) Study Group. *J. Am. Coll. Cardiol.* **21**:920-925.
205. Scognamiglio,R., Negut,C., Ramondo,A., Tiengo,A., and Avogaro,A. 2006. Detection of coronary artery disease in asymptomatic patients with type 2 diabetes mellitus. *J. Am. Coll. Cardiol.* **47**:65-71.
206. Hermans,M.P., Levy,J.C., Morris,R.J., and Turner,R.C. 1999. Comparison of insulin sensitivity tests across a range of glucose tolerance from normal to diabetes. *Diabetologia* **42**:678-687.

207. Bonora,E., Formentini,G., Calcaterra,F., Lombardi,S., Marini,F., Zenari,L., Saggiani,F., Poli,M., Perbellini,S., Raffaelli,A. et al 2002. HOMA-Estimated Insulin Resistance Is an Independent Predictor of Cardiovascular Disease in Type 2 Diabetic Subjects: Prospective data from the Verona Diabetes Complications Study. *Diabetes Care* **25**:1135-1141.
208. Mather,K.J., Hunt,A.E., Steinburg,H.O., Paradisi,G., Hook,G., Katz,A., Quon,M.J., and Baron,A.D. 2001. Repeatability characteristics of simple indices of insulin resistance: implications for research applications. *J. Clin. Endocrinol. Metab.* **86**:5457-5464.
209. Kahn,S.E., Hull,R.L., and Utzschneider,K.M. 2006. Mechanisms linking obesity to insulin resistance and type 2 diabetes. *Nature* **444**:840-846.
210. Steiner,G. 1995. Dyslipoproteinemias in diabetes. *Clin. Invest. Med.* **18**:282-287.
211. Byrne,C.D., Maison,P., Halsall,D., Martensz,N., Hales,C.N., and Wareham,N.J. 1999. Cross-sectional but not longitudinal associations between non-esterified fatty acid levels and glucose intolerance and other features of the metabolic syndrome. *Diabet. Med.* **16**:1007-1015.
212. Yamagishi,K., Nettleton,J.A., and Folsom,A.R. 2008. Plasma fatty acid composition and incident heart failure in middle-aged adults: the Atherosclerosis Risk in Communities (ARIC) Study. *Am. Heart J.* **156**:965-974.
213. Donnelly,K.L., Smith,C.I., Schwarzenberg,S.J., Jessurun,J., Boldt,M.D., and Parks,E.J. 2005. Sources of fatty acids stored in liver and secreted via lipoproteins in patients with nonalcoholic fatty liver disease. *J. Clin. Invest* **115**:1343-1351.
214. Diraison,F., Moulin,P., and Beylot,M. 2003. Contribution of hepatic de novo lipogenesis and reesterification of plasma non esterified fatty acids to plasma triglyceride synthesis during non-alcoholic fatty liver disease. *Diabetes Metab* **29**:478-485.
215. Murakami,K., Sasaki,S., Takahashi,Y., Uenishi,K., Watanabe,T., Kohri,T., Yamasaki,M., Watanabe,R., Baba,K., Shibata,K. et al 2008. Lower estimates of delta-5 desaturase and elongase activity are related to adverse profiles for several metabolic risk factors in young Japanese women. *Nutr. Res.* **28**:816-824.
216. Pan,D.A., Lillioja,S., Milner,M.R., Kriketos,A.D., Baur,L.A., Bogardus,C., and Storlien,L.H. 1995. Skeletal muscle membrane lipid composition is related to adiposity and insulin action. *J. Clin. Invest* **96**:2802-2808.
217. Kotronen,A., Seppanen-Laakso,T., Westerbacka,J., Kiviluoto,T., Arola,J., Ruskeepaa,A.L., Oresic,M., and Yki-Jarvinen,H. 2009. Hepatic stearoyl-CoA desaturase (SCD)-1 activity and diacylglycerol but not ceramide concentrations are increased in the nonalcoholic human fatty liver. *Diabetes* **58**:203-208.
218. Chevalier,M.M., Wiley,J.H., and Leveille,G.A. 1972. Effect of dietary fructose on fatty acid synthesis in adipose tissue and liver of the rat. *J. Nutr.* **102**:337-342.

219. Shillabeer,G., Hornford,J., Forden,J.M., Wong,N.C., Russell,J.C., and Lau,D.C. 1992. Fatty acid synthase and adipsin mRNA levels in obese and lean JCR:LA-cp rats: effect of diet. *J. Lipid Res.* **33**:31-39.
220. Brown,M.S., and Goldstein,J.L. 2006. Biomedicine. Lowering LDL--not only how low, but how long? *Science* **311**:1721-1723.
221. Kearney,P.M., Blackwell,L., Collins,R., Keech,A., Simes,J., Peto,R., Armitage,J., and Baigent,C. 2008. Efficacy of cholesterol-lowering therapy in 18,686 people with diabetes in 14 randomised trials of statins: a meta-analysis. *Lancet* **371**:117-125.
222. Horton,J.D., Cohen,J.C., and Hobbs,H.H. 2009. PCSK9: a convertase that coordinates LDL catabolism. *J. Lipid Res.* **50 Suppl**:S172-S177.
223. Leffondre,K., Abrahamowicz,M., Siemiatycki,J., and Rachet,B. 2002. Modeling smoking history: a comparison of different approaches. *Am. J. Epidemiol.* **156**:813-823.
224. Ford,E.S. 2005. Risks for all-cause mortality, cardiovascular disease, and diabetes associated with the metabolic syndrome: a summary of the evidence. *Diabetes Care* **28**:1769-1778.
225. Angiolillo,D.J., Sabata,M., Alfonso,F., and Macaya,C. 2004. "Candy wrapper" effect after drug-eluting stent implantation: deja vu or stumbling over the same stone again? *Catheter. Cardiovasc. Interv.* **61**:387-391.
226. Belardinelli,R., Paolini,I., Cianci,G., Piva,R., Georgiou,D., and Purcaro,A. 2001. Exercise training intervention after coronary angioplasty: the ETICA trial. *J. Am. Coll. Cardiol.* **37**:1891-1900.
227. Farb,A., Sangiorgi,G., Carter,A.J., Walley,V.M., Edwards,W.D., Schwartz,R.S., and Virmani,R. 1999. Pathology of acute and chronic coronary stenting in humans. *Circulation* **99**:44-52.
228. Takahashi,Y., Watanabe,H., Murakami,M., Ohba,T., Radovanovic,M., Ono,K., Iijima,T., and Ito,H. 2007. Involvement of transient receptor potential canonical 1 (TRPC1) in angiotensin II-induced vascular smooth muscle cell hypertrophy. *Atherosclerosis* **195**:287-296.
229. Landsberg,J.W., and Yuan,J.X. 2004. Calcium and TRP channels in pulmonary vascular smooth muscle cell proliferation. *News Physiol Sci.* **19**:44-50.
230. Lewis,R.S. 2007. The molecular choreography of a store-operated calcium channel. *Nature* **446**:284-287.
231. Graier,W.F., Simecek,S., Bowles,D.K., and Sturek,M. 1994. Heterogeneity of caffeine- and bradykinin-sensitive Ca²⁺ stores in vascular endothelial cells. *Biochem. J.* **300**:637-641.

232. Fleenor, B.S., and Bowles, D.K. 2009. Exercise training decreases the size and alters the composition of the neointima in a porcine model of percutaneous transluminal coronary angioplasty (PTCA). *J. Appl. Physiol* **107**:937-945.
233. Antonucci, D., Valenti, R., Santoro, G.M., Bolognese, L., Trapani, M., Cerisano, G., Boddi, V., and Fazzini, P.F. 1998. Restenosis after coronary stenting in current clinical practice. *Am. Heart J.* **135**:510-518.
234. Hammoud, T., Tanguay, J.F., and Bourassa, M.G. 2000. Management of coronary artery disease: Therapeutic options in patients with diabetes. *J. Am. Coll. Cardiol.* **36**:355-365.
235. Lee, I.M., Sesso, H.D., Oguma, Y., and Paffenbarger, R.S., Jr. 2003. Relative intensity of physical activity and risk of coronary heart disease. *Circulation* **107**:1110-1116.
236. Berlin, J.A., and Colditz, G.A. 1990. A meta-analysis of physical activity in the prevention of coronary heart disease. *Am. J. Epidemiol.* **132**:612-628.
237. Diabetes Prevention Program Research Group 2002. Reduction in the Incidence of Type 2 Diabetes with Lifestyle Intervention or Metformin. *N Engl J Med* **346**:393-403.
238. Andersson, L. 2003. Identification and characterization of AMPK α 3 mutations in the pig. *Biochem. Soc. Trans.* **31**:232-235.
239. Nilius, B., Owsianik, G., Voets, T., and Peters, J.A. 2007. Transient Receptor Potential Cation Channels in Disease. *Physiol. Rev.* **87**:165-217.
240. Sturek, M., Stehno-Bittel, L., and Obye, P. 1991. Modulation of ion channels by calcium release in coronary artery smooth muscle. In *Electrophysiology and Ion Channels of Vascular Smooth Muscle Cells and Endothelial Cells*. N. Sperelakis, and Kuriyama, H., editors. Elsevier. New York. 65-79.
241. Cheng, K.T., Liu, X., Ong, H.L., and Ambudkar, I.S. 2008. Functional Requirement for Orai1 in Store-operated TRPC1-STIM1 Channels. *J. Biol. Chem.* **283**:12935-12940.
242. Mani, B.K., Brueggemann, L.I., Cribbs, L.L., and Byron, K.L. 2009. Opposite regulation of KCNQ5 and TRPC6 channels contributes to vasopressin-stimulated calcium spiking responses in A7r5 vascular smooth muscle cells. *Cell Calcium* **45**:400-411.
243. Frischauf, I., Muik, M., Derler, I., Bergsmann, J., Fahrner, M., Schindl, R., Groschner, K., and Romanin, C. 2009. Molecular determinants of the coupling between STIM1 and Orai channels: Differential activation of Orai1,2,3 channels by a STIM1 coiled-coil mutant. *J. Biol. Chem.* **(In press)**.
244. Hu, G., Oboukhova, E.A., Kumar, S., Sturek, M., and Obukhov, A.G. 2009. Canonical transient receptor potential channels expression is elevated in a porcine model of metabolic syndrome. *Molecular Endocrinology* **23**:689-699.

245. Lafont,A., Guzman,L.A., Whitlow,P.L., Goormastic,M., Cornhill,J.F., and Chisolm,G.M. 1995. Restenosis after experimental angioplasty. *Circ. Res.* **76**:996-1002.
246. Post,M.J., Borst,C., and Kuntz,R.E. 1994. The relative importance of arterial remodeling compared with intimal hyperplasia in lumen renarrowing after balloon angioplasty. A study in the normal rabbit and the hypercholesterolemic Yucatan micropig. *Circulation* **89**:2816-2821.
247. Dluhy,R.G., and McMahon,G.T. 2008. Intensive Glycemic Control in the ACCORD and ADVANCE Trials. *N Engl J Med* **358**:2630-2633.
248. Barrett-Connor,E. 1997. Does hyperglycemia really cause coronary heart disease? *Diabetes Care* **20**:1620-1623.
249. Neeb,Z.P., Alloosh,M., Long,X., Bratz,I.N., Edwards,J.M., Lee,L., Chalasani,N., and Sturek,M. 2009. Severe coronary artery disease in Ossabaw miniature swine with metabolic syndrome. *To be determined (In preparation)*.
250. Ross,R. 1986. The pathogenesis of atherosclerosis -- an update. *N. Engl. J. Med.* **314**:488-500.
251. Bean,B.P., Sturek,M., Puga,A., and Hermsmeyer,K. 1986. Calcium channels in muscle cells isolated from rat mesenteric arteries: modulation by dihydropyridine drugs. *Circ. Res.* **59**:229-235.
252. Bowles,D.K., Hu,Q., Laughlin,M.H., and Sturek,M. 1997. Heterogeneity of L-type calcium current density in coronary smooth muscle. *Am. J. Physiol. : Heart Circ. Physiol.* **273**:H2083-H2089.
253. Wangsness,P.J., Martin,R.J., and Gahagan,J.H. 1977. Insulin and growth hormone in lean and obese pigs. *Am. J. Physiol.* **233**:E104-E108.
254. Brisbin,Jr.I.L., and Mayer,J.J. 2001. Problem pigs in a poke: a good pool of data. *Science* **294**:1280-1281.
255. Turner,N., Hulbert,A.J., and Else,P.L. 2006. Limits to physical performance and metabolism across species. *Curr. Opin. Clin. Nutr. Metab Care* **9**:691-696.
256. Sacks,D.B., Bruns,D.E., Goldstein,D.E., Maclaren,N.K., McDonald,J.M., and Parrott,M. 2002. Guidelines and recommendations for laboratory analysis in the diagnosis and management of diabetes mellitus. *Clin. Chem.* **48**:436-472.
257. Boden,G., and Shulman,G.I. 2002. Free fatty acids in obesity and type 2 diabetes: defining their role in the development of insulin resistance and beta-cell dysfunction. *Eur. J. Clin. Invest* **32 Suppl 3**:14-23.
258. Gotto,A.M. 2002. Lipid management in diabetic patients: lessons from prevention trials. *Am. J. Med.* **112 Suppl 8A**:19S-26S.

259. Sturek,M., Kunda,K., and Hu,Q. 1992. Sarcoplasmic reticulum buffering of myoplasmic calcium in bovine coronary artery smooth muscle. *J. Physiol. (Lond.)* **451**:25-48.
260. Lemos,V.S., Poburko,D., Liao,C.H., Cole,W.C., and van,B.C. 2007. Na⁺ entry via TRPC6 causes Ca²⁺ entry via NCX reversal in ATP stimulated smooth muscle cells. *Biochem. Biophys. Res. Commun.* **352**:130-134.
261. Neeb,Z.P., Edwards,J.M., Alloosh,M.A., Mokolke,E.A., and Sturek,M. 2009. Coronary artery disease and Ca²⁺ signaling in metabolic syndrome. *To be determined (In preparation)*.
262. Ashida,T., and Blaustein,M.P. 1987. Regulation of cell calcium and contractility in mammalian arterial smooth muscle: The role of sodium-calcium exchange. *J. Physiol. (Lond.)* **392**:617-635.
263. Arnon,A., Hamlyn,J.M., and Blaustein,M.P. 2000. Na⁺ entry via store-operated channels modulates Ca²⁺ signaling in arterial myocytes. *Am. J. Physiol. Cell Physiol.* **278**:C163-C173.
264. Zeng,W., Yuan,J.P., Kim,M.S., Choi,Y.J., Huang,G.N., Worley,P.F., and Muallem,S. 2008. STIM1 Gates TRPC Channels, but Not Orai1, by Electrostatic Interaction. *Mol. Cell* **32**:439-448.
265. Rosker,C., Graziani,A., Lukas,M., Eder,P., Zhu,M.X., Romanin,C., and Groschner,K. 2004. Ca(2+) signaling by TRPC3 involves Na(+) entry and local coupling to the Na(+)/Ca(2+) exchanger. *J. Biol. Chem.* **279**:13696-13704.
266. Lemos,V.S., Poburko,D., Liao,C.H., Cole,W.C., and Breemen,C.v. 2007. Na⁺ entry via TRPC6 causes Ca²⁺ entry via NCX reversal in ATP stimulated smooth muscle cells. *Biochem. Biophys. Res. Commun.* **352**:130-134.
267. Bowles,D.K., Heaps,C.L., Turk,J.R., Maddali,K.K., and Price,E.M. 2004. Hypercholesterolemia inhibits L-type calcium current in coronary macro-, not microcirculation. *J. Appl. Physiol.* **96**:2240-2248.
268. Wamhoff,B.R., Dixon,J.L., and Sturek,M. 2001. Exercise training prevents altered coronary smooth muscle L-type calcium channel function in diabetic dyslipidemia. *Circulation* **104**:II-157 (Abstr.)
269. Launay,P., Cheng,H., Srivatsan,S., Penner,R., Fleig,A., and Kinet,J.P. 2004. TRPM4 regulates calcium oscillations after T cell activation. *Science* **306**:1374-1377.
270. Ullrich,N.D., Voets,T., Prenen,J., Vennekens,R., Talavera,K., Droogmans,G., and Nilius,B. 2005. Comparison of functional properties of the Ca²⁺-activated cation channels TRPM4 and TRPM5 from mice. *Cell Calcium* **37**:267-278.
271. Phillips,R.W., Panepinto,L.M., Spangler,R.S., and Wheeler,L.R. 1978. Insulin secretion in Yucatan miniature swine selected for glucose intolerance. *Diabetes* **27**:497-497, (Abstr.)

272. Phillips,R.W., Panepinto,L.M., Will,D.H., and Case,G.L. 1980. The effects of alloxan diabetes on Yucatan miniature swine and their progeny. *Metabolism* **29**:40-45.
273. Du,Z.Q., Fan,B., Zhao,X., Amoako,R., and Rothschild,M.F. 2008. Association Analyses Between Type 2 Diabetes Genes and Obesity Traits in Pigs. *Obesity* **17**:323-329.
274. Panepinto,L.M., Phillips,R.W., Wheeler,L.R., and Will,D.H. 1978. The Yucatan miniature pig as a laboratory animal. *Lab. Anim. Sci.* **28**:308-313.
275. Mokolke,E.A., and Sturek,M. 2001. Cardiac dysfunction in a swine model of diabetic dyslipidemia.
276. Xi,S., Yin,W., Wang,Z., Kusunoki,M., Lian,X., Koike,T., Fan,J., and Zhang,Q. 2004. A minipig model of high-fat/high-sucrose diet-induced diabetes and atherosclerosis. *Int. J. Exp. Pathol.* **85**:223-231.
277. Larsen,M.O., and Rolin,B. 2004. Use of the Gottingen minipig as a model of diabetes with special focus on type 1 diabetes research. *ILAR J.* **45**:303-313.
278. Spurlock,M.E., and Gabler,N.K. 2008. The Development of Porcine Models of Obesity and the Metabolic Syndrome. *J. Nutr.* **138**:397-402.
279. Stribling,H.L., Brisbin,Jr.I.L., Sweeney,J.R., and Stribling,L.A. 1984. Body fat reserves and their prediction in two populations of feral swine. *J. Wildl. Manage.* **48**:635-639.
280. Buhlinger,C.A., Wangsness,P.J., Martin,R.J., and Ziegler,J.H. 1978. Body composition, *in vitro* lipid metabolism and skeletal muscle characteristics in fast-growing, lean and in slow-growing, obese pigs at equal age and weight. *Growth* **42**:225-236.
281. Brisbin,I.L., Jr., Geiger,R.A., Graves,H.B., Pinder,J.E., III, Sweeney,J.M., and Sweeney,J.R. 1977. Morphological characterizations of two populations of feral swine. *Acta Theriol.* **22**:75-85.
282. Kempson,S.A., Edwards,J.M., Osborn,A., and Sturek,M. 2008. Acute inhibition of the betaine transporter by ATP and adenosine in renal MDCK cells. *Am. J. Physiol. Renal Physiol.* **295**:F108-F117.
283. Krolewski,A.S., Warram,J.H., Valsania,P., Martin,B.C., Laffel,L.M.B., and Christlieb,A.R. 1991. Evolving natural history of coronary artery disease in diabetes mellitus. *Am. J. Med.* **90**:56S-60S.
284. Neel,J.V. 1962. Diabetes mellitus: a "thrifty" genotype rendered detrimental by "progress"? *Am. J. Hum. Genet.* **14**:353-362.

285. Larsen,M.O., Wilken,M., Gotfredsen,C.F., Carr,R.D., Svendsen,O., and Rolin,B. 2002. Mild streptozotocin diabetes in the Göttingen minipig- A novel model of moderate insulin deficiency and diabetes. *Am J Physiol Endocrinol Metab* **282**:E1342-E1351.
286. Larsen,M.O., Rolin,B., Wilken,M., Carr,R.D., and Gotfredsen,C.F. 2003. Measurements of Insulin Secretory Capacity and Glucose Tolerance to Predict Pancreatic b-Cell Mass *In Vivo* in the Nicotinamide/Streptozotocin Gottingen Minipig, a Model of Moderate Insulin Deficiency and Diabetes. *Diabetes* **52**:118-123.
287. Maclean,N., and Oglivie,R.F. 1955. Quantitative estimation of the pancreatic islet tissue in diabetic subjects. *Diabetes* **4**:367-376.
288. Vozarova,B., Stefan,N., Lindsay,R.S., Saremi,A., Pratley,R.E., Bogardus,C., and Tataranni,P.A. 2002. High alanine aminotransferase is associated with decreased hepatic insulin sensitivity and predicts the development of type 2 diabetes. *Diabetes* **51**:1889-1895.
289. Marchesini,G., Brizi,M., Bianchi,G., Tomassetti,S., Bugianesi,E., Lenzi,M., McCullough,A.J., Natale,S., Forlani,G., and Melchionda,N. 2001. Nonalcoholic fatty liver disease: a feature of the metabolic syndrome. *Diabetes* **50**:1844-1850.
290. Bugianesi,E., Gastaldelli,A., Vanni,E., Gambino,R., Cassader,M., Baldi,S., Ponti,V., Pagano,G., Ferrannini,E., and Rizzetto,M. 2005. Insulin resistance in non-diabetic patients with non-alcoholic fatty liver disease: sites and mechanisms. *Diabetologia* **48**:634-642.
291. Wieckowska,A., McCullough,A.J., and Feldstein,A.E. 2007. Noninvasive diagnosis and monitoring of nonalcoholic steatohepatitis: present and future. *Hepatology* **46**:582-589.
292. Adams,L.A., Lymp,J.F., St,S.J., Sanderson,S.O., Lindor,K.D., Feldstein,A., and Angulo,P. 2005. The natural history of nonalcoholic fatty liver disease: a population-based cohort study. *Gastroenterology* **129**:113-121.
293. Chen,N.X., O'Neill,K.D., Chen,X., Duan,D., Wang,E., Edwards,J.M., Sturek,M., and Moe,S.M. 2007. Fetuin-A uptake in bovine vascular smooth muscle cells is calcium dependent and mediated by annexins. *Am. J. Physiol. Renal Physiol.* **292**:F599-F606.
294. Faeh,D., Minehira,K., Schwarz,J.M., Periasamy,R., Park,S., and Tappy,L. 2005. Effect of fructose overfeeding and fish oil administration on hepatic de novo lipogenesis and insulin sensitivity in healthy men. *Diabetes* **54**:1907-1913.
295. Mehta,K., Van Thiel,D.H., Shah,N., and Mobarhan,S. 2002. Nonalcoholic fatty liver disease: pathogenesis and the role of antioxidants. *Nutr. Rev.* **60**:289-293.
296. Utzschneider,K.M., and Kahn,S.E. 2006. The Role of Insulin Resistance in Nonalcoholic Fatty Liver Disease. *Journal of Clinical Endocrinology Metabolism* **91**:4753-4761.

297. Jensen,L.O., Thayssen,P., Mintz,G.S., Maeng,M., Junker,A., Galloe,A., Christiansen,E.H., Hoffmann,S.K.S., Pedersen,K.E., Hansen,H.S. et al 2007. Intravascular ultrasound assessment of remodelling and reference segment plaque burden in type-2 diabetic patients. *Eur Heart J* **28**:1759-1764.
298. Stratmann,B., and Tschoepe,D. 2009. Atherogenesis and atherothrombosis--focus on diabetes mellitus. *Best. Pract. Res. Clin. Endocrinol. Metab* **23**:291-303.
299. Hollenbeck,C.B. 1993. Dietary fructose effects on lipoprotein metabolism and risk for coronary artery disease. *Am. J. Clin. Nutr.* **58**:800S-809S.
300. Balk,E.M., Lichtenstein,A.H., Chung,M., Kupelnick,B., Chew,P., and Lau,J. 2006. Effects of omega-3 fatty acids on serum markers of cardiovascular disease risk: a systematic review. *Atherosclerosis* **189**:19-30.
301. Dixon,J.L., Stoops,J.D., Parker,J.L., Laughlin,M.H., Weisman,G.A., and Sturek,M. 1999. Dyslipidemia and vascular dysfunction in diabetic pigs fed an atherogenic diet. *Arterioscler. Thromb. Vasc. Biol.* **19**:2981-2992.
302. Liem,T.K., Vouyouka,A., Dixon,J., Shukla,S., Silver,D., Krause,G., and Sturek,M.S. 1999. Role of diabetes and hyperlipidemia in the uptake of cholesterol in arterial low shear regions. *Surg. Forum* **L**:429-432.
303. Roberts,T.M., Sturek,M., Dixon,J.L., and Hardin,C.D. 2001. Alterations in the oxidative metabolic profile in vascular smooth muscle from hyperlipidemic and diabetic swine. *Mol. Cell. Biochem.* **217**:99-106.
304. Mokolke,E.A., Hu,Q., Turk,J.R., and Sturek,M. 2004. Enhanced contractility in coronary arteries of diabetic pigs is prevented by exercise. *Equine Comp. Exercise Physiol.* **1**:71-80.
305. Hainsworth,D.P., Katz,M.L., Sanders,D.A., Sanders,D.N., Wright,E.J., and Sturek,M. 2002. Retinal capillary basement membrane thickening in a porcine model of diabetes mellitus. *Comp. Med.* **52**:523-529.
306. Korte,F.S., Mokolke,E.A., Sturek,M., and McDonald,K.S. 2005. Exercise improves impaired ventricular function and alterations of cardiac myofibrillar proteins in diabetic dyslipidemic pigs. *J. Appl. Physiol.* **98**:461-467.
307. Thomas,T.R., Pellecia,J., Rector,R.S., Sun,G.Y., Sturek,M., and Laughlin,M.H. 2002. Exercise training does not reduce hyperlipidemia in pigs fed a high fat diet. *Metabolism* **51**:1587-1595.
308. Mokolke,E.A., Wang,M., and Sturek,M. 2002. Exercise training enhances coronary smooth muscle cell sodium-calcium exchange activity in diabetic dyslipidemic Yucatan swine. *Ann. N. Y. Acad. Sci.* **976**:335-337.
309. Liu,Y., Rector,R.S., Thomas,T.R., Taylor,J.A., Holiman,D.A., Henderson,K.K., Welshons,W.V., and Sturek,M. 2004. Lipoproteins during the estrous cycle in swine. *Metabolism* **53**:140-141.

310. Lichtenstein,A.H., Ausman,L.M., Jalbert,S.M., and Schaefer,E.J. 1999. Effects of Different Forms of Dietary Hydrogenated Fats on Serum Lipoprotein Cholesterol Levels. *N Engl J Med* **340**:1933-1940.
311. Payne,G.A., Borbouse,L., Kumar,S., Neeb,Z.P., Alloosh,M., Sturek,M., and Tune,J.D. 2009. Perivascular adipose-derived leptin exacerbates coronary endothelial dysfunction in metabolic syndrome via a PKC- α dependent pathway. *Arterioscler. Thromb. Vasc. Biol.* **(Submitted)**.
312. Ziegler,M.G., Sturek,M., Alloosh,M., and Unthank,J.L. 2009. Peripheral artery collateral formation after femoral artery occlusion in Ossabaw miniature swine with metabolic syndrome. *To be determined (In preparation)*.
313. Kassab,G.S., Choy,J.S., Svendsen,M., Sinha,A.K., Alloosh,M., Sturek,M., Huo,Y., Sandusky,G.E., and Hermiller,J. 2009. A novel system for reconstruction of coronary artery lumen profile in real-time: a preclinical validation. *Am. J. Physiol. : Heart Circ. Physiol.* **297**:H485-H492.
314. Habegger,K.M., Tackett,L., Sealls,W.J., Bell,L.N., Awad,M., Blue,E., Gallagher,P.J., Sturek,M., Alloosh,M.A., Steinberg,H.O. et al 2009. Fatty acid-induced plasma membrane cholesterol accrual and insulin resistance. *Diabetologia* **(Submitted)**.
315. Ertas,G., Van Beusekom,H.M., and Van der Giessen,W.J. 2009. Late stent thrombosis, endothelialisation and drug-eluting stents. *Neth. Heart J.* **17**:177-180.
316. Tharp,D.L., Wamhoff,B.R., Turk,J.R., and Bowles,D.K. 2006. Upregulation of intermediate-conductance Ca^{2+} -activated K^{+} channel (IKCa1) mediates phenotypic modulation of coronary smooth muscle. *Am. J. Physiol Heart Circ. Physiol* **291**:H2493-H2503.
317. Van,A.T., Fransen,P., Guns,P.J., Herman,A.G., and Bult,H. 2007. Altered Ca^{2+} handling of smooth muscle cells in aorta of apolipoprotein E-deficient mice before development of atherosclerotic lesions. *Cell Calcium* **41**:295-302.
318. Christen,T., Verin,V., Bochaton-Piallat,M.L., Popowski,Y., Ramaekers,F., Debruyne,P., Camenzind,E., Van Eys,G., and Gabbiani,G. 2001. Mechanisms of neointima formation and remodeling in the porcine coronary artery. *Circulation* **103**:882-888.
319. Chung,I.M., Gold,H.K., Schwartz,S.M., Ikari,Y., Reidy,M.A., and Wight,T.N. 2002. Enhanced extracellular matrix accumulation in restenosis of coronary arteries after stent deployment. *J. Am. Coll. Cardiol.* **40**:2072-2081.
320. Owens,G.K. 1995. Regulation of differentiation of vascular smooth muscle cells. *Physiol. Rev.* **75**:487-517.
321. Lompré,A.M. 1999. Sarcoplasmic reticulum in vascular cells in hypertension and during proliferation. *Clin. Exp. Pharmacol. Physiol.* **26**:553-557.

322. Côrtes,S.D.F., Lemos,V.S., Corriu,C., and Stoclet,J.C. 1996. Changes in angiotensin II receptor density and calcium handling during proliferation in SBR aortic myocytes. *Am. J. Physiol. Heart Circ. Physiol.* **271**:H2330-H2338.
323. Masuo,M., Toyo-oka,T., Shin,W.S., and Sugimoto,T. 1991. Growth-dependent alterations of intracellular Ca²⁺-handling mechanisms of vascular smooth muscle cells: PDGF negatively regulates functional expression of voltage-dependent, IP₃- mediated, and Ca²⁺-induced Ca²⁺ release channels. *Circ. Res.* **69**:1327-1339.
324. Montero,M., Alvarez,J., Scheenen,W.J.J., Rizzuto,R., Meldolesi,J., and Pozzan,T. 1997. Ca²⁺ homeostasis in the endoplasmic reticulum: coexistence of high and low [Ca²⁺] subcompartments in intact HeLa cells. *J. Cell Biol.* **139**:601-611.
325. Porter,K.R., and Palade,G.E. 1957. Studies on the endoplasmic reticulum. III. Its form and distribution in striated muscle cells. *J. Biophys. Biochem. Cytol.* **3**:269-300.
326. Villa,A., Podini,P., Panzeri,M.C., Söling,H.D., Volpe,P., and Meldolesi,J. 2003. The endoplasmic-sarcoplasmic reticulum of smooth muscle: immunocytochemistry of vas deferens fibers reveals specialized subcompartments differentially equipped for the control of Ca²⁺ homeostasis. *J. Cell Biol.* **121**:1041-1051.
327. Devine,C.E., Somlyo,A.V., and Somlyo,A.P. 1972. Sarcoplasmic reticulum and excitation-contraction coupling in mammalian smooth muscle. *J. Cell Biol.* **52**:690-718.
328. Somlyo,A.V. 1980. Ultrastructure of vascular smooth muscle. In *Vascular Smooth Muscle*. D.F.Bohr, Somlyo,A.P., and Sparks,H.V., editors. American Physiological Society. Bethesda, MD. 33-67.
329. Sanders,K.M. 2008. Regulation of smooth muscle excitation and contraction. *Neurogastroenterol. Motil.* **20 Suppl 1**:39-53.
330. Bowles,D.K., Hu,Q., Laughlin,M.H., and Sturek,M. 1998. Exercise training increases L-type calcium current density in coronary smooth muscle. *Am. J. Physiol. : Heart Circ. Physiol.* **275**:H2159-H2169.
331. Guo,R.W., Wang,H., Gao,P., Li,M.Q., Zeng,C.Y., Yu,Y., Chen,J.F., Song,M.B., Shi,Y.K., and Huang,L. 2009. An essential role for stromal interaction molecule 1 in neointima formation following arterial injury. *Cardiovasc. Res.* **81**:660-668.
332. Okon,E.B., Golbabaie,A., and Breemen,C. 2008. Paracrine effects of endothelial cells in a diabetic mouse model: capacitative calcium entry stimulated thromboxane release. *Horm. Metab Res.* **40**:645-650.

333. Pulver-Kaste,R.A., Barlow,C.A., Bond,J., Watson,A., Penar,P.L., Tranmer,B., and Lounsbury,K.M. 2006. Ca²⁺ source-dependent transcription of CRE-containing genes in vascular smooth muscle. *Am. J. Physiol Heart Circ. Physiol* **291**:H97-105.
334. Saleh,S.N., Albert,A.P., Peppiatt-Wildman,C.M., and Large,W.A. 2008. Diverse properties of store-operated TRPC channels activated by protein kinase C in vascular myocytes. *J. Physiol* **586**:2463-2476.
335. Flemming,R., Xu,S.Z., and Beech,D.J. 2003. Pharmacological profile of store-operated channels in cerebral arteriolar smooth muscle cells. *Br. J. Pharmacol.* **139**:955-965.
336. Wang,Y., Deng,X., Hewavitharana,T., Soboloff,J., and Gill,D.L. 2008. Stim, ORAI and TRPC channels in the control of calcium entry signals in smooth muscle. *Clin. Exp. Pharmacol. Physiol* **35**:1127-1133.
337. Trepakova,E.S., Csutora,P., Hunton,D.L., Marchase,R.B., Cohen,R.A., and Bolotina,V.M. 2000. Calcium Influx Factor Directly Activates Store-operated Cation Channels in Vascular Smooth Muscle Cells. *J. Biol. Chem.* **275**:26158-26163.
338. Xu,S.Z., and Beech,D.J. 2001. TrpC1 is a membrane-spanning subunit of store-operated Ca(2+) channels in native vascular smooth muscle cells. *Circ. Res.* **88**:84-87.
339. Hogan,P.G., and Rao,A. 2007. Dissecting ICRAC, a store-operated calcium current. *Trends Biochem. Sci.* **32**:235-245.
340. Abdullaev,I.F., Bisailon,J.M., Potier,M., Gonzalez,J.C., Motiani,R.K., and Trebak,M. 2008. Stim1 and Orai1 Mediate CRAC Currents and Store-Operated Calcium Entry Important for Endothelial Cell Proliferation. *Circ. Res.* **103**:1289-1299.
341. Brueggemann,L.I., Markun,D.R., Henderson,K.K., Cribbs,L.L., and Byron,K.L. 2006. Pharmacological and electrophysiological characterization of store-operated currents and capacitative Ca(2+) entry in vascular smooth muscle cells. *J. Pharmacol. Exp. Ther.* **317**:488-499.
342. Pani,B., Cornatzer,E., Cornatzer,W., Shin,D.M., Pittelkow,M.R., Hovnanian,A., Ambudkar,I.S., and Singh,B.B. 2006. Up-regulation of transient receptor potential canonical 1 (TRPC1) following sarco(endo)plasmic reticulum Ca²⁺ ATPase 2 gene silencing promotes cell survival: a potential role for TRPC1 in Darier's disease. *Mol. Biol. Cell* **17**:4446-4458.
343. Sweeney,M., Yu,Y., Platoshyn,O., Zhang,S., McDaniel,S.S., and Yuan,J.X.J. 2002. Inhibition of endogenous TRP1 decreases capacitative Ca²⁺ entry and attenuates pulmonary artery smooth muscle cell proliferation. *Am J Physiol Lung Cell Mol Physiol* **283**:L144-L155.

344. Tai,K., Hamaide,M.C., Debaix,H., Gailly,P., Wibo,M., and Morel,N. 2008. Agonist-evoked calcium entry in vascular smooth muscle cells requires IP3 receptor-mediated activation of TRPC1. *Eur. J. Pharmacol.* **583**:135-147.
345. Takahashi,Y., Watanabe,H., Murakami,M., Ono,K., Munehisa,Y., Koyama,T., Nobori,K., Iijima,T., and Ito,H. 2007. Functional role of stromal interaction molecule 1 (STIM1) in vascular smooth muscle cells. *Biochem. Biophys. Res. Commun.* **361**:934-940.
346. Dehaven,W.I., Jones,B.F., Petranka,J.G., Smyth,J.T., Tomita,T., Bird,G.S., and Putney,J.W., Jr. 2009. TRPC channels function independently of STIM1 and Orai1. *J. Physiol* **587**:2275-2298.
347. Zakharov,S.I., Mongayt,D.A., Cohen,R.A., and Bolotina,V.M. 1999. Monovalent cation and L-type Ca^{2+} channels participate in calcium paradox-like phenomenon in rabbit aortic smooth muscle cells. *J. Physiol. (Lond.)* **514**:71-81.
348. Lee,C.H., Poburko,D., Sahota,P., Sandhu,J., Ruehlmann,D.O., and van Breeman,C. 2001. The mechanism of phenylephrine-mediated $[Ca^{2+}]_i$ oscillations underlying tonic contraction in the rabbit inferior vena cava. *J. Physiol. (Lond.)* **534**:641-650.
349. Chau,W.H., Lee,W.H., Lau,W.H., Kwan,Y.W., Au,A.L., and Raymond,K. 2003. Role of Na^+/H^+ exchanger in acetylcholine-mediated pulmonary artery contraction of spontaneously hypertensive rats. *Eur. J. Pharmacol.* **464**:177-187.
350. Kwan,H.Y., Shen,B., Ma,X., Kwok,Y.C., Huang,Y., Man,Y.B., Yu,S., and Yao,X. 2009. TRPC1 associates with BK(Ca) channel to form a signal complex in vascular smooth muscle cells. *Circ. Res.* **104**:670-678.

Curriculum Vita

Zachary Paul Neeb

Education

Doctor of Philosophy in Cellular and Integrative Physiology

Minor: Diabetes and Obesity

Jan. 2006 – Feb. 2010

Indiana University

Indianapolis, IN

Bachelor of Science in Biology

Aug. 2001 – Dec. 2005

Purdue University

Indianapolis, IN

Awards

CTSI Fellowship NIH UL1 RR025761 (Aug. 2009 – Jan. 2010)

2009 Keystone Symposia Dissecting the Vasculature Scholarship (Apr. 2009)

IU School of Medicine Translational Research Fellowship (Aug. 2007 – Aug. 2008)

Moenkhaus Physiology Graduate Fellowship Award (2007)

Multidisciplinary Undergraduate Research Institute scholarship (2005)

National Science Foundation Educational Research for Undergraduates (2005)

Skills

Angiography

Percutaneous vascular intervention (stenting/balloon angioplasty)

Intravascular ultrasound

Coronary blood flow in anesthetized swine/dogs

Localized drug infusion into coronary circulation

Sterile organ/tissue procurement from large mammals

Organ, cell, and primary culture

Enzymatic isolation of arterial endothelium and smooth muscle

Mechanical isolation of in-stent media and neointima

Fluorescence Ca²⁺ imaging

Patch clamp electrophysiology

Radioactive materials

PCR (quantitative, semi-quantitative, real time, and linear)

DNA/RNA/Protein isolation

ELISA/EMSA

Pull-down assay

Mini/Maxi preparation of plasmid DNA and protein

Publications

Zachary P. Neeb, Mouhamad Alloosh, Jason M. Edwards, Ivan Mwesigwa, Ian N. Bratz, Lydia Lee, Romil Saxena, Naga Chalasani, Michael Sturek. Diet-induced dyslipidemia in metabolic syndrome is necessary to elicit severe coronary artery disease and non-alcoholic steatohepatitis. (submitted)

Zachary P. Neeb, Mouhamad Alloosh, Xin Long, Jason M. Edwards, Ian N. Bratz, Michael Sturek. Store-operated Ca²⁺ influx predicts coronary artery disease and is induced by dyslipidemia in metabolic syndrome and type 2 diabetes. (submitted)

Zachary P. Neeb, Jason M. Edwards, Mouhamad Alloosh, Xin Long, Eric Mokolke, Michael Sturek. Novel metabolic syndrome and coronary artery disease in Ossabaw compared to Yucatan swine. (submitted)

Jason M. Edwards*, **Zachary P. Neeb***, Mouhamad A. Alloosh, Ian N. Bratz, Alexander G. Obukhov, Michael Sturek. Exercise training decreases TRPC-mediated Ca²⁺ influx associated with metabolic syndrome and coronary atherosclerosis. Cardiovascular Research. 2009 (In press). * denotes equal contribution.

Léna Borbouse, Gregory M. Dick, Shawn B. Bender, U. Deniz Dincer, Gregory A. Payne, **Zachary P. Neeb**, Ian N. Bratz, Michael Sturek, Johnathan D. Tune. Impaired Functional Expression of Coronary BKCa Channels in Metabolic Syndrome. Am J Physiol Heart Circ Physiol. 2009 Nov;297(5):H1629-37.

Ian N. Bratz, Gregory M. Dick, Johnathan D. Tune, Jason M. Edwards, **Zachary P. Neeb**, Unize D. Dincer, Michael Sturek. Impaired capsaicin-induced relaxation of coronary arteries in porcine model of the metabolic syndrome. American Journal of Heart Physiology Heart Circulation Physiology. 2008 Jun; 294(6):H2489-96.

Roland W. Pfaeffle, Chad S. Hunter, Jesse J. Savage, Mario Duran-Prado, Rachel D. Mullen, **Zachary P. Neeb**, Urs Eiholzer, Volker Hesse, Nadine G. Haddad, Heike M. Stobbe, Werner F. Blum, Johannes F.W. Weigel, Simon J. Rhodes. Three novel missense mutations within the LHX4 gene are associated with variable pituitary hormone deficiencies. *Journal of Clinical Endocrinology Metabolism*. 2008 Mar; 93(3):1062-71.

Presentations/Abstracts

Zachary P. Neeb, Mouhamad Alloosh, Romil Saxena, Naga Chalasani, Michael Sturek. Dyslipidemia in metabolic syndrome is necessary to elicit severe coronary artery disease and non-alcoholic steatohepatitis. *Experimental Biology*. April, 2010 Conference, Anaheim, CA.

Zachary P. Neeb, Mouhamad Alloosh, Jason M. Edwards, Ian N. Bratz, Michael Sturek. Store-operated Ca^{2+} influx predicts coronary artery disease and is induced by dyslipidemia in metabolic syndrome and type 2 diabetes. *Experimental Biology*. April, 2010 Conference, Anaheim, CA.

Aaron J. Trask, Paige S. Katz, **Zachary P. Neeb**, Mouhamad Alloosh, Michael Sturek, Pamela Lucchesi. Coronary artery microvascular narrowing downstream of stent implantation. *Experimental Biology*. April, 2010 Conference, Anaheim, CA.

Aaron J. Trask, Paige S. Katz, **Zachary P. Neeb**, Mouhamad Alloosh, Michael Sturek, Pamela Lucchesi. Inward coronary artery microvessel remodeling in Ossabaw swine with metabolic syndrome. *Experimental Biology*. April, 2010 Conference, Anaheim, CA.

Zachary P. Neeb, Xin Long, Michael Sturek. Store-operated Ca^{2+} influx in coronary smooth muscle cells predicts coronary atherosclerosis in the metabolic syndrome. CTSI conference. Indianapolis, IN. 3rd place poster presentation.

Zachary P. Neeb, Xin Long, Eric Mokolke, Jason Edwards, Mouhamad Alloosh, Michael Sturek. Adenosine A2a/b receptor-mediated vasodilation is antagonized by adenosine A1 receptor in coronary circulation of healthy Ossabaw swine. *Experimental Biology*. April, 2009 Conference, New Orleans.

Zachary P. Neeb, Xin Long, Michael Sturek. Store-operated Ca^{2+} influx in coronary smooth muscle cells predicts coronary atherosclerosis in the metabolic syndrome. Keystone Symposia. February 2009, Vancouver, British Columbia, Canada.

Rolf P. Kreutz, MD, Mouhamad Alloosh, MD, **Zachary P. Neeb**, MS, Yvonne Kreutz, MS, David A. Flockhart, MD, PhD, Michael Sturek, PhD. Metabolic Syndrome in Ossabaw Miniature Swine is Associated with Increased Sensitivity of Platelet Aggregation to Adenosine Diphosphate. *Arteriosclerosis, Thrombosis, and Vascular Biology*. April, 2009 Conference, Washington, D.C.

Zachary P. Neeb, Jason M. Edwards, Ian N. Bratz, Mouhamad A. Alloosh, Michael Sturek. Increased cholesterol is vital to the development of coronary artery disease and type 2 diabetes in Ossabaw swine. *Experimental Biology*. April 2008, San Diego Conference.

Zachary P. Neeb, Jason M. Edwards, Ian N. Bratz, Mouhamad A. Alloosh, Michael Sturek. Increased cholesterol in metabolic syndrome Ossabaw swine precedes store-operated Ca^{2+} influx and the development of coronary artery disease. Experimental Biology. April 2008, San Diego Conference.

Zachary P. Neeb, Jason M. Edwards, Ian N. Bratz, Mouhamad A. Alloosh, C. Schultz, K. Thompson, T. Cunha, Michael Sturek. Occlusive, diffuse coronary artery disease in Ossabaw miniature swine with metabolic syndrome. Experimental Biology. April 2008, San Diego Conference.

Ian N. Bratz, **Zachary P. Neeb**, Mouhamad A. Alloosh, Michael Sturek. Increased cholesterol is vital to impairment of TRPV1 channel-mediated relaxation of coronary artery in Ossabaw miniature swine model of metabolic syndrome. Experimental Biology. April 2008, San Diego Conference.

Jason M. Edwards, **Zachary P. Neeb**, Jim P. Byrd, Mouhamad A. Alloosh, Eric A Mokolke, Michael Sturek. Diffuse coronary atherosclerosis in Ossabaw miniature swine with metabolic syndrome compared to Yucatan swine. Experimental Biology. April 2008, San Diego Conference.

Guoqing Hu, **Zachary P. Neeb**, Michael Sturek, Alexander G. Obukhov. Expression level of canonical transient receptor potential (TRPC) channels is increased in the adrenal medulla of Ossabaw miniature pig manifesting the metabolic syndrome. Experimental Biology. April 2008, San Diego Conference.

Xin Long, Jason M. Edwards, **Zachary P. Neeb**, Mouhamad A. Alloosh, Michael Sturek. Upregulation of adenosine A1 receptor in atherosclerosis in the metabolic syndrome and in the *in vitro* organ culture model of coronary atherosclerosis. Experimental Biology. April 2008, San Diego Conference.

Zachary P. Neeb, Jason M. Edwards, Michael Sturek. Increased TRP Channel-Mediated Influx in Hypercholesterolemic Ossabaw Miniature Swine Coronary Artery Smooth Muscle Cells. Arteriosclerosis, Thrombosis, and Vascular Biology. April 2007 ATVB Conference, Chicago, IL.

Zachary P. Neeb, Jason M. Edwards, Michael Sturek. Increased TRP Channel-Mediated Influx in Hypercholesterolemic Ossabaw Miniature Swine Coronary Artery Smooth Muscle Cells. Experimental Biology. April 2007 Conference, Washington, D.C.

Matthew Franz, **Zachary P. Neeb**, Krista Cowan, Braden Duffin, Tim Pommer, Hazim El-Mounayri, Paul Herring, Omar El-Mounayri, Ben Snyder. Biomechanics of Smooth Muscle Cell Differentiation: Development of and Experimental Study Using an Innovative *In Vitro* Mechanical System. IU Medical School Department of Cellular and Integrative Physiology. July 2005 IUPUI UROP Summer Poster Symposium.